EFFECTS OF DETAILING AND FIBERS ON THE STATIC AND BLAST BEHAVIOUR OF HIGH-STRENGTH CONCRETE BEAMS

By

CHARLEMAGNE JUNIOR CHARLES

Thesis submitted to the
Faculty of Graduate Studies and Research in partial
fulfillment of the requirements for the degree of
Master of Applied Sciences
in Civil Engineering

uOttawa

Department of Civil Engineering
Faculty of Engineering
University of Ottawa

© Charlemagne Junior Charles, Ottawa, Canada, 2019

ABSTRACT

The CSA S850 Blast standard provides guidelines that can be used to enhance the blast performance of reinforced concrete structures. In the case of beams, the standard requires the use of top continuity (compression) bars and well-detailed transverse steel to ensure strength and ductility under blast loads. However, the requirements in the CSA S850 standard are intended for normal-strength concrete structures. Given the increased use of high-strength concrete (HSC) in practice, there is a need to explore the effects of modern blast designs on the behavior of HSC structures subjected to blast loads.

Accordingly, this project examines the effect of modern reinforcement detailing on the static, dynamic and post-blast performance of high-strength concrete beams. The study further examines the ability to use fibers to relax such detailing and simplify construction. A total of seventeen beams are tested. Static testing is conducted under four-point bending, with blast testing conducted using the University of Ottawa shock-tube. The post-blast behavior of the beams is assessed by conducting residual static tests on the blast-damaged specimens. The parameters investigated include the effects of: blast detailing vs. nominal detailing, steel fibers, the effect of longitudinal steel ratio (in compression and tension) and tie spacing.

The results show that under static loads, the use of blast detailing significantly improves the flexural behavior of the beams in terms of ductility. Likewise, the provision of continuity (compression) bars and closely spaced ties is found to improve blast performance by better controlling displacements, increasing blast resistance, limiting damages and allowing for important post-blast residual capacity. The use of steel fibers and relaxed detailing (increased tie spacing) is found to increase resistance and improve cracking behavior under static loads, with an ability to match the blast performance of more heavily-detailed HSC specimens. The use of fibers also allowed for substantial post-blast capacity. Finally, the steel ratio (in tension, in compression and in the transverse direction) was found to affect the blast behavior of the HSC beams.

In addition to the experiments, the analytical study predicts the static and blast response of the tested beams using sectional analysis and non-linear SDOF modeling. Results show that the analysis methodology was able to predict the static and blast responses of the blast-detailed and fiber-reinforced HSC beams with reasonable accuracy.

ACKNOWLEDGMENTS

First, the author wishes to extend his deepest gratitude and sincere appreciation to his thesis supervisor, Dr. HASSAN AOUDE, who offers his unconditional support and knowledge throughout this research.

The author would like to thank Dr. MUSLIM MAJEED for his help in the lab. In particular, YANG LI and ROUKAYA BASTAMI are owed a special thanks for their personal and professional support.

As well, the author would also like to thank his fellow colleagues HYUNCHUL JUNG, WESAM NJEEM, and JORDAN GANDIA AND FAWWAZ IBRAHIM for their help with the process of preparing, casting and testing his various specimens.

The author wishes to further extend his sincere thanks and gratitude to his thesis supervisor, Dr. HASSAN AOUDE, for his financial assistance and to the UNIVERSITY OF OTTAWA EXCELLENCE SCHOLARSHIP.

The author would also like to thank his mother, JEANNE ESPERA, his sister, LINDA ESPERA, for supporting him throughout the course of life.

Finally, the author would like to extend a special thanks to his fiancée ANGE UMUTONI, who through a perfect balance of encouragement, humor, and motivation has allowed the author to complete his work.

NOTATIONS

Symbol	Definition
A	Area impacted by the blast pressure
d_b	Steel reinforcement bar diameter
d_f	Fiber diameter
E_c	Modulus of elasticity, concrete
E_s	Modulus of elasticity, steel
f_{ctf}	Fiber reinforced concrete tensile stress
f_{cu}	Unconfined concrete stress
f_{cuf}	Unconfined fiber reinforced concrete stress
$f_{c'}$	Compressive concrete strength
$f_{cu'}$	Unconfined compressive concrete strength
$f_{cuf'}$	Unconfined compressive fiber reinforced concrete strength
$f_{dc'}$	Design compressive concrete strength
f_{du}	Design steel ultimate stress
f_{dy}	Design steel yield stress
$f_{fct,eq}$	Equivalent flexural strength
f_s	Steel stress
f_{sh}	Steel strain hardening stress
f_u	Steel ultimate stress
f_y	Steel yield stress
F_m	Mean load
I_r	Reflected impulse
K_{LM}	Load mass transformation factor
L_d	Driver length
l_f	Fiber length
m	Total mass of the system
P_r	Reflected pressure

P_d	Driver pressure
R	Building of the member
RI_v	Reinforcing index
t_P	Positive phase duration
u	Deflection at mid-height
$\ddot{u}$	Acceleration at mid-height
v_f	Fiber volume ratio
s	Steel strain
ε_{sh}	Steel strain hardening strain
ε_u	Steel ultimate strain
ε_y	Steel yield strain
$\dot{\varepsilon}$	Dynamic Strain rate
$\dot{\varepsilon}_s$	Static strain rate
Δ_y	Displacement at yielding of reinforcing bar
Δ_{85}	Displacement when load reached 85% of peak load
Δ_{res}	Residual displacement
Δ_{max}	Maximum displacement
θ_{max}	Maximum support rotation
τ_{bond}	Matrix bond strength

ACRONYMS

Acronym	Definition
ACI	American Concrete Institute
ASTM	American Society of Testing and Materials
ATC	Applied Technology Council
BLS	Blast loading simulator
CEB	Comité euro-international du béton
CSA	Canadian Standards Association
DIF	Dynamic increase factor
FRP	Fiber-reinforced polymer
HL	Hairline (crack width)
HS	High strength (steel reinforcement)
HSC	High strength concrete
HSFRC	High strength fiber reinforced concrete
HSS	Hollow steel section
LTD	Load transfer device
LVDT	Linear variable displacement transducer
NBCC	National Building Code of Canada
NS	Normal strength (steel reinforcement)
NSC	Normal strength concrete
NSR	Normal strength reinforcement
RPC	Reactive powder concrete
SCC	Self-consolidating concrete
SDOF	Single degree of freedom
SFRC	Steel fiber reinforced concrete
SHPB	Split Hopkinson Pressure Bar
TNT	Trinitrotoluene
UFC	Unified Facilities Criteria

TABLE OF CONTENTS

LIST OF FIGURES

LIST OF FIGURES

CHAPTER 1: INTRODUCTION

1.1 GENERAL CONTEXT

Recently, there has been growing concern about the structural safety of structures exposed to blast loads. Events such as the bombing of the Murrah Federal Building in Oklahoma City in 1995 (Hinman & Hammond, 1997) and the destruction of more than 30 buildings by the Lac Mégantic rail disaster in 2013 (Lacoursière et al., 2015) demonstrate the vulnerability of structures to blast-induced failures. As a result, it is becoming increasingly important to ensure bridges, transportation systems, government offices, and vulnerable public buildings are blast resistant.

The use of high-strength concrete (HSC) is now commonly used in construction due to its increased strength, stiffness and durability characteristics. While important research exists on the behavior of HSC structures under static and earthquake loads, research on the blast behavior of HSC structures is scarce. It is well known that concrete shows increased brittleness as its strength is increased, and this can raise concerns about the ductility of HSC elements subjected to blast loads.

Modern blast codes such as the Canadian CSA S850 Blast standard, have been developed to better protect structures against bomb blasts(CSA, 2012). In the case of reinforced concrete structures, the standard provides detailing requirements that allow for improved performance under extreme dynamic loading. In the case of flexural members, the standard requires the use of top continuity bars and well-detailed transverse steel to ensure strength and ductility. However, the requirements in the CSA S850 standard are intended for normal-strength concrete structures, and there is a need to adapt design rules for more advanced materials such as high-strength concrete.

Accordingly, this project examines the effect of modern blast detailing, including the use of top continuity (compression) bars and closely spaced ties, on the static and dynamic performance of high-strength concrete beams. The study further examines the potential of using steel fibers in HSC to relax such detailing and simplify construction which can in turn reduce construction cost and time.

1.2 RESEARCH OBJECTIVES

The primary objective of this experimental research is to investigate the effect of blast detailing as required by the CSA S850 standard on the static and dynamic behavior of high-strength concrete beams (with $f_c' \geq 80$ MPa). To achieve this objective, a large set of HSC and beams designed according to modern blast rules (provision of continuity bars and closely-spaced transverse steel) are tested under quasi-static four-point bending and simulated

blast loads using a shock-tube. Specimens showing residual strength from blast testing are further tested under static loads to assess their residual strength and energy-dissipation capacity when compared to undamaged beams. Moreover, the thesis also examines the potential of using steel fibers to relax the detailing required by modern blast codes by testing companion beams with moderate amounts of fibers and intermediate (relaxed) detailing.

A secondary objective of the thesis is to study the suitability of using non-linear single-degree-of-freedom (SDOF) analysis to predict the dynamic response of the blast-detailed and fiber-reinforced HSC beams.

1.3 SCOPE

As part of the experimental research, seventeen beams are tested, including seven beams under four-point quasi-static bending, and ten beams under simulated blast loading. Eight blast-damaged beams are further tested under static loads to assess their post-blast residual strength and ductility. The following parameters are investigated in this study:

- **The effect of reinforcement detailing in HSC beams**: by comparing the response of the test beams with blast detailing to a companion set of beams with nominal detailing tested by Algassem (2016);
- **The effect of steel fibers and ability of fibers to relax detailing in HSC beams**: by testing a companion set of high-strength fiber-reinforced concrete (HSFRC) beams with moderate amount of hybrid fibers and intermediate detailing;
- **The effect of single and repeated loading**: by testing a selected number of specimens under single and repeated blast loads;
- **The effect of longitudinal tension reinforcement ratio**: by testing plain HSC and HSFRC beams constructed with 2-15M (ρ_s = 1.6%), 2-20M (ρ_s = 2.4%), and 2-25M (ρ_s = 4.1%) bars;
- **The effect of longitudinal compression reinforcement ratio:** by testing beams with either 6 mm wire of 10M bars as compression reinforcement;
- **The effect of tie spacing in the HSC beams:** by testing companion beams with d/4 (s=50 mm) and d/2 (s=100mm) tie spacing.

As part of the analytical study, material constitutive models for HSC, HSFRC and steel reinforcement, including the effects of strain-rates are used to conduct sectional and member analysis in order to develop resistance functions for the beams under static and dynamic conditions. The dynamic functions are then used to conduct non-linear single-degree-of-freedom (SDOF) analysis to predict the blast response of the beams.

1.4 THESIS BREAKDOWN

This thesis contains eight chapters, which is divided as follows:

Chapter 1 - Introduction:

- Introduces the significance of this experimental research, describes the objectives and defines the scope of the thesis.

Chapter 2 - Literature review:

- Provides general background information on previous studies, with a focus on previous studies examining the effects of steel detailing, HSC and fibers on the high strength concrete on the static and dynamic response of reinforced concrete beams.

Chapter 3 - Experimental program:

- Describes the experimental program, including specimen designs, material properties, test setups (static, blast and residual) and testing protocols.

Chapter 4 – Experimental static results:

- Presents the individual results for the beams tested under static loads.

Chapter 5 – Experimental dynamic results:

- Presents the individual results for the beams tested under blast loads. The results from the post-blast residual tests are also presented.

Chapter 6 – Discussion of the Static, Dynamic, and Residual results:

- Discusses the effects of the test parameters, including the effects of Blast Detailing, Fibers, tension-steel ratio, compression steel ratio, tie spacing on the static and dynamic responses of the beams;
- Discusses the effects of the parameters on the dynamic resistance curves;
- Discusses the post-blast residual static tests and compares the residual capacity and ductility of the blast-damaged beams to the undamaged companions.

Chapter 7 – Dynamic and static analysis:

- Predicts the static response of the tested beams using sectional analysis;
- Predicts the dynamic response of the tested beams using non-linear single-degree-of-freedom (SDOF) analysis.

Chapter 8 – Conclusion:

- Presents the conclusions from the experimental and analytical research and provides recommendations for further research.

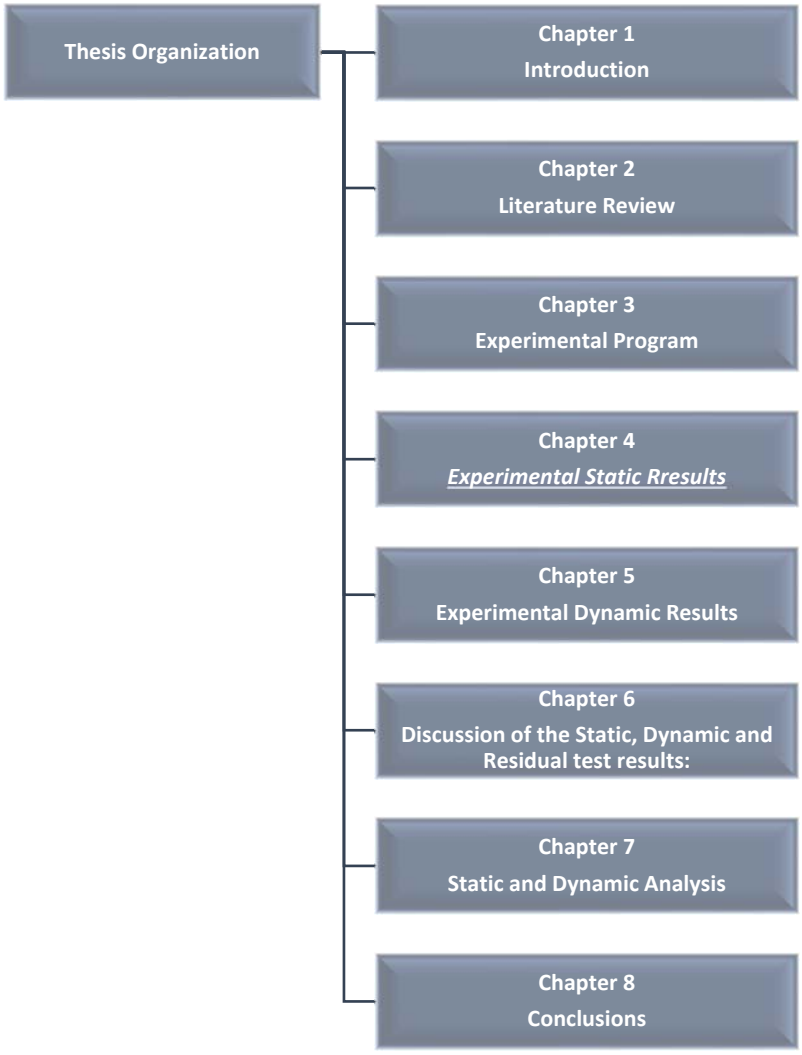

Figure 1-1 Thesis organization

CHAPTER 2: LITERATURE REVIEW

2.1 CHAPTER OVERVIEW

This chapter provides a literature review related to high-strength concrete, steel detailing and fibers on the static and blast behavior of reinforced concrete beams. The first section briefly introduces high-strength concrete and the influence of fibers on key HSC properties. The next section presents a review of previous research on the static behavior of HSC beams, with a focus on the effects of reinforcement detailing and fibers. The third and fourth sections review previous studies that have examined the effects of detailing and fibers on the dynamic (impact and blast) performance of beams. The final section summarizes the detailing requirements for beams in the Canadian CSA S850 Blast Design Standard.

2.2 HIGH-STRENGTH CONCRETE AND BENEFITS OF FIBERS

According to the American Concrete Institute (ACI), high-strength concrete (HSC) can be defined as concrete with a compressive strength which exceeds 55 MPa (ACI MCP, 2015). The Canadian CSA A23.3-14 standard does not explicitly define HSC but imposes certain design restrictions and more stringent requirements when the concrete strength exceeds 60 MPa (CSA, 2014). It is also noted that the current blast design standard (CSA S850-12, section 9.2.2.2) imposes restrictions on the design strength of concrete in blast-resistant structures to 80 MPa.

When compared to normal-strength concrete, HSC presents several enhancements which include increased strength, stiffness, and durability. As a result, HSC has gained increased acceptance as a structural material in building and bridge applications (ACI363R, 2010). On the other hand, it is well known that concrete becomes more brittle as its compressive strength is increased. The addition of steel fibers in high-strength concrete solves this problem by increasing its toughness and ductility in compression, with an added benefit of improved tensile post-cracking resistance.

Mansur et al., (1999) investigated the compressive behavior of HSC having compressive strengths (f'_c) from 70 to 120 MPa, reinforced with steel fibers at the content of 0.5% to 1.5% by volume of concrete (40-120 kg/m^3). Results showed no increase in the peak strength with the addition of fibers. However, the toughness and post-peak response significantly increased, with a change in the failure mode, from brittle to ductile. As shown in **Figure 2-1**, the toughness of HSC concrete increases proportionally with the increase in fiber content. Based on the results, Mansur presented a model that can be used to predict the stress-strain response of fiber-reinforced HSC in compression.

The effects of steel fibers on the tensile response of HSC has been studied by several researchers. Like all other conventional concretes, High Strength Concrete shows brittle response in tension, with failure after first cracking. The addition of fibers allows concrete

to carry tensile stresses after cracking, resulting in an enhancement in tensile post-cracking strength and toughness. The ability of fibers to bridge cracking also improves the tension response of high-strength concrete. Song and Hwang (2004) studies the compressive response, splitting tensile resistance and flexural toughness of HSC reinforced by 0.5%, 1%, 1.5% and 2% steel fibers. Results show that the use of fibers improved the splitting tensile resistance and toughness index of high-strength concrete, especially when using higher fiber contents (see **Figure 2-2)**.

The effects of steel fibers on the dynamic response of high-strength concrete have also been examined by several researchers. Wang et al., (2011) investigated the high strain rate compressive response of high strength fiber reinforced concrete (HSFRC) under high-velocity impact using a Split-Hopkinson pressure bar (SHPB) device. Results showed that the DIF for plain HSC indicated similar values when compared to the calculated CEB–FIP equation. However, this model overestimated the dynamic response of HSFRC, especially above the transition strain rate of 30/s. This study also found that under high-velocity impact loading, fibers were able to better control damage in HSC due to the holding effect of the fibers. It was also found that the presence of fibers increased the strength and energy absorption of HSFRC when compared to HSC, resulting in better impact resistance. Based on this study, the authors proposed a model to predict the high strain rate compressive response of HSFRC (see **Figure 2-3**):

$$DIF = \frac{f_{c,imp}}{f_{cm}} = \begin{cases} \left(\frac{\dot{\varepsilon}_c}{\dot{\varepsilon}_{c0}}\right)^{1.026\alpha} & \text{for } \dot{\varepsilon}_c \le (30 + 23i)s^{-1} \\ \eta\left(\frac{\dot{\varepsilon}_c}{\dot{\varepsilon}_{c0}}\right)^{k} & \text{for } \dot{\varepsilon}_c > (30 + 23i)s^{-1} \end{cases} \qquad 2\text{-}1$$

Where: i: 0 for plain concrete and 1 for FRC

$\dot{\varepsilon}_c$: strain rate (s^{-1}) in the range from 3 X 10^{-6} to 300 s^{-1}

$\dot{\varepsilon}_{co}$: quasi-static strain rate in compression, taken as 3 X 10^{-6} s^{-1}

$\eta = \gamma_s(1 - 0.3392i)$; $k = (1 + 0.05i)/3$; $\log\log\gamma_s = 6.156\alpha - 1$

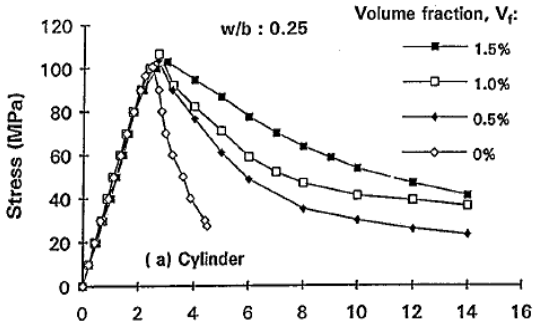

Figure 2-1- Stress-strain response of HSFRC with different fiber contents (Mansur et al., 1999)

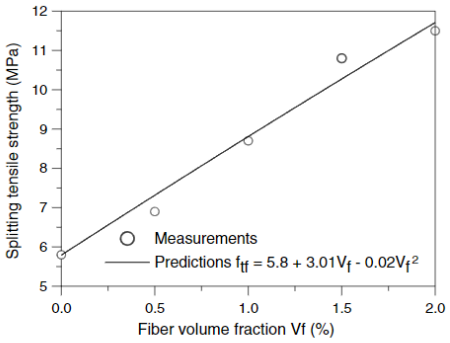

Fig. 2. Effect of fiber volume on splitting tensile strength.

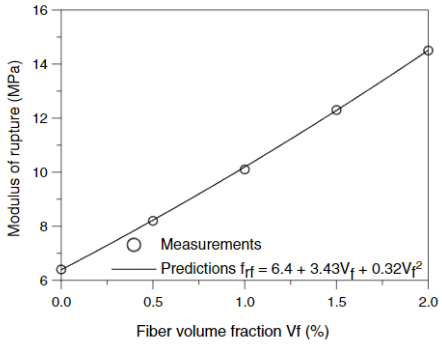

Fig. 3. Effect of fiber volume on modulus of rupture.

Table 3
Toughness index at various fiber volume fractions

Fiber volume fraction (%)	Toughness index		
	I_5	I_{10}	I_{30}
0	1.0	1.0	1.0
0.5	3.0	4.8	8.2
1.0	3.3	6.2	12.4
1.5	4.2	8.3	17.8
2.0	6.5	11.8	20.6

Figure 2-2- Effect of fibers on the splitting strength, modulus of rupture of HSC (Song and Hwang, 2004)

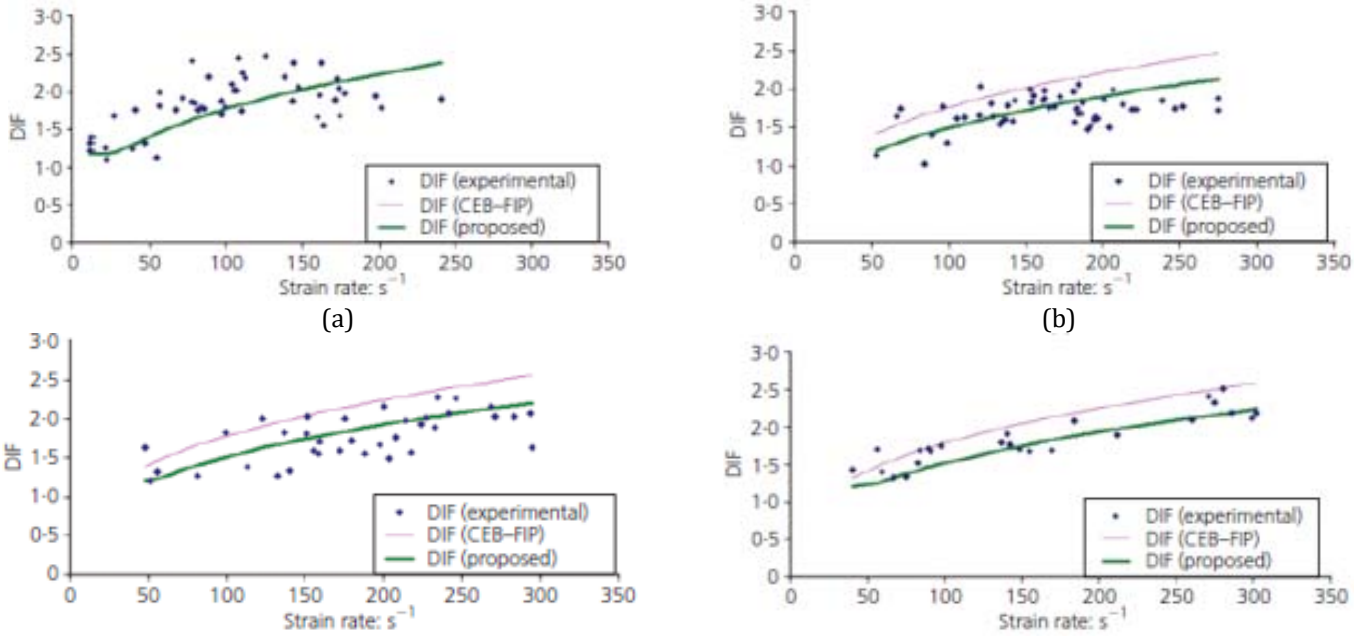

Figure 2-3 - Comparison of CEB–FIP equation with proposed equation at high strain rates from about 10–300 s1: (a) plain HSC; (b) SF-HSC; (c) PE-HSC; (d) HY-HSC (Wang et al., 2011).

2.3 PREVIOUS RESEARCH ON BEHAVIOR OF HSC BEAMS UNDER STATIC LOADING

2.3.1 OVERVIEW OF PREVIOUS TESTS

Over the years several studies have been conducted to examine the effect of concrete strength on the flexural behavior of reinforced concrete beams (Sarkar et al., 1997); (Shin et al., 1999) and (Ashour 2000). These studies have investigated the effects of concrete strength, beam dimensions (a/d ratio, beam depth), longitudinal steel ratio and shear reinforcement on HSC beam behavior. A few previous studies have also examined the effects of reinforcement detailing and fibers on the shear and flexural response of HSC beams as summarized in the following sub-sections and shown in **Table 2.1** and **Table 2.2**.

2.3.2 EFFECT OF REINFORCEMENT DETAILING

Rashid and Mansur (2005) presented one of the more comprehensive studies in the literature on the effects of reinforcement detailing on the flexural response of high-strength concrete beams. The testing program included 16 doubly-reinforced beams with cross-sectional dimensions of 250×400 mm and a total length of 3600 mm. The main parameters investigated were: concrete compressive strengths ($f'_c = 43 - 126\ MPa$), tensile reinforcement ratio ($\rho_t = 1.25 - 5.31\%$), compressive reinforcement ratio ($\rho_c = 0.3 - 0.94\%$), transverse reinforcement ratio ($\rho_r = 0.62 - 1.85$). The author found that increasing the tensile reinforcement ratio resulted in a lower ductility index but increased the moment resistance of the specimens (**Figure 2-4-b**). Results showed that compression reinforcement and lateral ties had a more influential effect on the post-peak behavior of the beams, enhancing ductility and toughness, with no significant effects on maximum load and stiffness. The use of compression bars and closely-spaced ties, confined and increased the toughness of concrete in compression, which improved the post-peak ductility of the beams. However, the use of compression bars with nominal ties spacing (s = 200 mm, s=d/2) resulted in premature buckling of the compression steel, which reduced beam ductility. In contrast, reducing the spacing of the transverse steel (s= 66.7 mm, s=d/5.5) improved the load-bearing capacity, toughness, and ductility of the beams (see **Figure 2-4-e**). Based on this study, the authors recommended the use of d/4 ties when designing doubly-reinforced HSC beams.

Ashour et al. (2000) studied the effects of concrete strength and tensile steel ratio by testing nine 200 mm x 250 mm x 3080 mm doubly-reinforced HSC beams under four-point load as shown in **Figure 2-5**. The beams were designed with different compressive strengths ($f'_c = 48 - 102\ MPa$), tension reinforcement ratio ($\rho_t = 1.18 - 2.37\%$), and compression reinforcement ratio of (ρ_c = 0 -0.15%). Results showed that concrete strength had minimal effects on the load-deflection responses of the beams with low reinforcement ratio. On the other hand, the influence of concrete strength was more pronounced in beams having higher tensile steel ratios, with a 15 % increase in maximum load at $f'_c = 102$ MPa when compared to $f'_c = 48$ MPa when ρ_t = 2.37 %. However, at lower reinforcement ratios (ρ_t = 1.18 & 1.77%), specimens with compressive strengths of (f'_c) $48, 78\ and\ 102\ MPa$ showed similar peak loads. The authors also noted, with the addition of transverse and compression reinforcement, the displacement ductility increased with higher tension reinforcement ratio

up to $\rho_t = 1.77\%$. However, a reduction of 12.5% in ductility was recorded at a reinforcement ratio of $\rho_t = 2.37\%$. Also, slight improvement of the displacement ductility was noticeable with higher strength concrete for doubly reinforced beams.

Sharifi and Maghsoudi (2014) presented another study that investigated the flexural behavior of HSC beams with both tension and compression reinforcement. A total of six (200 mm x 300 mm x 2000 mm) singly-reinforced and doubly-reinforced beams were tested under static loads. The beams had three different tension-steel ratios ($\rho_t = 4.81, 5.38, \text{and } 6.80\%$) and compression steel ratios ($\rho_c = 2.44, 2.69, \text{and } 3.40\%$). The results show that increasing the tensile reinforcement ratio enhanced the maximum resistance of the beams but reduced the ductility. As seen in **Figure 2-5**, the use of compression bars improved the deflection response and ductility of the beams having moderate steel ratios. On the other hand, the doubly reinforced and singly-reinforced specimens showed similar load-displacement curves at the maximum reinforcement ratio ($\rho_t = 6.80\%$ and $\rho_c = 3.40\%$).

Kwan et al. (2006) conducted an analytical study that examined the effects of detailing on the flexural response of beams having cross-sections of 300mm x 600mm. The parametric study examined the effects of concrete strength as well as the tension, compression and confinement reinforcement ratios. As shown in **Figure 2-7**, the analysis showed that higher tension-steel ratio (ρ_t) resulted in lower ductility (μ) in the HSC beams. The authors noted that fixing the tension reinforcement ratio (ρ_t), while increasing both the compression and/or confining reinforcement ratio increased the ductility factor (μ). To maintain a minimum ductility factor of μ=3.32, the authors proposed the following equations for (1) compression reinforcement, (2) confinement reinforcement, and (3) combined compression and confining reinforcements, with all cases having a fixed allowable tension to balanced steel ratio of $\rho_b = 0.75\%$:

$$\mathbf{3350\ \rho_c = f_c - 30} \qquad (2\text{-}2)$$

$$\mathbf{54\ f_r = f_c - 30} \qquad (2\text{-}3)$$

$$\mathbf{3350\ \rho_c + 54\ f_r = f_c - 30} \qquad (2\text{-}4)$$

Where: f_c: Compressive strength, f_r: Confining stress; ρ_c: compression steel ratio.

Table 2.1 - Summary of previous research on the Effect of Reinforcement Detailing in HSC beams

Authors	No. of Beams	Test Method	Type of Concrete	Beam Dimensions			Concrete Comp. strength f'_c (MPa)	Longitudinal Reinforcement		Transverse Reinforcement	
				B × H × L (mm × mm × mm)				Tension ρ_t (%)	Compression ρ_c (%)	Spacing S (mm)	Steel Ratio ρ_r (%)
Rashid et al. (2005)	16	4P bending	NSC HSC	250	400	3600	43-126	1.25-5.31	0.3-0.94	66.7-200	0.62-1.85
Ashour (2000)	9	4P bending	NSC HSC	200	250	3080	48-102	1.18-2.37	-	150	-
Sharifi and Maghsoudi (2014)	6	4P bending	HSC	200	300	2000	67-78	4.81-6.80	2.44-3.40	45-65	-
Kwan et al. (2006)	6	4P bending	NSC HSC	150	150	1000	30-90	0.2-1.2	0-2.5	150-200	-

Note: NSC: Normal Strength Concrete; HSC: High Strength Concrete; 4P: four-point bending test.
W: width of the beam, H: height of the beam, L: length of the beam

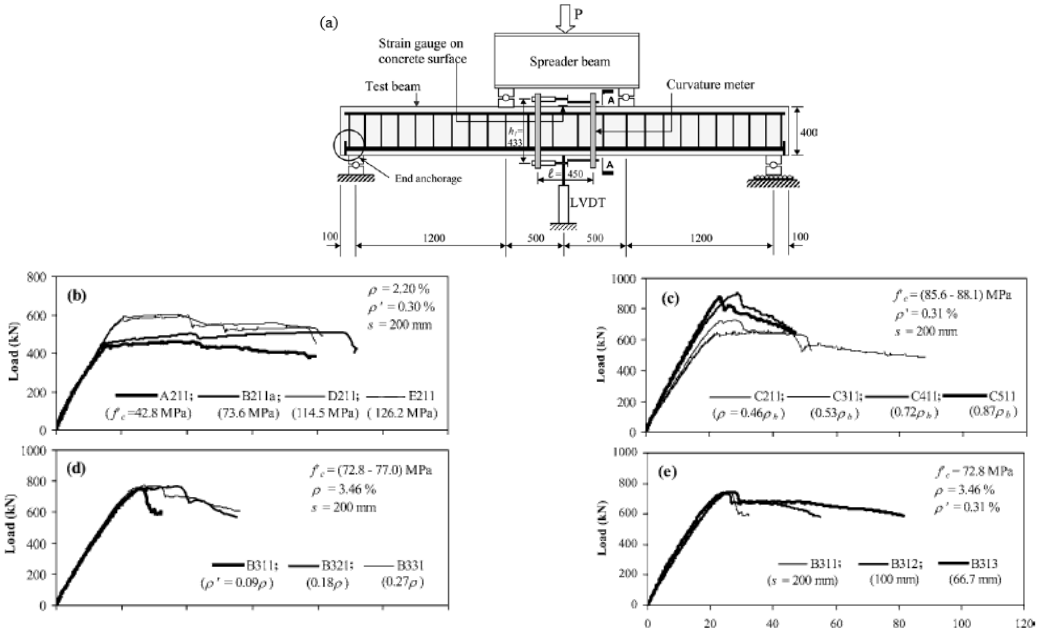

Figure 2-4 – (a) Experimental setup and beam design; Load-deflection response showing effects of: (b) concrete strength; (c) tensile reinforcement; (d) compression reinforcement; and (e) transverse steel. (Rashid et al. 2005)

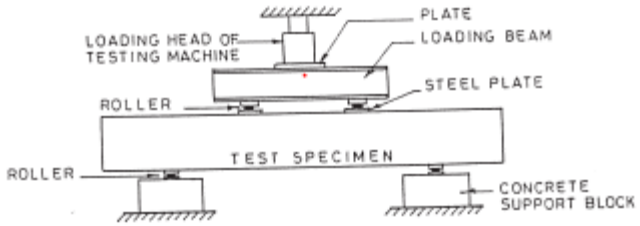

(a) Testing arrangement.

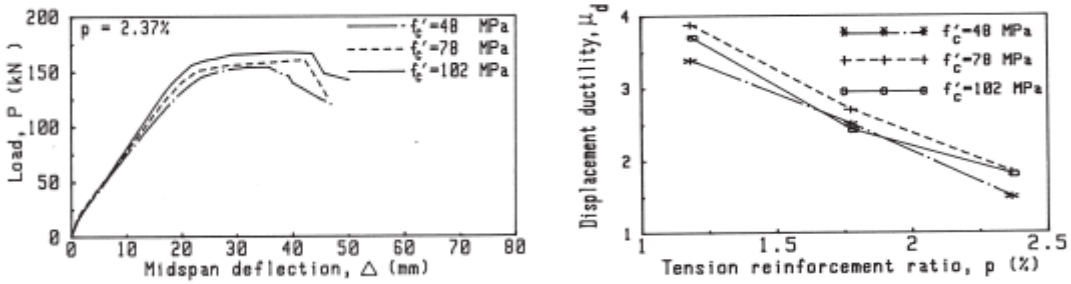

(b) Effect of concrete strength on beam response (c) Effect of tension steel ratio on displacement ductility

Figure 2-5 – Setup and results on HSC beams having varied concrete strength and steel ratios (Ashour, 2000)

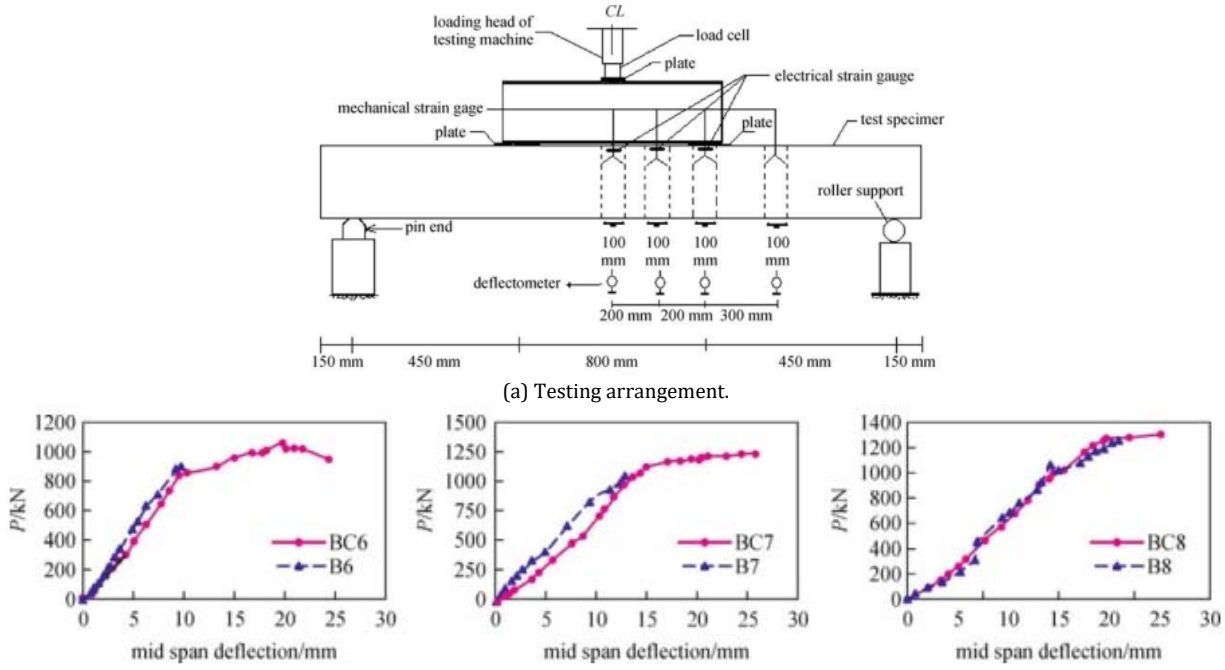

(a) Testing arrangement.

(b) Displacement beam curves at midspan load

Figure 2-6 – Beam Setup and Load-Displacement curves (Sharifi and Maghsoudi, 2014)

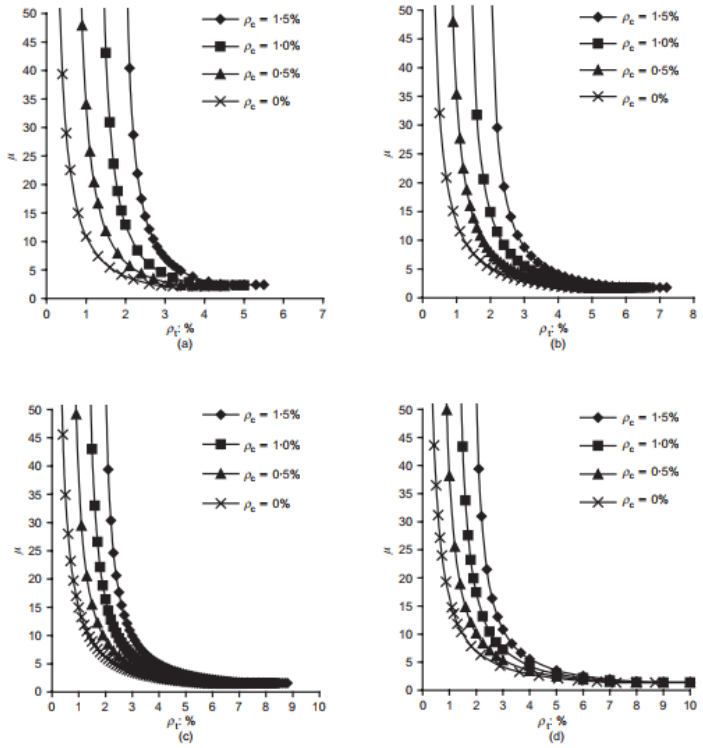

Figure 2-7 – Ductility factors of sections with compression reinforcement (Kwan et al. 2006)

2.3.3 EFFECT OF STEEL FIBERS

As previously noted, high-strength concrete (HSC) has a limited tensile capacity and exhibits a brittle failure under compression. The addition of steel fibers to HSC reduces the brittleness of HSC, increases tensile strength, and improves the post-cracking behavior, energy absorption capacity and ductility of high-strength concrete (Plizzari et al., 2000). A few studies investigated the benefits of implementing steel fibers in high-strength concrete beams tested under static loads as shown in **Table 2.2.**

Biolzi and Cattaneo (2017) examined the shear-flexure response of thirty-six fiber reinforced concrete beams ($f'_c = 40 - 90\ MPa$),) under four-point bending as shown in **Figure 2-8**. The parameters investigated were the influence of fibers and transverse steel on the crack patterns, ultimate shear capacities, and failure modes. The authors reported that the addition of 1% fibers significantly increased the shear and flexure capacity of the HSC beams, and was sufficient to replace transverse reinforcement. In general, results confirmed the benefits of using fibers to improve strength, stiffness, and ductility of specimens with and without stirrups. In addition, the use of fibers resulted in better damage control and reduced crack spacings and crack widths.

Tahenni et al. (2016) examined the shear behavior of twenty-four high strength fiber reinforced concrete beams (100 mm x 150 mm x 1100 mm), built with and without stirrups under quasi-static load. The major factors considered were the volume of the steel fibers (0, 0.5, 1.0, 2.0, and 3.0%), and the aspect ratio of the two fibers used in this study (l_f/d_f = 65 and 80). Results showed that fibers at volumes ≥ 1% provided better shear resistance when compared to stirrups. The use of 2% and 3% fibers controlled diagonal cracking and increased shear resistance, changing the failure mode from shear to flexure. Similarly, it was found that the shear capacity increased by 47% and 88% with fiber contents of 0.5% and 3%, respectively. Moreover, using fibers with higher aspect ratios and using higher fiber volume fractions were found to improve the ductility ratio (see **Figure 2-9**). Also, the authors mentioned that HSFRC is well suited for dynamic loading (e.g. earthquakes) due to its increased and the ability of fibers to prevent brittle and catastrophic failure.

Noghabai et al. (2000) presented another study that investigated the shear and flexure behavior of HSC beams reinforced with different types of fibers as shown in **Table 2.1**. The main parameters investigated were fiber type and fiber volume (0.5%, 0.75%, and 1%) content. Results showed that fibers restrained the propagation of cracks and reduced crack widths, resulting in enhanced stiffness and toughness. Fibers also increased the shear capacity of the beams by 49% to 107% at fiber volume fractions of 0.5% to 1%. It was found that the depth of the beams affected the failure mode and effectiveness of the fibers.

While most previous studies are focused on shear, a few previous studies have examined the effects of steel fibers on the flexural performance of HSC beams. Ashour and Wafa (1993) investigated the flexural behavior of eight HSFRC beams (cross-section of 300 x 170 mm; with fiber contents of 0, 0.5, 1 and 1.5%) under four-point bending. The authors noted that

the addition of fibers improved HSC's response in terms of compressive strength, modulus of rupture, splitting tensile strength, flexural strength, showing increases of 5.1, 50.7, 62.3, and 20% when adding 1% fibers. Similarly, the addition of 1.5 % fibers increased the ductility and the toughness of the beams by 3.38, 3.52, and 5.26, respectively. The authors also found that adding 1.5% of steel fibers to HSC reduced crack widths and improved the energy absorption capacity and ductility of the beams. As shown in **Figure 2-10**, the test results showed that the presence of fibers increased the length of the plastic hinge zone, which was found to be proportional to the fiber content.

Table 2.2 – Summary of previous research on the Effect of Fibers

Authors	No. of Beams	Test Method	Type of Concrete	Beam Dimensions W × H × L (mm × mm × mm)			Concrete Comp. strength f'_c (MPa)	Longitudinal Reinforcement		Transverse Reinforcement		Fibers				
								Tension ρ_t (%)	Compression ρ_c (%)	Spacing S (mm)	Steel Ratio ρ_r (%)	*Type*	*Content (%)*	L_f *(mm)*	d_f *(mm)*	*Aspect Ratio*
Biolzi et al (2017	36	4P bending	NSC HSC	150	300	2400 2900 3400	40-90	1.1	0.4	150	0.3	HE	1.0	30	-	48
Tahenni et al. (2016)	24	4P bending	HSC	100	150	1100	65	1.4	0.9	-	0.4	HE	0.0 0.5 1.0 2.0 3.0	35 60	0.5 0.7	65 80
Noghabai (2000)	32	4P bending	NSC HSC	200	250 300 500 700	1500 3600 6000	46-93	2.9 3.0 3.1 4.3 4.5	-	100 180	-	HE P	0.5 0.75 1	30 60 50	0.6	-
Ashour and Wafa (1993)	18	4P bending	NSC HSC	150	150	1000	93	0.37 2.84 4.58		150-200	-	HE	0 0.5 1	60	0.8	75

Note: W: width of the beam, H: height of the beam, L: length of the beam, L_f: Length of the fiber d_f: diameter of the fibers;
HE: Hooked-End fibers; P: Polyolefin fibers

(a) Testing arrangement

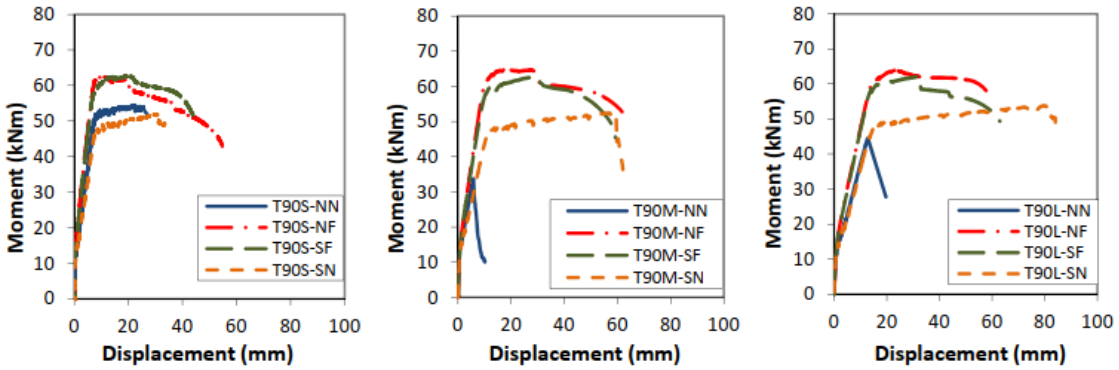

(b) Displacement beam curves at midspan load

Figure 2-8 – Beam Setup and Moment-Displacement curves (Biolzi et al, 2017)

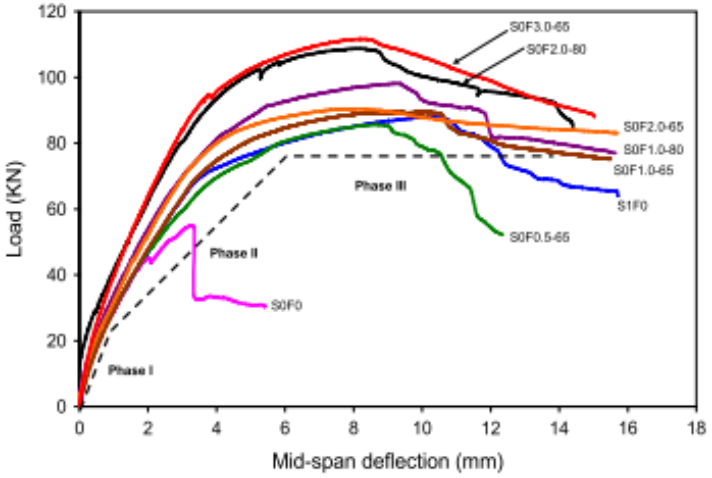

(a) Load-Displacement beam curves

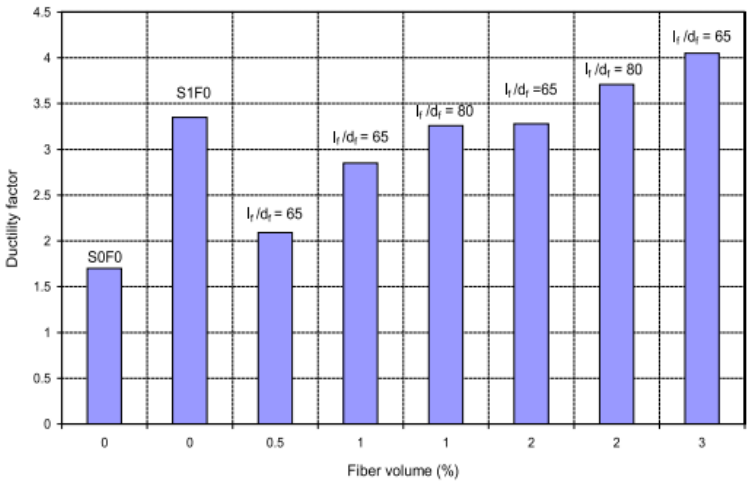

(b) Evolution of the ductility factor with the steel fiber content

Figure 2-9 – Beams test results and ductility as a function of fiber volume and type (Tahenni et al, 2017)

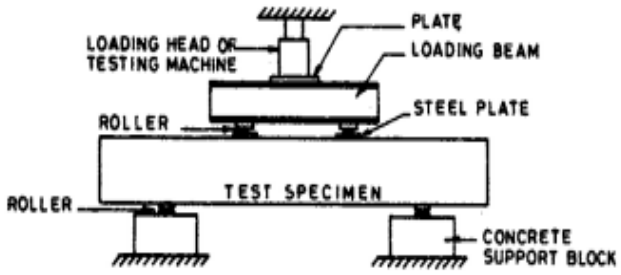

(a) Testing arrangement

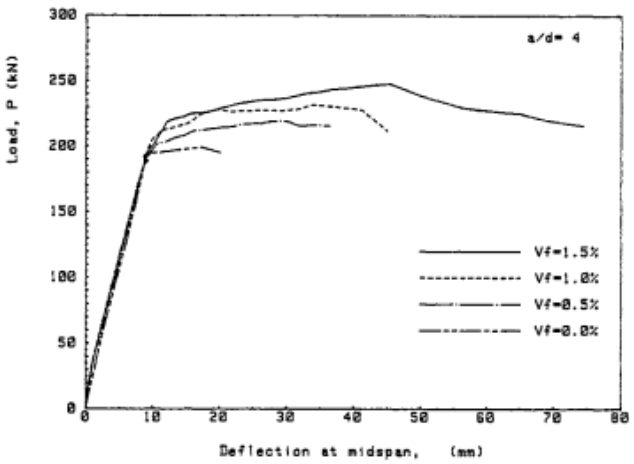

(b) Experimental versus midspan deflection for HSFRC beams with (a) aid= 4,

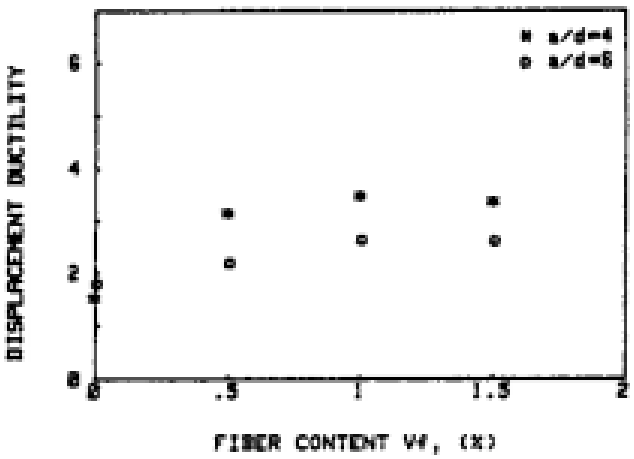

(c) Relationship between displacement, and steel fiber contents

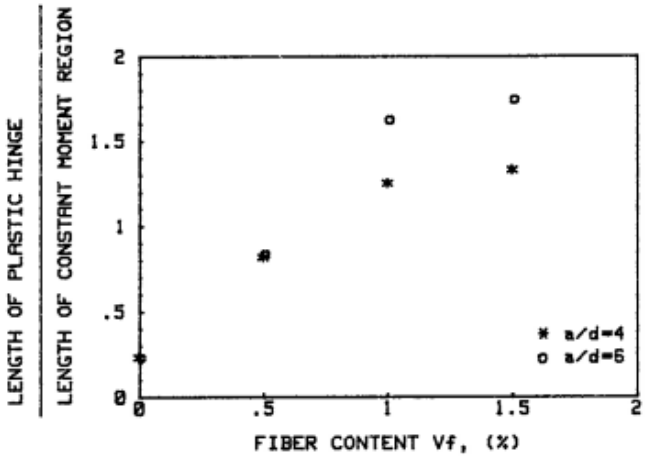

(d) Evolution of the ductility factor with the steel fiber content

Figure 2-10 – Beams setup and results for HSFRC beams tested in flexure (Ashour et al, 1992)

2.4 PREVIOUS IMPACT AND BLAST RESEARCH ON EFFECTS OF STEEL DETAILING

This section summarizes previous studies that have examined the effect on steel detailing on the impact and blast performance of beams, including those studies which examined the effects of transverse reinforcement and compression reinforcement detailing (see **Table 2.3** and **Table 2.4**).

2.4.1 PREVIOUS IMPACT TESTS

Louw et al. (1992) investigated the response of a series cantilever reinforced concrete columns having concrete strengths varying between 17 to 37 MPa under impact loading. A total of 36 columns were cast, with varied longitudinal reinforcement ratios of 1.5 to 3% and stirrups spacings between 100 to 250 mm. The specimens were subjected to impact loading at varying velocities (6.4 to 7.1 m/s) by varying the striker mass from 650 to 1450 kg. It was found that concrete strength and the shear reinforcement ratio had a greater influence on the shear resistance of the specimens. On the other hand, the longitudinal reinforcement ratio had a greater effect on the flexural strength of the beam-columns.

Fujikake et al. (2009) conducted an analytical study investigating the impact responses of reinforced concrete (RC) beams with concrete strength (f'_c) of 42 MPa. In total, twelve beams (102 mm x 178 mm x 2000 mm) were tested having the following longitudinal configurations: Tensile reinforcement ratio of $(\rho_t) = 1.26\,\%$ and Compressive reinforcement ratio of $(\rho_c) = 1.26\,\%$; Tensile reinforcement ratio of $(\rho_t) = 2.46\,\%$ and Compressive reinforcement ratio of $(\rho_c) = 0.4\%$; Tensile reinforcement ratio of $(\rho_t) = 2.46\,\%$ and Compressive Reinforcement ratio of $(\rho_c) = 2.46\,\%$. The main parameters investigated in this study were the effects of longitudinal reinforcement ratios in tension and compression. Results showed that the longitudinal reinforcement ratio influenced the failure mode of the beams. Beams with lower longitudinal steel reinforcement displayed only flexural failures while the use of higher ratios resulted in flexural failure and greater local damage near the impact point. The amount of compression steel influenced the degree of local failure, with reduced damage as the compression ratio increased. The authors also concluded that increasing the compression steel ratio increased the resistance of the RC beams under impact loading.

Saatci and Vecchio (2009) examined the shear behavior of reinforced concrete beams with concrete strength varying from 47 *to* 53 MPa subjected to impact loading. Eight RC beams having a cross-section of 410x250 mm and length of 4880 mm were tested under free-falling drop-weights at the midspan. The beams were double-reinforced with the same reinforcement ratio in tension and compression ($\rho_t = \rho_c = 4.78\%$) but had four transverse reinforcement ratios: $\rho_r = 0, 0.1, 0.2, 0.4\%$. All beams developed shear plugs and severe diagonal shear cracks under the impact point, regardless of their shear capacity. Specimens with higher transverse steel ratios and shear capacities absorbed more energy and sustained

more impacts (see **Figure 2-11**). Beams with lower transverse steel ratios suffered greater damage under the same or lower impact loads.

Tachibana et al. (2010) conducted a series of impact beam experiments on a series of doubly reinforced beams constructed with different reinforcement ratios. Eight beams were built with constant transverse reinforcement (ties spaced at 50 mm), while the longitudinal reinforcement ratio in tension and compression varied between 0.29 and 1.27%. The beams were subjected to impact loading using three masses: 150 kg, 300 kg and 450 kg. Results showed that the resulting impulse from the impact was proportional to the ratio of the momentum of the impacting mass divided by the static ultimate bending capacity $M_{col}/\ P_u$. Also, maximum displacement was found to be inversely proportional to the impact force. Moreover, the maximum displacement was proportional to the impact energy divided by the static ultimate bending capacity $E_{col}/\ P_m$.

Adhikary et al. (2015) studied the impact response of thirty beams using a drop-weight impact loading machine with 300 kg of mass, with six beams tested under quasi-static loading. The main parameters studied were the effect longitudinal steel ratio (tension and compression; $\rho_t = \rho_c = 0.47, 0.64$ and 1.00) and transverse reinforcement ratio ($\rho_r = 0 - 0.56$). The study found that maximum midspan deflection increased with an increase in drop height or impact velocity. The authors note that the presence of inertia forces can cause different failure modes in RC beams under dynamic versus static loading, with a greater tendency for shear failure under impact loads. In this study no shear failure occurred in flexural-dominant beams, however greater localized failure with greater concrete crushing was noted with increasing drop-height. The author also noted that increasing the longitudinal reinforcement increased the impact of load resistance and decreased the maximum midspan deflection. Also, it was found that beams without transverse reinforcement suffered more damages at equivalent impact force and resulted in early failure (see **Figure 2-12**).

Othman and Marzouk (2016) examined the impact response of High Strength Concrete plates with compressive strength (f'_c) ranging from 80 to 160 MPa. The test consisted of dropping a 475 kg steel weight at the mid-point of six reinforced concrete plates having varying steel ratios ($\rho_c = \rho_t = 1, 2,$ and 3%. Specimens with higher longitudinal steel reinforcement ratios resulted in lower displacements and higher impact energy capacity at similar impact loads (See **Figure 2-13**). On the other hand, the failure mode and crack patterns were observed to be more dependent on the reinforcement arrangement (i.e. two layers vs. 1 layer of bars) as opposed to the reinforcement ratio. Results also showed that the displacements were further reduced with improvements in dynamic performance for specimens with fibers. Specimens with a fiber content of 3% resulted in higher dynamic performance when compared to steel fiber contents of 1% and 2%.

2.4.2 PREVIOUS BLAST TESTS

Feldman et al. (1962) conducted an early study that examined the behavior of reinforced concrete beams subjected to impulse loading. In total thirty-three beams with a cross-section of 150 mm x 300 mm), and a length of either 2743 or 3860 mm, were tested with a blast simulator. The compressive strength and the yield strength of steel reinforcement were 45 MPa and 328 MPa respectively. The variables investigated included: tension reinforcement ratio ($\rho_t = 0.16 - 0.72\%$), compression reinforcement ratio ($\rho_c = 0$ – 2.44 %) and transverse reinforcement ratio ($\rho_r = 1.47 - 3.33\%$). Results showed that the yield strength of steel reinforcement showed an increase of 40 to 50% under rapid rates of loading (10^0 in/in/sec) when compared to static loading (10^{-5} in/in/sec). Results also showed that the compression bars increased the flexural response of the beams, resulting in higher ductility (See **Figure 2-14**). The provision of compression bars also allowed the beams to sustain additional bellows, even after crushing had already occurred in the compression zone. Furthermore, reducing the tie spacing provided additional confinement of the concrete, which in turn increased the ductility and prevented buckling of the compression bars. The authors also noted that the ties configuration (welded, hooked at the top or hooked at the bottom) or small differences in tie spacing did not significantly affect the dynamic performance of the beams.

Thiagarajan et al. (2015) presented a study that examined the response of doubly reinforced concrete slabs under blast loads. The slabs were designed with normal strength concrete ($f'_c = 28\ MPa$), high strength concrete ($f'_c = 107 MPa$) and reinforced with either normal strength reinforcement (NR) or high-strength low-alloy vanadium reinforcement (HSLA-V). The dynamic tests were conducted using a blast load simulator (BLS). Substitution with either HSC concrete or HSLA-V bars led to improved blast behavior when compared to slabs built with conventional concrete and steel materials. For example, HSC slabs had reduced peak and residual deflections when compared to normal strength concrete slabs with the same thickness. The spacing of the steel reinforcement was also found to affect the blast performance of the slabs. The use of 100 mm reinforcement layout in the slabs resulted in higher ductility and better control of deflections when compared to the use of 200 mm detailing for both the HSC and NSC slabs (**Figure 2-15**).

Table 2.3- Summary of previous impact and blast research on the Effect of Reinforcement Detailing

Study	Test method	Specimen Test	Number of Specimens	Beam Dimensions			Concrete Strength (MPa)	Longitudinal Reinforcement Ratio (ρ) %		Transverse Reinforcement			Parameters investigated								
				W (mm)	H (mm)	L (mm)		Tension	Compression	Full Span / Shear Span	Spacing (mm)	Ratio (ρ) %	Concrete Strength	Tension reinf. Ratio	Comp. reinf. Ratio	Shear reinf. Ratio	Stirrups in constant moment region	Impact mass weight	Fiber Reinf.	Spacing detailing contribution	Effect of loading rate (dynamic vs. static)
Louw et al. (1992)	D-W	Column	36	150	350	1600	17-37	1.5-3	1.5-3	F-S S-S	100 250 350	-	√	√	√	-	-	√	-	-	-
Kazunori et al. (2009)	D-W	Beam	12	102	178	2000	42	1.26 2.46	0.4 1.26 2.46	F-S	75	-	√	√	√		√	√	-	-	√
Saatci et al. (2009)	D-W	Beam	8	250	410	4880	47-63	4.78	4.78	F-S	0 100 150 300	0 0.1 0.2 0.4	√	√	√	√	√	√		√	√
Tachibana et al. (2010)	D-W	Beam	8	150 300	100 250 400	1000 2000 4000	24	0.49 0.95 1.61 2.43	0.49 0.95 1.61 2.44	-	50	-	√	√	√	-	√	√	-	-	√
Huynh et al. (2015)	D-W	Beam Column	3 13	250	250	2000	80-167	-	-	F-S	-	-	√	√	√	--	-	√	-	-	√
Adhikari et al. (2015)	I-L	Beam	36	150	250	1700	30-50	0.47 0.64 1.00	0.47 0.64 1.01	-	-	-	√	√	√	-	-	-	√	-	√
Othman et al. (2016)	D-W	Slabs	6	1950	1950	100	80-160	0.47 0.64 1.00	0.47 0.64 1.01	-	-	-	√	√	√	-	-	-	√	-	√

Note: D-W : Drop Weight HR : High Rate I-L : Impact loading
W : Width H : Height L: Length
F-S : Full Span S-S : Shear Span

Table 2.4- Summary of previous blast research on the Effect of Reinforcement Detailing

Study	Test method	Specimen Test	Number of Specimens	Beam Dimensions			Concrete Strength (MPa)	Longitudinal Reinforcement Ratio (ρ) %		Transverse Reinforcement			Parameters investigated							
				W (mm)	H (mm)	L (mm)		Tension	Compression	Full Span / Shear Span	Spacing (mm)	Ratio (ρ) %	Concrete Strength	Tension reinf. Ratio	Comp. reinf. Ratio	Shear reinf. Ratio	Stirrups in constant moment region	Fiber Reinf.	Spacing detailing contribution	Effect of loading rate (dynamic vs. static)
Feldman and Siess et al. (1952)	P-L	Beam	31	150	300	2743 3048	41	2.44 3.33 5.55	2.44	F-S	178	0.5	√	√	√	√	√	-	√	-
Thiagarajan et al. (2017)	A-B	Slab	8	860	100 200	1626	40 200	-	-	-	100	-	√	√	√	-	√	√	-	√

Note: A-B : Air Blast P-L : Pneumatic Loading R-L : Rapid Loading

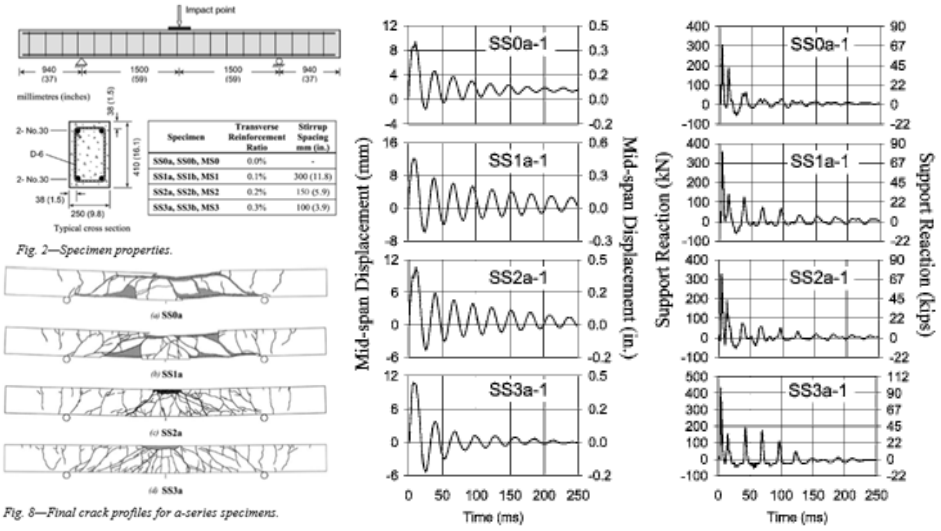

Figure 2-11 - Midspan displacements, support reactions and crack patterns (Saatci, 2009)

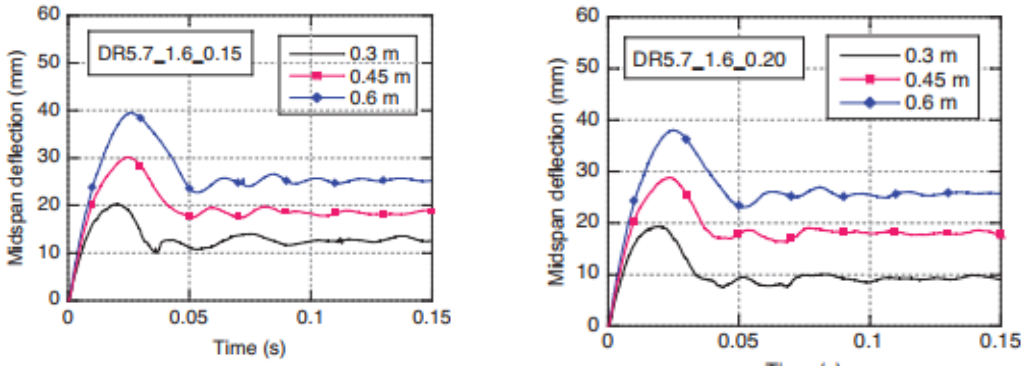

Figure 2-12 - Comparison of the specimens (Adhikary, 2015)

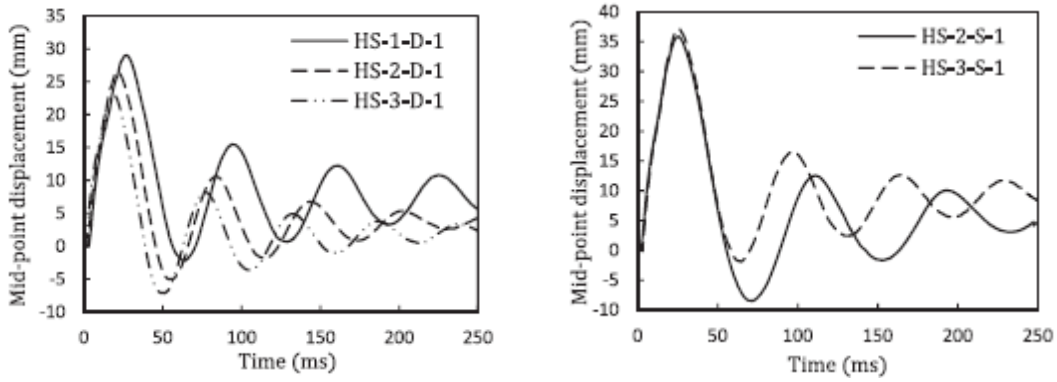

(a) With Top Reinforcement (b) Without Top Reinforcement

Figure 2-13 - Influence of the main reinforcement ratio on mid-point displacement (Othman and Marzouk, 2016).

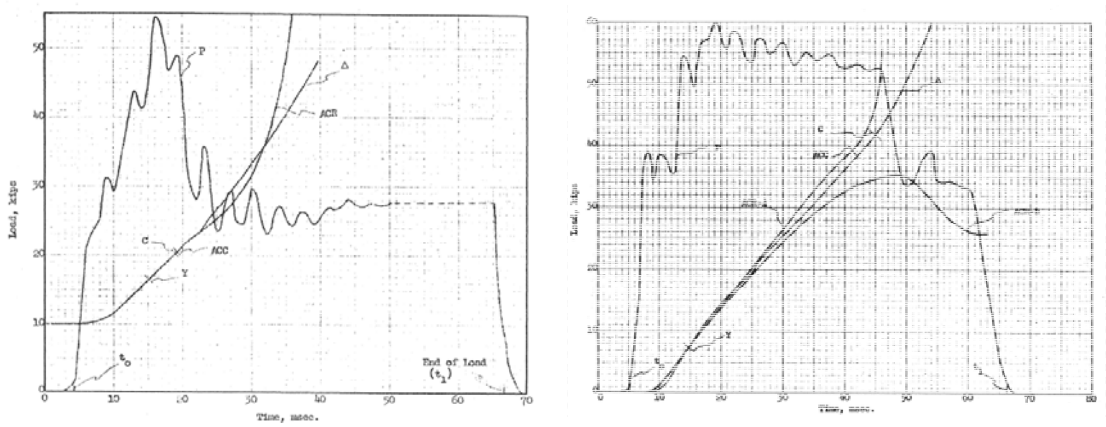

(a) Singly Reinforcement (b) Doubly Reinforcement

Figure 2-14 - Load and Midspan Displacement of a Singly and Doubly reinforced beam (Feldman and Siess 1962)

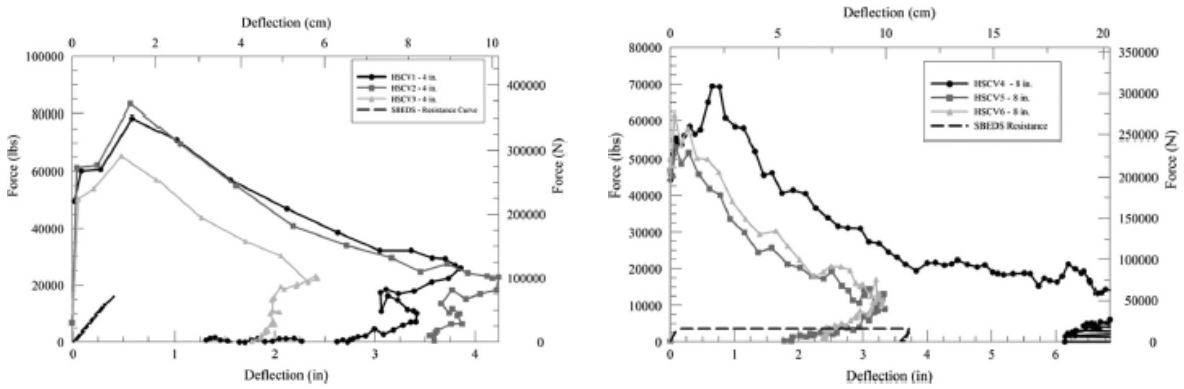

(a) 4 in. (101.6 mm) bar spacing (b) 8 in. (203.2 mm) bar spacing

Figure 2-15 - Dynamic resistance curves for slabs (Thiagarajan, 2017)

2.5 PREVIOUS IMPACT AND BLAST RESEARCH ON EFFECTS OF FIBERS IN BEAMS

This section summarizes previous studies that have examined the effect of steel fibers on the impact and blast performance of beams (see Table 2.5).

2.5.1 PREVIOUS IMPACT TESTS

Banthia et al. (1987) assessed the impact performance of fifty beams, twelve of which were built with steel (1.5%) and polypropylene (0.5%) fibers. The specimens were subjected to impact loading which consisted of dropping a hammer that weighed 345 kg (see **Figure 2-16**). The main parameters investigated were the effect of fibers and transverse reinforcement. Results demonstrated that HSC is a rate-sensitive material as the impact strengths and fracture energies increased at higher stress-rates. As expected, plain HSC showed brittle failure under the impact, while adding longitudinal steel with sufficient stirrups changed the behavior to ductile (see **Figure 2-16**). The addition of fibers changed the brittle response of HSC and improved the ductility and failure mode of the beams. The authors noted that steel fibers increased the dynamic resistance and fracture energies with failure controlled by fiber pullout, while polypropylene fibers were weaker and failed by fracture. Also, transverse reinforcement was found to be very effective in increasing the ductility of the beams.

Min et al. (2014) investigated the effect of steel fibers and shear reinforcement in beams subjected to impact loading. In total seven specimens (160 mm x 290 mm x 2200 mm) were tested, having a concrete strength (f'_c) ranging between 50.4 and 71.9 MPa and fiber contents of 0.75%. Results showed that the use of fibers in beams without shear reinforcements increased the energy absorption capacity and ductility when compared to specimens with shear reinforcement. Also, steel fiber reinforced concrete specimens were found to resist more impact loads with fewer damages. Therefore, the authors concluded that steel fibers can be used to reduce or replace stirrups in beams subjected to impact.

Huynh et al. (2015) presented a study which examined the drop-weight impact response of high-Strength concrete (concrete compressive strength: f'_c=80-115 MPa) and reactive powder concrete columns with 2.5% steel fibers (f'_c= 130 -167 MPa). The study included sixteen specimens, including thirteen beam-columns and three beams. The study found that the axial load and load eccentricity influenced both the impact resistance and the failure mode of the beams. As shown in **Figure 2-17**, the use of steel fibers in RPC considerably improved the impact performance of the beams-columns when compared to HSC specimens. Results also showed that adding fibers to RPC specimens improved shear resistance, changing the failure mode from brittle to ductile in flexure.

Ulzurrun and Zanuy (2017) presented a further study investigating the impact performance of HSFRC beams without shear reinforcement. Seven FRC (125 mm x 250 mm x 2000 mm) beams with concrete strength (f'_c) of 48 – 65 MPa were built with three volumetric fractions (0%, 0.5%, and 1.0%) and different types of fibers (smooth, hooked and prismatic). Specimens without steel fibers exhibited brittle shear failure. The addition of 0.5% smooth steel fibers was able to prevent shear failure, however, shear failures occurred when using hooked and prismatic fibers. Conversely, the use of 1.0% of steel fibers prevented shear failure for all fiber types and resulted in flexural failure. It was found that specimens with prismatic fibers showed the poorest performance against impact. Results also showed that specimens with smooth fibers showed an increase in toughness, crack-bridging capacity and maximum impact loading when compared to hooked and prismatic fibers (as seen in **Figure 2-18**).

Jin et al. (2017) conducted an experimental and numerical study on a series of FRC beams tested under impact loading. Twelve fiber reinforced concrete beams ($f'_c = 42 - 60\ MPa$) were tested, with a cross-section of 400 mm x 200 mm and a length of 2800 mm. The variables included the fiber content (0%, 1%, 2% and 3%) and the transverse reinforcement ratio (0%, 0.25% and 0.5%). Results show that the impact resistance of the beams increased with the addition of fibers and transverse reinforcement. In general, lower maximum and residual displacements were recorded in specimens with higher fiber content (3%) and transverse steel ratio (0.5%). For example, reducing the spacing of the stirrups from 200 mm to 100 mm decreased the maximum deflection by 45% for the specimen with 2% fibers. Similarly use of 3% fibers and transverse ratio of 0.25% showed decreases of 145%, 42% and 29% in displacements when using 0%, 1%, 2% fibers (see Error! Reference source not found.).

Yoo et al. (2007) examined the effect of steel fibers on the impact resistance of a series of four Ultra-High-Performance Concrete (UHPC) beams under drop-weight impact loading. The main parameters were the tension reinforcement ratio ($\rho_t = 0$, 0.53%, 1.06% and 1.71%), fiber content (0% vs. 2%) and fiber type. The authors found that the addition of steel fibers decreased the maximum and residual deflections and improved the residual capacity of the beams after impact. Furthermore, the steel fibers increased the number of cracks, prevented local failure at the surface and redistributed the tensile stresses. It was also found that beams without fibers showed a 39% decrease in the moment capacity. UHPC specimens with twisted steel fibers resulted in less microcracking compared to smooth steel fiber (See **Figure 2-20**).

2.5.2 PREVIOUS BLAST TESTS

The purpose of three-part papers from Magnusson et al. (2010) was to investigate the flexural and shear behavior of reinforced concrete and steel fiber reinforced concrete beams under air blast loading. In total, eighty-nine beams were tested having a concrete compressive strength ranging from 30 to 200 MPa, tensile reinforcement ratio varying between 2.8% and 2.5%, and steel fibers (either 0% or 1.0% percent by volume). Results show that the ductility and the deformation capacity of the beams were independent of the compressive strength of concrete. It was found that the specimens with high reinforcement ratio without steel fibers failed in shear, however, the beams with a low reinforcement ratio failed in flexure. The authors also found that the presence of fibers increased the shear capacity of the beams, preventing shear failure and increased the ductility of the beams.

Algassem (2016) tested twenty beams built with self-consolidating concrete (SCC), HSC and HSFRC under static and blast loads. The parameters investigated were the effect of concrete strength, longitudinal reinforcement ratio (ρ_t, ranging from 1.02 and 2.41 %), presence of stirrups, and effect of fibers (at volumetric ratios of either 0.5% and 1%). Results showed that a higher longitudinal tensile reinforcement ratio enhanced the blast performance of the HSC and HSFRC beams by reducing the maximum and residual mid-span displacements. Transverse reinforcement played a predominant role in preventing shear failure in the plain HSC beams. HSFRC specimens reduced the maximum and residual mid-span displacements while improving overall blast capacity in comparison to HSC beams with no fibers. In addition, 1% of fibers were sufficient to replace transverse reinforcement and prevent shear failure (**Figure 2-21**). Fibers also improved damage control and reduced concrete crushing in the compression zone. HSC beams with higher longitudinal steel ratio had a greater amount of damage and concrete loss in the midspan beam region.

Lee et al. (2018) investigated the structural response of Steel Fiber Reinforced Concrete (SFRC) beams under impact and blast loading. In total, ten SFRC beams were cast. The impact test consisted of dropping a 300 kg hammer at the midspan of the beams. The remaining five SFRC beams were subjected to simulated blast tests using a shock tube. The steel fibers were added at contents of either 0.5% or 1%, with beams built with and without stirrups. Results showed the addition of steel fibers enhanced the load-carrying capacity, impact resistance, energy absorption capacity, while also lowering maximum and residual displacements. Higher amounts of steel fibers provided better structural performance but the use of 1% fibers was unable to prevent brittle shear failure in any of the test types. Conversely, providing the beams with transverse reinforcement prevented shear failure and changed the failure mode to flexure. As shown in **Figure 2-22**, a combination of the steel fibers and stirrups provided an improved response under both impact and blast loads when compared to the use of fibers without stirrups.

Table 2.5- Summary of previous impact and blast research on the Effect of Fibers

Study	Test method	Specimen Test	Number of Specimens	Beam Dimensions			Concrete Strength	Longitudinal Reinforcement Ratio (ρ) %		Transverse Reinforcement			Parameters investigated							
				W (mm)	H (mm)	L (mm)		Tension	Compression	Full Span / Shear Span	Spacing (mm)	Ratio (ρ) %	Concrete Strength	Tension reinf. Ratio	Comp. reinf. Ratio	Shear reinf. Ratio	Stirrups in constant moment region	Fiber Reinf.	Spacing detailing contribution	Effect of loading rate (dynamic vs. static)
Banthia et al. (1987)	D.W	Beam	62	100	125 150	1200 1400 1525	42-82	0.7 1.42	-	F.S	100	0.13 0.19	√	√	√	-	√	√	-	-
Min et al. (2014)	D.W	Beam	7	160	290	2200	50-115	1.0 1.1	1.0 1.1	F-S	100	-	√	√	√	√	√	√	-	-
Huynh et al. (2015)	D-W	Beam Column	13	250	50	2000	80-167	-	-	F-S	-	-	√	√	√	--	-	√	-	-
Ulzurrun et al. (2017)	D.W	Beam	7	125	250	2000	48-65	1.6	01.6	F-S	-	-	√	√	√	√	√	√	-	-
Jin et al. (2017)	D.W	Beam	12	200	400	2800	42-60	2.8	0.5		0 100 200	0 0.25 0.50	√	√	√	√	√	√	-	-
Yoo et al. (2017)	D-W	Beam	10	150	220	2500	150	1.5	0.75	F-S	80	1.41	√	√	√		√		√	√
Magnusson et al. (2014)	A-B	Beam	89	160	300	1720	30 200	1.1 2.5	0.8	F-S	200	-	√	√	√	-	√	√	-	√
Algassem et al. (2016)	Blast	Beam	0	125	250	2440	85	1.02 1.59 2.41	-	S-S	100	0.3	√	√	-	√	-	√	-	-
Lee et al. (2018)	Blast	Beam	15	125	250	2438	43	1.14	0.2	S-S	125	0.42	√	√	√	√	√	√	-	√

Note: A-B : Air Blast, P-L : Pneumatic Loading R-L : Rapid Loading

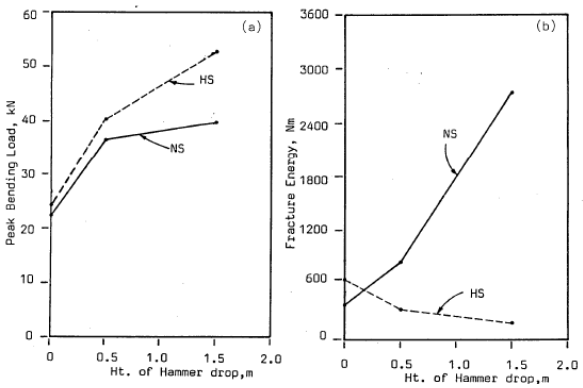

a) High Strength Concrete vs. Plain Concrete

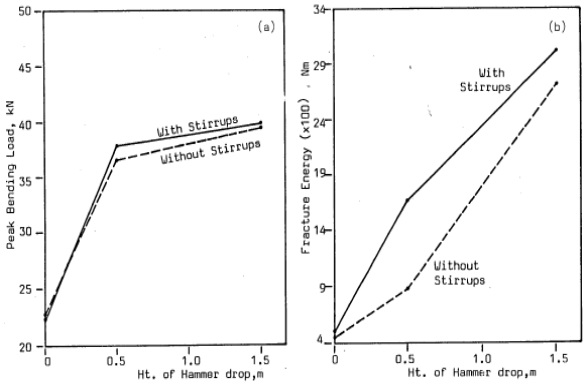

b) Plain Concrete with or without Stirrups

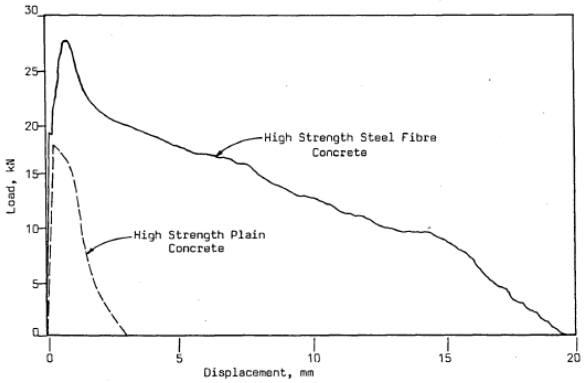

c) High Strength Concrete with or without Fibers

Figure 2-16 - Comparison of the specimens (Banthia, et al.1987)

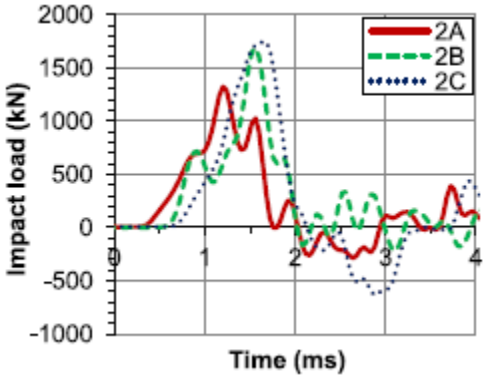

(a) Red: HSC, Green: HSC-core-RPC shell, Black: RPC

Figure 2-17 - Uniaxial stress-strain of HSC, HSC-core-RPC shell and RPC (Huynh, 2015)

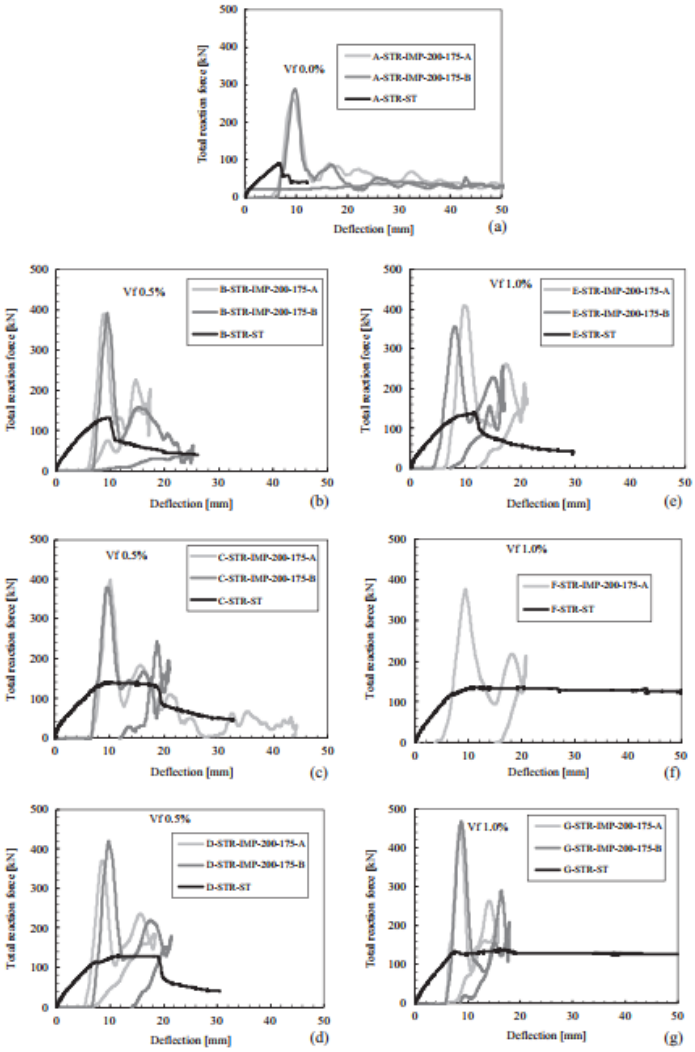

Figure 2-18 - Load–deflection curves of the C2- and the S2-series specimens Ulzurrun et al. (2017)

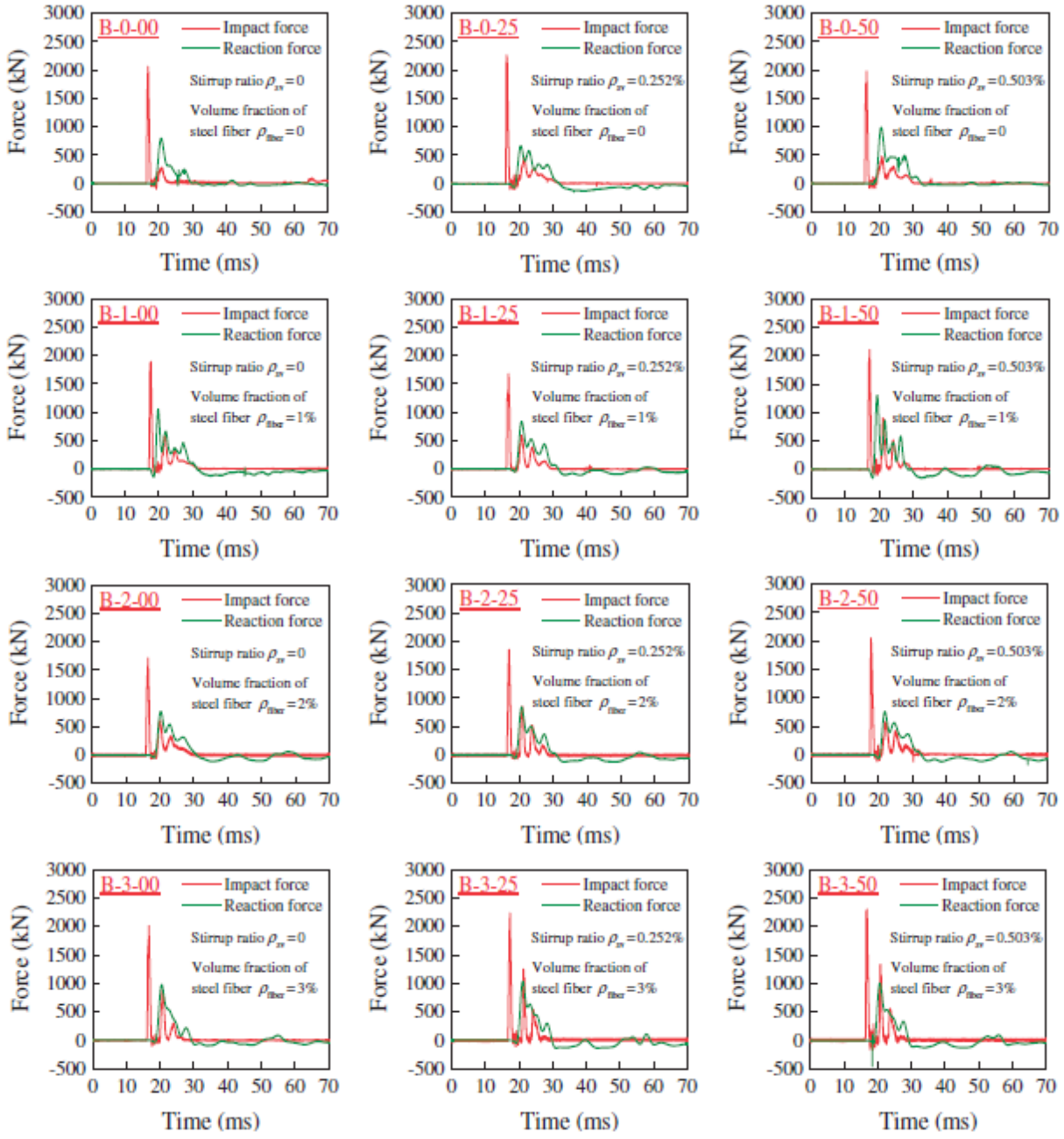

Figure 2-19 - Time histories of the impact forces and reaction forces recorded in the impact tests (Jin et al. 2017)

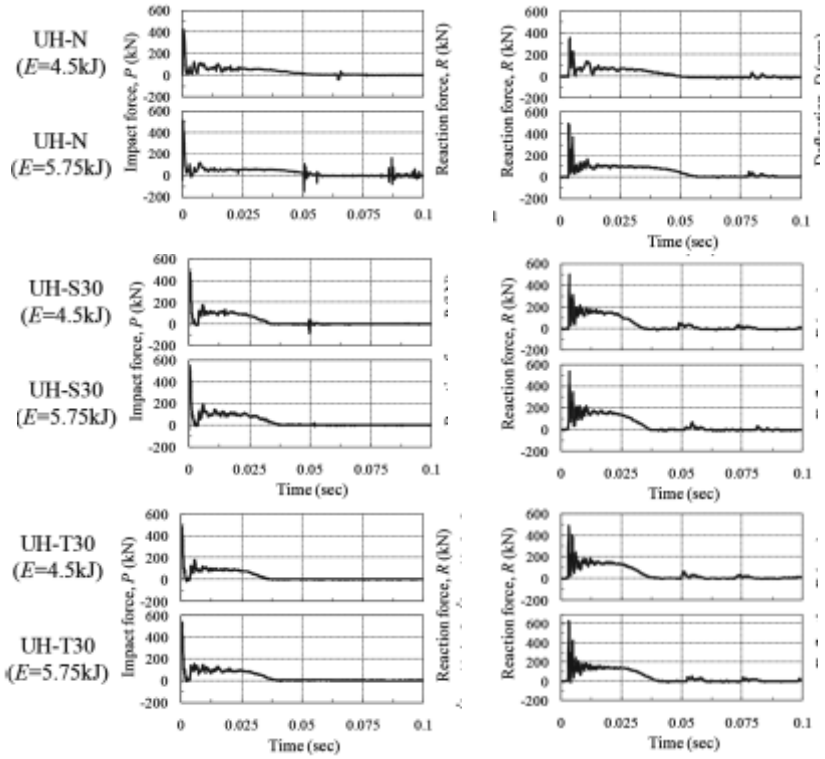

(a) Impact force (b) Reaction force

Figure 2-20 - Impact responses of the UHPC beams (Yoo et al., 2017)

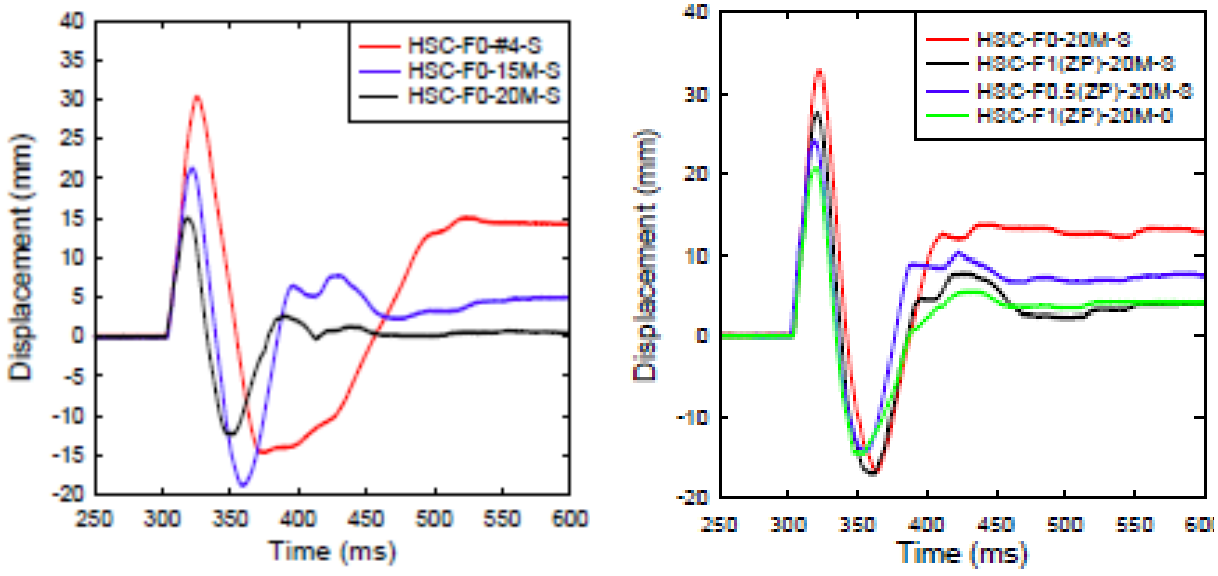

(a) (b)

Figure 2-21- Displacement time histories; effects of the reinforcement ratio (a) without steel fibers, (b) with steel fibers (Algassem, 2016)

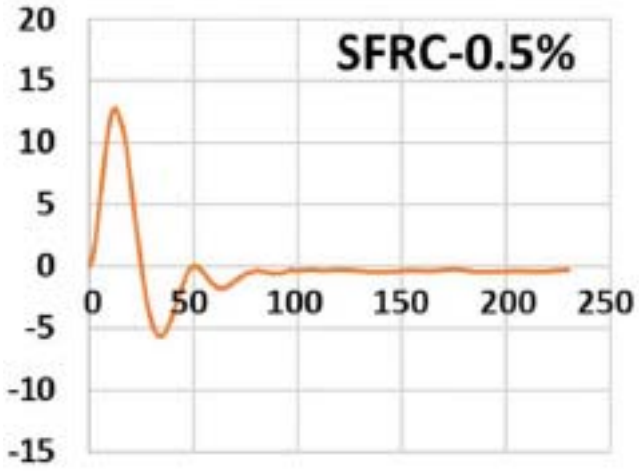

(a) Displacement-time graph with fibers

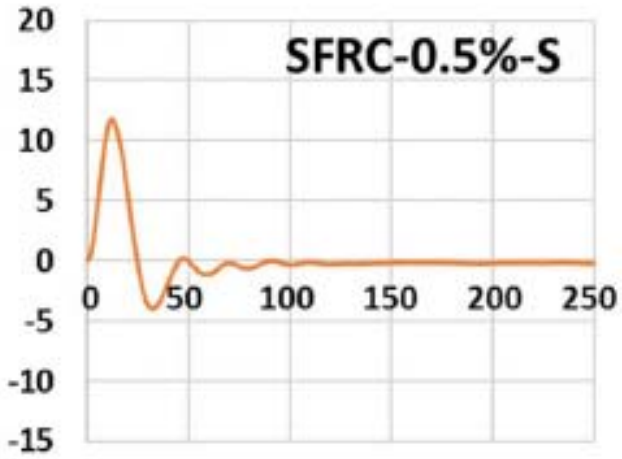

(b) Displacement-time graph with fibers and stirrups

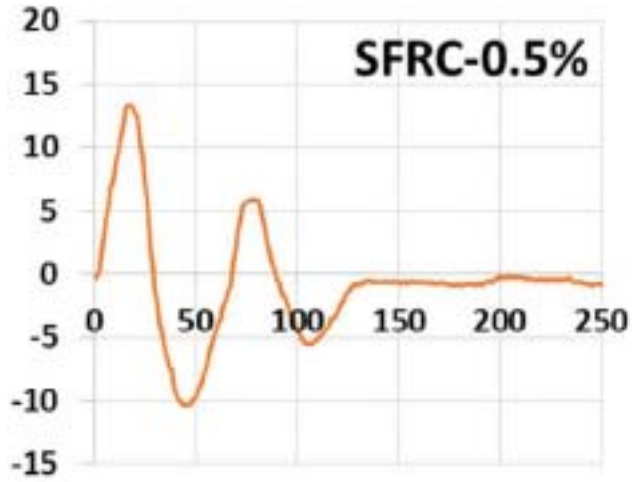

(c) Displacement-time graph with fibers

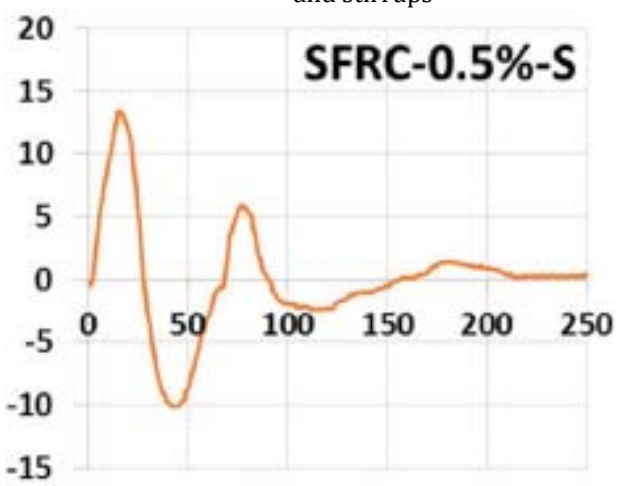

(d) Displacement-time graph with fibers and stirrups

Figure 2-22 - (a, b) Impact test, (c, d) Blast test – (Lee, 2018)

2.6 REVIEW OF CSA S850 DETAILS REQUIREMENTS FOR BEAMS

The Canadian CSA S850 standard (Design and Assessment of Buildings Subjected to Blast Loads) and the Department of Defense's UFC 03-340-02 (Structures to Resist the Effects of Accidental Explosions) are the two main documents used in the protective design of blast-resistant structures. These two documents enforce strict detailing requirements in primary elements in reinforced concrete structures such as beams and columns. According to the CSA S850 standard, the following requirements apply to beams with a factored axial compressive force not exceeding $0.10A_g f'_c$ [clause 9.2.4.1]:

- The provisions only apply to beams with a clear span, not less than four times its effective depth. Deep beams with a clear span-to-effective depth ratio of 4 and less are beyond the scope of the standard [clause 9.2.4.2].
- At any section of a flexural member, the areas of top reinforcement and bottom reinforcement shall each be not less than $1.4\, b_w d/f_y$, and the reinforcement ratio, ρ, shall not exceed 0.025. At least two effectively continuous bars shall be provided at both top and bottom [clause 9.2.4.3].
- The positive moment resistance at the face of a joint shall be not less than one-half of the negative moment resistance provided at that face of the joint. Neither the negative nor the positive moment resistance at any section along the member length shall be less than one-quarter of the maximum moment resistance provided at the face of either end joint [clause 9.2.4.4].
- Transverse reinforcement shall consist of closed hoops with 135° hooks and will be made up of one piece of reinforcement. The transverse reinforcement shall be provided over the clear span of the beam with the first hoop located not more than 50 mm from the face of the supporting member. The maximum spacing of the hoops shall not exceed [clause 9.2.4.5]:
    - $\frac{d}{4}$;
    - eight times the diameter of the smallest longitudinal bars;
    - 24 times the diameter of the hoop bars; or
    - 300 mm.
- The shear resistance of beams shall be equal to the shear force [applied on the member]. The moments corresponding to probable strength shall be calculated using $1.25\, f_{ds}$, where f_{ds} is the specified yield stress of reinforcement at the face of the joint, the SIF, and the DIF in clause 7.3 [clause 9.2.4.6].

- Shear reinforcement for diagonal tension shall be designed to the requirements of CAN/CSA A23.3, with the following exceptions [clause 9.2.4.7]:
    - a) values of β=0.10 and θ=45° shall be used throughout the clear length of the beam; and b) the transverse reinforcement required to resist diagonal tension shall be hoops over the clear length of the member. Open stirrups, either single or double leg, shall not be used.

2.7 SUMMARY AND DISCUSSION OF PREVIOUS WORK AND SYNTHESIS

The following points can be drawn from the literature review:

- Several studies have examined the effect of concrete strength and steel detailing on the flexural behavior of HSC beams tested under quasi-static loads. This research shows that provision of compression bars and closely spaced ties can enhance the ductility of HSC beams, with no significant effects on maximum load and stiffness. The tie spacing has an important effect on the stability of top compression reinforcement where the use of large tie spacing can cause bar buckling.

- Several studies have investigated the effects of fibers on the shear and flexural response of HSC beams. Tahenni et al. (2016) and Biolzi et al. (2017) noted that 1% fibers increased shear resistance and flexure ductility and was sufficient to replace transverse reinforcement in HSC beams. Ashour & Wafa (1993) also observed that the addition of fibers controlled the propagation of cracks, enhanced stiffness and improved toughness/ductility in flexural-dominant beams.

- The behavior of reinforced concrete beams under impact has been investigated by many researchers. Among previous studies, a few have focused on the effect of detailing and fibers. Louw et al. (1992), and Fujikake et al. (2009) observed that the longitudinal reinforcement ratio influenced the failure mode of beams tested under impact loading. Improved detailing and use of top compression bars reduced damages in the compression zone. Similarly, Saatci and Vecchio (2009) observed that higher transverse steel ratios increased impact resistance and damage tolerance of beams tested under impact. Banthia et al. (1987) and others concluded that the addition of fibers can increase the ductility and energy absorption capacity of reinforced concrete beams subjected to dynamic impact loading.

- Very limited studies have focused on the blast performance of beams, especially in the case of beams built with high-strength concrete. Algassem (2016) conducted one of the few studies in this area and examined the effect of longitudinal steel ratio and fibers on the blast performance of singly-reinforced HSC beams. The study found that HSC beams can suffer brittle concrete compression failures under blast loading. The use of 1% steel fibers reduced such damage and was able to replace stirrups in the beam shear spans. No research has examined the blast performance of doubly-reinforced HSC beams. Moreover, no studies have examined the effect of steel detailing (tie spacing, compression steel ratio, etc.) on the blast performance of such beams. There is a need for research on the ability of modern blast detailing (i.e. as required in the CSA-S850 standard) to improve the blast performance of HSC beams. Research is also needed to study the ability of steel fibers to relax such detailing.

CHAPTER 3: EXPERIMENTAL PROGRAM

3.1 CHAPTER OVERVIEW

This experimental research program consists of constructing and testing sixteen beams specimens built with high-strength concrete, fibers and varying types of detailing. Six of the specimens were tested under quasi-static four-point bending, and the remaining ten under simulated blast loading. The parameters investigated include the effects of reinforcement detailing, concrete type (plain HSC vs. HSFRC), longitudinal steel ratio and tie spacing. This chapter describes the test specimens, material parameters, test setups, and testing procedures.

3.2 DESCRIPTION OF TEST SPECIMENS

A total of seventeen reinforced concrete beams was designed, built and tested in this research program. Six of the beams were tested under quasi-static four-point bending and ten specimens were tested under simulated blast loading using the University of Ottawa Shock-tube. The test matrix includes eleven high strength concrete (HSC) beams and five high strength fiber reinforced concrete (HSFRC) beams built with hybrid steel fibers added at a ratio of 0.75% by volume of concrete (60 kg/m^3). The design details of the specimens are summarized in **Figure 3-1**. All beams had a length of 2440 mm, with cross-sectional dimensions of 125 mm x 250 mm. In all cases, the beams were tested over a simply supported span of 2232 mm, with a constant moment region of 750 mm and two equal shear spans of 741 mm. The majority of the beams were double-reinforced, with two tension and two compression bars as continuity reinforcement. Tension reinforcement consisted of either 2-15M, 2-20M or 2-25M bars (longitudinal steel ratios, ρ = 1.6%, 2.42% and 4.1%), while the compression reinforcement consisted of either 2-10M bars (most beams) or 2-6 mm bars made from non-deformed steel wire (compression steel ratios, ρ' = 0.78% or 0.25%). It is noted that the tension steel ratios fall within the limits in the CSA S850 Standard of $\rho \leq 2.5\%$, but resulted in "under-reinforced" and "over-reinforced" conditions for the beams with 15M/20M and 25M bars, respectively, with provided-to-balanced steel ratios of ρ/ρ_b = 0.28, 0.42 and 0.72, when not accounting for the compression bars. Transverse reinforcement in most beams consisted of closed hoops made from 6 mm wire, spaced at s = 50 mm (d/4) or 100 mm (d/2) throughout the span for the beams with "blast" and "intermediate" detailing, respectively. Two beams in the 25M set and the control beams tested by Algassem (2016) were singly reinforced and provided with open stirrups made from 6mm wire, spaced at s = 100mm in the shear spans only. All specimens had the same 35 mm of bottom clear cover.

Table 3-1 provides the design properties of the beams including Specimen ID, concrete type, fiber content, V_f (in %), tension and compression steel size and tie spacing. The nomenclature follows the following logic:

CONCRETE TYPE - FIBER (%) – TOP REBAR SIZE - BOTTOM REBAR SIZE - STIRRUP

For example, HSC-F0-15M-10M-d/4 is the ID for a beam constructed with plain HSC, 15M tension bars, 10M compression bars and closed hoops spaced at d/4 throughout the beam span. Similarly, HSC-F0.75%-15M-10M-d/2 is the companion beam with fiber-reinforced HSC and intermediate ties at d/2, while HSC-F0-25M is the plain HSC beam built with 25M bars and nominal detailing (singly reinforced and stirrups in shear span only).

Table 3-1 - Specimen Series and Specifications

Series		Specimen ID	Concrete Type	Fiber content Vf (%)	Tension Longitudinal Reinforcement Properties		Compression Longitudinal Reinforcement Properties		Transverse Reinforcement Properties	Test type [2]
					Type	ratio ρ (%)	Type	ratio ρ' (%)	Tie Spacing (mm)	
HSC	15M	HSC-F0-15M-10M-d/4	HSC	0	2-15M	1.6	2-10M	0.78	50	S
		HSC-F0-15M-10M-d/4	HSC		2-15M	1.6	2-10M	0.78	50	D
		HSC-F0-15M-10M-d/4[x1]	HSC		2-15M	1.6	2-10M	0.78	50	D
	20M	HSC-F0-20M-10M-d/4	HSC		2-20M	2.42	2-10M	0.78	50	S
		HSC-F0-20M-10M-d/4	HSC		2-20M	2.42	2-10M	0.78	50	D
		HSC-F0-20M-10M-d/2	HSC		2-20M	2.42	2-10M	0.78	100	D
		HSC-F0-20M-6M-d/2	HSC		2-20M	2.42	2-6M	0.25	100 [1]	D
	25M	HSC-F0-25M	HSC		2-25M	4.1	0	-	100 [1]	S
		HSC-F0-25M	HSC		2-25M	4.1		-	100	D
		HSC-F0-25M-10M-d/4	HSC		2-25M	4.1	2-10M	0.78	50	S
		HSC-F0-25M-10M-d/4	HSC		2-25M	4.1	2-10M	0.78	50	D
HSFRC	15M	HSC-F0.75-15M-10M-d/2	HSFRC	0.75	2-15M	1.6	2-10M	0.78	100	S
		HSC-F0.75-15M-10M-d/2	HSFRC		2-15M	1.6	2-10M	0.78	100	D
	20M 20M	HSC-F0.75-20M-10M-d/2	HSFRC		2-20M	1.6	2-10M	0.78	100	S
		HSC-F0.75-20M-10M-d/2	HSFRC		2-20M	1.6	2-10M	0.78	100	D
	25M	HSC-F0.75-25M-10M-d/2	HSFRC		2-25M	4.1	2-10M	0.78	100	S
		HSC-F0.75-25M-10M-d/2	HSFRC		2-25M	4.1	2-10M	0.78	100	D

[1] These beams were designed with nominal detailing (open stirrups in shear spans only)
[2] S = beam tested under static load, D = beam tested under dynamic load, D[x1] = replicate beam tested under single blast

Steel cages details **Cross-section**

(a) 15M Series

HSC-F0.75-15M-10M-d/2

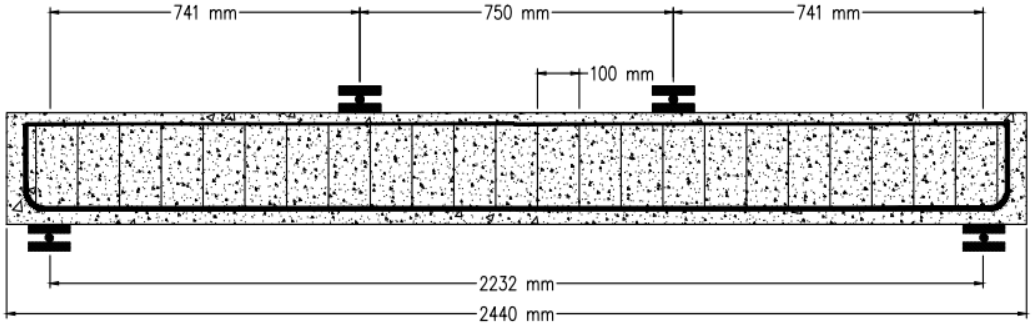

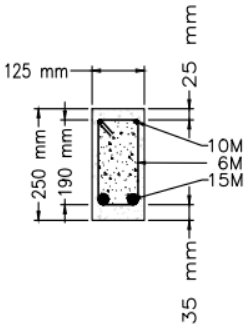

HSC-F0-15M-10M-d/4

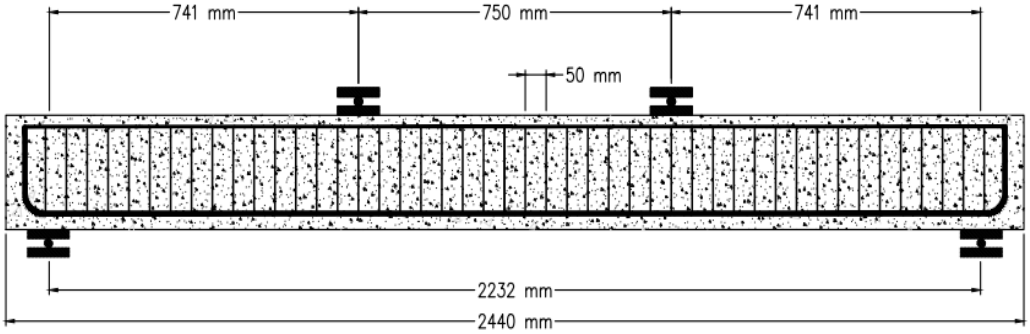

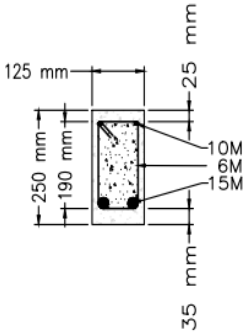

(b) 20M Series

HSC-F0-20M-6M-d/2
HSC-F0-20M-10M-d/2
HSC-F0.75-20M-10M-d/2

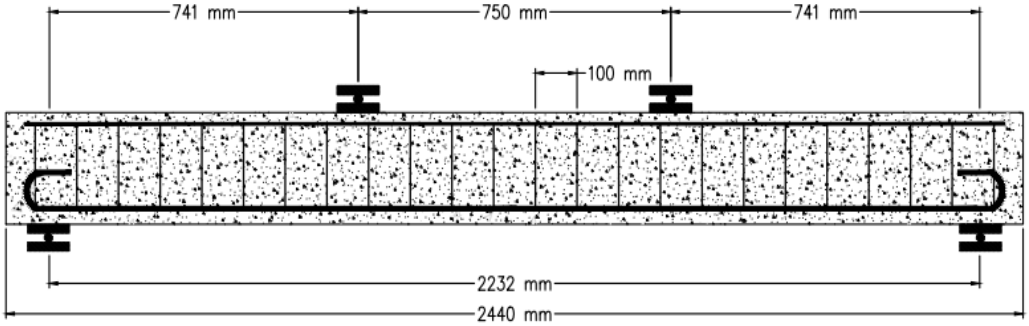

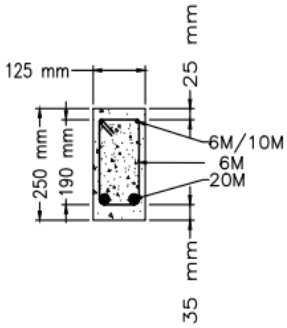

HSC-F0-20M-10M-d/4

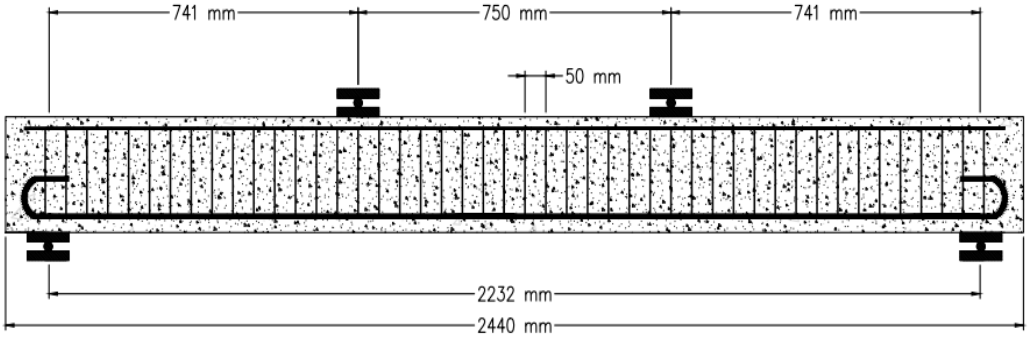

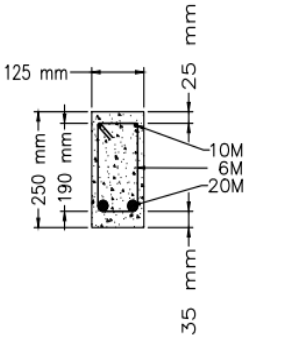

(c) 25M Series

Steel cages details **Cross-section**

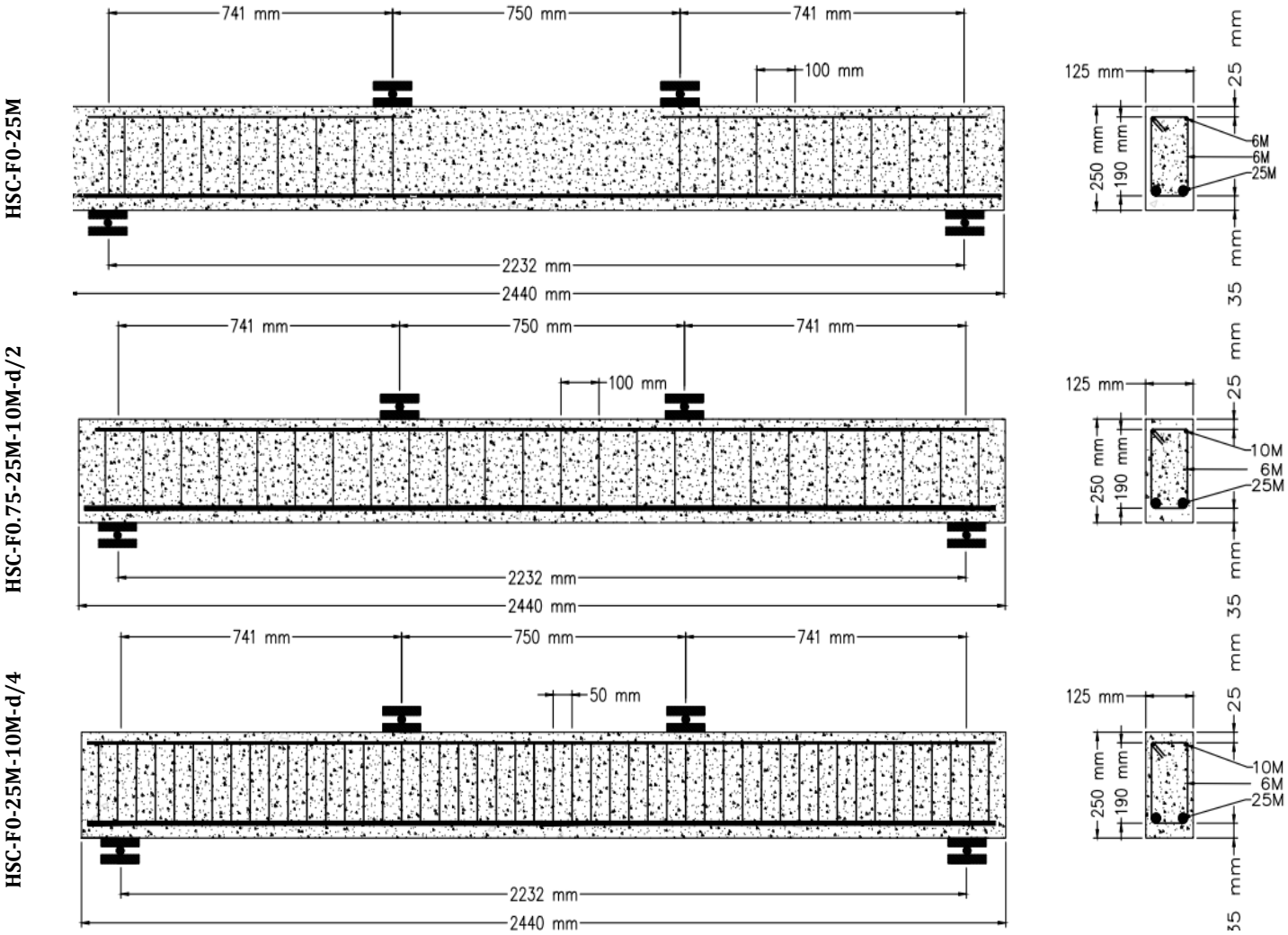

Figure 3-1 - Specimen dimensions and reinforcement details

3.2.1 CONCRETE PARAMETERS

The plain high strength concrete (HSC) and fiber-reinforced HSC (HSFRC) were mixed at the Structures Laboratory of the University of Ottawa. All seventeen beams used the same base HSC mix which had a target strength of 100 MPa. As seen in **Table 3-2**, the mix contained Portland cement (Trillium Cement / Element GU TYPE 1), silica fume, slag, fine aggregates (sand), and two sizes of coarse aggregate (9.5 mm and 19 mm). Liquid admixtures in the mix consisted of MasterGlenium 7500 super-plasticizer and MasterSet R 100 retarder. The water-to-cement (w/c) ratio was 0.27, and the steel f fibers added to the FRC specimen consisted of a hybrid mix of 0.25% of micro-fibers and 0.5% of hooked-end steel fibers. **Figure 3-2** shows typical materials used in the mixtures.

Table 3-2 - Properties of High strength concrete

Mix Design Component		Content Density	Quantity for two beams
Portland Cement (GU)		440.3 kg/m3	67.14 kg
Slag		193.6 kg/m3	29.52 kg
Silica Fume		56.7 kg/m3	8.64 kg
Fine Aggregate	Sand	872.1 kg/m3	133 kg
Coarse Aggregate	9.5 mm	661 kg/m3	100.8 kg
	19 mm	662 kg/m3	100.8 kg
Water		185.6 kg/m3	28.3 kg
Super Plasticizer		13.1 L/m3	2 L or 2.2 L
Retarder		3.3 L/m3	0.5 L
Steel Fibers	0.25% BELM	19.5 kg/m3 of concrete	2.86 L
	0.5%ZP305	39 kg/m3 of concrete	5.71 L

Cement


Slag


Silica fume


Super-plasticizer


Coarse Aggregate (19 mm)


(9.5 mm)


Sand


Retarder


Steel Fiber (ZP)


Steel Fiber (OL)

Figure 3-2 - Materials used in the base HSC mix

3.2.2 STEEL REINFORCEMENT PARAMETERS

Five different steel reinforcement types were used in the construction of the specimens. The first type consisted of non-deformed "6M" non-deformed steel wire, having a diameter, d_b = 6.3 mm and cross-sectional area of A_b = 32 mm^2. This steel was used for the closed-hoops or stirrups, as compression steel in one beam. The remaining steel consisted of either 10M, 15M, 20M or 25M used for the tension and compression steel (d_b = 11.3, 16.0, 19.5 and 25.2 mm; A_b = 100, 200, 300 and 500 mm^2).

Three coupons for each type of steel reinforcement were tested in direct tension using a 600 kN Galdabini Sun 60 Universal Testing Machine as shown in **Figure 3-3**. The steel specimens were subjected to an axial tension rate of 5 mm/min, whereas the displacements were measured with an axial extensometer - model 3542 Epsilon Technology Corporation – having a gauge length of 50 mm. **Table 3-3** provides the properties of each type in terms of yield strain ($\boldsymbol{\varepsilon_y}$) and Strength ($\boldsymbol{f_y}$), ultimate strain ($\boldsymbol{\varepsilon}_u$) and strength ($\boldsymbol{f_u}$) and strain at rupture ($\boldsymbol{\varepsilon}_r$). Typical stress-strain relationships for each rebar are shown in **Figure 3-4**. It is noted that the 25M could not be tested due to equipment limitations, therefore data for this bar type is not reported.

Figure 3-3 - Galdabini Steel Coupon Testing Setup

Table 3-3 - Steel reinforcement mechanical properties

ID	Steel Reinforcement	Bar Diameter d_b (mm)	Bar Area A_b (mm^2)	Yield		Ultimate		Rupture
				Strain ε_y	Strength f_y (MPa)	Strain ε_u	Strength f_u MPa)	ε_r
6M	Non-deformed	6.35	32	0.003	561	0.056	615	0.070
10M	Regular	11.3	100	0.0020	475	0.150	590	0.204
15M	Regular	16.0	200	0.0023	436	0.144	584	0.228
20M	Regular	19.5	300	0.0021	430	0.160	565	0.233

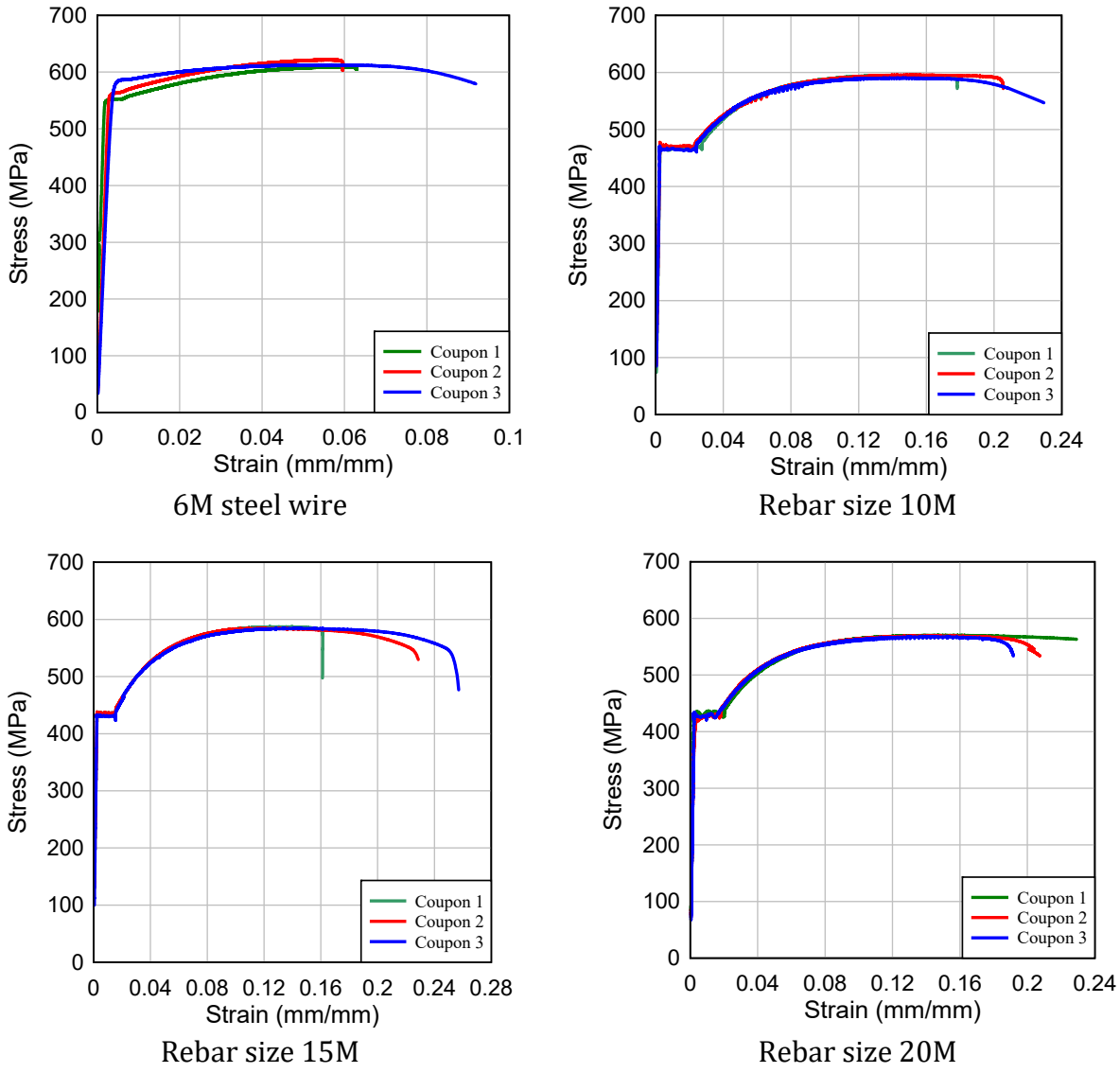

Figure 3-4 - Steel reinforcement stress-strain relationships for 6M, 10M, 15M & 20M bar types

3.2.3 STEEL FIBER PARAMETERS

Two types of fibers were used in the high-strength fiber-reinforced concrete beams. To allow for a workable mix with moderate fiber content (0.75% = 60 kg/m^3), a hybrid mix of steel fibers, consisting of 0.25% micro-fibers (OL) and 0.5% of macro hooked-end fibers. **Table 3-4** presents the properties of the two fibers in term of: Length L_f (mm), Diameter d_f (mm), Aspect Ratio (mm/mm) and Tensile Strength (MPa). The ZP fibers had hooked-ends with 30 mm length and tensile strength of 1350 MPa, whereas the smooth OL fibers had a length of 13 mm and tensile strength of 2750 MPa. Photos of both fibers are shown in **Figure 3-5**.

Table 3-4 Steel fiber properties

Fiber ID	Fiber Name	Length L_f (mm)	Diameter d_f (mm)	Aspect Ratio (mm/mm)	Tensile Strength (MPa)
ZP	ZP 305	30	0.55	55	1350
OL	OL	13	0.20	65	2750

(a) ZP 305 fiber

(b) OL fiber

(c) side by side comparison of ZP and OL

Figure 3-5 - (a) ZP Fiber (b) OL Fiber (c) side by side comparison of ZP and OL

3.3 CONSTRUCTION OF TEST SPECIMENS

The sixteen beams were built in the structural laboratory at the University of Ottawa. The construction process was as follows: constructing the formwork and steel cages, installing the strain gauges, casting of the beams and curing of the specimens.

3.3.1 PREPARATION

The first construction phase consisted of building a wood formwork to cast the beams. A 4'× 8' sheet of plywood with 1/2" thickness was placed at the base, which was divided equally into 7 sections by 3/4" thick plywood. Then, 2" × 4" studs were placed to provide lateral support on the sides when casting the specimens (see **Figure 3-7(a)**)

Typical steel cages after construction are shown in **Figure 3-6**. To allow for proper anchorage and development the 15M bars had 90° hooks, while the 20M bars had 180° hooks. The 25M bars were kept straight due to the limitations of the bending equipment in the lab. To monitor strains in the steel bars, strain gauges were installed at the midpoint of the longitudinal steel bars as seen in **Figure 3-7(b)**. The strain gauges for static and dynamic specimens were of the120 Ω and 350 Ω type respectively. Two gauges were placed on the longitudinal bars, with one gauge placed on one of the compression bars in each beam. Prior to casting form oil was applied with a roller and brush on the inside face of the formwork. Lastly, the cages were inserted into the form and were placed on top of a 35 mm chair to allow for proper coverage on the underside of the beams.

In all cases, HSC and HSFRC concrete were mixed using a large electric pan mixer with a capacity of 225 L at the University of Ottawa Structures Laboratory (**Figure 3-7(c)**. The

mixing procedure consisted of measuring all mix materials, dry mixing the cement/sand/aggregates, gradually adding water, and finally the steel fibers. The entire mix took approximately five-ten minutes, after which the concrete was directly poured into the form while being vibrated with a poker vibrator to ensure proper consolidation of concrete. In total, two beams, two flexural prisms, and six cylinders were cast per batch. Thereafter, the specimens were covered with moist burlap and plastic was placed on top of the burlap to prevent the specimens from drying out. All the specimens were cured for seven days, then removed from the form where they were air-cured until testing.

Steel cages

(a) 15M-10M-d/2

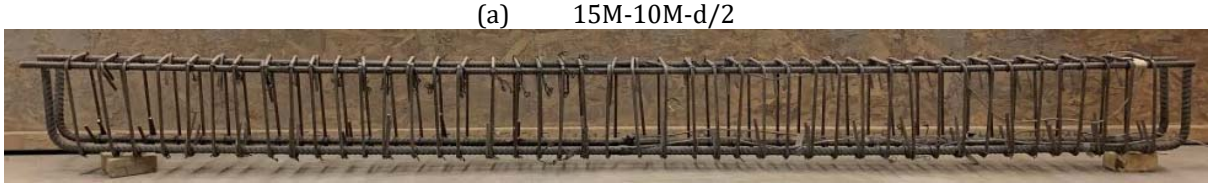

(b) 15M-10M-d/4

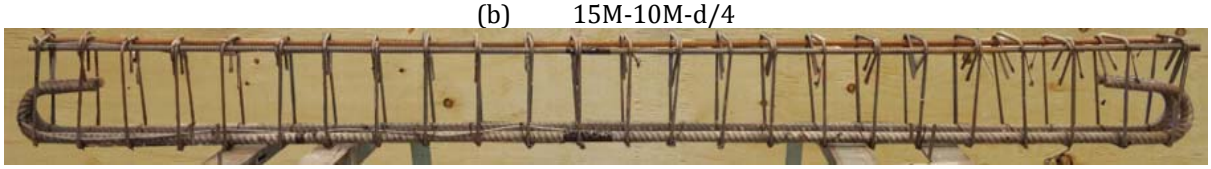

(c) 20M-10M-d/2

(d) 25M-0M-d/2

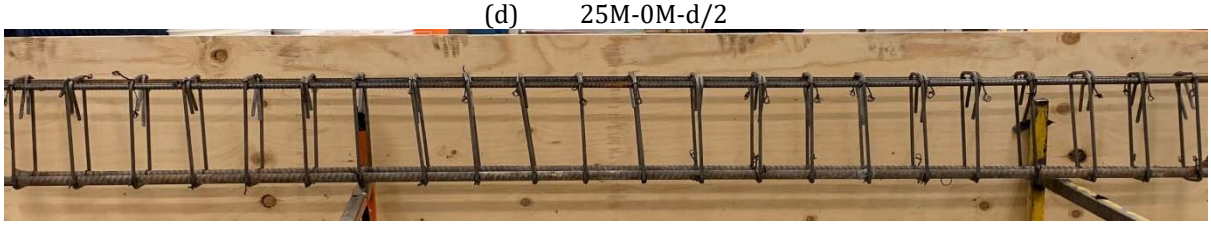

(e) 25M -10M-d/2

(f) 25M -10M-d/4

Figure 3-6 - Steel Reinforcement Details

(a) Beams in formwork before casting

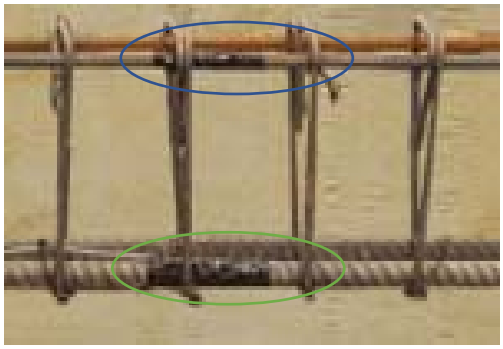

(b) Strain gauges after installation

(c) Pan mixer

(d) Casting of the beams with vibration

Figure 3-7 – Construction and casting photos

3.3.2 FRESH STATE PROPERTIES

The ASTM C1611 "Standard Test Method for Slump of Hydraulic-Cement Concrete" was used to record the slump for each mix. The test consisted of pouring three layers of concrete which were rodded individually twenty-five times. The mold was lifted after leveling the top of the concrete. The slump was recorded by measuring the vertical distance (height) between the top of the upturned cone and the top of the concrete. **Table 3-5** presented the slump test values for each of the HSC and HSFRC mixes, while sample photos are shown in **Figure 3-8**.

Table 3-5 – Concrete Fresh State Material Properties

Series		Specimen ID	Concrete Type	Fiber content Vf (%)	ASTM C143 Slump (mm)	Test type
HSC	15M	HSC-F0-15M-10M-d/4	HSC	0	193	S
		HSC-F0-15M-10M-d/4	HSC		200	D
		HSC-F0-15M-10M-d/4[x1]	HSC		195	D
	20M	HSC-F0-20M-10M-d/4	HSC		200	S
		HSC-F0-20M-10M-d/4	HSC		190	D
		HSC-F0-20M-10M-d/2	HSC		195	D
		HSC-F0-20M-6M-d/2	HSC		190	D
	25M	HSC-F0-25M	HSC		205	S
		HSC-F0-25M	HSC		200	D
		HSC-F0-25M-10M-d/4	HSC		205	S
		HSC-F0-25M-10M-d/4	HSC		200	D
Hybrid HSC	15M	HSC-F0.75-15M-10M-d/2	HSFRC	0.75	130	S
		HSC-F0.75-15M-10M-d/2	HSFRC		135	D
	20M	HSC-F0.75-20M-10M-d/2	HSFRC		137	S
		HSC-F0.75-20M-10M-d/2	HSFRC		130	D
	25M	HSC-F0.75-15M-10M-d/2	HSFRC		140	S
		HSC-F0.75-15M-10M-d/2	HSFRC		140	D

(a) HSC (b) HSFRC

Figure 3-8- Concrete slump test

3.4 HARDENED FRESH STATE PROPERTIES

For every mix, two flexural concrete prisms and six cylinders were prepared and cured for seven days. The cylinders and prisms were tested to get the compressive strength and flexural strength/toughness of the samples.

3.4.1 COMPRESSIVE CYLINDER TEST

Each cast included six 100 mm × 200 mm cylinders. Four of the cylinders were tested under pure axial compression in accordance with ASTM C39 "Standard Test Method for Compressive Strength of Cylindrical Concrete Specimens" to get the compressive strength at 7 days and 28 days. The results of these tests are presented in **Table 3-6**. The last two cylinders were tested to obtain both compressive strength and stress-strain relationships using a set of two LVDTs on the day of testing. In all cases, the tests were conducted using a PILOT CONTROLS machine with 1000 KN capacity. **Figure 3-9** shows typical stress-strain curves for plain HSC and HSFRC. Typical cylinders after testing are shown in **Figure 3-9 (b).**

(a) Picture of the Setup

(b) Compression test

(c) Stress-strain test

Figure 3-9- Cylinder Testing Setup

Table 3-6 – Concrete compressive strength summary

Series		Specimen ID	Concrete Type	Fiber content Vf (%)	Cylinder Test Compressive Strength (MPa)			Test type
					7 days	28 days	day of beam test	
HSC	15M	HSC-F0-15M-10M-d/4	HSC	0	75	98	105	S
		HSC-F0-15M-10M-d/4	HSC		79	101	115	D
		HSC-F0-15M-10M-d/4[x1]	HSC		85	100	114	D
	20M	HSC-F0-20M-10M-d/4	HSC		79	95	116	S
		HSC-F0-20M-10M-d/4	HSC		85	100	114	D
		HSC-F0-20M-10M-d/2	HSC		80	103	100	D
		HSC-F0-20M-6M-d/2	HSC		80	103	100	D
	25M	HSC-F0-25M	HSC		83	112	112	S
		HSC-F0-25M	HSC		82	95	98	D
		HSC-F0-25M-10M-d/4	HSC		83	112	112	S
		HSC-F0-25M-10M-d/4	HSC		82	95	98	D
HSFRC	15M	HSC-F0.75-15M-10M-d/2	HSFRC	0.75	75	87	94	S
		HSC-F0.75-15M-10M-d/2	HSFRC		78	90	100	D
	20M	HSC-F0.75-20M-10M-d/2	HSFRC		75	87	94	S
		HSC-F0.75-20M-10M-d/2	HSFRC		78	90	100	D
	25M	HSC-F0.75-15M-10M-d/2	HSFRC		78	107	110	S
		HSC-F0.75-15M-10M-d/2	HSFRC		78	107	118	D

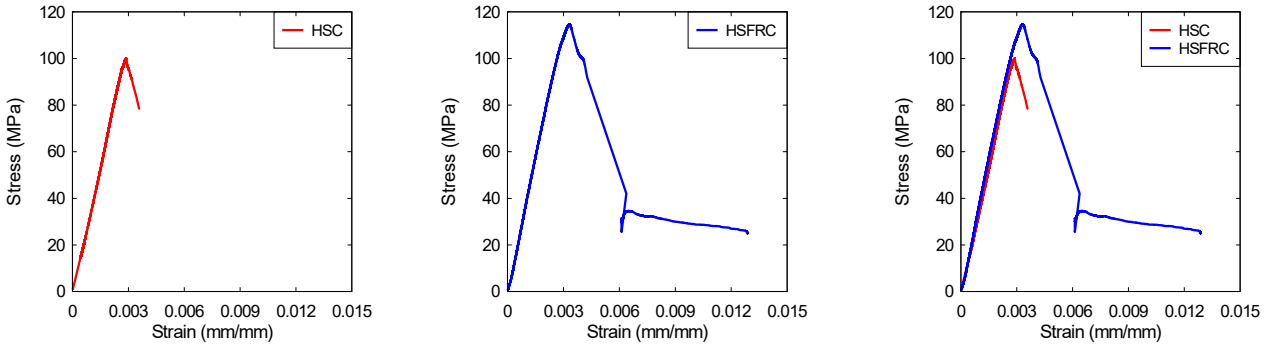

(a) (b) (c)

Figure 3-10- Stress Strain relationship

(a) HSC (b) HSFRC

Figure 3-11- Sample concrete cylinder testing failures

3.4.2 FLEXURE TOUGHNESS

From each batch, two prisms with dimensions of 100 mm x 100 mm x 400 mm were built and tested to determine the modulus of rupture and toughness properties (for HSFRC). Testing was conducted using a GALDABINI SUN 60 Universal Testing Machine, with the prisms tested under four-point loading in accordance with the ASTM C1609 standard which is shown in **Figure 3-12**. As quantified in ASTM C1609, the test started with an initial loading rate varying between 0.025 mm/min to 0.075 mm/min. However, beyond a deflection of L/900, the rate varied from 0.05 to 0.2 mm/min. During testing, the loading rate was kept constant under deflection control of 0.075 mm/min. Deflections were measured using a "Japanese yoke" and two LVDTs. The test results are summarized in **Table 3-7**, and load-deformation curves are listed in **Figure 3-12**.

Figure 3-13 shows typical samples for HSC (before testing) and HSFRC (after testing). During testing, the plain HSC displayed linear elastic response and exhibited brittle failure after first cracking. In contrast, the addition of steel fibers to the HSC improved the pre-peak and post-peak response as seen in **Figure 3-14**, allowing HSFRC to carry significant post-cracking stresses with improved toughness.

Figure 3-12- GALDABINI SUN 60 Universal Floor Standing Testing Machine

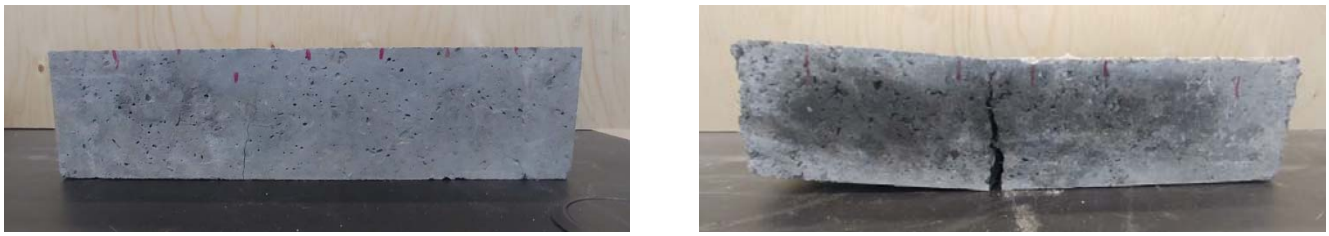

(a) HSC *(b) HSFRC*

Figure 3-13- HSC and HSFRC Flexural Prism Toughness Testing Failures

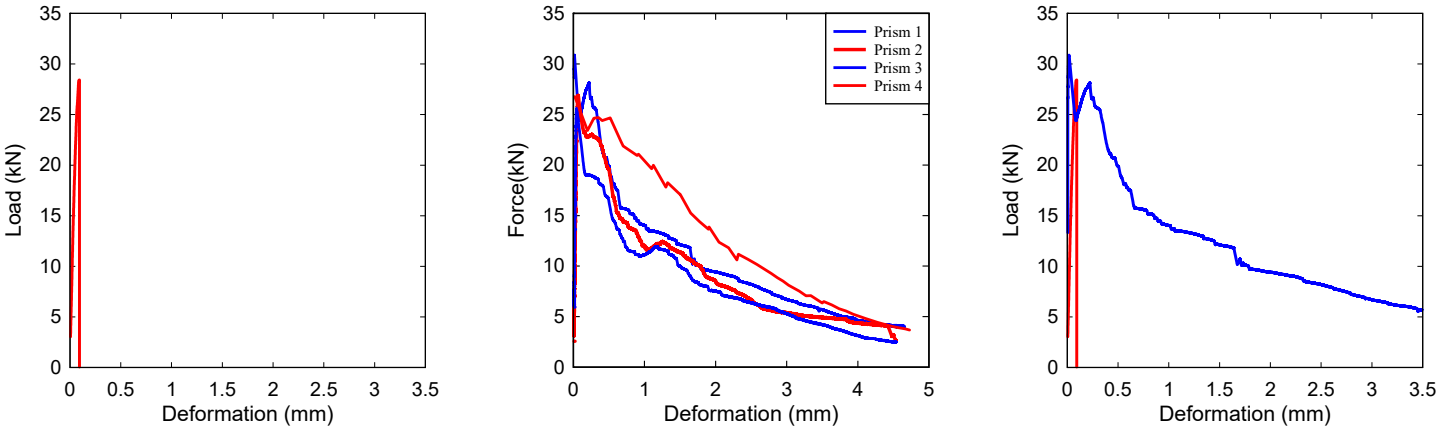

(a) HSC (b) HSFRC (c) HSC vs HSFRC

Figure 3-14- Flexural prism Load-Deflection Curve Samples for HSC and HSFRC

Table 3-7 – Results from the ASTM C1609 toughness tests

Concrete Mix	ASTM C1609										
	P_1	δ_1	P_p	δ_p	f_1	f_p	P_{600}	f_{600}	P_{150}	f_{150}	T_{150}
HSC	28.42	0.09	28.42	0.09	8.62	8.62	-	-	-	-	1.86
HSFRC	30.88	0.02	30.88	0.02	9.26	9.26	15.80	4.74	7.90	2.37	32.2

L = Span Length (300 mm), (L/600 = 0.5, L/150 =2)
P_1= First-Peak Load (kN)
δ_1= Net Deflection at First-Peak Load (mm)
P_p= Peak Load (kN)
δ_p= Net Deflection at Peak Load (mm)
f_1= First-Peak Strength (MPa)
f_p= Peak Strength (MPa)
P_{600}= Residual Load at net deflection of L/600 (kN)
f_{600}= Residual Strength at net deflection of L/600 (MPa)
P_{150}= Residual Load at net deflection of L/150 (kN)
F_{150}= Residual Strength at net deflection of L/150 (MPa)
T_{150}= Area under load vs. net deflection curve (0 to L/150), (kN*mm)
FT = Flexural Toughness Factor = (T_{150}*L)/(L/150 *b*d^2)

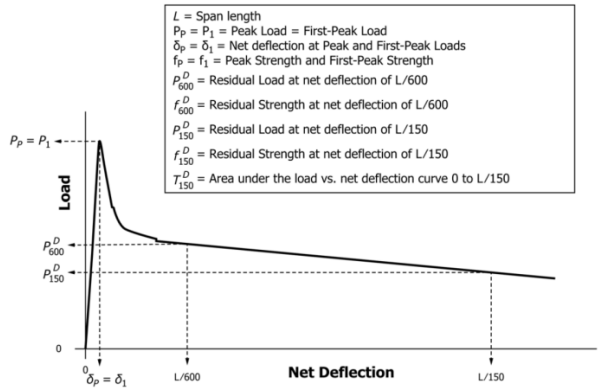

3.5 EXPERIMENTAL SETUP

3.5.1 STATIC TESTING

A total of six beams were subjected to quasi-static four-point bending loading with simply supported boundary conditions. The beams were tested over a span of 2232 mm, with two concentrated loads distanced at 750 mm (central constant moment region) and two equal shear spans of 741 mm. As seen in **Figure 3-15** and **Figure 3-16**, the loading was applied using a hydraulic jack and manually operated pump. The load was then transferred to an I-Beam which distributed the load as two-point loads located at 375 mm from the center of the beam. The loading was monitored using two load cells located at the supports as well at the jack location, and deflections were recorded at mid-span with a displacement cable transducer (DCT). The tensile strains in the steel longitudinal reinforcement were captured using the strain gauges glued to the reinforcement bars at mid-span. A data acquisition system was used to record the load, deflections and strains readings.

All static specimens followed the same loading sequence. In the first step, a 20 kN was applied to detect first cracking. If the first hairline crack was not found, the load was augmented incrementally by 10kN until it appeared. Thereafter, the load was increased in 20 kN intervals, until yielding. In the post-yield range, loading was changed to displacement-control using 10 mm increments until failure of the beam or reaching the maximum displacement (150 mm) of the hydraulic jack. In some cases, testing was stopped earlier if the leading beam-ends began touching the specimens.

It is noted that several beams were tested after blast testing using the same setup to assess their residual capacity. The residual tests were conducted in displacement control using increments of 20 mm until beam failure or when the test setup capacity was exceeded.

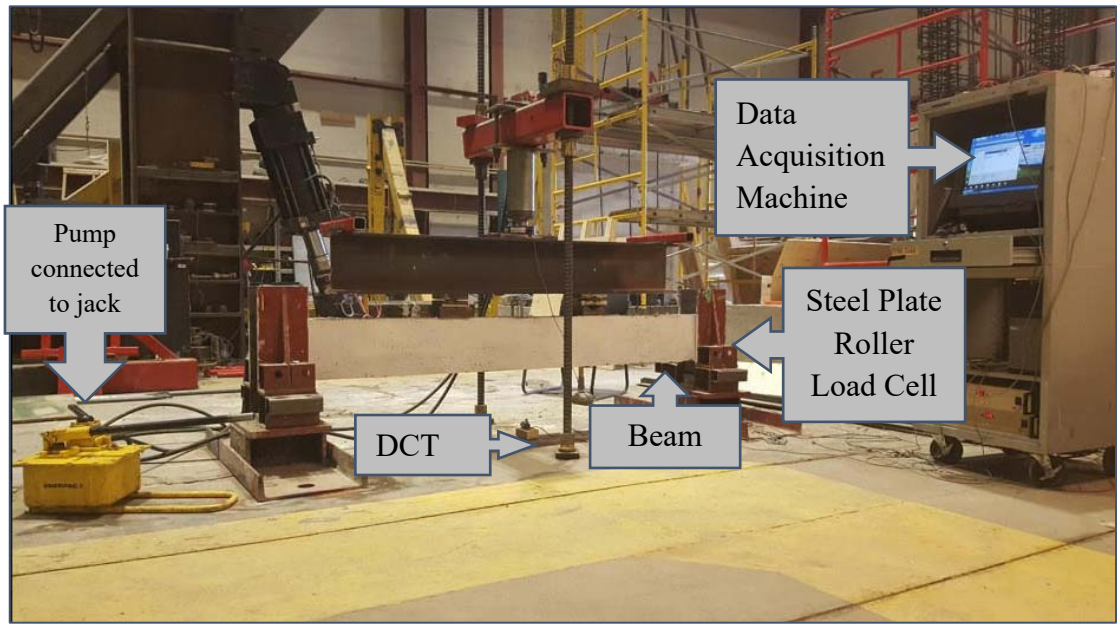

Figure 3-15 - Beam specimen prior to static testing

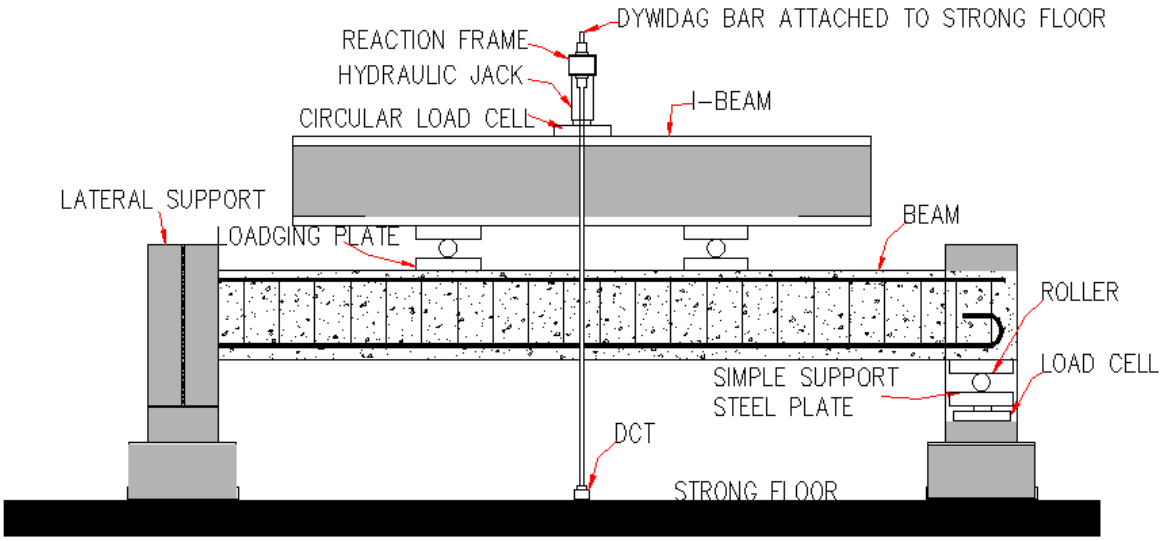

Figure 3-16 - Loading device and support details (sketch)

3.5.2 BLAST TESTING

3.5.2.1 SHOCK TUBE

Dynamic blast testing was conducted using the University of Ottawa shock-tube (Lloyd et al. 2011; Saatcioglu et al. 2011). The shock-tube can simulate the shock waves generated by the detonation of high explosives in the far-field range. As illustrated in **Figure 3-17** and **Figure 3-18** the shock tube consists of four main sections: a variable-length driver, spool section, expansion chamber, and rigid end test frame (with 2 m x 2 m square opening).

The driver length varies between 305 mm (1 ft) to 5158 mm (17 ft). It is used to generate the blast energy and controls the duration of the shockwave, while the driver pressure determines the magnitude of the peak reflected pressure of the shock wave. This study used a constant driver length of 2743 mm (9 ft). The second component is the spool section which is composed of a double diaphragm firing system placed between the expansion chamber section and the driver and is used to control the release of compressed air. The diaphragm system has two sets of aluminum sheets. the first set blocks the opening of the driver and the second set of sheets blocks the opening of the expansion chamber. When the specified pressure is reached, the pressurized air is released from the spool, which ruptures the aluminum foils, thereby releasing the pressure into the expansion chamber. This compressed-air travels along the length of the expansion section until it reaches the specimen at the rigid end frame. Meanwhile, the lateral load transfer device (LTD) collects the shockwaves and transfers the pressure onto the specimens. The pressure at the rigid end frame section is known as the “reflected pressure” and is measured using two pressure sensors placed at the side and bottom of the shock-tube end-frame.

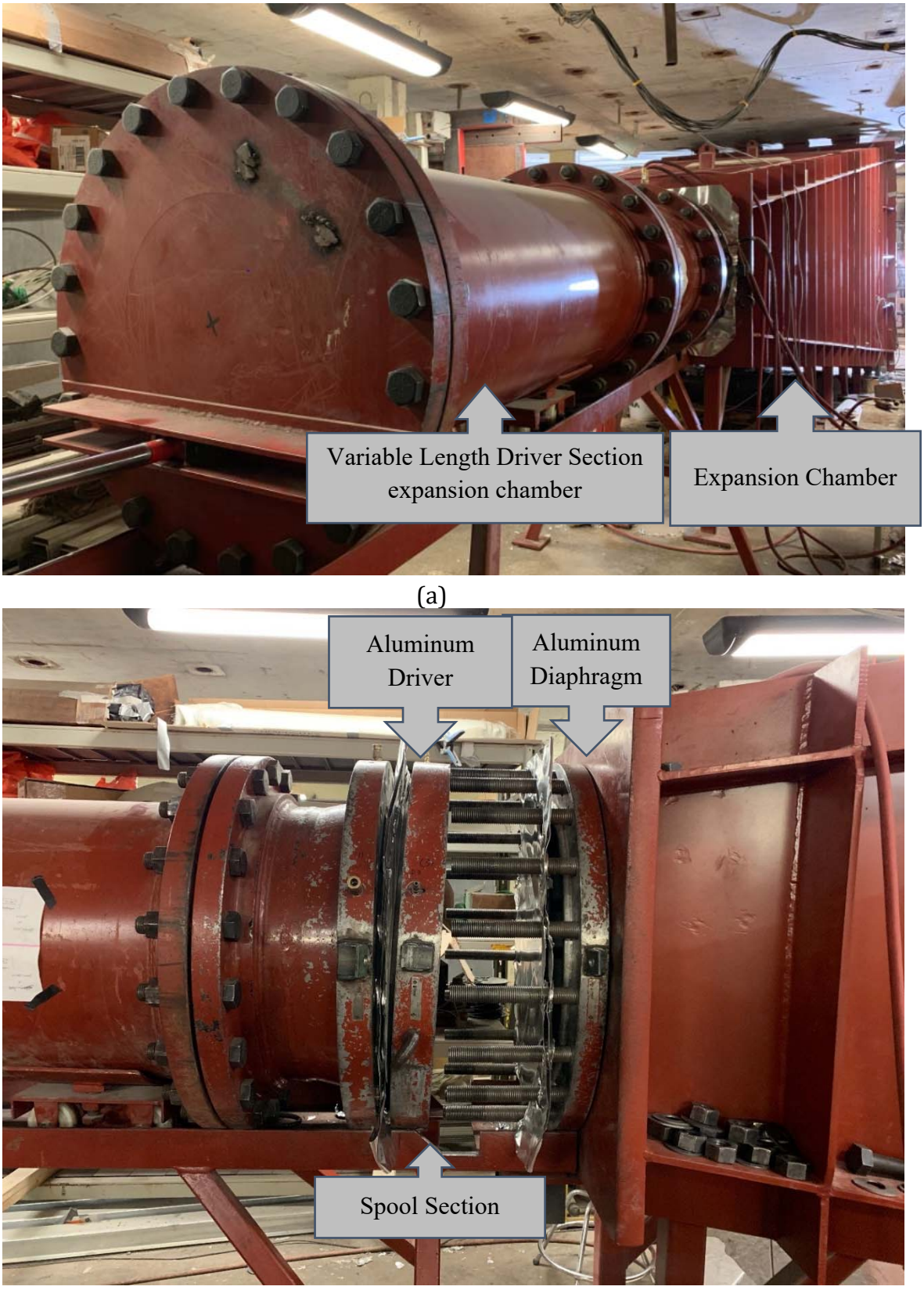

Figure 3-17- Shock Tube (a) Driver Section, (b) Spool Section

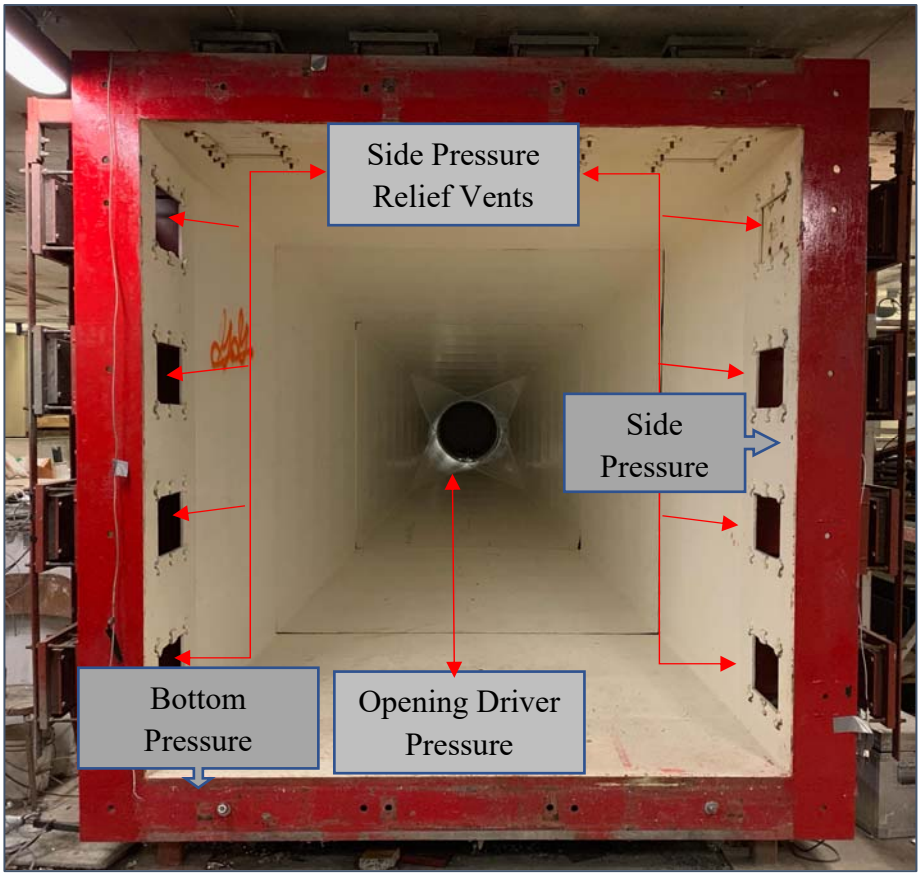

(a)

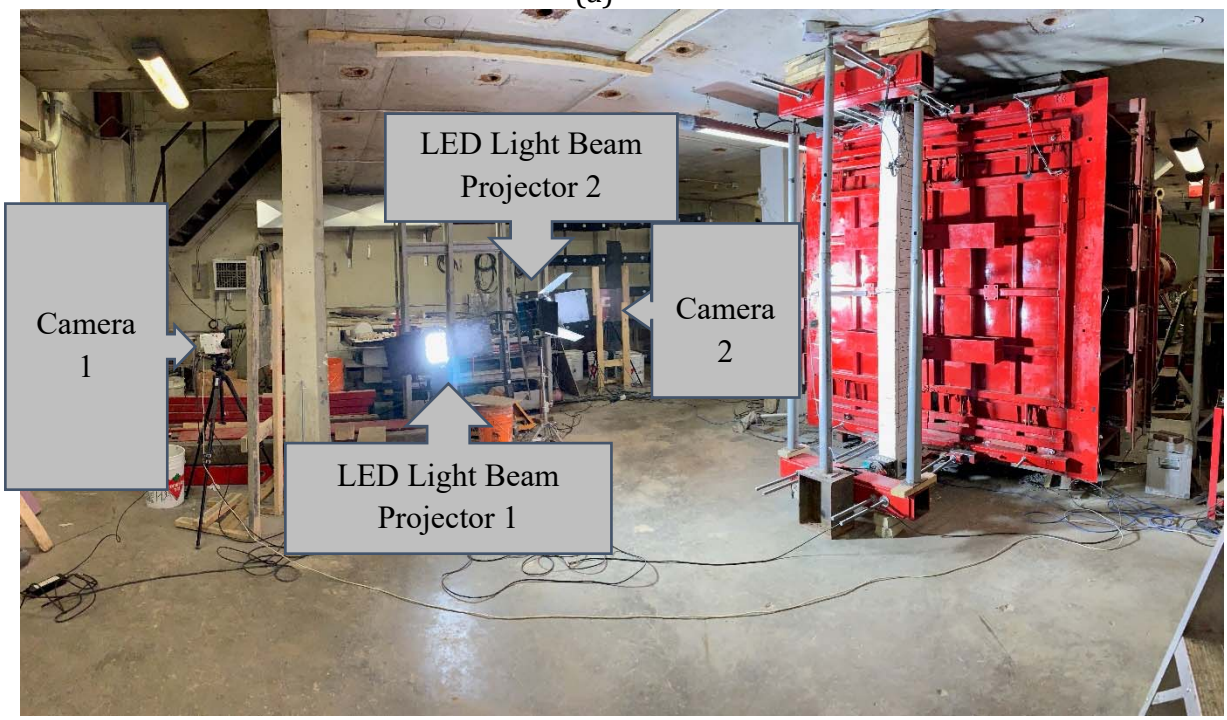

(b)

Figure 3-18- Sock Tube (a) Rigid End Test Frame Section, (b) Beam Setup

3.5.2.2 LATERAL LOAD TRANSFER DEVICE

The lateral load transfer device (LTD) redirects the blast pressure generated by the shock-tube end-frame opening onto the beams. The test fixture was designed to duplicate the loading pattern in the static tests and collects and transfers the blast pressure as to two concentric point loads. As shown in **Figure 3-19**, the lateral load transfer device covers the entire 2 m x 2 m shock-tube opening and is composed of two side-by-side rigid steel panels (height: 2032 mm; width:1000 mm). The LTD also consists of hollow steel section (HSS) members and rigid plates as seen in **Figure 3-19**. Sliding hinges are placed at the top and bottom supports, which allow free lateral movement of the middle portion of the LTD (Jacques, 2016). To redirect the shockwaves to the specimen, two I-steel load-transfer beams with a dimension of 160 mm x 165 mm x 1200 mm are attached to the LTD (see **Figure 3-19**).

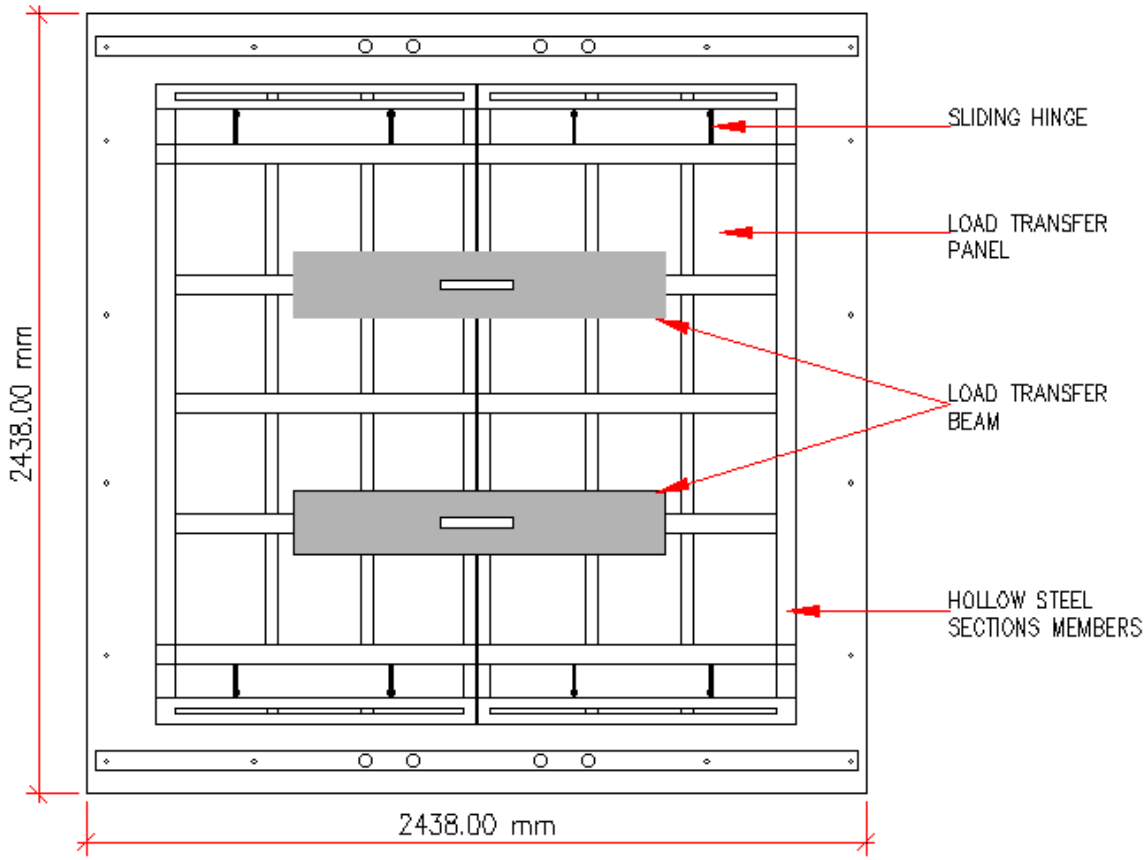

Figure 3-19 - Lateral load transfer device section details

3.5.2.3 SUPPORTS

The beams were secured to the shock-tube using simple supports that allowed rotation and closely replicated the conditions found in the static tests. The setup results in a 2232 mm unsupported span, with two shear spans of 741 mm and a constant moment region of 750 mm. Both top and bottom supports were identical consisting of front and rear support components. The front supports consist of 1000 mm long, 152 x 152 mm square HSS section with an integrated load cell, which is connected using four 19 mm diameter threaded rods. The rear supports consist of 500 mm long 51 x 51 mm HSS, with an additional 440 mm long HSS section to simulate a roller condition. A schematic of the setup is shown in **Figure 3-20** and **Figure 3-21**.

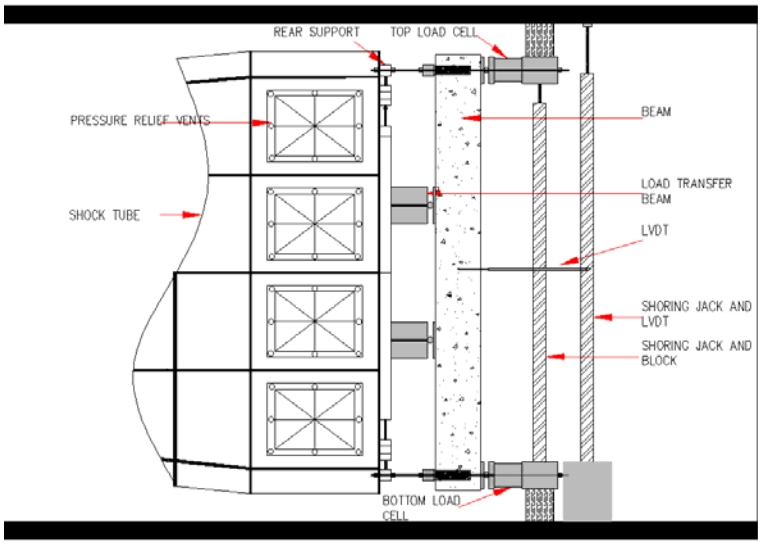

Figure 3-20 - Dynamic experimental setup - Side view

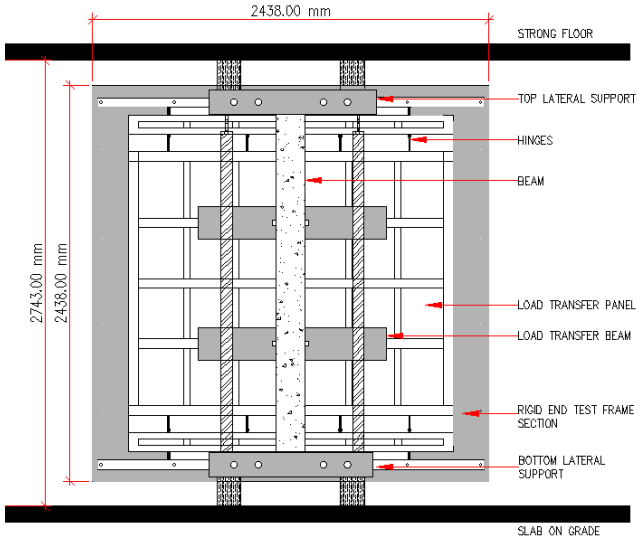

Figure 3-21 - Dynamic experimental setup - Front view

3.5.2.4 DATA ACQUISITION SYSTEM

A Yokogawa SL 1000 High-speed Data Acquisition unit, capable of recording 100,000 data points per second (100,000 Hz), was used to record data from the LVDTs strain gauges and dynamic reactions and pressure gages using a trigger system. The data is exported for full analysis through software XViewer in a .csv format.

3.5.2.5 HIGH-SPEED VIDEO CAMERA

All dynamic tests were recorded with AOS Technology X-PRI high-speed camera to capture the response of the specimens at each blast. The camera has a resolution of 800x600 pixels and rate of 1000 frames per second. During the tests, the camera was installed at the side of the beams, with a second camera placed at 45 degrees.

3.5.2.6 PRESSURE SENSORS

Two PCB Piezotronics Model #112A22 piezoelectric pressure sensors were installed at the side and bottom of the end frame to record complete pressure-time histories for each blast wave and send a trigger signal to record the data.

3.5.2.7 LINEAR VARIABLE DISPLACEMENT TRANSDUCERS (LVDT)

Two linear variable displacement transducers (LVDT), Celesco model CLWF-300, with a 300 mm gauge length were installed at the mid and third span of each beam to measure the lateral displacements of the beams during blast loading. The mid-span LVDT recorded the maximum and residual displacement, while the third span LVDT is used in case of failure of the middle LVDT. Another LVDT was installed at the bottom of the end-frame to correct for any shock-tube movement during testing.

3.5.2.8 STRAIN GAUGES

In total three strain gauges were installed at the mid-span of the longitudinal reinforcement rebars (1 on the top and 2 on the bottom steel as seen in **Figure 3-22**). The strain gauges used were FLA-6-350-11 with a length of 6 mm and an electrical resistance of 350 ohms.

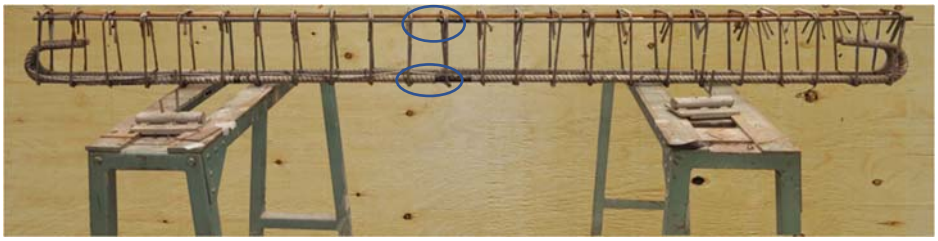

Figure 3-22 - Specimen 20M-10M-d/2 with two strain gauges at the bottom steel and one strain gauge at the top

3.5.2.9 EXPERIMENTAL PROCEDURE

Dynamic testing was conducted by testing the specimens under gradually increasing pressures until failure. The testing sequence aimed at examining the response of the beams under elastic, yield and ultimate conditions, with the Blasts selected to allow for direct comparison with the previous tests on the nominally detailed specimens tested by Algassem (2016)

The shockwaves' properties are obtained by adjusting the driver length and pressure. In this study, the driver length was kept constant at 2745mm (9 ft) with the driver pressure varied. **Table 3-8** provides a summary of the resulting blast properties, including the average, reflected pressure, reflected impulse, and positive phase duration. Sample pressure-time histories are shown in **Figure 3-23**.

For the 15 M beams with plain HSC, the blast sequence was as follows: Blast A (30 psi), Blast B (50 psi), and Blast C (70 psi). An additional blast was applied in the case of the beam with fibers: Blast D (90 psi). Similarly, the sequence in the 20M series consisted of Blast A (30 psi), Blast C (70 psi), and Blast D (90 psi). The beams in the 25 M series were subjected to Blast C (70 psi) and Blast D (90 psi) only, except for the HSFRC specimen, which was subjected to an addition Blast load at 100 psi (Blast E).

Table 3-8 – Blast test properties

Blast ID	Approximate Driver Pressure P_d kPa	Reflected Pressure P_r kPa	Reflected Impulse I_r kPa-ms	Positive Phase Duration t_P ms
A	207 (30)	46.34	372.90	19.75
B	345 (50)	57.82	582.42	21.25
C	483 (70)	70.81	701.37	21.43
D	621 (90)	97.70	1001.43	27.81
E	690 (100)	89.32	1312.96	26.85

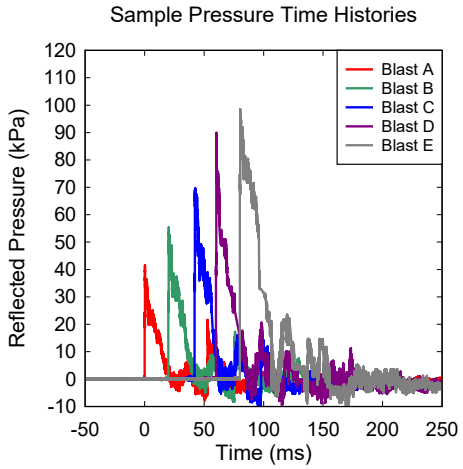

Figure 3-23 - Typical pressure-time histories for Blasts A-E

CHAPTER 4: EXPERIMENTAL RESULTS – STATIC TESTS

4.1 CHAPTER OVERVIEW

This section summarizes the experimental test results of the specimen tested under quasi-static four-point bending. The static results for the seven beams cast with High Strength Concrete (HSC), and High Strength Fiber Reinforced Concrete (HSFRC) are presented in **Table 4-1**. The individual response and behavior of the beams are documented in this chapter. The results are further discussed/compared in **Chapter 6**.

The results for each specimen are presented in Figures and Tables. The figures include the following: (1) load vs. displacement curve, (2) load vs. strain for longitudinal reinforcement, (3) a graph of load vs. flexural and shear crack widths, (4) a graph of flexural and shear crack widths vs. displacement and (5) a pictorial description of the damage in the beams at various stages during testing.

Data from the load-displacement curves includes the following: (1) the yield load (P_y) and maximum load (P_{max}), (2) Displacement at yield (Δ_{yield}), at 85% of peak load (Δ_{max}) and at end of testing or failure (Δ_{end}), (3) stiffness, (4) Ductility: $\Delta_{max}/\Delta_{yield}$ and $\Delta_{end}/\Delta_{yield}$, (5) Toughness: areas under the load-deflection curve until Δ_{max} and Δ_{end} and (A_{max} and A_{end}) as presented graphically in **Figure 4-1**.

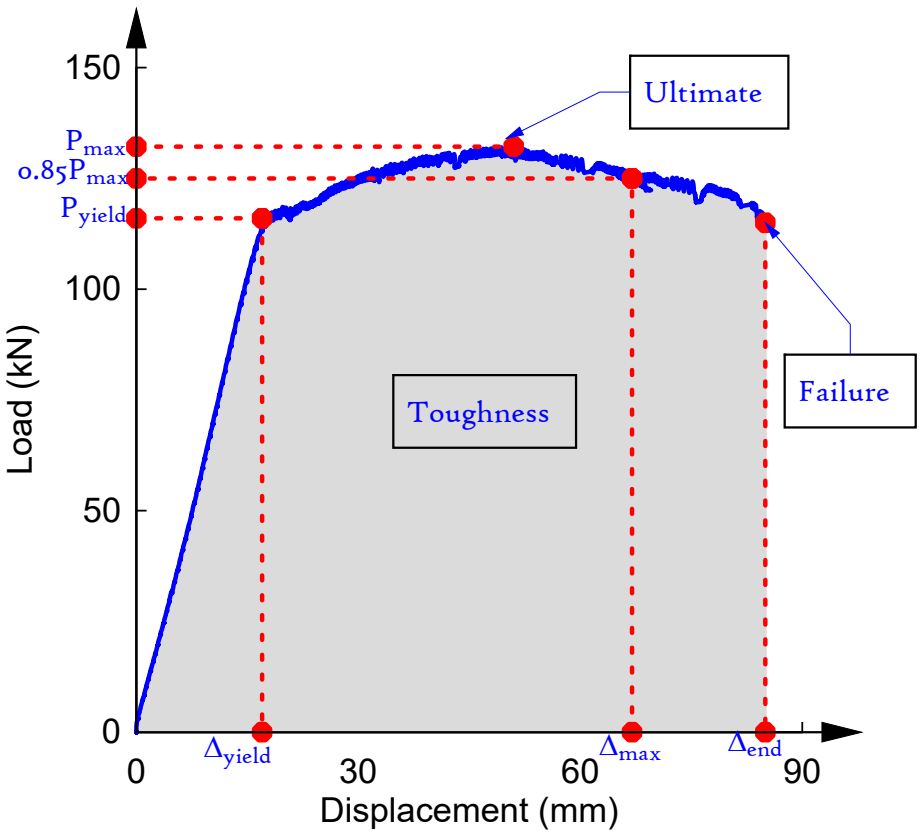

Figure 4-1 - Load vs. mid-span deflection curve

Table 4-1 – Static Testing Data Summary

Series	ID	Concrete Type	Fiber content V_f (%)	Load		Displacement			Stiffness	Ductility		Toughness (kN-mm)		Damage Mechanism
				P_y (kN)	P_{max} (kN)	Δ_{yield} (mm)	Δ_{max} (mm)	Δ_{end} (mm)	K (N/mm)	$\frac{\Delta_{max}}{\Delta_{yield}}$	$\frac{\Delta_{end}}{\Delta_{yield}}$	A_{max}	A_{end}	
15M	HSC-F0-15M-10M-d/4	HSC	0	105	108	16	149	149	6562	9.3	9.3	14018	14018	Flexure
	HSC-F0.75-15M-10M-d/2	HSFRC	0.75	112	117	11	98.8	102	10181	8.9	9.3	9997	10234	Flexure + Bar Rupture
20M	HSC-F0-20M-10M-d/4	HSC	0	127	131	13	150	150	9411	11.5	11.5	18889	18889	Flexure
	HSC-F0.75-20M-10M-d/2	HSFRC	0.75	160	168	15	37	100	10667	2.5	6.8	4781	12494	Flexure
25M	HSC-F0-25M	HSC	0	-	202	-	-	18	11098	-	-	-	1920	Shear
	HSC-F0-25M-10M-d/4	HSC	0	220	225	19.2	80	120	11458	4.2	6.3	14734	19734	Flexure
	HSC-F0.75-25M-10M-d/2	HSFRC	0.75	240	248	19.3	70	125	12435	3.5	6.5	13931	22811	Flexure

4.2 RESULTS OF THE 15M SERIES

4.2.1 HSC-F0-15M-10M-D/4

The first beam in the 15M series was built with plain high strength concrete, 2-15M tension bars, 2-10M continuity (compression) bars, and closed ties spaced at 50 mm (d/4) throughout the span, meeting the blast detailing requirement of the CSA S850 standard. **Table 4-1** and **Figure 4-2 to Figure 4-4** summarize the results for this beam.

The first flexural hairline cracks appeared at a displacement of 2.38 mm (20 kN). Yielding of longitudinal bars occurred at a displacement of 16 mm (P_{yield} = 105 kN; see **Figure 4-3**). The beam reached a maximum load (P_{max}) of 108 kN (17mm). The top cover concrete in the midspan region started crushing at a displacement of 24 mm which resulted in a sudden drop in load to 98 kN. However, the provision of compression bars and ties prevented failure allowing the beam to sustain pronounced post-yield deflections until the end of testing at a large deflection of 149 mm. Damage at failure was limited to spalling of cover concrete in the midspan constant moment region, with no buckling of the compression bars, nor severe crushing of confined concrete within the core (**Figure 4-4**). The results demonstrate the important ductility that can be provided by blast detailing, even under quasi-static loading.

a) Load – Mid-Span Deflection

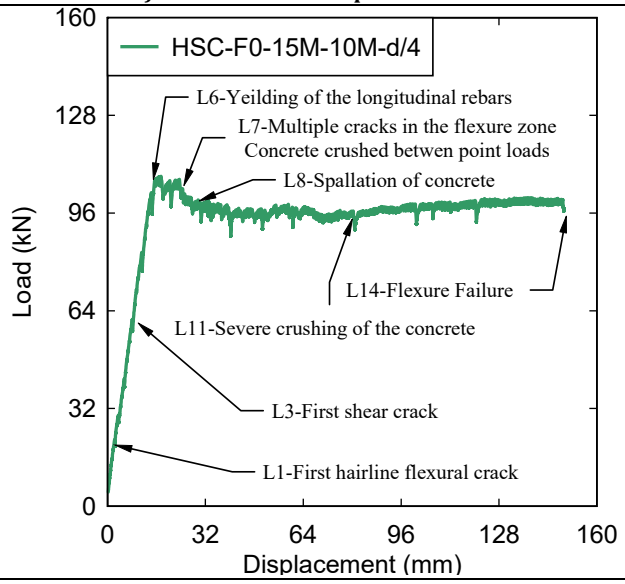

Data Summary	
P_{max} (kN)	108
Δ_{end} (mm)	149
K (N/mm)	6750
$\frac{\Delta_{end}}{\Delta_{yield}}$	9.3
A_{max}	14018

b) Condition of beam after static test

Failure Mechanism
Flexure: excessive deformation with top cover spalling

Figure 4-2 Residual test results for beam HSC-F0-15M-10M-d/4

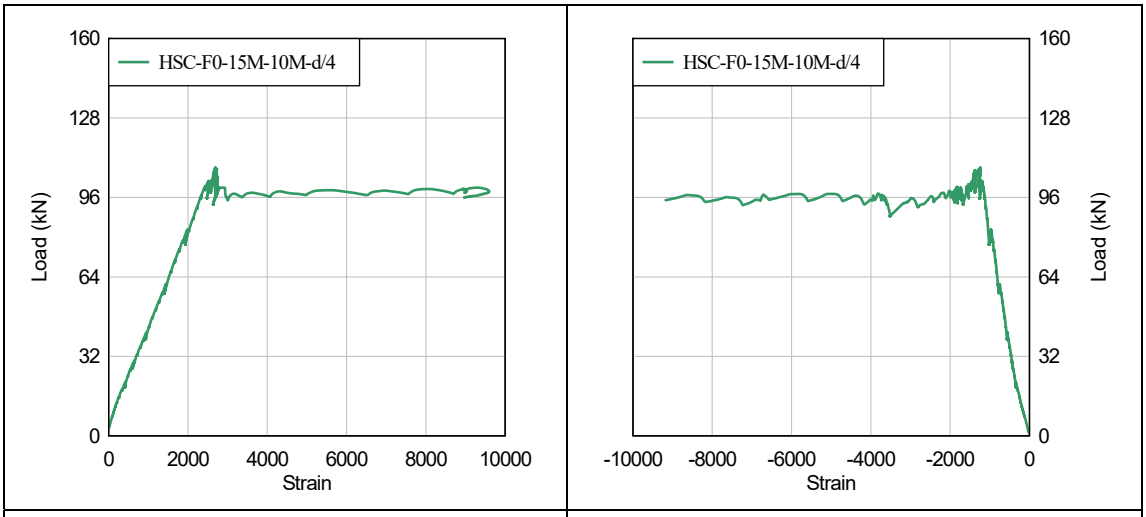

(a) Tensile strain in longitudinal bars

(b) Compressive strain in longitudinal bars

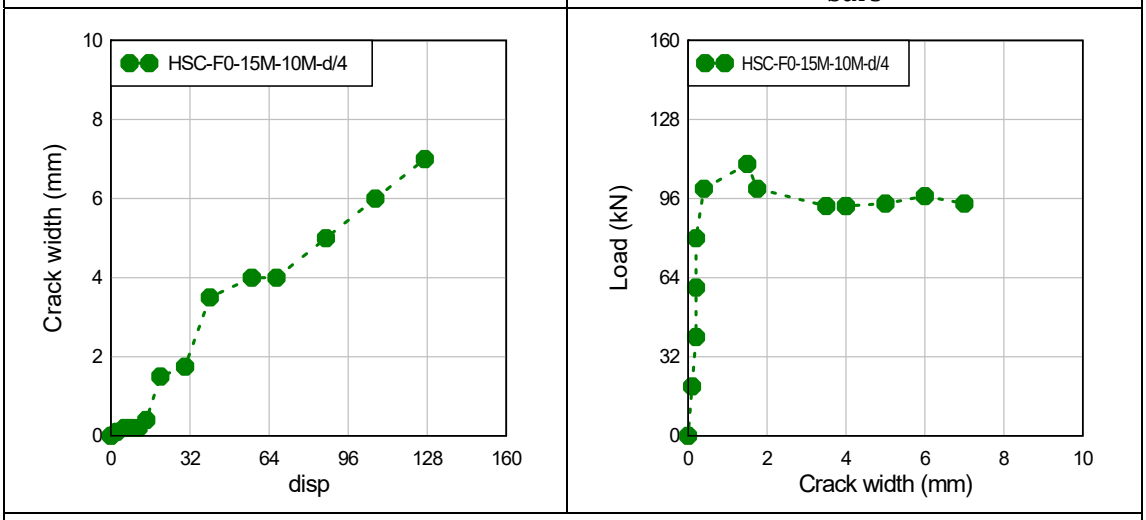

(c) Maximum crack width (flexure)

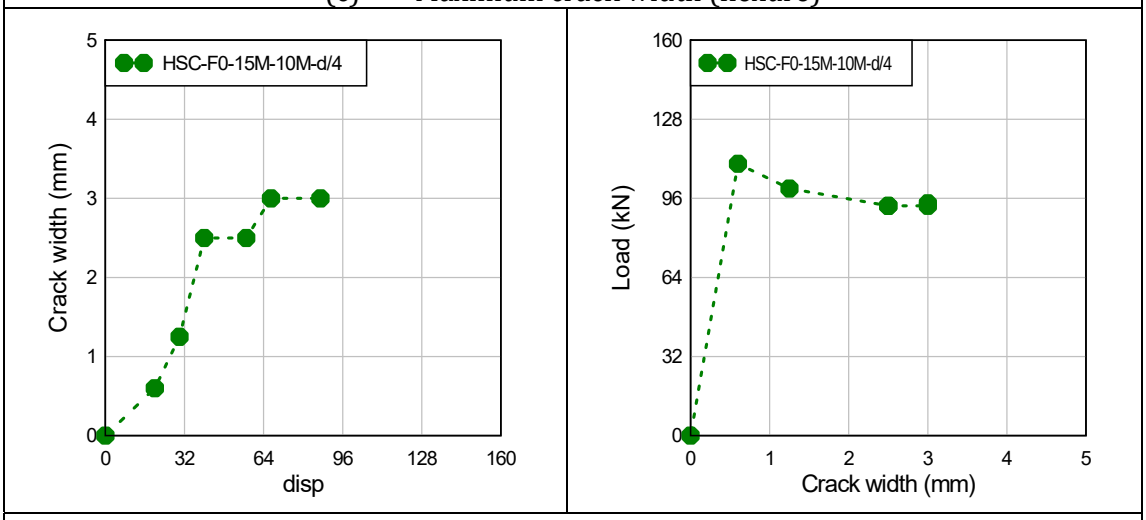

(d) Maximum crack width (shear)

Figure 4-3 - Experiment results for beam HSC-F0-15M-10M-d/4

<table>
<tr><th colspan="3">Experimental Results</th><th>Comments</th></tr>
<tr><td>Load stage</td><td>2P (kN)</td><td>Mid-span deflection (mm)</td><td rowspan="3">First hairline cracks appear</td></tr>
<tr><td>L1</td><td>20.0</td><td>2.4</td></tr>
<tr><td colspan="3">  </td></tr>
<tr><td>Load stage</td><td>2P (kN)</td><td>Mid-span deflection (mm)</td><td rowspan="3">Yielding of the longitudinal bars in tension

Formation of Flexural-shear cracks</td></tr>
<tr><td>L6</td><td>108</td><td>16</td></tr>
<tr><td colspan="3"> 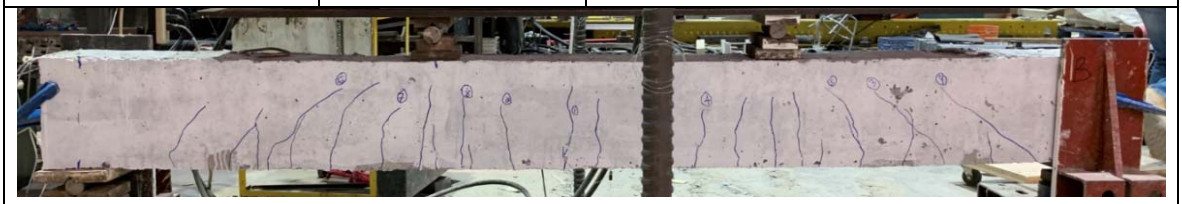 </td></tr>
<tr><td>Load stage</td><td>2P (kN)</td><td>Mid-span deflection (mm)</td><td rowspan="3">Concrete crushing in the cover regiuon in the midspan compression zone</td></tr>
<tr><td>L11</td><td>94</td><td>87</td></tr>
<tr><td colspan="3"> 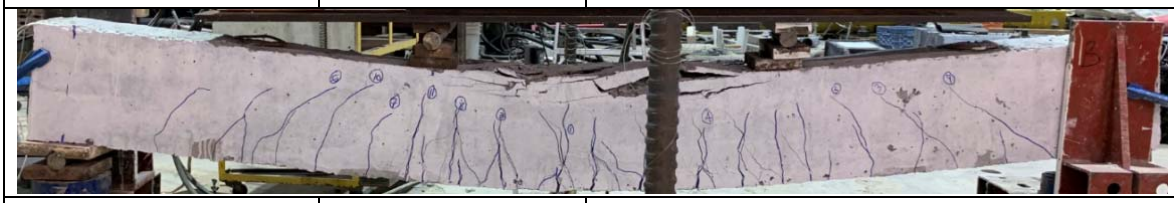 </td></tr>
<tr><td>Load stage</td><td>2P (kN)</td><td>Mid-span deflection (mm)</td><td rowspan="3">End of testing

Large Deflection with damage limited to top cover spalling.

Beam can still carry load</td></tr>
<tr><td>L14</td><td>94</td><td>127</td></tr>
<tr><td colspan="3">  </td></tr>
<tr><td colspan="3"> 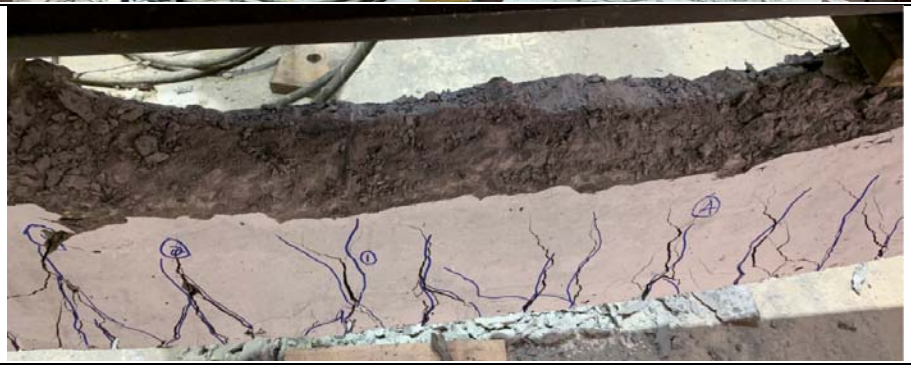 </td><td>Compression rebars did not buckle, the core is well confined</td></tr>
</table>

Figure 4-4 - Major events for specimen HSC-F0-15M-10M-d/4

4.2.2 HSC-F0.75-15M-10M-D/2

The second specimen in the 15M series was built with high strength fiber reinforced concrete (HSFRC) and had similar properties to the previous beam, with the exception of the addition of 0.75% fibers and the use of relax, "intermediate" detailing with ties spaced at s = 100 mm (d/2). The test results for this beam are provided in **Table 4-1** and **Figure 4-5** to **Figure 4-7**.

As opposed to the previous beam, the first flexural hairline cracks appeared at 40 kN (displacement of 3.1mm) due to fibers. Yielding occurred when the displacement reached 11 mm, at an applied load (P_{yield}) of 112 kN. The addition of fibers allowed for an increase in stiffness (K= 10181 N/mm) and maximum load (P_{max}= 117 kN at 22 mm) when compared to the 15M beam with plain HSC and blast detailing. After yielding the first localized crack appeared at a displacement of 32 mm (112 kN), growing to a maximum width of 6 mm. The progressive application of load proportionally increased localized the crack width at this location. As shown in **Figure 4-5**, the localized crack eventually propagated from the tension zone into the core region of the beam, reaching a maximum width of 17 mm at a displacement of 72 mm (100 kN). The localized cracking eventually led to the rupture of the tension reinforcement, with the beam reaching a large deformation of (Δ_{end}) of 102 mm (load before failure = 88 kN). It is noted that unlike the previous beam, the top cover region damage remained well controlled.

a) Load – Mid-Span Deflection

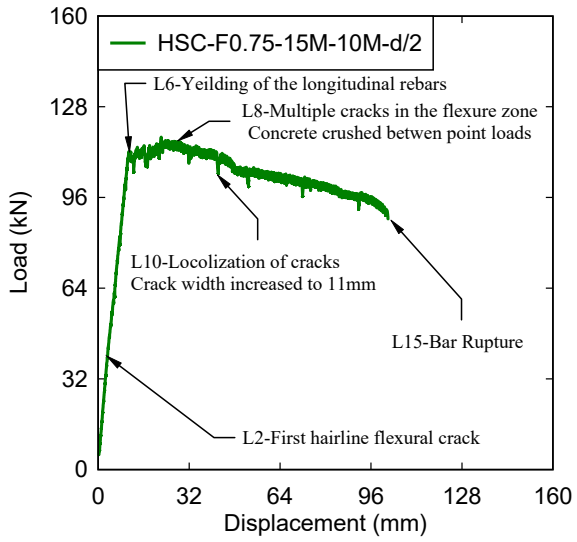

Data Summary	
P_{max} (kN)	117
Δ_{end} (mm)	102
K (N/mm)	10181
$\frac{\Delta_{end}}{\Delta_{yield}}$	9.3
A_{max}	10234

b) Condition of the beam after static test

Failure Mechanism
Tension Bar rupture

Figure 4-5 Residual test results for beam HSC-F0.75-15M-10M-d/2

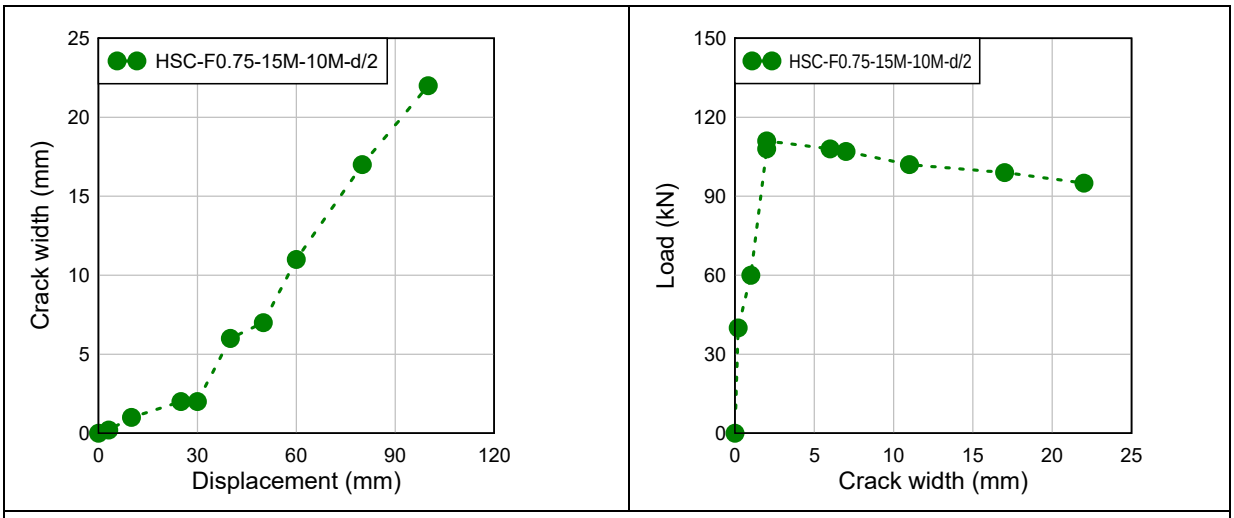

(a) Maximum crack width (flexure)

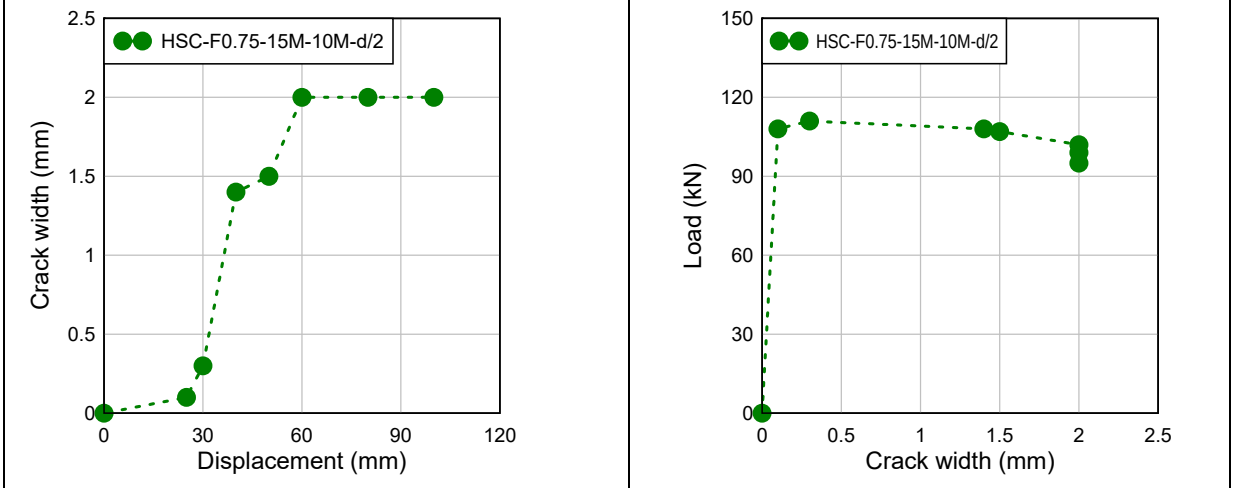

(b) Maximum crack width (Shear)

Figure 4-6 - Experiment results for beam HSC-F0.75-15M-10M-d/2

<table>
<tr><th colspan="3">Experimental Results</th><th>Comments</th></tr>
<tr><td>Load stage</td><td>2P (kN)</td><td>Mid-span deflection (mm)</td><td rowspan="3">First flexural hairline cracks</td></tr>
<tr><td>L2</td><td>40</td><td>3</td></tr>
<tr><td colspan="3">  </td></tr>
<tr><td>Load stage</td><td>2P (kN)</td><td>Mid-span deflection (mm)</td><td rowspan="3">Yielding of the longitudinal bars in tension

Multiple cracks from throughout span</td></tr>
<tr><td>L6</td><td>112</td><td>11</td></tr>
<tr><td colspan="3">  </td></tr>
<tr><td>Load stage</td><td>2P (kN)</td><td>Mid-span deflection (mm)</td><td rowspan="3">Crack localization started to show in the constant moment region of the beam</td></tr>
<tr><td>L10</td><td>104</td><td>42</td></tr>
<tr><td colspan="3"> 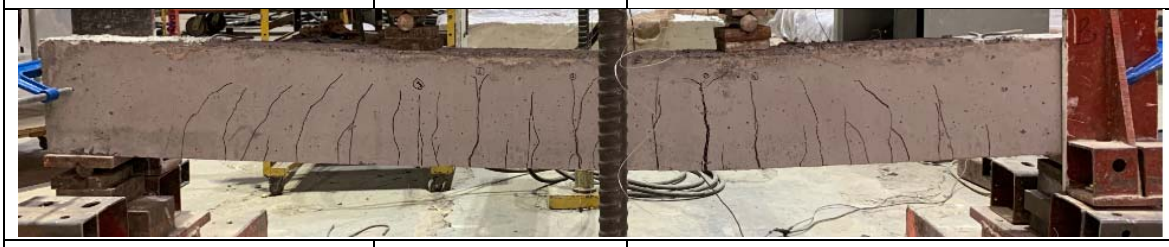 </td></tr>
<tr><td>Load stage</td><td>2P (kN)</td><td>Mid-span deflection (mm)</td><td rowspan="3">Flexure failure due to bar rupture at the localized crack location</td></tr>
<tr><td></td><td>88</td><td>102</td></tr>
<tr><td colspan="3">  </td></tr>
<tr><td>Bar rupture</td><td colspan="2">Limited cover crushing at failure</td><td rowspan="2">Close up pictures of the failure</td></tr>
<tr><td>  </td><td colspan="2">  </td></tr>
</table>

Figure 4-7 - Major events for specimen Hybrid-HSC-F0.75-20M-10M-d/2

4.3 RESULTS OF THE 20M SERIES

4.3.1 HSC-F0-20M-10M-D/4

This specimen followed the detailing requirements of the CSA S850 standard and was designed plain high strength concrete, 2-20M bars in tension, 2-10M layers of bars in compression and closed ties spaced at 50mm (d/4). The results for this beam are shown in **Table 4-1** and **Figure 4-8** to **Figure 4-10**.

The first flexural and shear hairline cracks appeared at displacements of 1.5 mm (30 kN) and 10 mm (100 kN), respectively. Yielding of the longitudinal bars occurred at a displacement of 15 mm (P_{yield} =127 kN; see **Figure 4-9**). The maximum load reached P_{max} = 131 kN (17 mm), which was followed by a sudden drop to 120 kN (60mm) due to concrete crushing in the top cover region. Once again blast detailing allowed for a well-defined post-yield plateau without further significant drops load in load until the end of testing. The confinement steel protected the core region, while also preventing buckling of the compression bars. The specimen maintained an average load of 125 kN load until the end of testing at a very large deformation (Δ_{end}) of 150 mm.

a) Load – Mid-Span Deflection

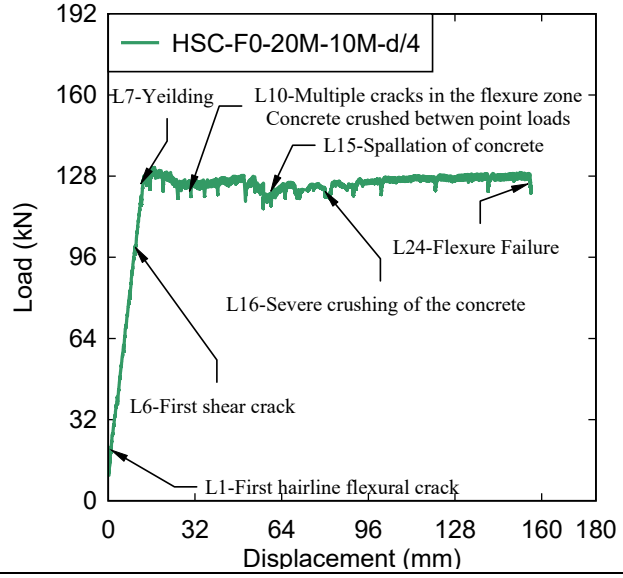

Data Summary

P_{max} (kN)	131
Δ_{end} (mm)	150
K (N/mm)	8333
$\frac{\Delta_{end}}{\Delta_{yield}}$	11.5
A_{max}	18889

b) Condition of the beam after static test

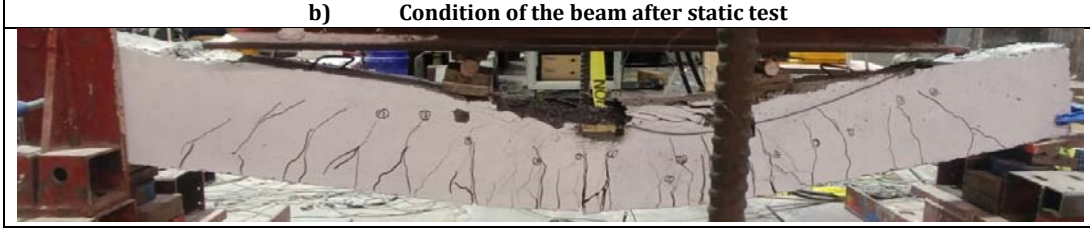

Failure Mechanism

Flexure failure: excessive deformation and spalling of top cover concrete

Figure 4-8 Residual test results for beam HSC-F0-20M-10M-d/4

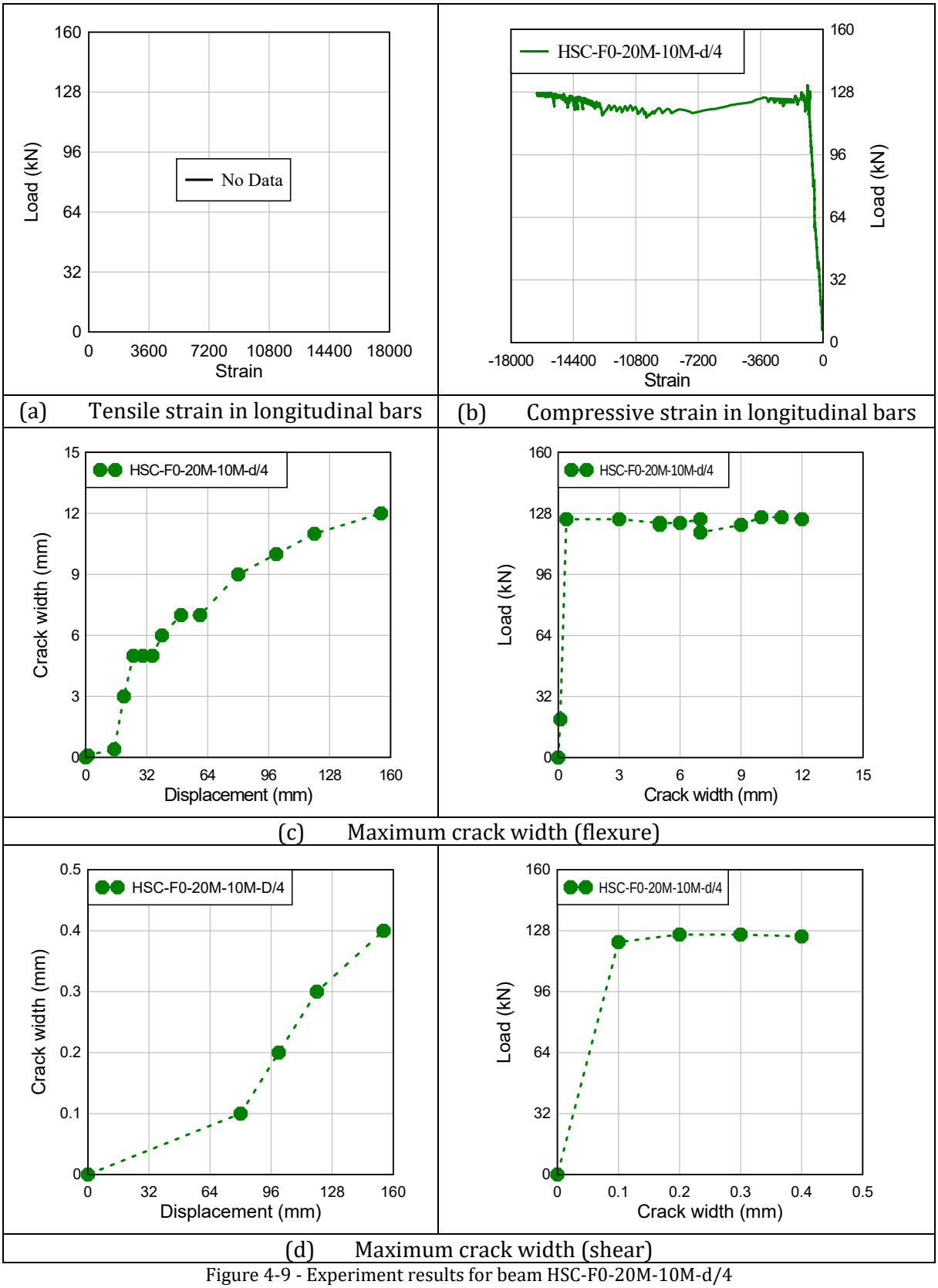

(a) Tensile strain in longitudinal bars

(b) Compressive strain in longitudinal bars

(c) Maximum crack width (flexure)

(d) Maximum crack width (shear)

Figure 4-9 - Experiment results for beam HSC-F0-20M-10M-d/4

Experimental Results			Comments
Load stage	2P (kN)	Mid-span deflection (mm)	First hairline crack appeared in the flexure zone
L1	20.0	1.5	
			
Load stage	2P (kN)	Mid-span deflection (mm)	Yielding of the longitudinal bars Flexure-shear cracks form in the shear spans
L7	125.0	15.0	
			
Load stage	2P (kN)	Mid-span deflection (mm)	Sudden crushing of the top cover concrete in the constant moment region
L18	122.0	80.0	
			
Load stage	2P (kN)	Mid-span deflection (mm)	Large deflection with spallation of cover concrete. Excessive deformation. Beam still carrying load.
L24	125.0	150.0	
			
Left		Right	
			

Figure 4-10 - Major events for specimen HSC-F0-20M-10M-d/4

4.3.2 HSC-F0.75-20M-10M-D/2

The second beam in the 20M series was designed with high strength fiber reinforced concrete with identical properties to the previous beam except for the use of intermediate ties (closed hoops, spaced at d/2 =100 mm), and fibers added at 0.75% by volume of concrete. The results are shown in **Table 4-1** and **Figure 4-11** to **Figure 4-13**.

The addition of fibers controlled early cracks, with flexural cracks appearing at a later stage (L2: displacement of 2.8 mm and a load of 40kN) when compared to the two previous beams. The yield (P_{yield}) and maximum (P_{max}) load recorded were 160 kN (15 mm) and 168 kN (25 mm), respectively. As seen in **Figure 4-11**, the load-displacement curve showed a rapid decrease in the load capacity after the peak, with the load reduced by 29 % (130 kN) at a displacement of 40 mm. This sudden drop is the result of gradual concrete crushing in the midspan compression zone. Thus, this specimen behaved differently when compared to the plain HSC beam with blast detailing, which kept the load constant until the end of testing. As testing continued, the load capacity of the beam continued to decrease, and the beam failed in flexure at a displacement of 100 mm (88 kN). As seen in **Figure 4-13**, the beam suffered severe crushing in compression with buckling of the top compression (10M) bars. In addition, the maximum localized crack width reached 25 mm, however, unlike the 15M series beam, bar rupture did not occur. The results demonstrate the importance of tie spacing in doubly-reinforced beams, even when using HSFRC.

a) Load – Mid-Span Deflection

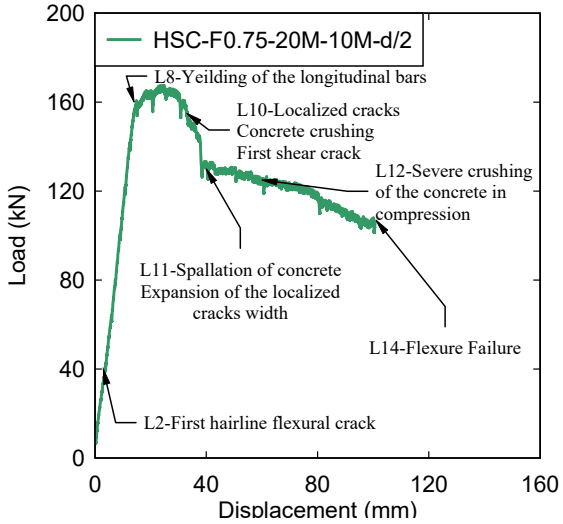

Data Summary	
P_{max} (kN)	168
Δ_{end} (mm)	100
K (N/mm)	10667
$\frac{\Delta_{end}}{\Delta_{yield}}$	6.8
A_{max}	12494

b) Condition of the beam after static test

Failure Mechanism
Flexure failure: crushing of concrete in compression with localized cracking

Figure 4-11 Residual test results for beam HSC-F0.75-20M-10M-d/2

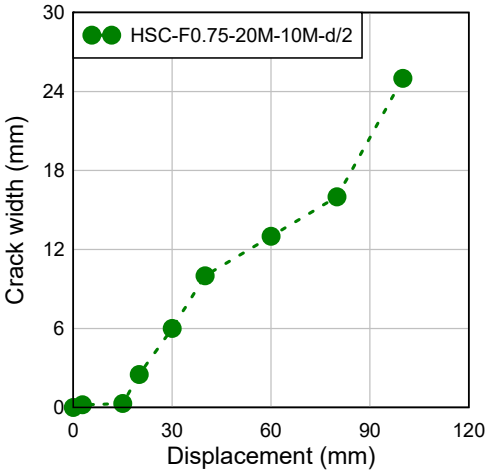

(a) Tensile strain in longitudinal bars

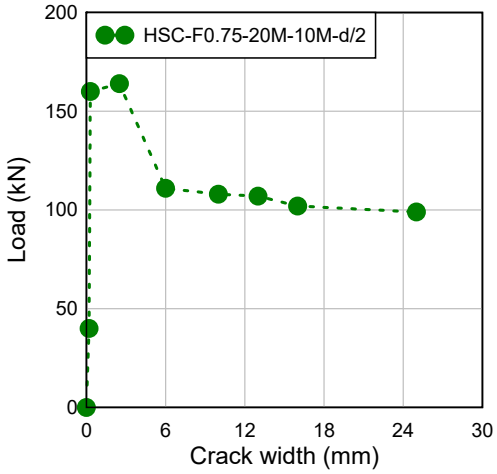

(b) Compressive strain in longitudinal bars

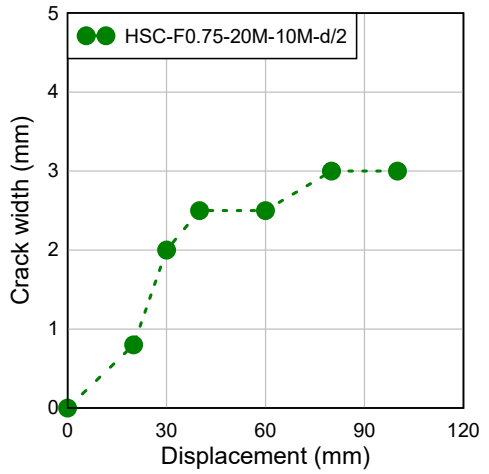

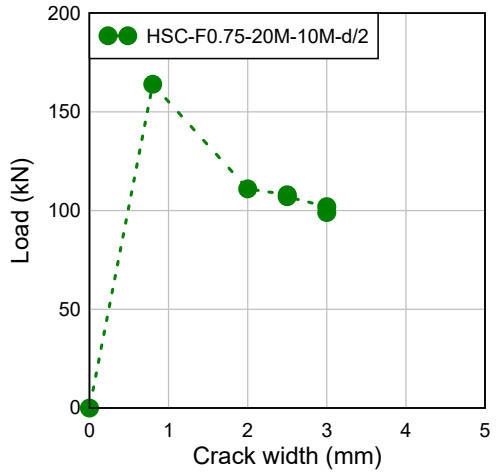

(c) Maximum crack width (flexure)

Figure 4-12 - Experiment results for beam HSC-F0.75-20M-10M-d/2

<table>
<tr><th colspan="3">Experimental Results</th><th>Comments</th></tr>
<tr><td>Load stage</td><td>2P (kN)</td><td>Mid-span deflection (mm)</td><td rowspan="3">First hairline cracks</td></tr>
<tr><td>L2</td><td>40</td><td>2.8</td></tr>
<tr><td colspan="3">  </td></tr>
<tr><td>Load stage</td><td>2P (kN)</td><td>Mid-span deflection (mm)</td><td rowspan="3">Propagation of flexural and shear cracks</td></tr>
<tr><td>L8</td><td>160</td><td>17</td></tr>
<tr><td colspan="3">  </td></tr>
<tr><td>Load stage</td><td>2P (kN)</td><td>Mid-span deflection (mm)</td><td rowspan="3">Localized cracking and crushing of concrete in constant moment region</td></tr>
<tr><td>L11</td><td>130</td><td>40</td></tr>
<tr><td colspan="3">  </td></tr>
<tr><td>Load stage</td><td>2P (kN)</td><td>Mid-span deflection (mm)</td><td rowspan="3">Further crushing and crack localization</td></tr>
<tr><td>L12</td><td>125</td><td>60</td></tr>
<tr><td colspan="3">  </td></tr>
<tr><td>Load stage</td><td>2P (kN)</td><td>Mid-span deflection (mm)</td><td rowspan="3">Crushing, severe crcak localization and bar buckling</td></tr>
<tr><td>L14</td><td>107</td><td>100</td></tr>
<tr><td colspan="3">   </td></tr>
</table>

Figure 4-13 - Major events for specimen Hybrid-HSC-F0.75-20M-10M-d/2

4.4 RESULTS OF THE 25M SERIES

4.4.1 HSC-F0-25M

The 25M series included three beams. This beam was designed with plain high strength concrete and singly-reinforced with 2-25M longitudinal bars and nominal detailing. Transverse reinforcement consisted of 6M U-shaped stirrups spaced at 100 mm in the shear spans only. **Table 4-1** provides the results of the beam while **Figure 4-14** to **Figure 4-16** show the static response of the beam

The first flexural hairline cracks were observed when the applied load reached 30 kN (2.7 mm). The continuous application of loads generated multiple flexural cracks, with the first diagonal shear cracks appearing at 11.5 mm (120 kN). At 16 mm (180 kN), the concrete started to crush under the loading plate. Shortly thereafter, the specimen experienced a sudden shear failure at a maximum load (P_{max}) of 202 kN and corresponding displacement (Δ_{end}) of 18.2 mm. The tension bars (2-25M) never yielded which resulted in zero ductility, though the strain data indicates that the strains were closed to yield. The results demonstrate the importance of providing sufficient transverse reinforcement in HSC beams, especially as the tension steel ratio increases.

a) Load – Mid-Span Deflection

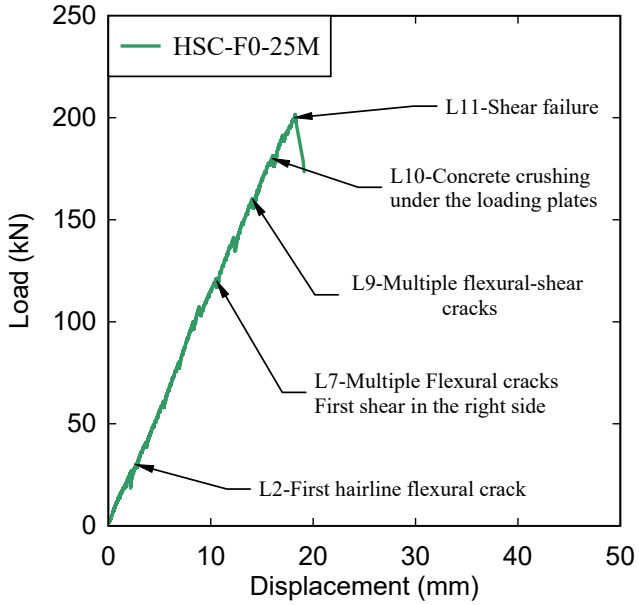

Data Summary	
P_{max} (kN)	202
Δ_{end} (mm)	18
K (N/mm)	11098
$\frac{\Delta_{end}}{\Delta_{yield}}$	-
A_{max}	1920

b) Condition of the beam after static test

Failure Mechanism
Shear

Figure 4-14 Residual test results for beam HSC-F0-25M

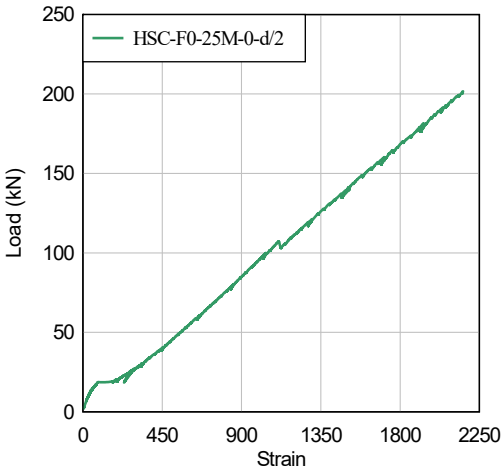

(a) Tensile strain in longitudinal bars

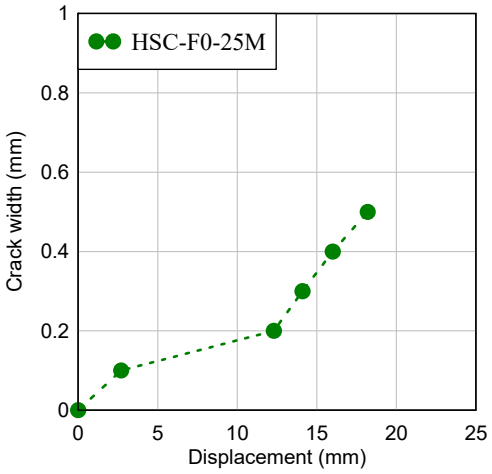

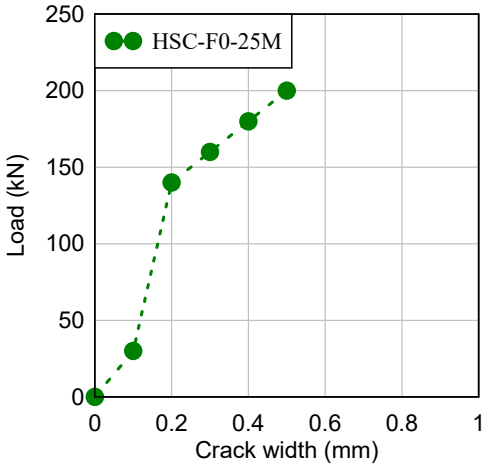

(b) Maximum crack width (flexure)

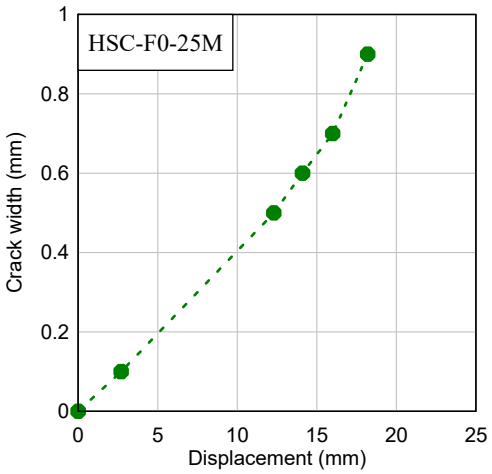

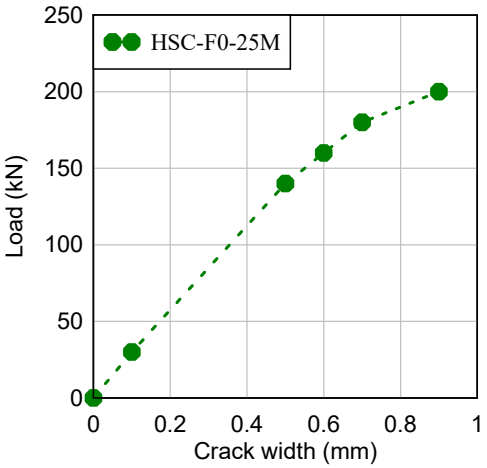

(c) Maximum crack width (Shear)

Figure 4-15 - Experiment results for beam HSC-F0-25M

<table>
<tr><th colspan="3">Experimental Results</th><th>Comments</th></tr>
<tr><td>Load stage</td><td>2P (kN)</td><td>Mid-span deflection (mm)</td><td rowspan="3">First hairline crack appeared in the flexure zone</td></tr>
<tr><td>L2</td><td>30.0</td><td>2.7</td></tr>
<tr><td colspan="3">  </td></tr>
<tr><td>Load stage</td><td>2P (kN)</td><td>Mid-span deflection (mm)</td><td rowspan="3">Flexure-shear cracks are formed in the shear spans

Crack width in the flexure zone reached 0.6mm</td></tr>
<tr><td>L9</td><td>160</td><td>14.1</td></tr>
<tr><td colspan="3">  </td></tr>
<tr><td>Load stage</td><td>2P (kN)</td><td>Mid-span deflection (mm)</td><td rowspan="3">Concrete started crushing where the point load is applied</td></tr>
<tr><td>L10</td><td>180</td><td>16</td></tr>
<tr><td colspan="3">  </td></tr>
<tr><td>Load stage</td><td>2P (kN)</td><td>Mid-span deflection (mm)</td><td rowspan="3">Sudden Shear-Compression in the shear span zone</td></tr>
<tr><td>L11</td><td>200.0</td><td>18.2</td></tr>
<tr><td colspan="3">  </td></tr>
<tr><td colspan="4">Shear Failure</td></tr>
<tr><td colspan="4">  </td></tr>
</table>

Figure 4-16 - Major events for specimen HSC-F0-25M

4.4.2 HSC-F0-25M-10M-D/4

This specimen was the second beam tested in the 25M Series. Unlike the previous specimen, this beam was detailed according to the requirements of the CSA S850 standard. In particular, the beam was doubly-reinforced, with 25M bars in tension and 10M bars in compression, and ties spaced at 50 mm (d/4). The results for this beam are presented in **Figure 4-17** to **Figure 4-19.**

At a displacement of 3.4 mm (40 kN), the first hairline cracks were recorded in the flexure region. The number of flexural and flexural shear cracks increased with the application of loads and resulted in the yielding of the tensile reinforcement at 19.2 mm (P_{yield} =220 kN). Thus, the blast detailing prevented shear failure when compared to the previous beam which failed at (P_{max}) 202 kN. Shortly after yielding, a sudden drop in the load occurred at 25mm (209 kN) due to concrete crushing. The closely spaced ties ensured the stability of the compression bars and confinement of core concrete which allowed for a sustained post-yield response and high ductility despite the high-tension steel ratio. Nonetheless, the high strain demands on the compression zone combined with the relatively small diameter compression bars resulted in buckling of the compression steel at 73 mm (210 kN). As a result, the load capacity rapidly decreased and displayed behavior which was different than the 15M and 20M blast detailed beams. The specimen failed in flexure at a displacement (Δ_{end}) of 120 mm (104.21 kN). The results demonstrate the beneficial effects of blast detailing while also pointing to the importance of increasing the compression steel ratio (bar size) in heavily-reinforced HSC beams.

a) Load – Mid-Span Deflection

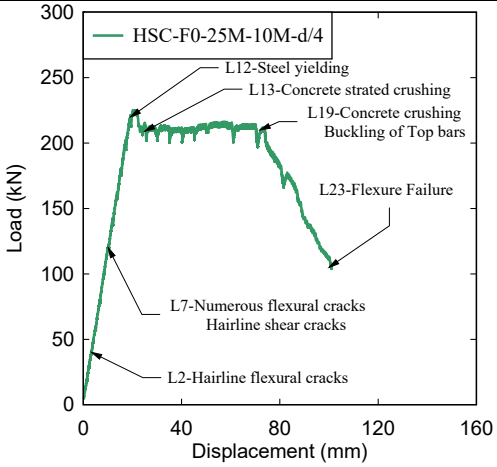

Data Summary	
P_{max} (kN)	225
Δ_{end} (mm)	120
K (N/mm)	11458
$\frac{\Delta_{end}}{\Delta_{yield}}$	6.25
A_{max}	19734

b) Condition of the beam after static test

Failure Mechanism
Flexure failure, excessive deflection, with severe crushing and buckling of compression bars

Figure 4-17 Residual test results for beam HSC-F0-25M-10M-d/4

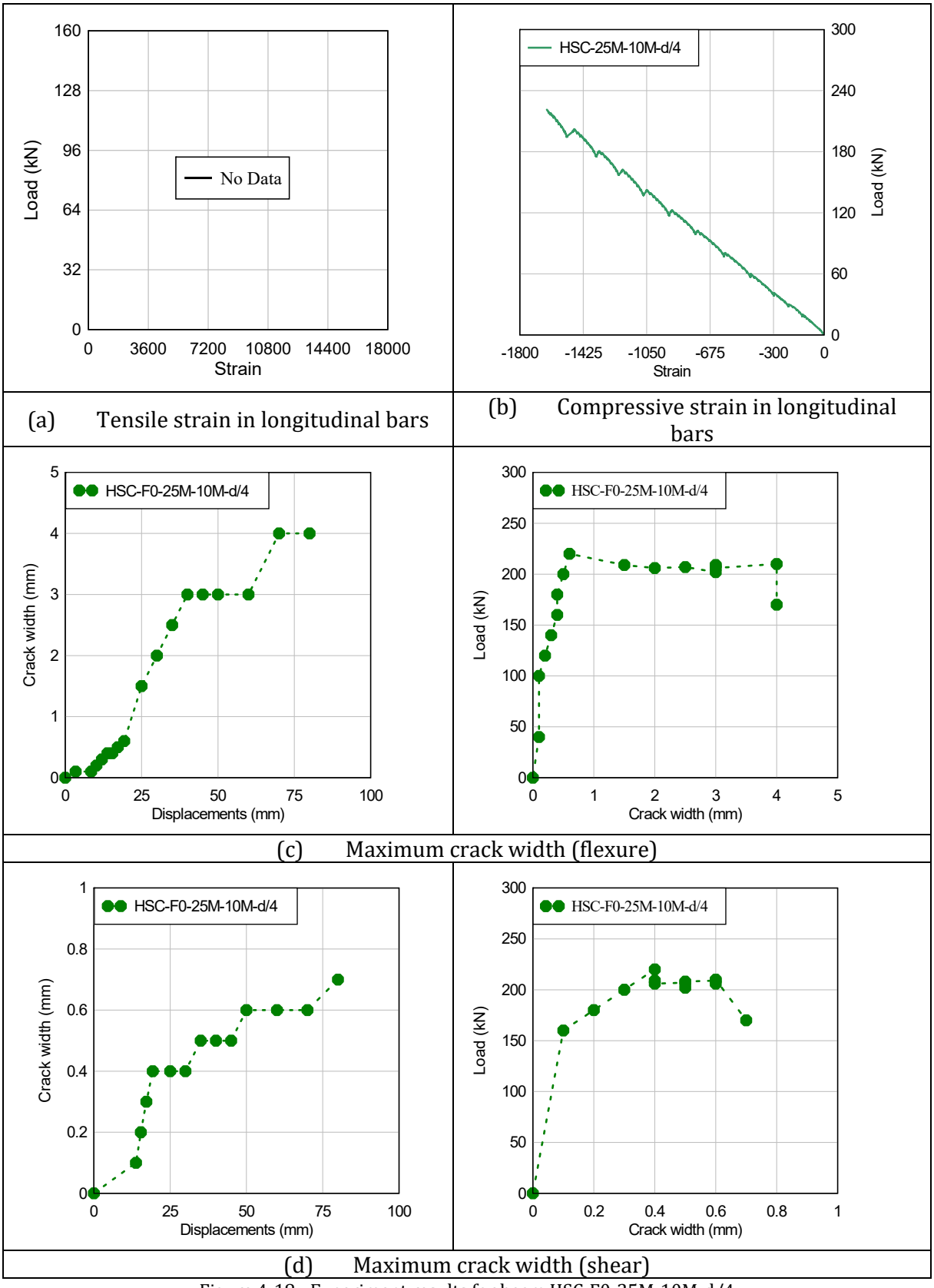

Figure 4-18 - Experiment results for beam HSC-F0-25M-10M-d/4

<table>
<tr><th colspan="3">Experimental Results</th><th>Comments</th></tr>
<tr><td>Load stage</td><td>2P (kN)</td><td>Mid-span deflection (mm)</td><td rowspan="3">The first hairline crack appeared in the flexure region</td></tr>
<tr><td>L3</td><td>40.0</td><td>3.4</td></tr>
<tr><td colspan="3">  </td></tr>
<tr><td>Load stage</td><td>2P (kN)</td><td>Mid-span deflection (mm)</td><td rowspan="3">Compression steel reinforcement yielding

Development of flexural-shear cracks</td></tr>
<tr><td>L12</td><td>220</td><td>19.5</td></tr>
<tr><td colspan="3">  </td></tr>
<tr><td>Load stage</td><td>2P (kN)</td><td>Mid-span deflection (mm)</td><td rowspan="3">Concrete began to crush between the two-point loads

Load started to decrease rapidly</td></tr>
<tr><td>L19</td><td>206.0</td><td>73.0</td></tr>
<tr><td colspan="3">  </td></tr>
<tr><td>Load stage</td><td>2P (kN)</td><td>Mid-span deflection (mm)</td><td rowspan="3">Beam Failure in Flexure

Concrete is severely crushed in between the two points loads; compression bars are buckled</td></tr>
<tr><td>L23</td><td>104.0</td><td>120</td></tr>
<tr><td colspan="3">  </td></tr>
<tr><td colspan="4">Buckling of the compression bars</td></tr>
<tr><td colspan="4">   </td></tr>
</table>

Figure 4-19 - Major events for specimen HSC-F0-25M-10M-d/4

4.4.3 HSC-F0.75-25M-10M-D/2

This specimen was the last beam tested under static loads and was built with 25M bars like the previous specimen but was built with high strength fibers reinforced concrete and intermediate ties spaced at s = 100 mm (d/2). The summary of the test results is provided in **Table 4-1** and **Figure 4-20** to **Figure 4-22**.

The first hairline cracks appeared in the flexure zone at an applied load of 50kN (3.2 mm) representing an increase when compared to the previous beam. As seen in **Figure 4-20,** the addition of fibers also allowed for increased yield (P_{yield}) and maximum (P_{max}) loads when compared to the previous beam, reaching 240 kN (19.3mm) and 248 kN (21 mm), respectively. The beam experienced visible macro fiber pullout in the tension region at a displacement of 35 mm (225 kN), which was followed by buckling of the top 10M bars at 67 mm (215 kN). Despite this, the hybrid confining effect of the intermediate ties and fibers increased the overall performance of the beam when compared to the companion beam designed with blast detailing. The beam showed large deflections with concrete crushing in the constant moment region and failed in flexure at a large deformation (Δ_{end}) of 125 mm (90 kN).

a) Load – Mid-Span Deflection

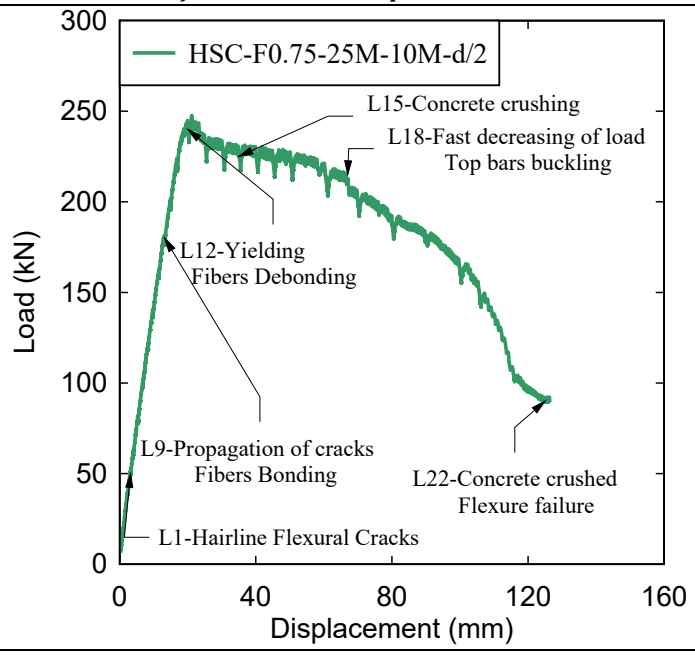

Data Summary	
P_{max} (kN)	248
Δ_{end} (mm)	125
K (N/mm)	12435
$\frac{\Delta_{end}}{\Delta_{yield}}$	6.47
A_{max}	22811

b) Condition of the beam after static test

Failure Mechanism
Flexure failure with crushing and buckling of top compression bars

Figure 4-20 Residual test results for beam HSC-F0-25M-10M-d/2

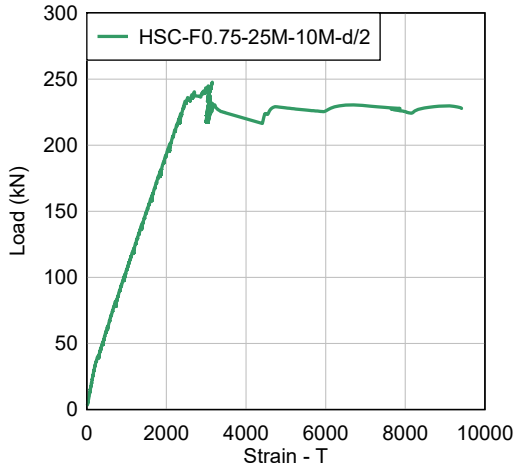

(a) Tensile strain in longitudinal bars

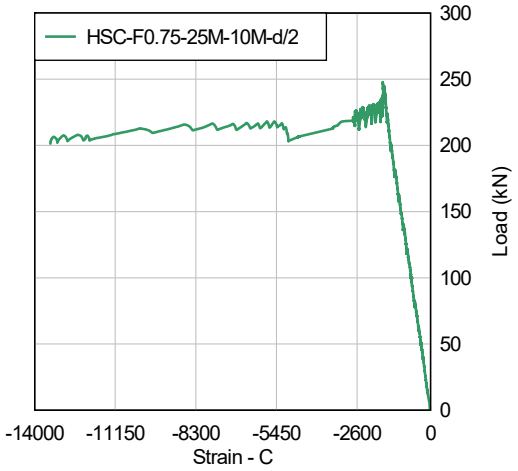

(b) Compressive strain in longitudinal bars

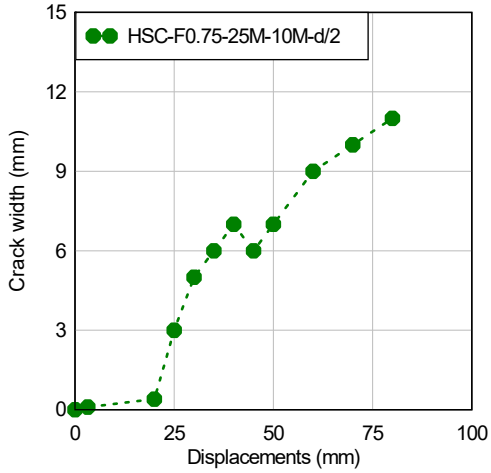

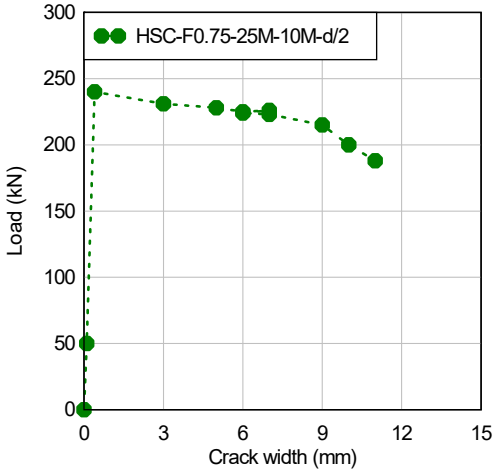

(c) Maximum crack width (flexure)

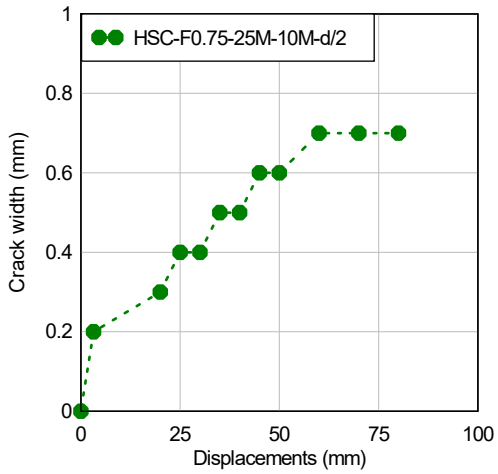

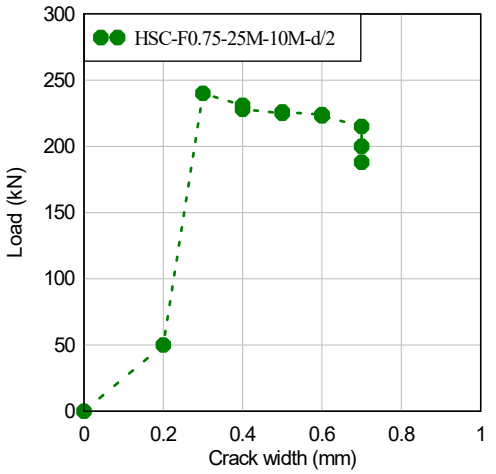

(d) Maximum crack width (Shear)

Figure 4-21 - Experiment results for beam HSC-F0.75-25M-10M-d/2

<table>
<tr><th colspan="3">Experimental Results</th><th>Comments</th></tr>
<tr><td>Load stage</td><td>2P (kN)</td><td>Mid-span deflection (mm)</td><td rowspan="3">First hairline crack showed in the flexure zone</td></tr>
<tr><td>L1</td><td>50.0</td><td>3.2</td></tr>
<tr><td colspan="3">  </td></tr>
<tr><td>Load stage</td><td>2P (kN)</td><td>Mid-span deflection (mm)</td><td rowspan="3">Propagation of cracks in the flexure zone
Shear cracks appeared in both shear spans</td></tr>
<tr><td>L9</td><td>180.0</td><td>13.2</td></tr>
<tr><td colspan="3">  </td></tr>
<tr><td>Load stage</td><td>2P (kN)</td><td>Mid-span deflection (mm)</td><td rowspan="3">Further propagation of cracking

Yielding of the longitudinal reinforcement</td></tr>
<tr><td>L15</td><td>225.0</td><td>35.0</td></tr>
<tr><td colspan="3">  </td></tr>
<tr><td>Load stage</td><td>2P (kN)</td><td>Mid-span deflection (mm)</td><td rowspan="3">Concrete in midspan region started crushing

Load started to decrease slowly</td></tr>
<tr><td>L18</td><td>223.0</td><td>50.0</td></tr>
<tr><td colspan="3">  </td></tr>
<tr><td>Load stage</td><td>2P (kN)</td><td>Mid-span deflection (mm)</td><td rowspan="3">Cracks fully extended to compression zone

Concrete in compression crushing despite fibers

Flexure Failure of the beam with bar buckling</td></tr>
<tr><td>L22</td><td>90.0</td><td>125.0</td></tr>
<tr><td colspan="3">  </td></tr>
<tr><td colspan="4">Buckling of the compression bars</td></tr>
<tr><td colspan="4">   </td></tr>
</table>

Figure 4-22 - Major events for specimen Hybrid-HSC-F0-25M-10M-d/2

CHAPTER 5: EXPERIMENTAL RESULTS - DYNAMIC TESTS

5.1 CHAPTER OVERVIEW

This chapter presents the experimental data collected for the ten beams tested under dynamic blast loading. **Section 5.2** provides a general summary of the data collected for each beam which includes the shockwave properties and beam response in terms of mid-span displacements, support rotation, and dynamic reactions. **Section 5.3** presents a detailed summary for each specimen, describing the results after each test shot and presenting additional data which includes pressure-impulse & pressure-displacement time histories, test photos, dynamic reactions, strain data, and residual load-deflection test results.

5.2 SUMMARY OF RESULTS OF EXPERIMENTS

Table 5-2 provides a summary of the dynamic test results including the shockwave parameters and the response of the beams after each blast. The blast properties include the driver pressure (P_d), reflected pressure (P_r), reflected impulse (I_r), positive phase duration (t_p) as defined in **Figure 5-1a**. Beam response is summarized in terms of maximum displacement (D_{max}), maximum support rotation (θ_{max}) and residual displacement (D_{res}) as illustrated in **Figure 5-1b.** It is noted that the displacements (maximum and residual) values presented are not cumulative. Finally, the peak dynamic load (P_{max}^D), corresponding to the sum of the dynamic reactions is also reported.

Table 5-2 also compares the experimental support rotations with the Response Limits (B1-B4) and Component Damage Levels in the CSA S850 standard (see **Table 5-1**). The response limits in the CSA S850 standard correspond to different support rotations (θ_{max}) or ductility ratios (μ_{max}). For singly-reinforced and doubly-reinforced beams, limits B1, B2, B3 and B4 are equivalent to $\mu_{max} = 1$, $\theta_{max} = 2°$ and 4°, $\theta_{max} = 5°$ and 6°, and $\theta_{max} = 10°$, respectively, with component damage levels given as: "Blowout" (greater than B4), "Hazardous failure" (between B4 and B3); "Heavy" (between B3 and B2); "Moderate" (between B2 and B1) and "Superficial" (less than B1).

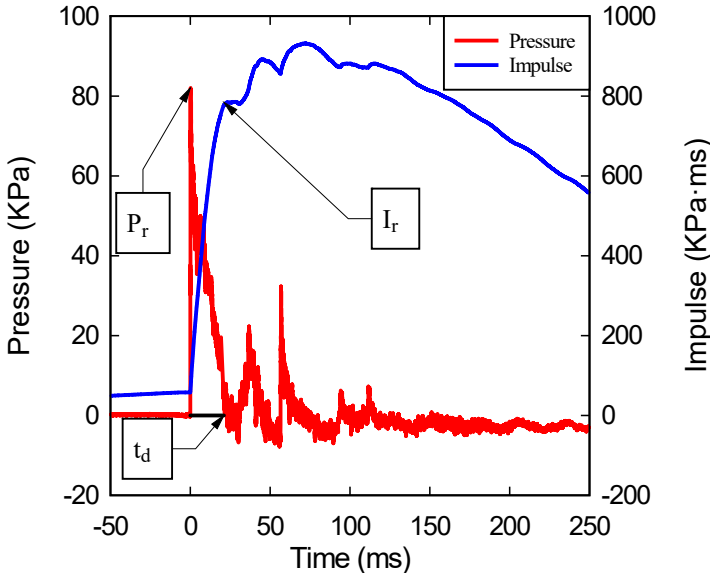

(a) Sample pressure and impulse time histories

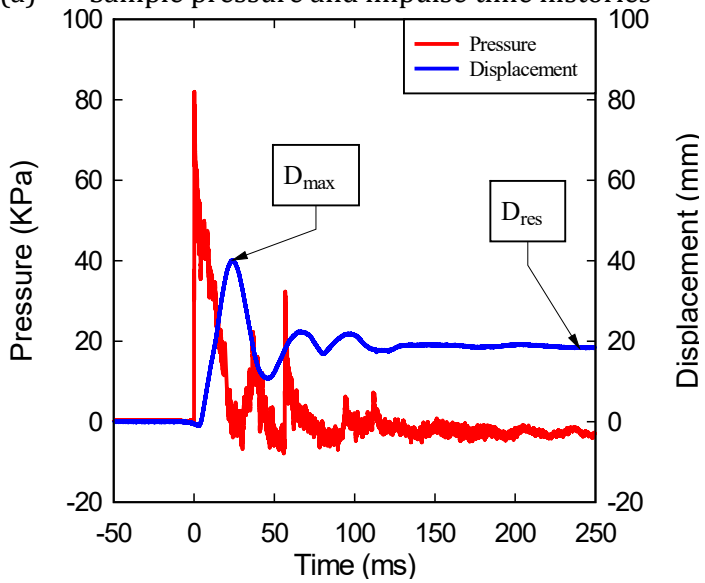

(b) Sample pressure and displacement time histories

Figure 5-1 - Blast A: Reflected pressure, impulse, and displacement time histories

Table 5-1 - CSA S850 Response Limits and Component Damage levels

Single-reinforced beam	**Double-reinforced beam**	**Response Limit**	**Expected Damage Level**
Angle	**Angle**		
θ <1°	θ <1°	<B1	Superficial
1°≤ θ <2°	1°≤ θ <4°	B2-B1	Moderate
2°≤ θ <5°	4°≤ θ <6°	B2-B3	Heavy
5°≤ θ <10°	6°≤ θ <10°	B3-B4	Hazardous
θ ≥ 10°	θ ≥ 10°	≥ B4	Blowout

Table 5-2- Dynamic Testing Data Summary

Beam ID	Blast ID	Driver pressure kPa (psi)	Shockwave properties			Displacement		Angle	Dynamic Reaction	Observed Damage	CSA S850 Response Limits and Component Damage[1]	
			P_r (kPa)	I_r (kPa-ms)	t_d (ms)	D_{max} (mm)	D_{res} (mm)	θ_{max} (°)	P_{max} (kN)		Response Limit	Expected Damage Level
HSC-F0-15M*	A	207 (30)	42.9	340.7	15.9	21.4	4.7	1.1	‡	Moderate Damage, F & S Cracks	B2-B1	Moderate
	B	345 (50)	58.6	516.0	17.6	124.0	22.0	6.4	‡	Extreme Damage, Concrete crushing	B3-B4	Hazardous
HSC-F0-20M*	A	207 (30)	39.2	360.0	18.4	15.1	0.2	0.8	‡	Moderate Damage, F & S Cracks	<B1	Superficial
	B	345 (50)	57.4	538.2	18.8	32.9	12.4	1.7	‡	Limited Damage, Flexural Cracks	B2-B1	Moderate
	C	483 (70)	68.8	702.6	20.4	118.1	71.7	6.1	‡	Extreme Damage, Concrete crushing	B3-B4	Hazardous
HSC-F0- 25M	C	483 (70)	78.5	746.2	20.6	30.9	5.1	1.5	217.3	Moderate Damage, F & S Cracks	B2-B1	Moderate
	D	621 (90)	91.4	1007.7	26.7	185.4	-	8.6	-	Extreme Damage, Concrete crushing	B3-B4	Hazardous
HSC-F0-15M-10M-d/4	A	207 (30)	46.3	372.9	19.8	17.7	4.2	0.9	103.7	Limited Damage, Flexural Cracks	<B1	Superficial
	B	345 (50)	57.8	582.4	21.3	33.1	18.0	1.6	135.8	Moderate Damage, F & S Cracks	B2-B1	Moderate
	C	483 (70)	70.8	701.4	21.4	63.4	45.2	3.0	134.7	Concrete crushing and Cover spalling	B2-B1	Moderate
HSC-F0-15M-10M-d/4[x1]	C	483 (70)	69.8	711.9	21.0	61.6	42.4	2.9	125.4	Moderate Damage, Cracks opening	B2-B1	Moderate
HSC-F0.75-15M-10M-d/2	A	207 (30)	33.4	335.5	19.3	10.8	1.1	0.5	93.7	No Damage, Few Hairlines Cracks	<B1	Superficial
	B	345 (50)	55.9	565.0	21.6	28.6	12.0	1.4	142.4	Limited Damage, Flexural Cracks	B2-B1	Moderate
	C	483 (70)	70.1	730.7	23.6	58.5	34.5	2.8	158.5	Moderate Damage, fiber pull-out	B2-B1	Moderate
	D	621 (90)	86.3	921.2	21.9	70.1	53.1	3.3	140.7	Moderate Damage, Crack localization	B2-B1	Moderate
HSC-F0-20M-6M-d/2	A	207 (30)	45.0	486.9	28.1	10.6	0.8	0.5	103.7	Limited Damage, Flexural Cracks	<B1	Superficial
	C	483 (70)	82.0	784.4	20.6	40.2	18.2	1.9	135.8	Moderate Damage, F & S Cracks	B2-B1	Moderate
	D	621 (90)	76.9	973.6	23.0	123.4	72.9	5.8	134.7	Extreme Damage, Concrete crushing	B3-B2	Heavy
HSC-F0-20M-10M-d/2	A	207 (30)	42.9	402.6	20.7	12.1	1.4	0.6	103.9	Limited Damage, Flexural Cracks	<B1	Superficial
	C	483 (70)	74.7	881.1	28.8	37.4	19.8	1.8	178.8	Moderate Damage, F & S Cracks	B2-B1	Moderate
	D	621 (90)	93.0	1099.4	29.4	72.4	49.7	3.5	170.7	Concrete crushing and Cover spalling	B2-B1	Moderate
HSC-F0-20M-10M-d/4	A	207 (30)	45.1	370.4	19.1	11.5	1.7	0.6	103.9	Limited Damage, Flexural Cracks	<B1	Superficial
	C	483 (70)	74.9	703.9	21.1	34.6	17.3	1.7	178.8	Moderate Damage, F & S Cracks	B2-B1	Moderate
	D	621 (90)	88.7	837.2	20.2	71.6	48.2	3.4	170.7	Concrete crushing and Cover spalling	B2-B1	Moderate
HSC-F0.75- 20M-10M-d/2	A	207 (30)	43.1	315.0	18.6	11.1	1.2	0.2	81.5	No Damage, Few Hairlines Cracks	<B1	Superficial
	C	483 (70)	68.7	706.5	21.3	36.5	15.2	1.1	217.3	Limited Damage, Flexural Cracks	B2-B1	Moderate
	D	621 (90)	89.9	896.9	25.7	49.9	27.4	1.8	206.1	Moderate Damage, fiber pull-out	B2-B1	Moderate
HSC-F0- 25M-10M-d/4	C	483 (70)	72.1	819.0	26.9	26.5	2.3	0.6	251.0	Moderate Damage, F & S Cracks	B2-B1	Moderate
	D	621 (90)	97.7	1001.4	27.8	45.1	14.9	2.2	284.2	Concrete crushing and Cover spalling	B2-B1	Moderate
HSC-F0.75- 25M-10M-d/4	C	483 (70)	80.4	637.0	20.7	21.6	3.4	1.0	208.0	No Damage, Few Hairlines Cracks	B2-B1	Moderate
	D	621 (90)	85.2	945.2	25.9	36.6	12.8	1.7	283.4	Limited Damage, Flexural Cracks	B2-B1	Moderate
	E	690 (100)	89.3	1313.0	26.9	54.7	21.6	2.6	252.8	Moderate Damage, fiber pull-out	B2-B1	Moderate

[1]: Flexural cracking: F; Shear cracking: S; *: Beams tested by Algassem (2016), ‡: No available data

5.3 RESULTS OF THE 15M SERIES

5.3.1 HSC-F0-15M-10M-D/4

This beam was built with plain HSC and was designed in accordance with the detailing requirements of the CSA S850 standard. The beam was reinforced with 2 - 15M bars in tension and 2 -10M bars in compression, with closed ties spaced at 50 mm (s = d/4) throughout the beam span. This beam was subjected to three dynamic blast loads: A (30 psi), B (50 psi), and C (70 psi) as reported in **Table 5-2**. Additional results are presented in **Figure 5-2** to **Figure 5-4**.

Blast A (30 psi) was intended to bring the 15M bars close to yielding and resulted in maximum and residual displacements of D_{max} = 17.7 mm and D_{res} = 4.2 mm, with the formation of hairline cracking. Blast B (50 psi) resulted in the formation of further flexural and flexural-shear cracks which extended the full depth of the beam section. The displacements reached D_{max} = 33.1 mm and D_{res} = 18 mm after this blast. Blast C (70 psi) resulted in a loss of concrete cover in the mid-span compression region, with D_{max} = 63.4 mm corresponding to maximum support rotation of θ_{max}= 3.02° and D_{res} = 45.2 mm.

After the dynamic blast test, the residual capacity of the beam was tested under four-point quasi-static bending. **Figure 4-2** shows the residual response of the beam. Considering the initial residual deformation of 67.4 mm, the beam reached a peak load of P_{max}^{R} =107.5 kN (similar to the original undamaged, P_{max}=108.1 kN) and continued to carry load of P_{end}^{R}=103.9 kN up to a displacement of Δ_{max}^{R} =150.9 mm, with failure occurring due to crushing of concrete in the mid-span region, without bar buckling.

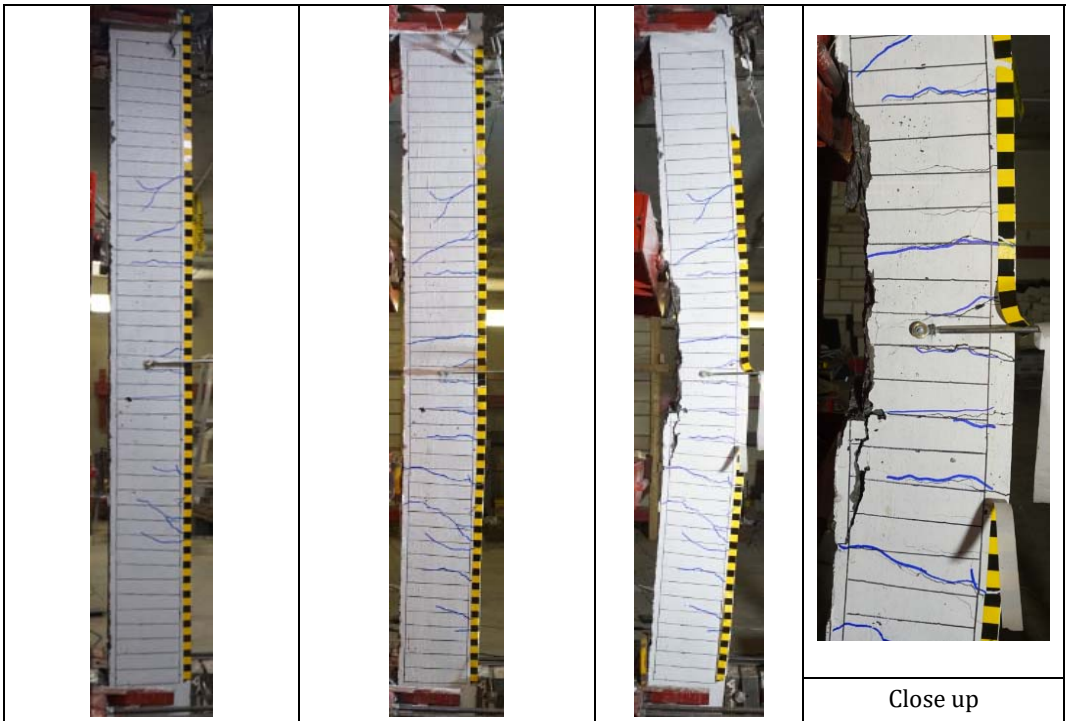

Figure 5-2 – HSC-F0-15M-10M-d/4 - Photographs at the end of Blasts A, B, and C

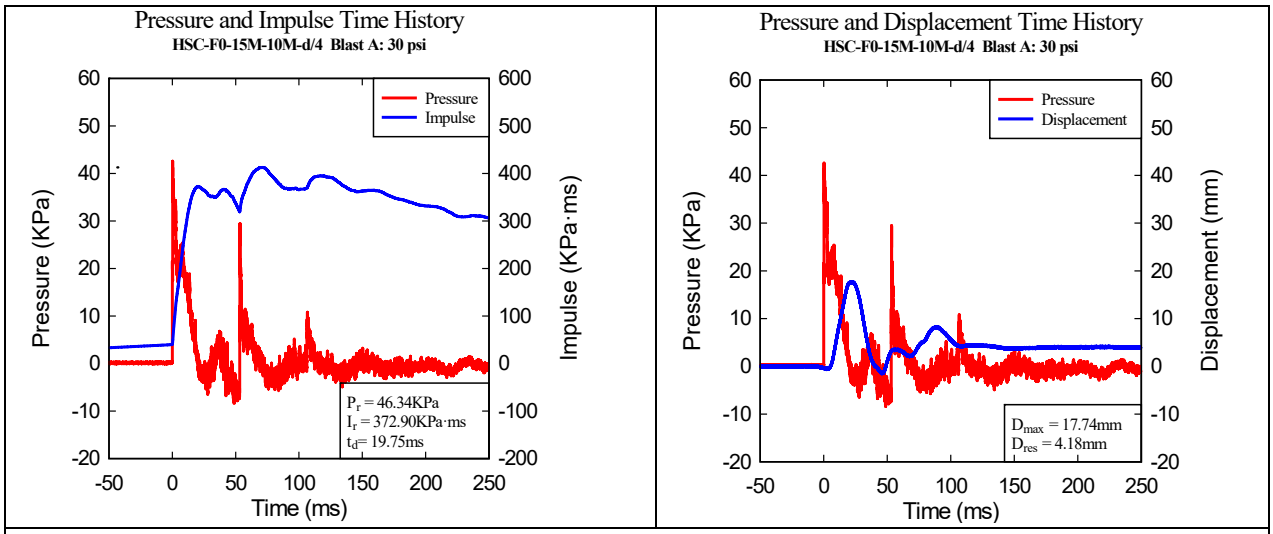

(a) Blast A: Reflected pressure, impulse, and displacement time histories

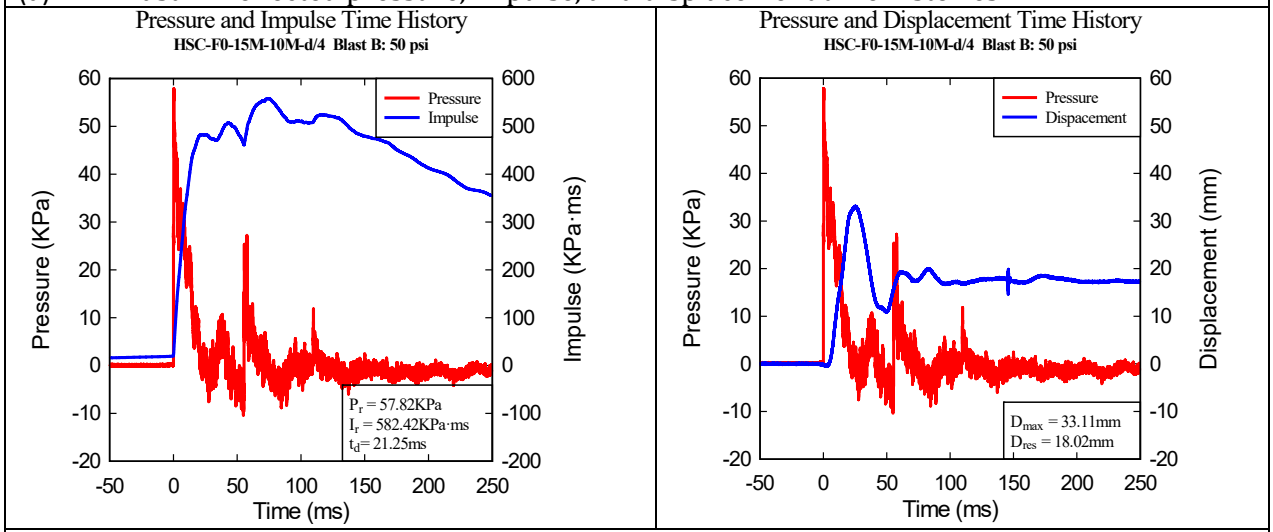

(b) Blast B: Reflected pressure, impulse, and displacement time histories

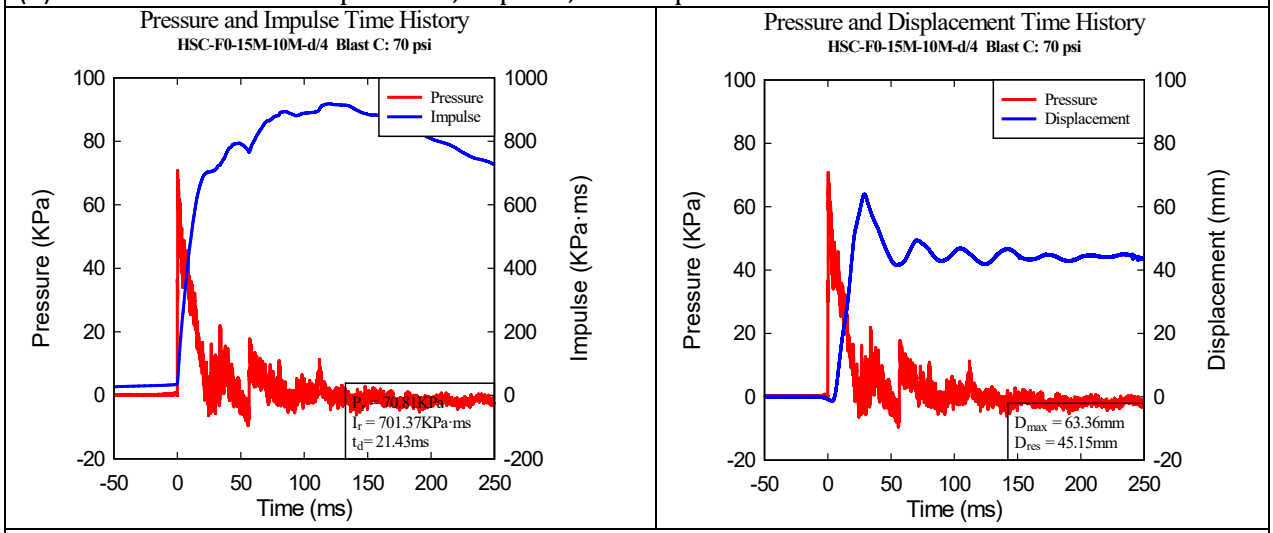

(c) Blast C: Reflected pressure, impulse, and displacement time histories

Figure 5-3 Recorded reflected pressure, impulse and displacement for Blasts A, B and C (HSC-F0-15M-10M-d/4)

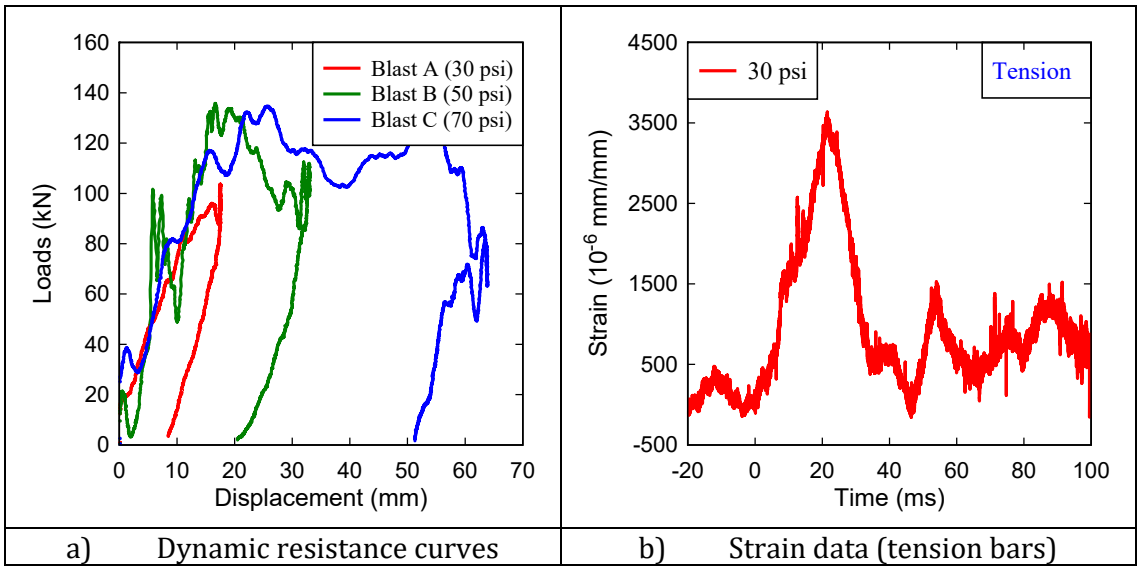

a) Dynamic resistance curves b) Strain data (tension bars)

Figure 5-4 Dynamic resistance curve and strain data (HSC-F0-15M-10M-d/4)

a) Residual test load-deflection result

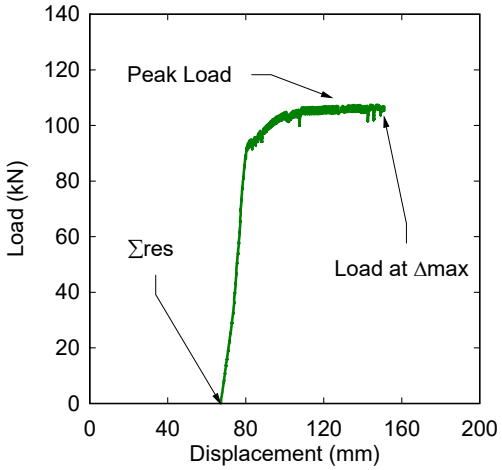

Data Summary	
∑res (mm)	63.2
P_{max}^{R} (kN)	107.5
Δ_{max}^{R} (mm)	150.9
P_{end}^{R} (kN)	103.9

b) Condition of the beam before residual test- after Blast C (70 psi)

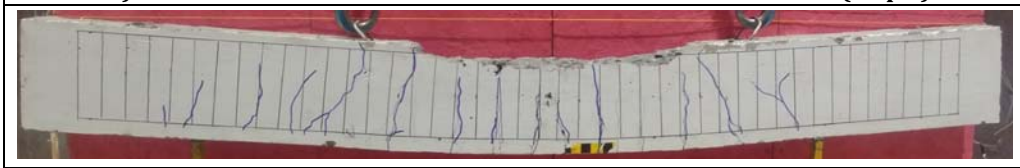

Comments

-After blast testing, the beam has lost the top cover concrete
-Maximum residual displacement of 63.36 mm

c) Condition of beam after Residual Test

Comments

-Beam is severely deformed but additional damage limited to growth and extension of cracks.
-Bars do not buckle
-Beam reached a maximum cumulative displacement of 158.75 mm

Figure 5-5 Residual test results for beam HSC-F0-15M-10M-d/4

5.3.2 HSC-F0- 15M-10M-D/4[X1]

This beam was identical to the previous beam but subjected to a single blast load of 70 psi (Blast C). Results are summarized in **Table 5-2** and **Figure 5-6** to **Figure 5-8**.

At Blast C, the beam suffered limited damages with concrete cracking in the constant moment region. Unlike the previous beam, this specimen did not experience spalling of concrete in the compression region. The maximum and residual displacements recorded during this test were D_{max} = 61.55 mm (θ_{max} = 2.9°) and D_{res} = 42.4 mm which were 3% and 6% lower compared to the beam tested under repeated blasts.

After blast testing, the beam was subjected tested under static loads to study its residual load-carrying capacity. The results for this test are provided in **Figure 5-9**. Taking into consideration the initial residual deformation (Δ_{res}=42.4 mm), the beam recorded a maximum load of P_{max}^{R} =102.9 KN, which represents 95% of the original (undamaged) beam capacity. The beam carried a load of P_{end}^{R}=95.2 kN at the end of testing at Δ_{max}^{R}=148.4 mm. The damage was limited to the top concrete cover and cracking.

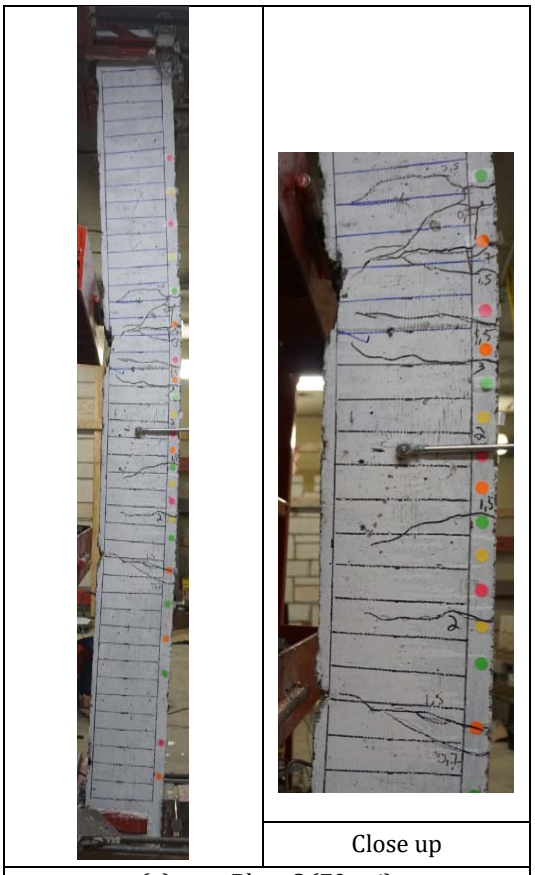

Close up

(a) Blast C (70 psi)

Figure 5-6 – HSC-F0-15M-10M-d/4[x1] - Photographs at the end of Blast C

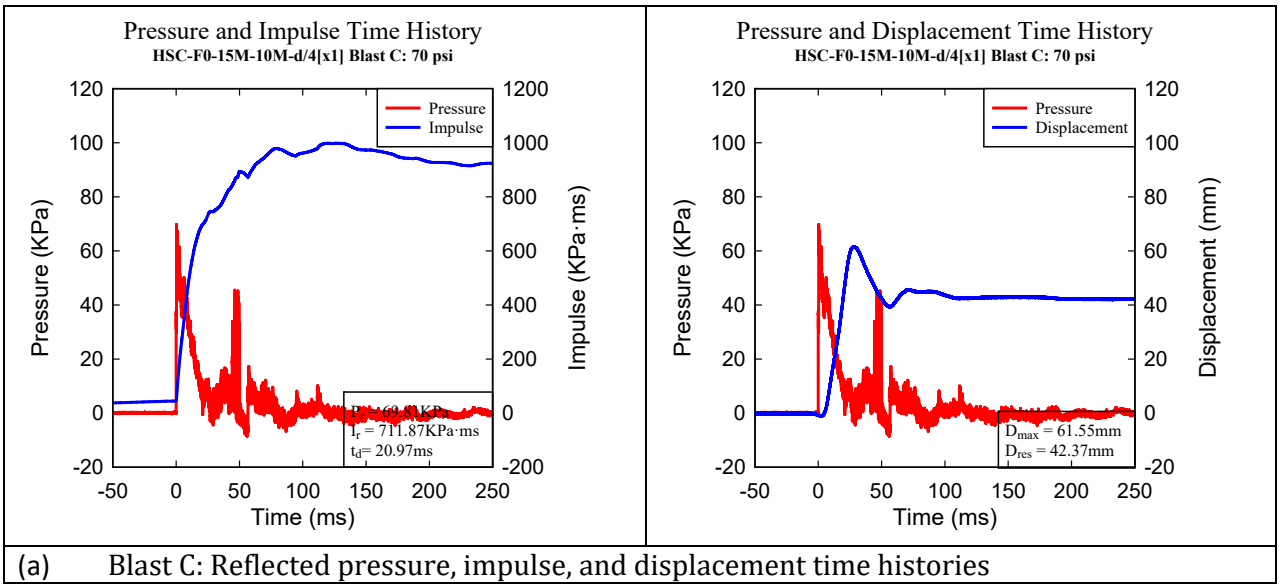

(a) Blast C: Reflected pressure, impulse, and displacement time histories

Figure 5-7 – Recorded reflected pressure, impulse, and displacement for Blasts A, B, and C (HSC-F0-15M-10M-d/4[x1])

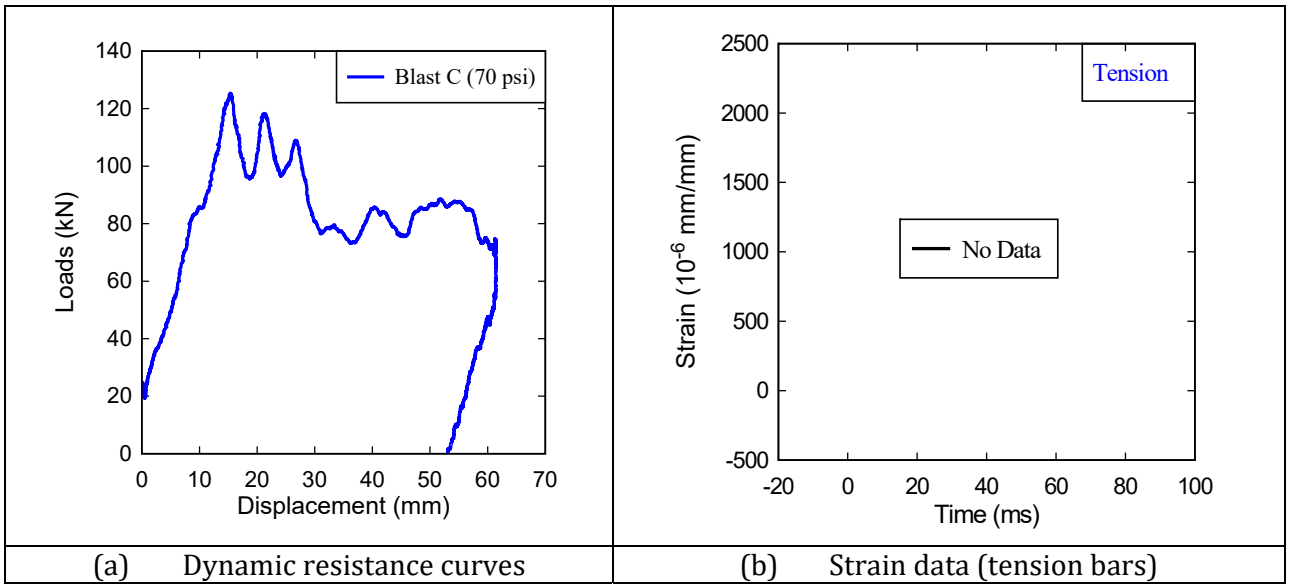

(a) Dynamic resistance curves (b) Strain data (tension bars)

Figure 5-8 – Dynamic resistance curve and strain data (HSC-F0-15M-10M-d/4[x1])

a) Residual test load-deflection result

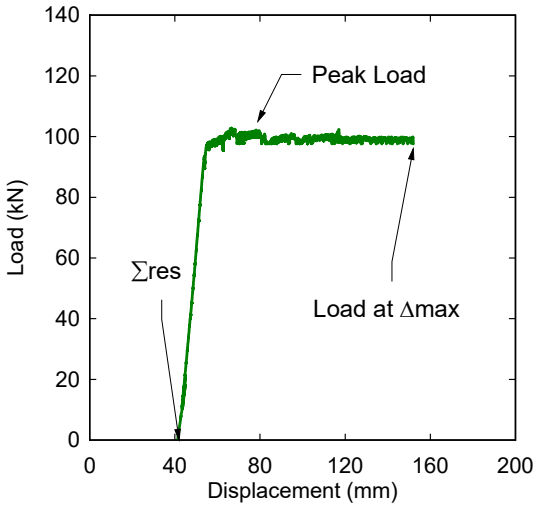

Data Summary	
∑res (mm)	42.4
$P_{max}{}^{R}$ (kN)	102.9
$\Delta_{max}{}^{R}$ (mm)	147.4
$P_{end}{}^{R}$ (kN)	97.6

b) Condition of beam before residual test- after Blast C (70 psi)

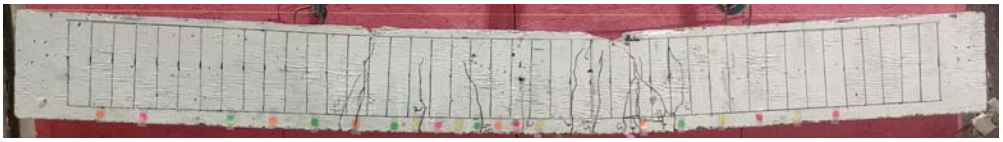

Comments

At end of blast testing beam shows cracking but no significant cover damage. Total residual displacement reaches 42.4 mm.

c) Condition of beam after Residual Test

Comments

Propagation of the flexural cracks.
Concrete cover crushes in the compression zone, with some cover spalling in tension region
Bar buckling does not occur

Figure 5-9 – Residual test results for beam HSC-F0-15M-10M-d/4[x1]

5.3.3 HSC-F0.75- 15M-10M-D/2

The third beam in the 15M series was built with HSFRC having 0.75% fibers with double-reinforcement (10M bars in compression) with intermediate ties spaced at 100 mm (d/2). Results are provided in **Table 5-2** and **Figure 5-10** to **Figure 5-12**. This specimen was subjected to four blast loads: A, B, C, and D (30, 50, 70 and 90 psi).

Blast A tested the beam within the elastic range, which resulted in the formation of hairline cracks in the flexural zone with displacements of D_{max} = 10.8 mm and D_{res} = 1.1 mm. Blast B pushed the specimen into the inelastic range, reaching displacements of D_{max} = 28.6 mm and D_{res} = 12.0 mm. Blast C inflicted moderate damages with lower displacements of D_{max} = 58.5 mm and D_{res} = 34.5 mm. Unlike the previous beams, this beam survived Blast C with damage limited to fiber pull-out at the location of the major cracks (cracks width: 5mm). Blast D was the final shot for this beam and resulted in maximum and residual displacements of D_{max} = 70.1 mm (θ_{max} = 2.3°) and D_{res} = 53.1 mm with crack localization with crack width of 15 mm. The fibers were effective in controlling crushing in the compression zone.

After the blast test, the residual capacity of the beam was tested under static loading. Results are shown in **Figure 5-13**. Considering the initial displacement, this beam reached a peak load of P_{max}^{R} =130.6 kN. The specimen carried a residual load of P_{end}^{R}=115.7 kN till failure to a very large displacement of Δ_{max}^{R} =151.1 mm. The damages were concentrated in the flexural region of the beam, with the expansion of the localized cracks, but no bar rupture.

Figure 5-10 – HSC-F0.75-15M-10M-d/2 - Photographs at the end of Blasts A, B, C and D

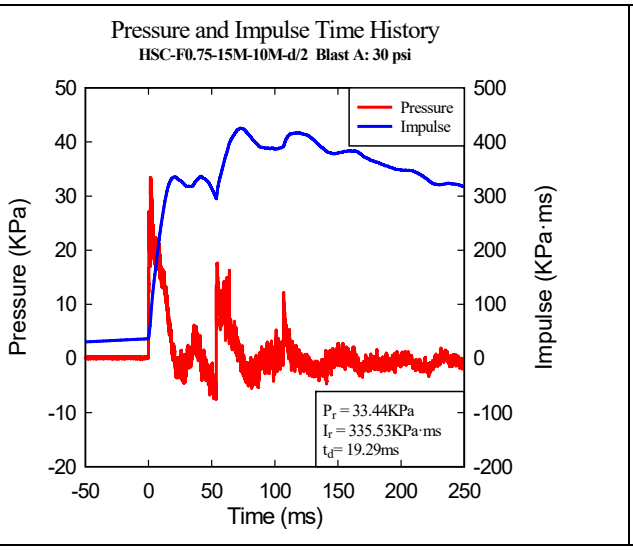

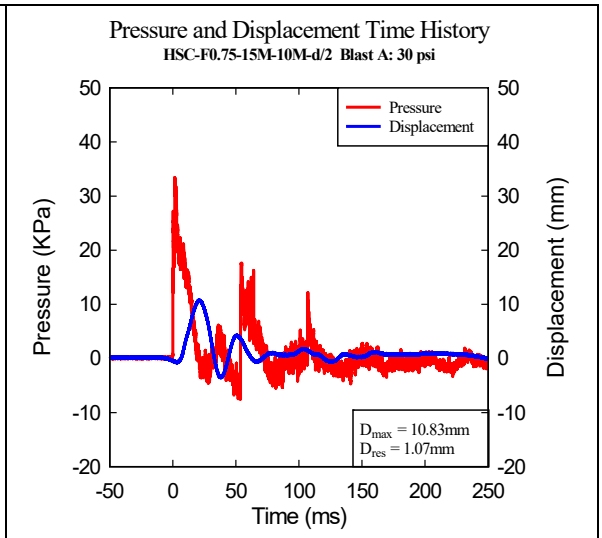

(a) Blast 1: Reflected pressure, impulse, and displacement time histories

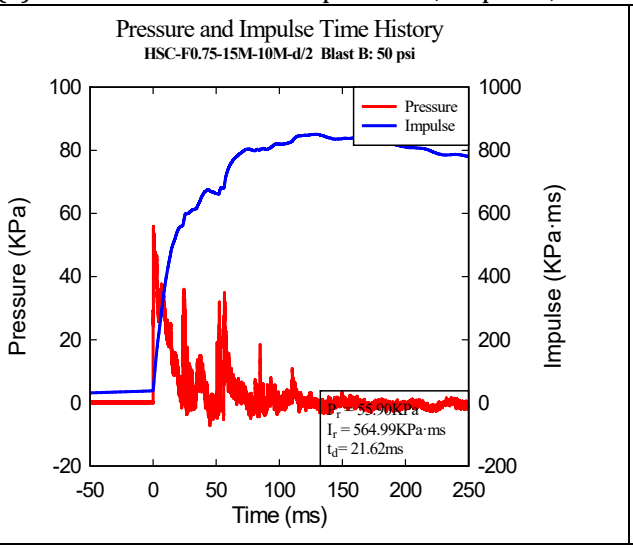

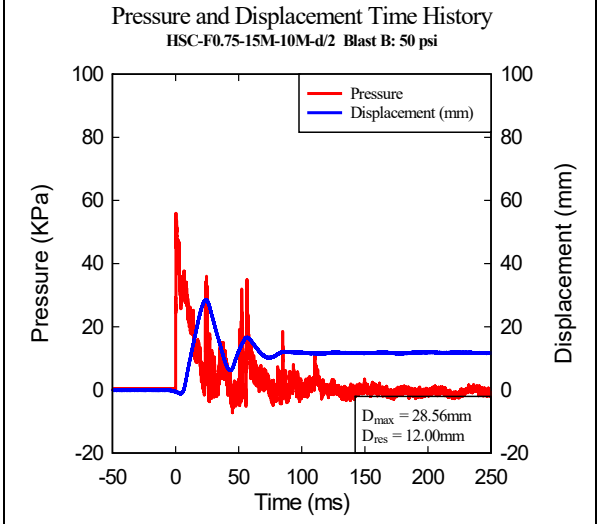

(b) Blast B: Reflected pressure, impulse, and displacement time histories

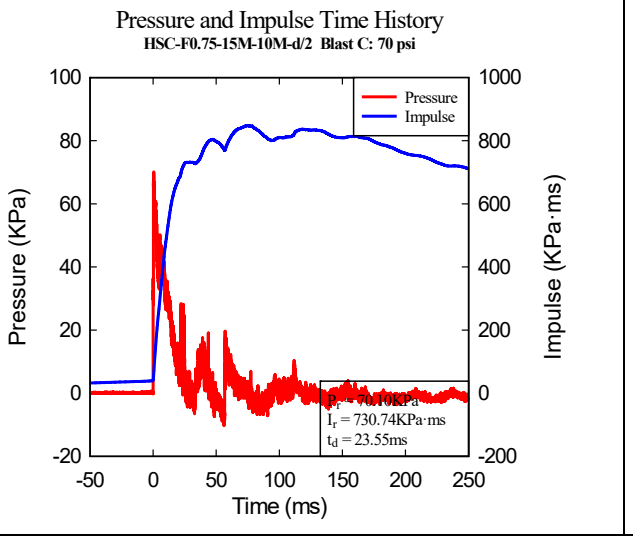

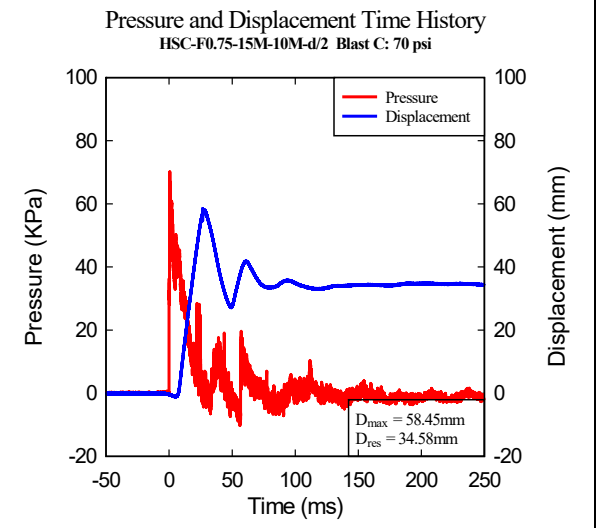

(c) Blast C: Reflected pressure, impulse, and displacement time histories

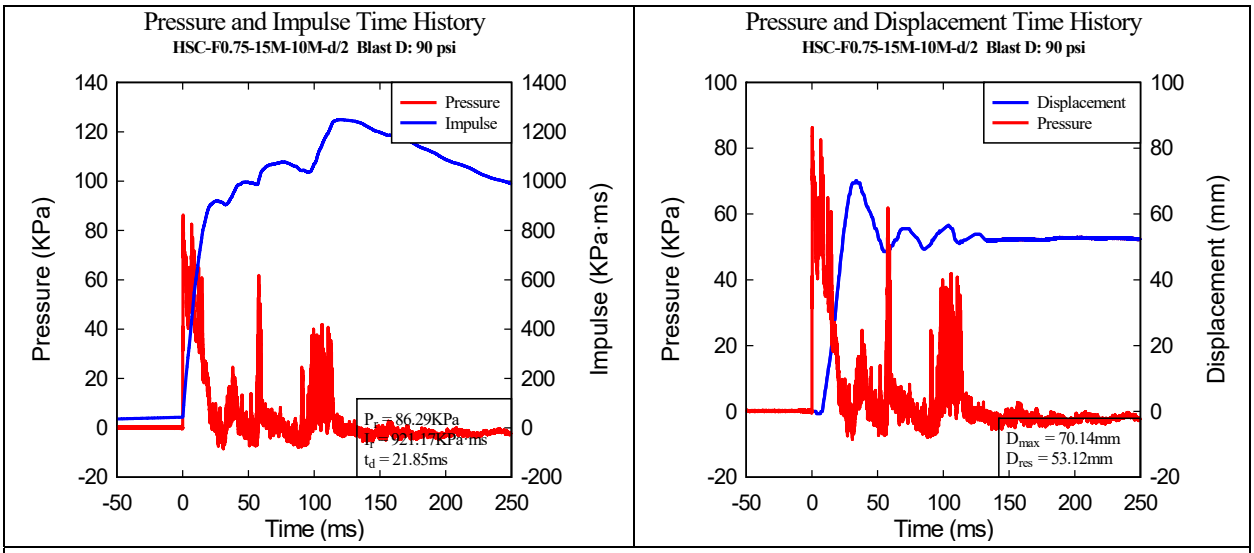

(d) Blast C: Reflected pressure, impulse, and displacement time histories

Figure 5-11 Recorded reflected pressure, impulse, and displacement for Blast A, B, C & D (HSC-F0.75-15M-10M-d/2)

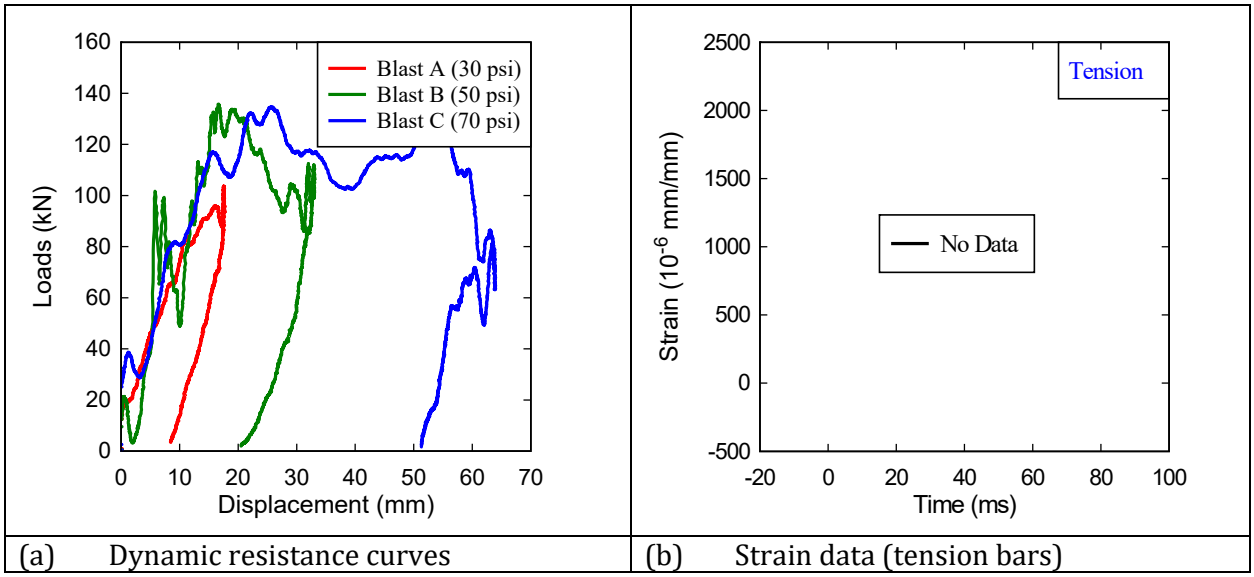

(a) Dynamic resistance curves (b) Strain data (tension bars)

Figure 5-12 Dynamic resistance curve and strain data (HSC-F0.75-15M-10M-d/2)

(a) Residual test load-deflection result	Data Summary	
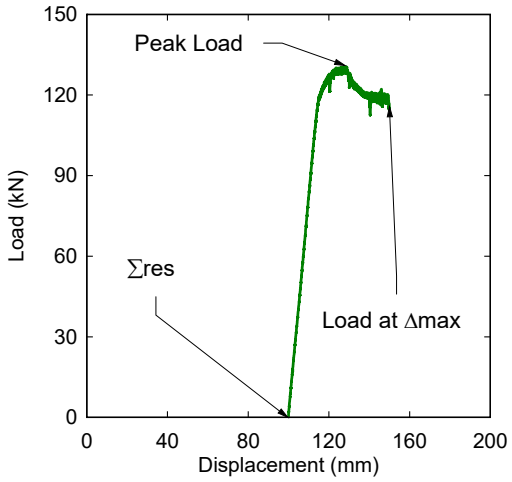	**∑res (mm)**	99.6
	P_{max}^{R} (kN)	130.6
	Δ_{max}^{R} (mm)	151.1
	P_{end}^{R} (kN)	115.7
(b) Condition of beam before residual test- after Blast D (90 psi)	**Comments**	
	-Flexural cracks are developed within the constant moment region of the beam. Localized cracks have formed. -Maximum displacement after blast testing reaches 99 mm.	
(c) Condition of beam after Residual Test	**Comments**	
	-Pronounced localized cracks. -Maximum cumulative displacement of 151 mm.	

Figure 5-13 Residual test results for beam HSC-F0.75-15M-10M-d/2

5.4 RESULTS OF THE 20M SERIES

5.4.1 HSC-F0-20M-6M-D/2

The 20M series included four beams designed with different detailing levels and concrete types. This beam was designed with plain high strength concrete and was doubly reinforced with 2-20M bars in the tension region and 2-6M bars in the compression region. Transverse reinforcement consisted of closed-ties spaced at 100 mm (d/2) throughout the beam span. The design of the transverse reinforcement and compression bars does not meet the requirements of the CSA-S850 standard. Results for this beam are summarized in **Table 5-2**, and **Figure 5-14** to **Figure 5-16**. This beam was subjected to three Blast loads: Blast A (30 psi), Blast C (70 psi) and Blast D (90 psi).

Blast A tested the beam within the elastic range and resulted in limited damages with a maximum and residual displacement of D_{max}= 10.6 mm and D_{res}= 0.7 mm. Blast C pushed the longitudinal tension-steel into the inelastic region, with the formation of flexural and flexural-shear cracks. The provision of compression reinforcement in the constant moment region prevented failure, with displacements of D_{max}= 40.2 mm and D_{res}= 18.2 mm and support rotation of 1.9°. Blast D caused severe flexure failure which was associated with crushing of concrete in the constant moment region, buckling of the small-diameter compression bars and cover spalling which exposed the tension bars (see **Figure 5-14**). The beam suffered displacements of D_{max}=123.4 mm (maximum support rotation of θ_{max} = 5.8°) and D_{res}=72.9 mm. Because of severe failure, the residual load-carrying capacity was not investigated.

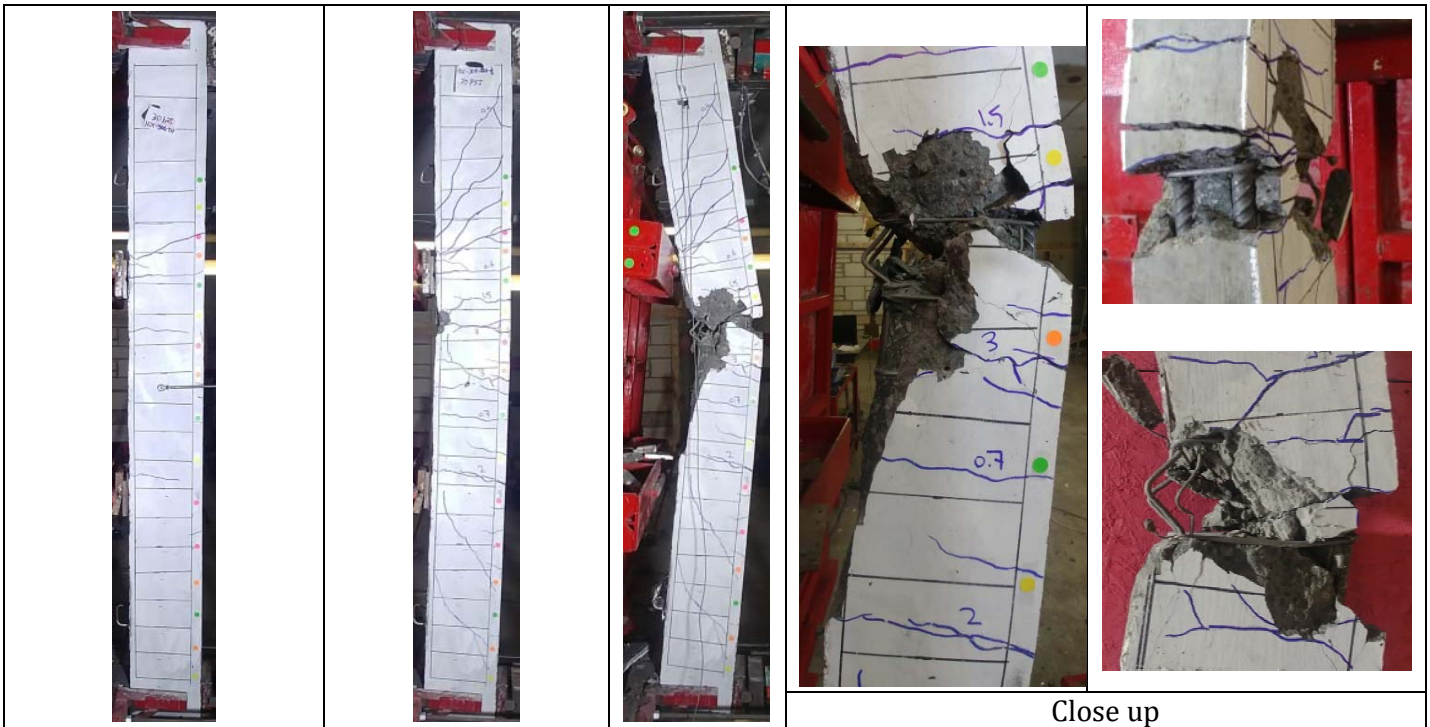

Figure 5-14 - HSC-F0-20M-6M-d/2 - Photographs at the end of Blasts A, C, and D

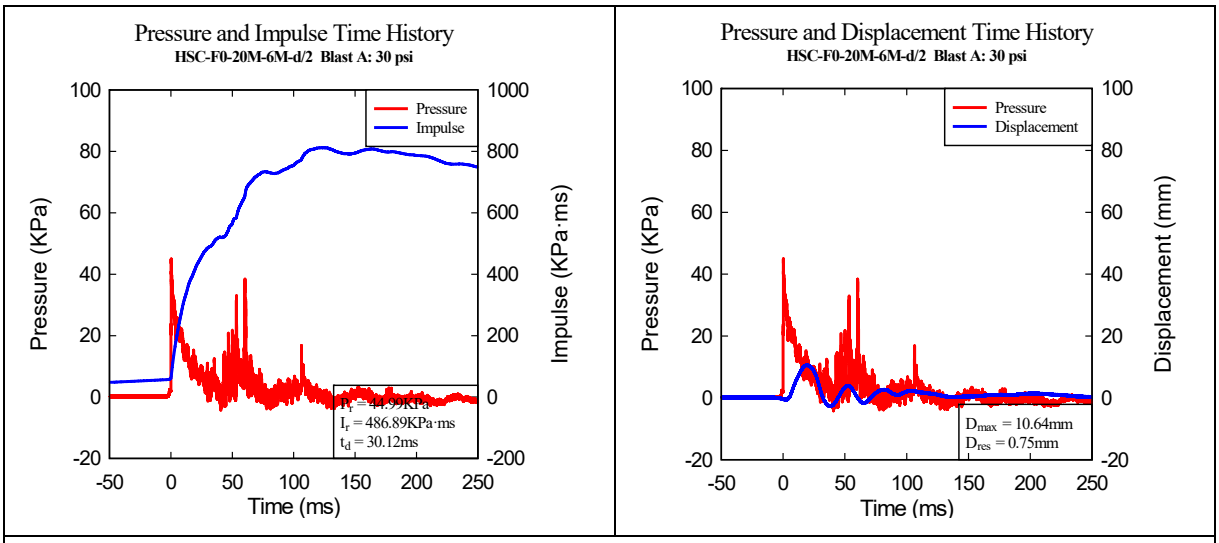

(a) Blast A: Reflected pressure, impulse, and displacement time histories

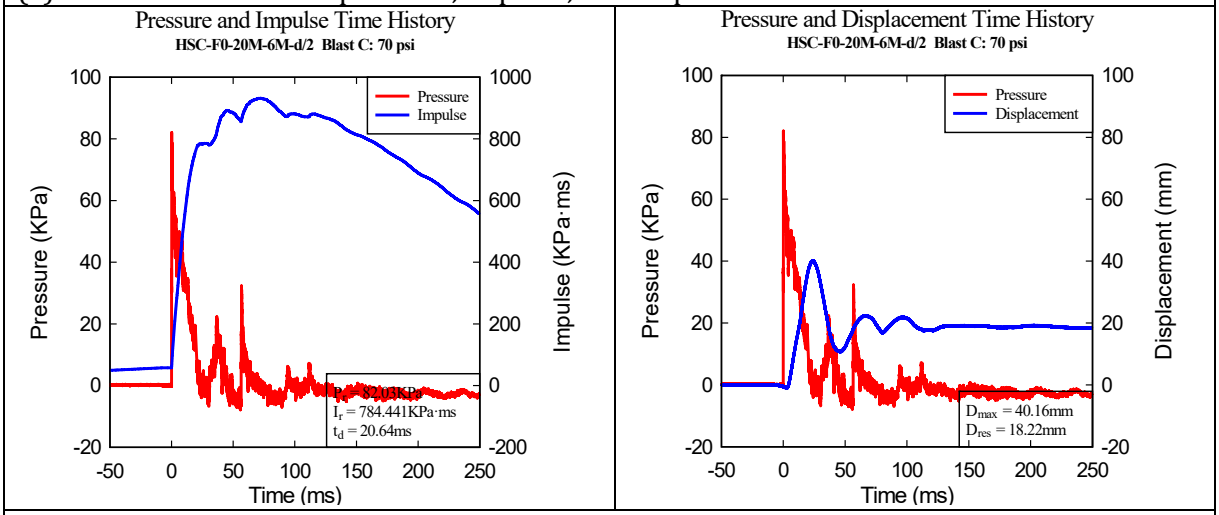

(b) Blast C: Reflected pressure, impulse, and displacement time histories

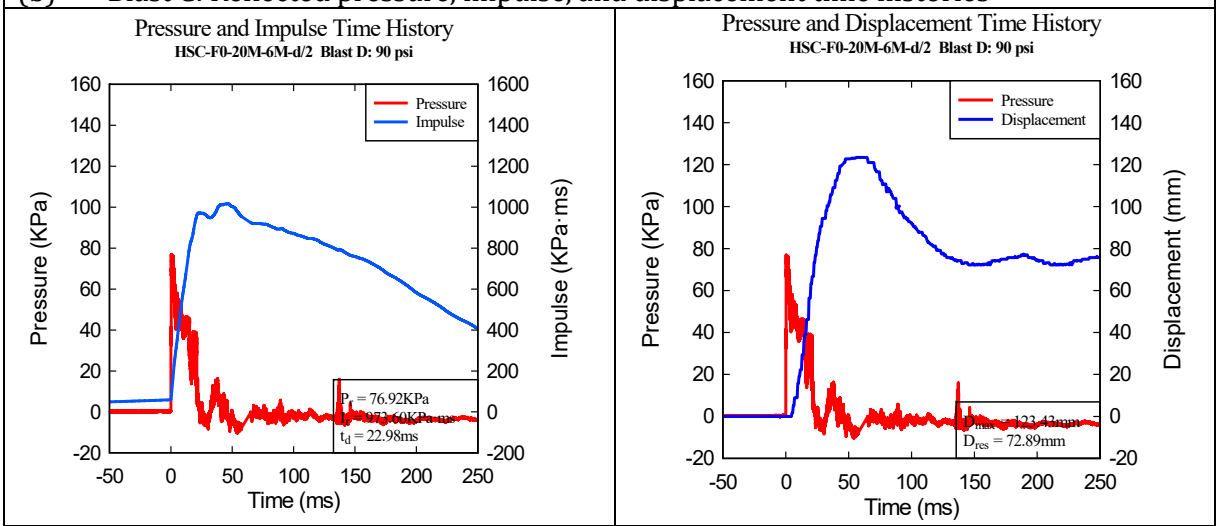

(c) Blast C: Reflected pressure, impulse, and displacement time histories

Figure 5-15 – Recorded reflected pressure, impulse and displacement for Blasts A, C and D (HSC-F0-20M-6M-d/2)

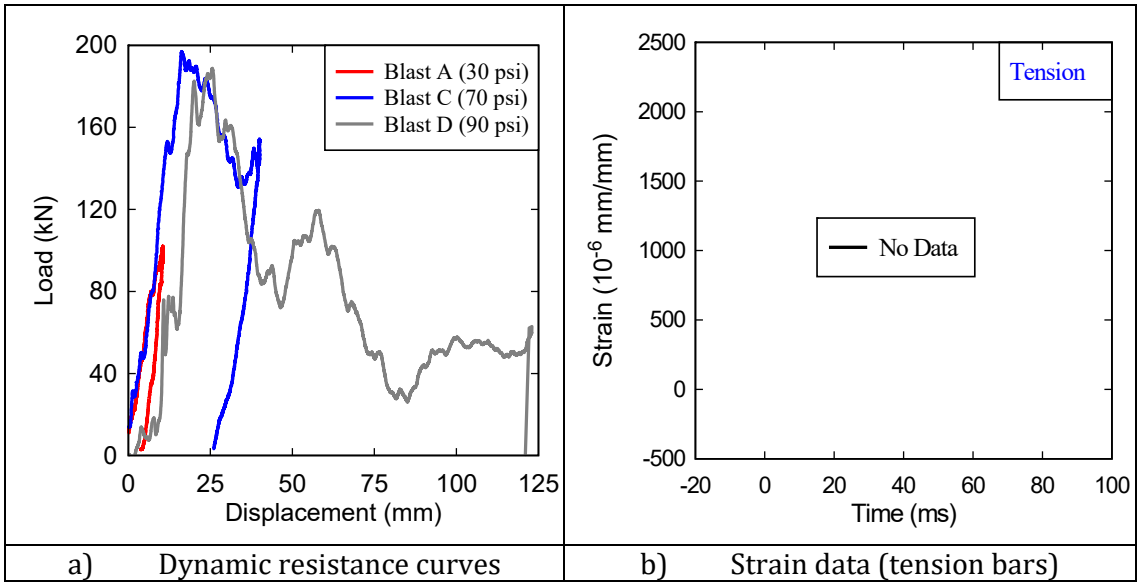

a) Dynamic resistance curves b) Strain data (tension bars)

Figure 5-16 – Dynamic resistance curve and strain data (HSC-F0-20M-6M-d/2)

5.4.2 HSC-F0-20M-10M-D/2

The second beam in the 20M series was cast with plain HSC with a similar design to HSC-F0-20M-6M-d/2, except for the use of 10M bars instead of 6M wires in compression. Testing sequence for this beam included: Blast A (30 psi), Blast C (70 psi) and Blast D (90 psi). The results are provided in **Table 5-2** and **Figure 5-17** to **Figure 5-19.**

Blast A tested the beam within the elastic range and resulted in flexural cracks with maximum and residual displacements of D_{max}= 12.1 mm and D_{res}= 1.4 mm. Blast C resulted in further developments of flexural and flexural-shear cracks which extended to the entire depth of the beam. After this blast, the displacements reached D_{max}= 37.4 mm and D_{res}= 19.8 mm. Blast D resulted in further cracking with spalling of concrete cover in the midspan compression region. Higher compression reinforcement prevented complete failure and limited the damages in the constant moment region when compared to the previous beam. The beam experienced pronounced deformations after this test with D_{max}= 72.6 mm (θ_{max}= 3.5°) and D_{res}=49.7 mm.

After blast testing the beam's residual capacity was assessed under static loads. Results are presented in **Figure 5-20**. With the initial displacement of ∑res= 72.4 mm, the maximum residual load reached P_{max}^{R}= 132.2 kN. The beam continued to carry load (P_{end}^{R}= 97.5 kN) until the end of testing at a displacement of Δ_{max}^{R} = 151.7 mm. Damage after the residual test consisted of concrete crushing in the midspan region and buckling of the longitudinal compression reinforcement bars due to the relatively large tie spacing of 100 mm (d/2).

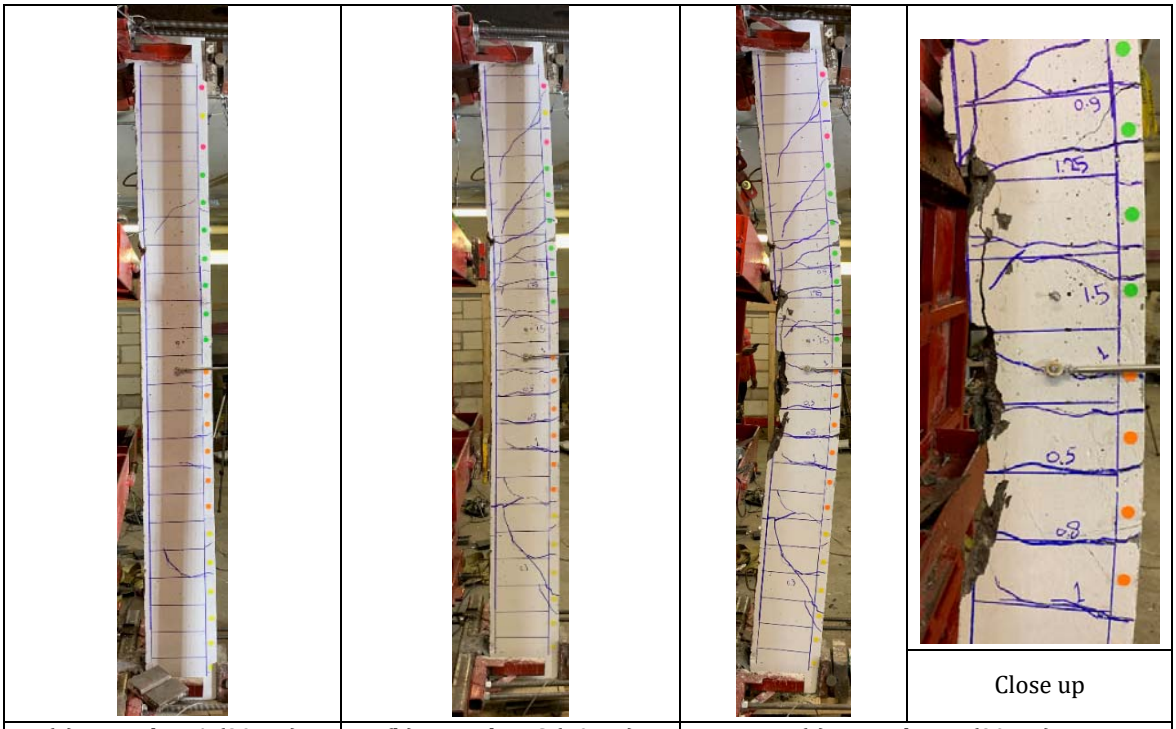

Figure 5-17 - Failure of the specimen at Blast A, C, and D

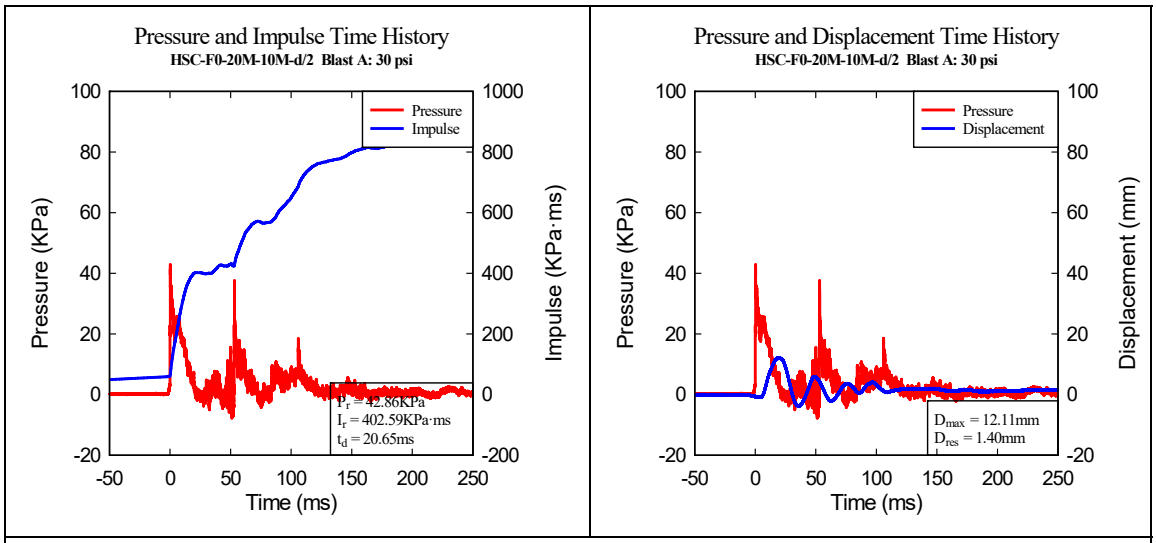

(a) Blast A: Reflected pressure, impulse, and displacement time histories

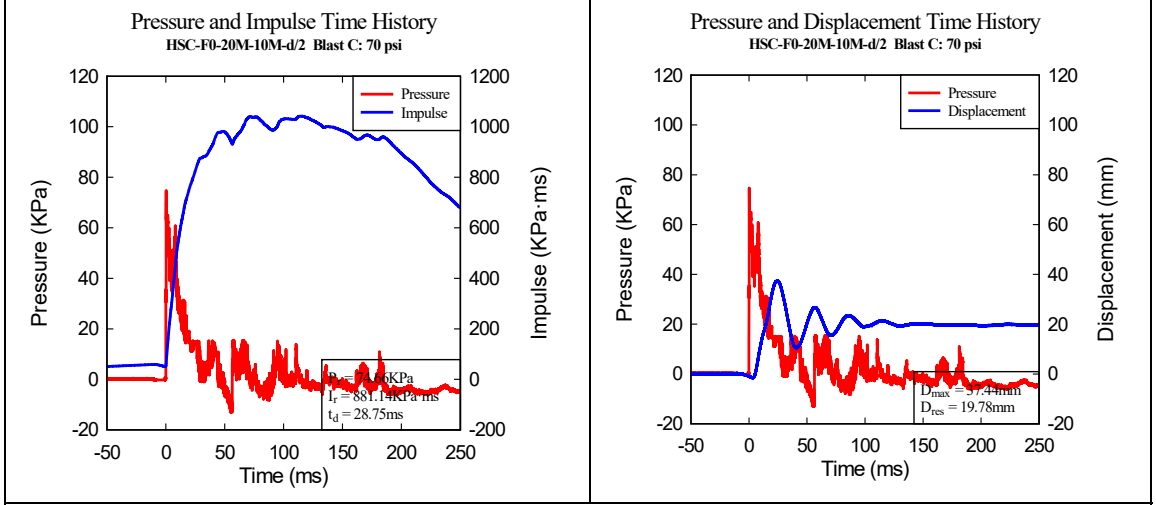

(b) Blast C: Reflected pressure, impulse, and displacement time histories

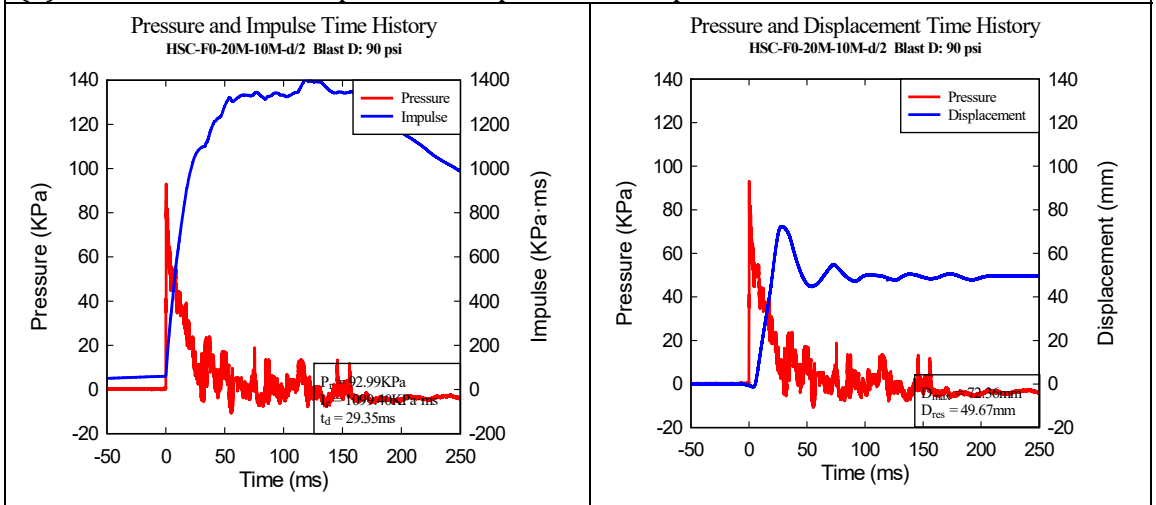

(c) Blast C: Reflected pressure, impulse, and displacement time histories

Figure 5-18 – Recorded reflected pressure, impulse, and displacement for Blasts A, B, and C (HSC-F0-20M-10M-d/2)

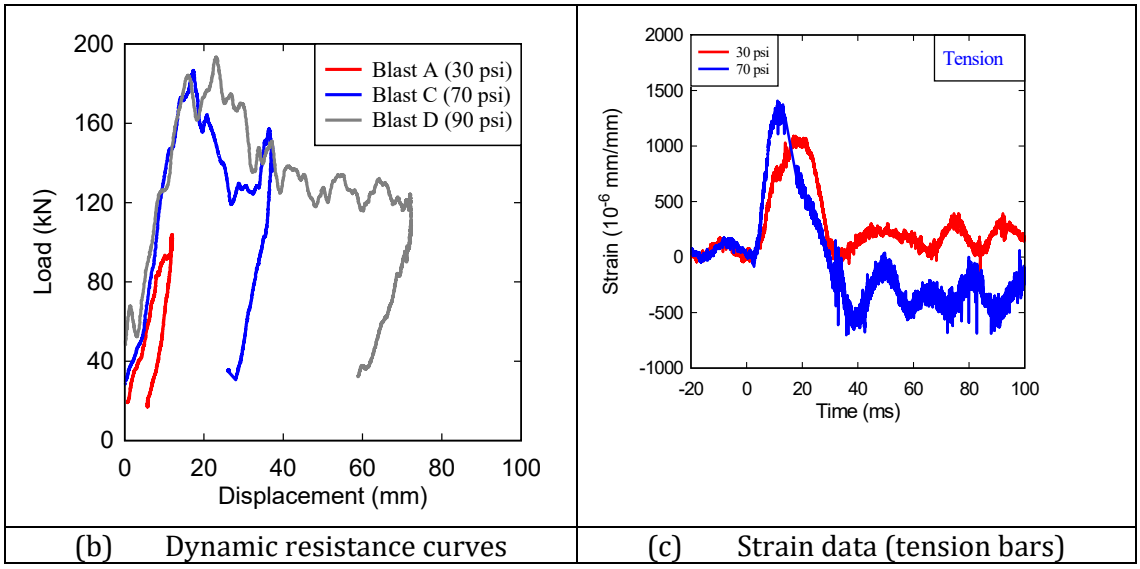

(b) Dynamic resistance curves (c) Strain data (tension bars)

Figure 5-19 Dynamic resistance curve and strain data (HSC-F0-20M-10M-d/2)

(a) Residual test load-deflection result

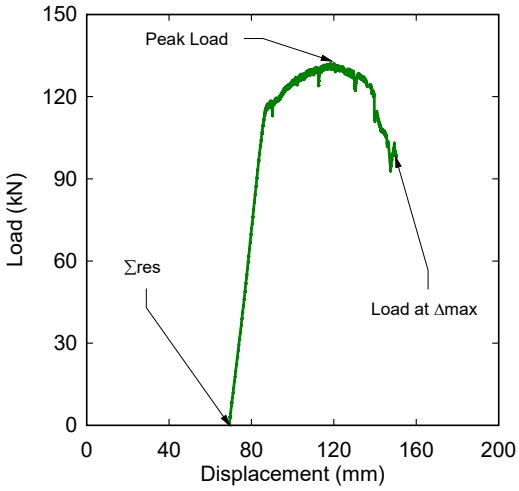

Data Summary	
∑res (mm)	70.8
P_{max}^{R} (Kn)	132.2
$\Delta_{max}{}^{R}$ (mm)	151.7
P_{end}^{R} (Kn)	98.1

(b) Condition of beam before residual test- after Blast D (90 psi)

Comments

-Specimen experienced crushing of cover concrete during the blast test
- Total residual displacement reached 71 mm.

(c) Condition of beam after Residual Test

Comments

-Damages in compression zone become more pronounced
-Buckling of the top compression bars

Figure 5-20 Residual test results for beam HSC-F0-20M-10M-d/2

5.4.3 HSC-F0-20M-10M-D/4

The third beam in the 20M series is similar to the previous beam except for reduced tie spacing of 50 mm (s = d/4) to meet the requirements of the CSA S850 standard. **Table 5-2** and **Figure 5-21** to **Figure 5-23** summarize the results for this beam. This beam was also tested under Blasts A, C, and D (30, 70 and 90 psi).

Blast A was meant to evaluate the behavior of the beam within the elastic range, and resulted in limited damages, with maximum and residual displacements of D_{max} = 11.5 mm and D_{res} = 1.7 mm, respectively. Blast C strained the longitudinal tension and compression reinforcements into the inelastic range, increased the number of flexural and flexural-shear cracks, with D_{max} = 34.6 mm and D_{res} = 17.3 mm. Blast D resulted in further crack opening, with crushing of cover concrete in compression. However, the provision of compression bars and closely spaced hoops confined the core concrete and prevented buckling, resulting in D_{max} = 71.6 mm and D_{res} = 48.2 mm, and a maximum support rotation (θ_{max}) of 3.4°.

After Blast D, the residual capacity of this beam was tested under static loading and the results are presented in **Figure 5-24.** Considering the initial residual from the blast test, the beam reached a peak residual load of P_{max}^{R} =139.3 kN. The beam continued to carry the load until reaching a maximum displacement of Δ_{max}^{R} = 150.4 mm, with crushing of concrete in the mid-span region but no buckling of compression steel.

Figure 5-21 – HSC-F0-20M-10M-d/4 – Photographs at the end of Blasts A, C, and D

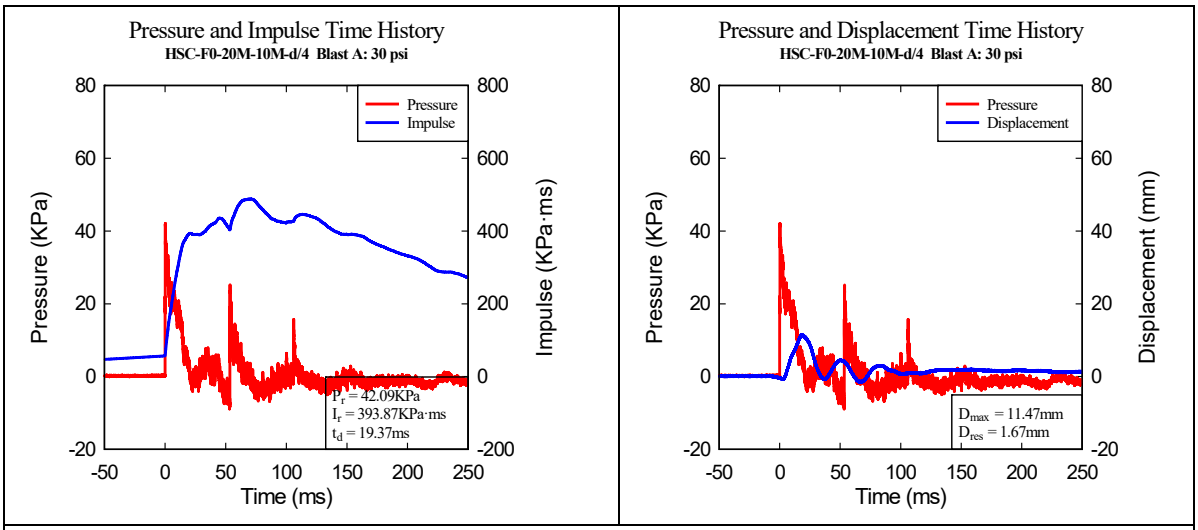

(a) Blast A: Reflected pressure, impulse, and displacement time histories

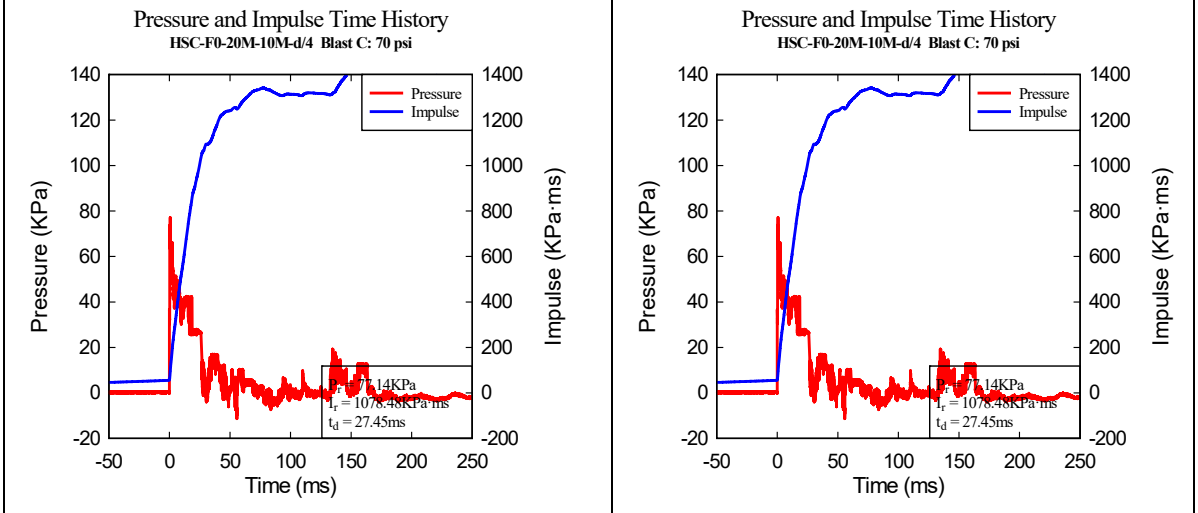

(b) Blast C: Reflected pressure, impulse, and displacement time histories

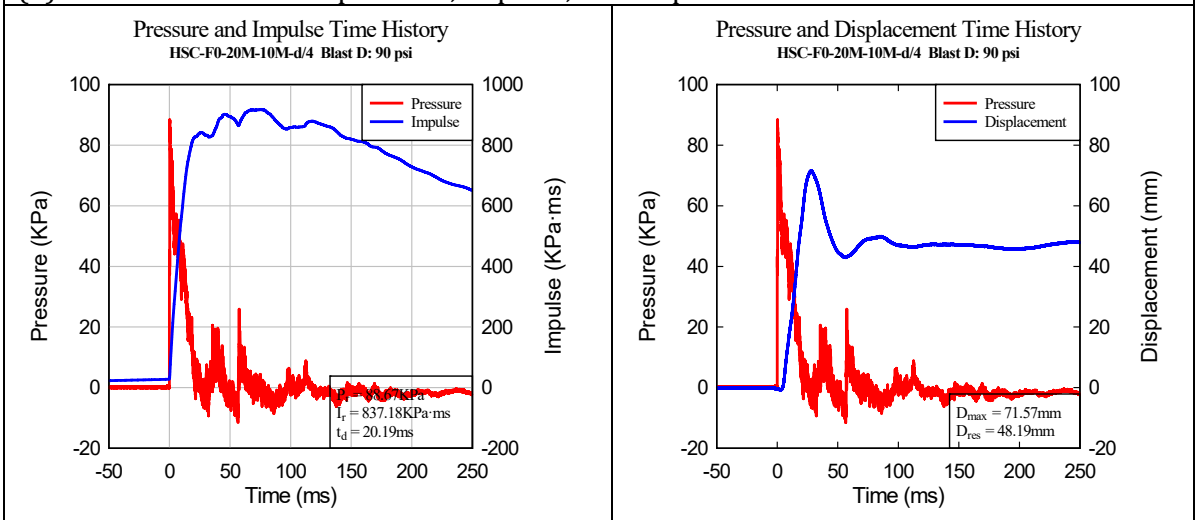

(c) Blast D: Reflected pressure, impulse, and displacement time histories

Figure 5-22 – HSC-F0-20M-10M-d/4 recorded reflected pressure, impulse, and displacement for Blasts A, C, and D

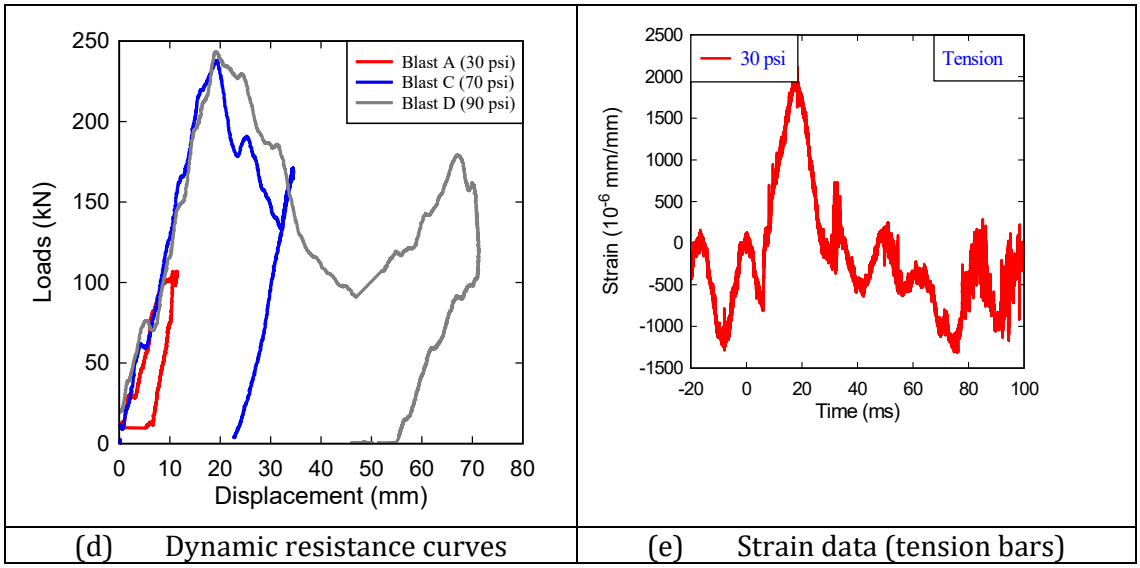

(d) Dynamic resistance curves (e) Strain data (tension bars)

Figure 5-23 Dynamic resistance curve and strain data (HSC-F0-20M-10M-d/4)

(a) Residual test load-deflection result	Data Summary	
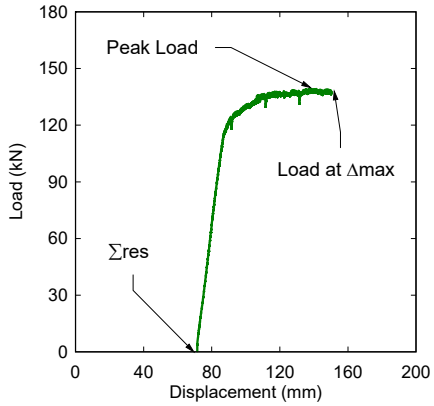	**∑res (mm)**	67.2
	P_{max}^R (kN)	139.3
	Δ_{max}^R (mm)	150.4
	P_{end}^R (kN)	131.8
(b) Condition of beam before residual test- after Blast D (90 psi)	**Comments**	
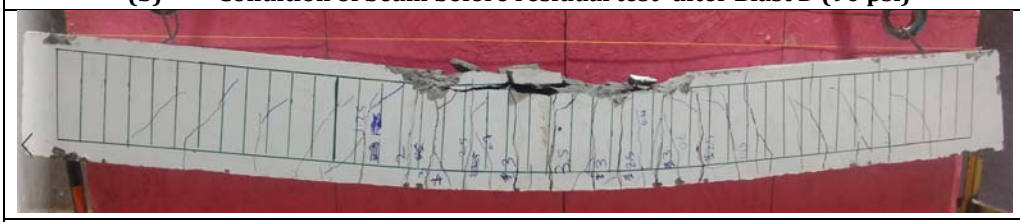	-Concrete crushing in the compression region. Total residual displacement after blast testing reaches 67 mm.	
(c) Condition of beam after Residual Test	**Comments**	
	-Excessive deformation. -Crushing becomes more severe but bar buckling is prevented. -Maximum displacement reaches 150.35 mm	

Figure 5-24 Residual test results for beam HSC-F0-20M-10M-d/4

5.4.4 HSC-F0.75-20M-10M-D/2

The final specimen in the 20M series was built with HSFRC having 0.75% fibers and intermediate tie spacing of 100 mm (d/2). Results of the blast test are provided in **Table 5-2** and **Figure 5-25** to **Figure 5-27.** This beam was subjected to three dynamic blast loads: A (30 psi), C (70 psi), and D (90 psi).

Blast A kept the longitudinal tension-steel within the elastic range and resulted in minor cracks. Support rotations remained below 1° with D_{max} = 11.1 mm and D_{res} = 1.2 mm. Blast C inflicted moderate damages with D_{max} = 36.5 mm and D_{res} = 15.2 mm, pushing the longitudinal tension reinforcement into the inelastic range. The last shot for this specimen was Blast D (90 psi), reaching D_{max} = 49.9 mm ((θ_{max}= 1.7°) and D_{res} = 1.7 mm. The addition of fibers reduced the displacements by half when compared to the previous beam, with no significant cover damage. The mean crack width recorded was 7 mm with visible fiber pullout across some cracks. However, the structural damage was limited to cracking, as the fibers held the concrete together.

After the dynamic blast test, the residual load-carrying capacity of the beam was tested under static bending. Results of the residual test are presented in **Figure 5-28.** Considering the total residual displacement after blast testing, ∑res =43.7 mm, the beam recorded a maximum residual load of P_{max}^{R} =162.9 kN. The beam supported a very large deflection (of Δ_{max}^{R}=150 mm), with damage limited to cracking at the end of testing, demonstrating the high post-blast resilience of the beam.

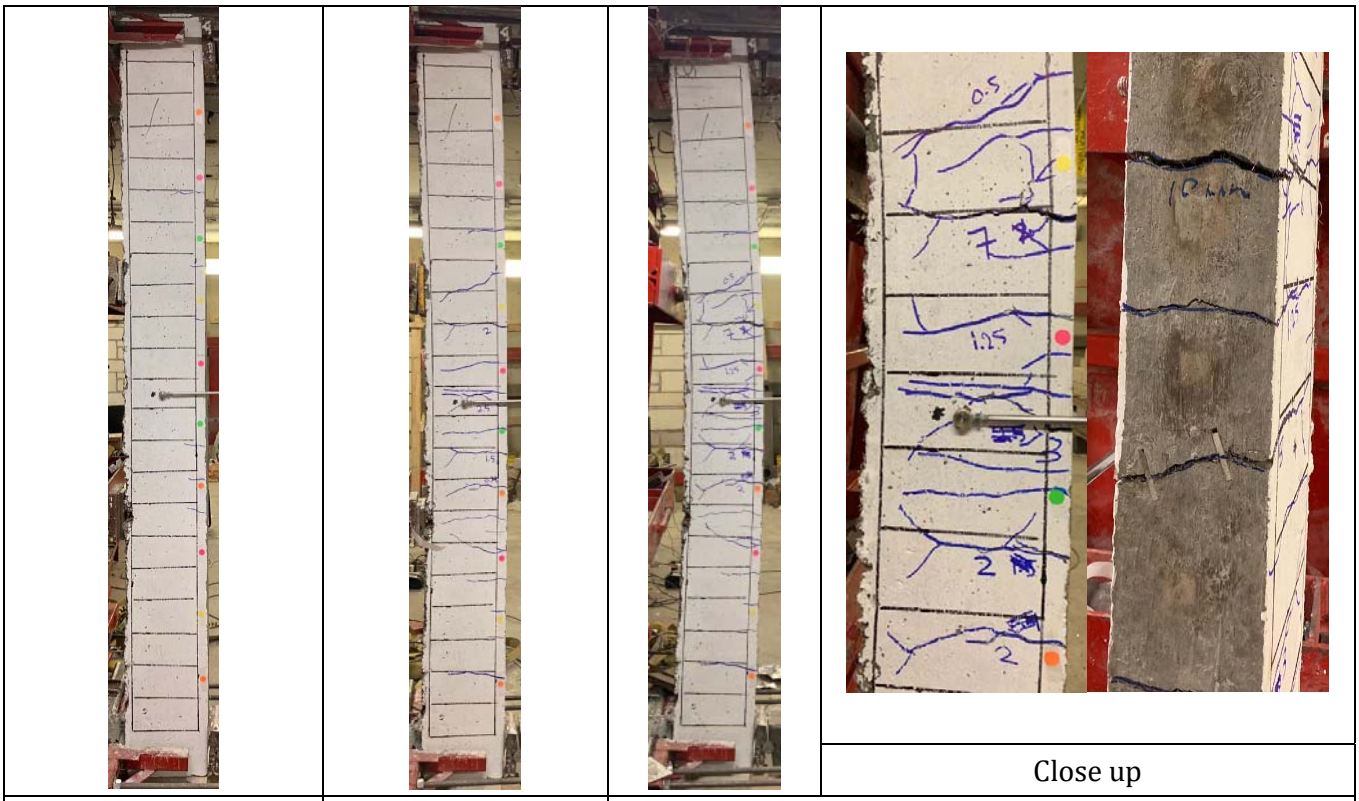

(a) Blast A (30 psi) (b) Blast C (70 psi) (c) Blast D (90 psi)

Figure 5-25 - HSC-F0.75-20M-10M-d/2 - Photographs at the end of Blasts A, C, and D

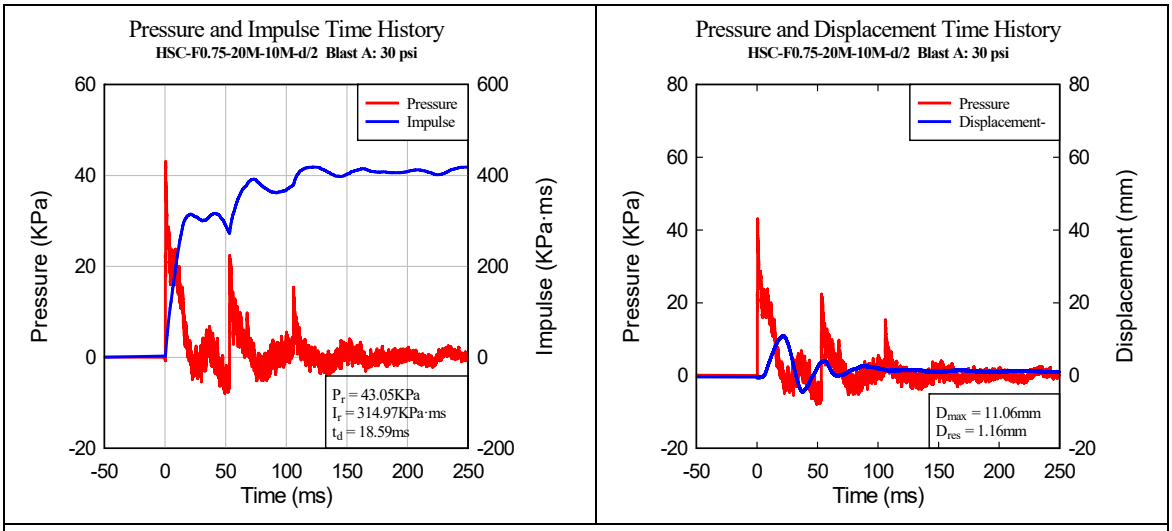

(a) Blast A: Reflected pressure, impulse, and displacement time histories

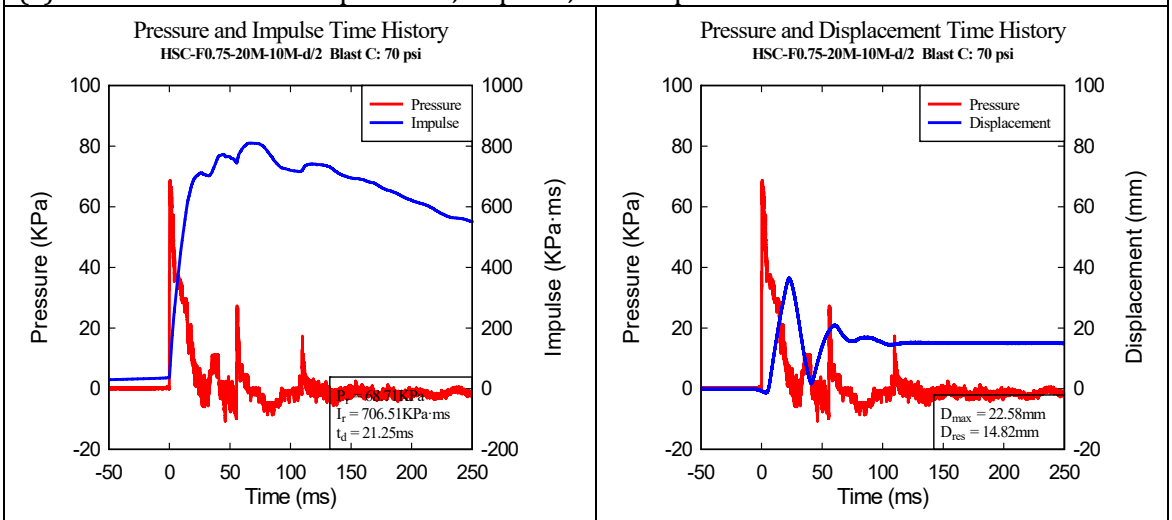

(b) Blast C: Reflected pressure, impulse, and displacement time histories

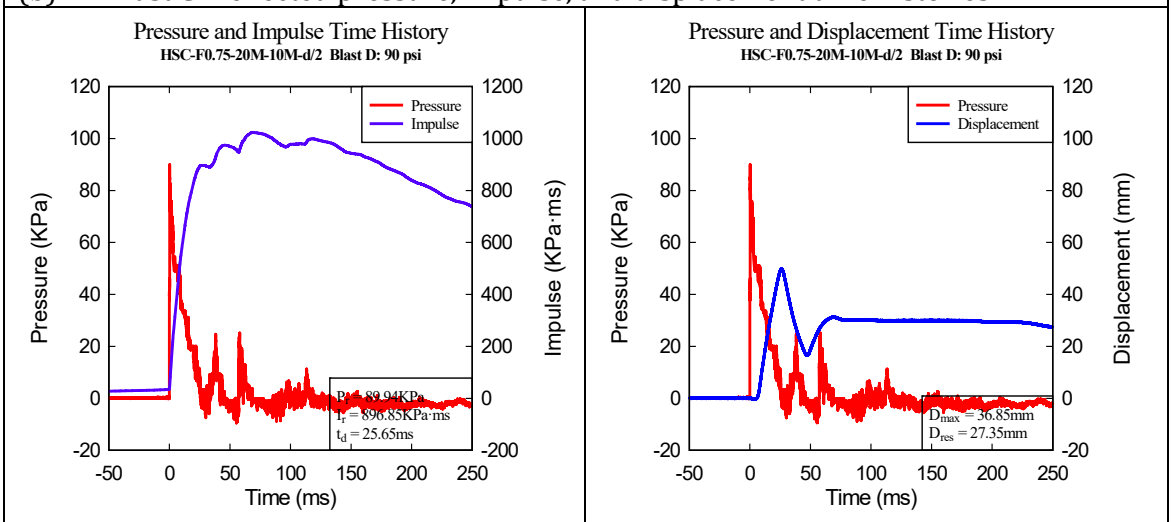

(c) Blast D: Reflected pressure, impulse, and displacement time histories

Figure 5-26 – HSC-F0.75-20M-10M-d/2 recorded reflected pressure, impulse, and displacement for Blasts A, C, and D

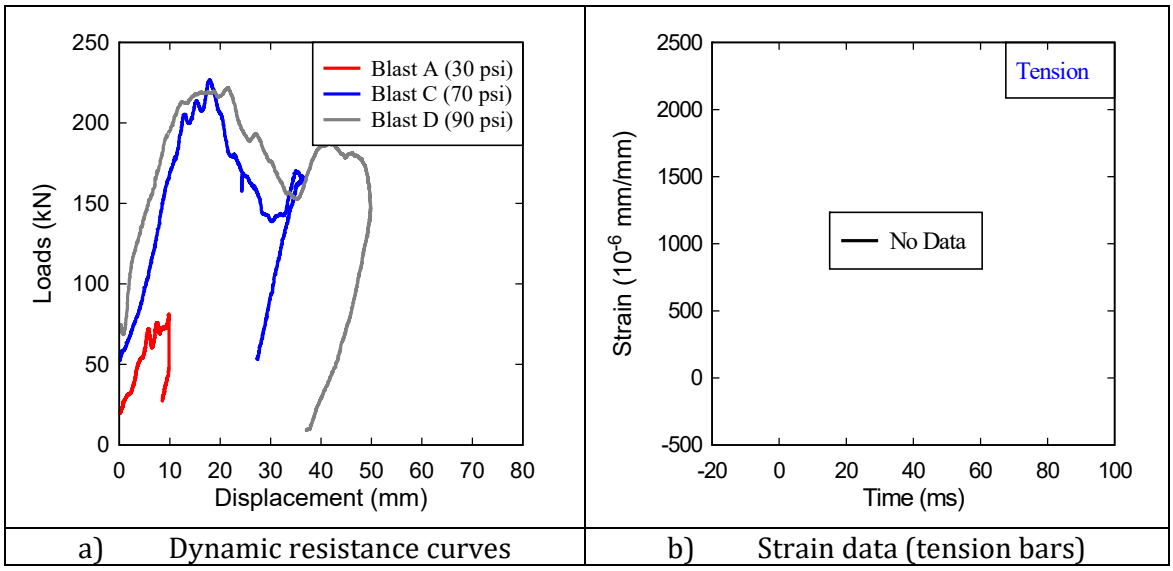

a) Dynamic resistance curves b) Strain data (tension bars)

Figure 5-27 – Dynamic resistance curve and strain data (HSC-F0.75-20M-10M-d/2)

(a) Residual test load-deflection result

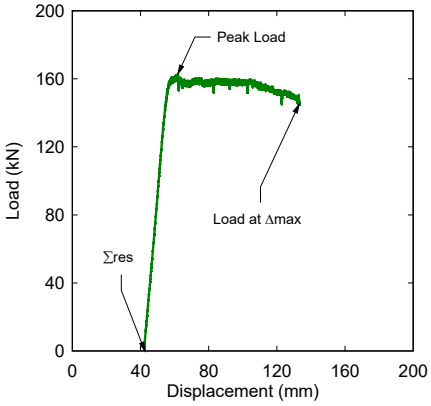

Data Summary	
Σres (mm)	43.7
P_{max}^R (kN)	162.9
Δ_{max}^R (mm)	134.0
P_{end}^R (kN)	150.6

(b) Condition of beam before residual test- after Blast D (90 psi)

Comments

-Damage at end of blast testing limited to flexural shear cracks.
-Total residual displacement reached 63.4 mm

(c) Condition of beam after Residual Test

Comments

-Beam is severely deformed but does not show significant damage.
-Cover concrete is still attached
-Beam reached a maximum cumulative displacement of 173.7 mm

Figure 5-28 – Residual test results for beam HSC-F0.75-20M-10M-d/2

5.5 RESULTS OF THE 25M SERIES

5.5.1 HSC-F0-25M

The first beam of the 25M series was designed with plain high strength concrete and singly-reinforced with 25M longitudinal bars. Transverse reinforcement consisted of U-shaped stirrups spaced at 100 mm in the shear spans only. Results of the blast test for this beam are found in **Table 5-2** and **Figure 5-29** to **Figure 5-30.** This specimen was subjected to two dynamic blast loads: C (70 psi), and D (90 psi).

Blast C brought the longitudinal tension reinforcement into the inelastic range with moderate beam damage consisting of shear and flexural cracks, and D_{max} = 30.1 mm and D_{res} = 5.1 mm at a support rotation of 1.5°. Blast D inflicted enough impact force to cause complete blowout failure of the specimen. Using the high-speed camera the maximum displacement was estimated to reach D_{max} = 185.4 mm, corresponding to a support rotation θ_{max}= 8.6°. In addition to the crushing, a concrete cover segment with 600 mm length spalled of the beam exposing the longitudinal reinforcement bars in the constant moment region. Because of the blowout failure, no residual test was carried out on this specimen.

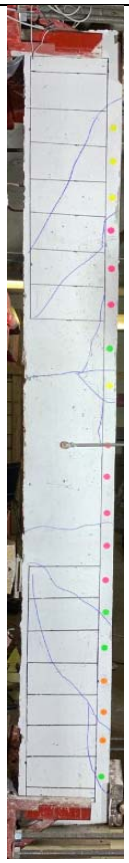

(a) Blast C (70 psi)

(b) Blast D (90 psi)

Close up

Figure 5-29 – HSC-F0-25M - Photographs at the end of Blasts C and D

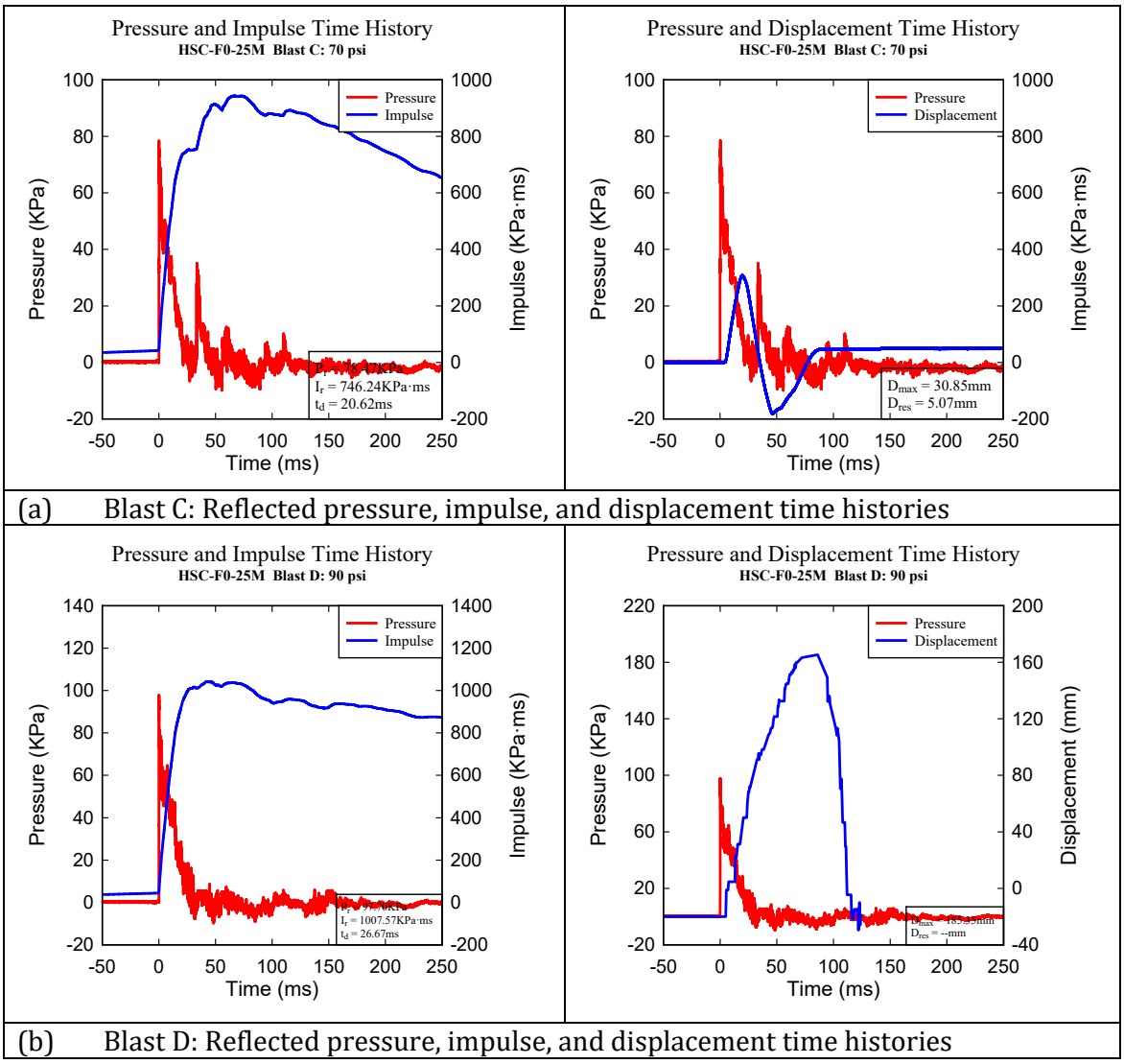

Figure 5-30 – HSC-F0-25M recorded reflected pressure, impulse and displacement for Blasts C and D.

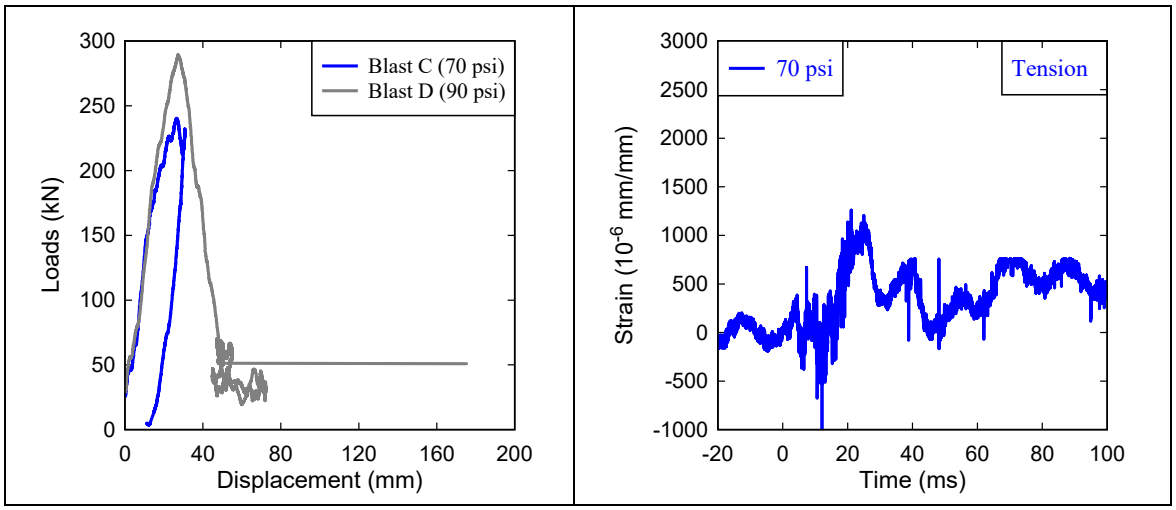

Figure 5-31 Dynamic resistance curve and strain data (HSC-F0-25M)

5.5.2 HSC-F0-25M-10M-D/4

The next beam in the 25M series was doubly reinforced in the longitudinal direction with 2-25M in tension region and 2-10M in the compression region, with closed ties spaced at 50 mm (s = d/4) throughout the beam span. **Table 5-2** shows the results along with **Figure 5.32** to **Figure 5-34**. Like the previous beam, the specimen was tested under Blast C and D pressures (70 and 90 psi)

Blast tested pushed the longitudinal reinforcement steel into the inelastic range, and resulted in flexural and shear cracks, with a maximum support rotation of 1.3° and maximum and residual displacements of D_{max} = 26.5 mm and D_{res} = 2.3 mm. Blast D (90 psi) was the last blast applied on this specimen and resulted in concrete crushing in the mid-span compression zone, but much more moderate damages as opposed to the blowout failure of the previous beam. The provision of compression and transverse ties protected the midspan compression region in this heavily reinforced specimen. This blast resulted in maximum and residual displacements of D_{max} = 45.1 mm (θ_{max}= 2.2°) and D_{res} = 14.9 mm.

Following the blast tests, the beam was tested under static loading to study its residual capacity. The maximum load recorded was P_{max}^{R}=201kN, which represents 88% of the original (undamaged) beam capacity. Other results for the residual test are summarized in **Figure 5-35**. Taking into consideration the total residual deformation after blast testing (∑res=57.2 mm), the beam continued to carry load up to a displacement of Δ_{max}^{R} =137.4 mm, with flexure failure associated with further crushing of concrete in the mid-span region and buckling of the bars in between the ties.

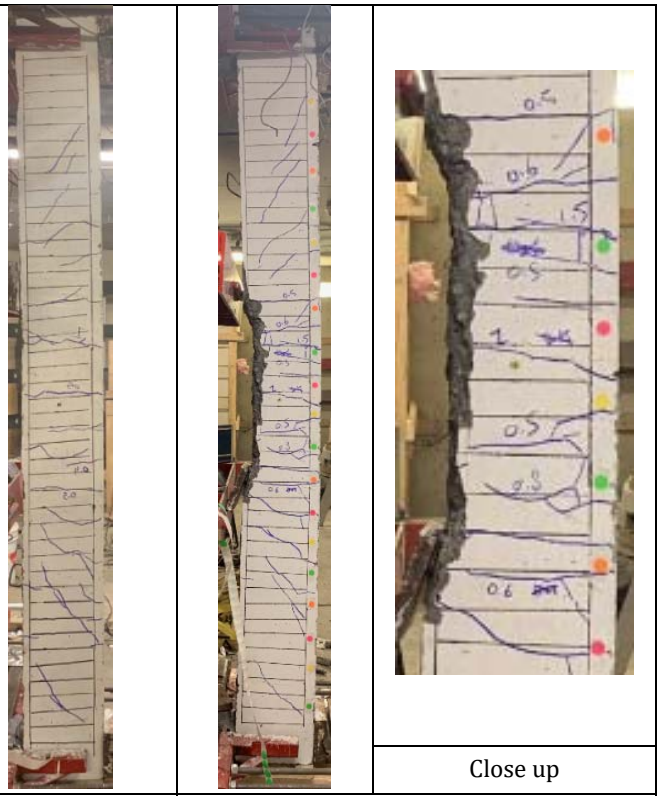

(b) Blast C (70 psi)	(c) Blast D (90 psi)	Close up

Figure 5.32 – HSC-F0-25M-10M-d/4 - Photographs at the end of Blasts C and D

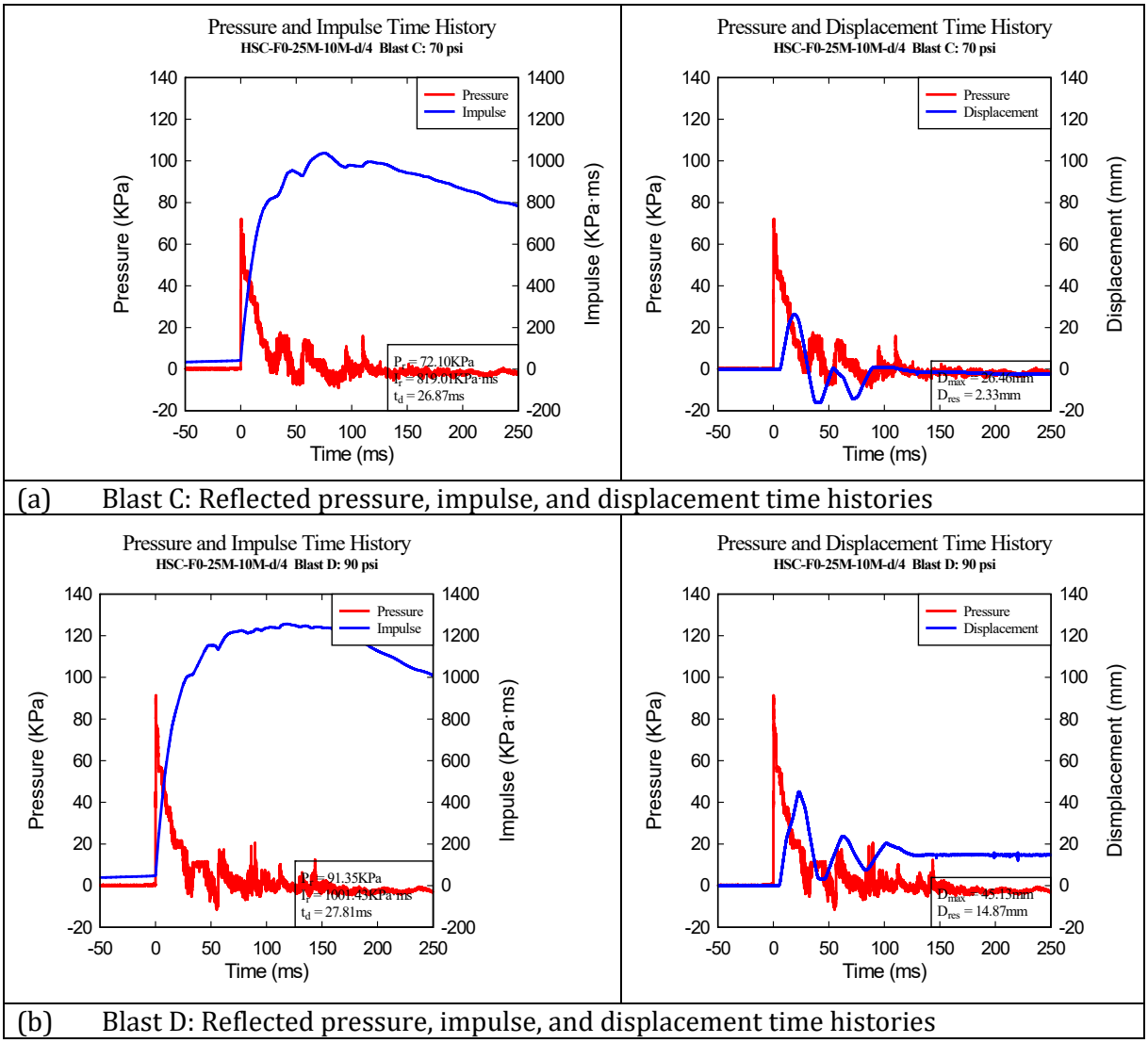

Figure 5-33 – HSC-F0-25M-10M-d/4 recorded reflected pressure, impulse, and displacement for Blasts C and D.

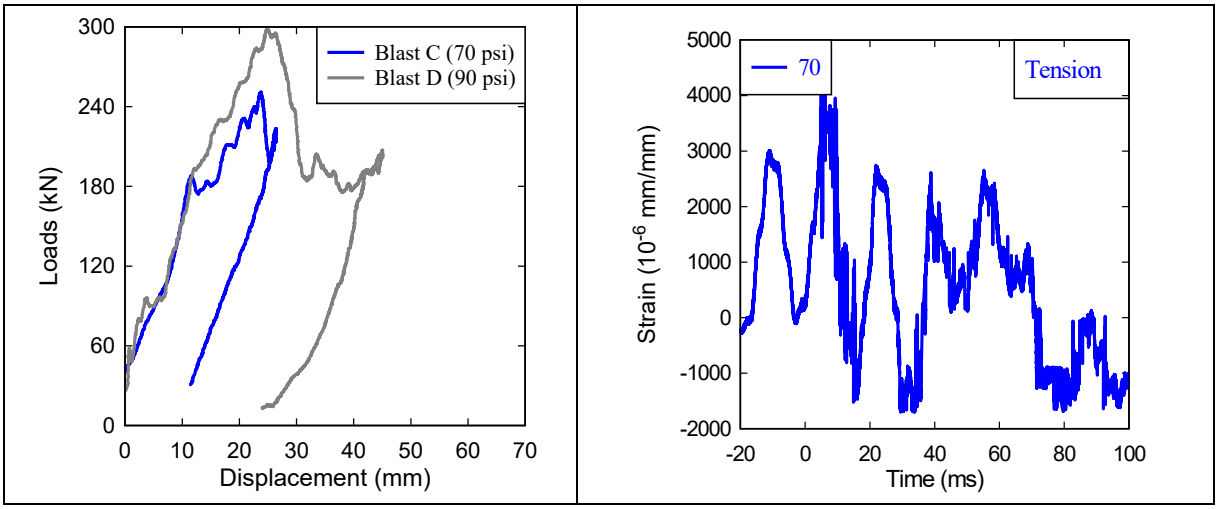

Figure 5-34 Dynamic resistance curve and strain data (HSC-F0-25M-10M-d/4)

(a) Residual test load-deflection result	Data Summary	
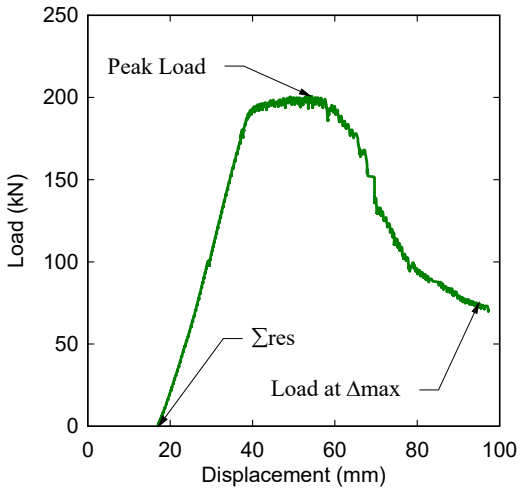	**∑res (mm)**	57.2
	P_{max}^{R} (kN)	201.0
	Δ_{max}^{R} (mm)	137.4
	P_{end}^{R} (kN)	70.0
(b) Condition of beam before residual test- after Blast D (90 psi)	**Comments**	
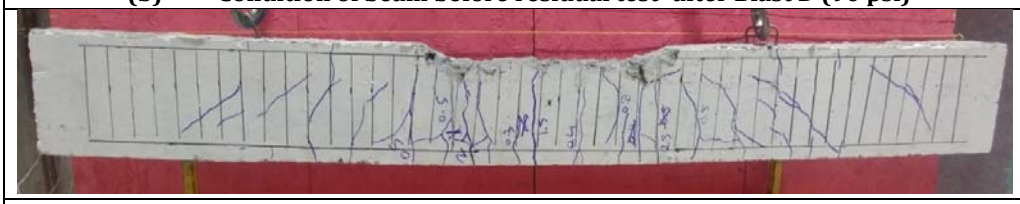	-Loss of cover concrete during blast testing -Total residual displacement of 48 mm	
(c) Condition of beam after Residual Test	**Comments**	
	-Concrete crushing in the compressive region becomes more severe and propagates to the core. -Slight buckling of compression bars within the closely spaced ties	

Figure 5-35 Residual test results for beam HSC-F0-25M-10M-d/4

5.5.3 HSC-F0.75-25M-10M-D/2

The last beam in the test program and in the 25M series was identical to the previous beam except for the use HSFRC containing 0.75% fibers and larger intermediate tie spacing of 100 mm (d/2). Results are provided in **Table 5-2** and **Figure 5-36** to **Figure 5-38**. This beam was also tested under Blasts C and D (70 and 90 psi).

Blast C tested the beam beyond yielding and resulted in maximum and residual displacements of D_{max} = 21.6 mm and D_{res} = 3.4 mm with limited damages. Blast D inflicted moderate damages that were limited to fiber pull-out, crack localization (the main crack reaches 5 mm) but no cover crushing or spalling. This blast resulted in a support rotation of 2.6°, with D_{max} = 36.6 mm and D_{res} = 12.8 mm. Since the beam showed low damage it was tested under another blast corresponding to Blast E (100 psi). This shot resulted in the further opening of the main cracks, and the displacements reached D_{max} = 54.7 mm (θ_{max}= 2.6°) and D_{res} = 21.6 mm. Despite flexural cracks openings, the fibers held the concrete together and secondary fragments were not generated.

After the final blast, the residual capacity of the beam was tested under static loading. Results are shown in **Figure 5-39**. The beam carried a maximum residual load of P_{max}^{R} =223 kN, which was 11% lower than the original (undamaged) beam capacity. Considering the initial residual deformation of 37.7 mm, the beam continued to carry a residual load of P_{end}^{R}= 83 kN until reaching a very large displacement of Δ_{max}^{R} = 153mm. The residual test resulted in more severe damages that were concentrated in the constant region of the beam.

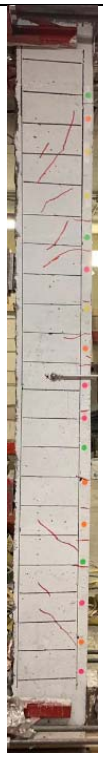

(a) Blast C (70 psi)

(b) Blast D (90 psi)

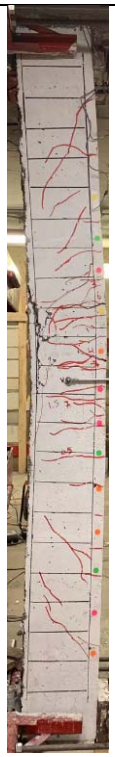

(c) Blast E (100 psi)

Close up

Figure 5-36 – HSC-F0.75-25M-10M-d/2 - Photographs at the end of Blasts C, D and E

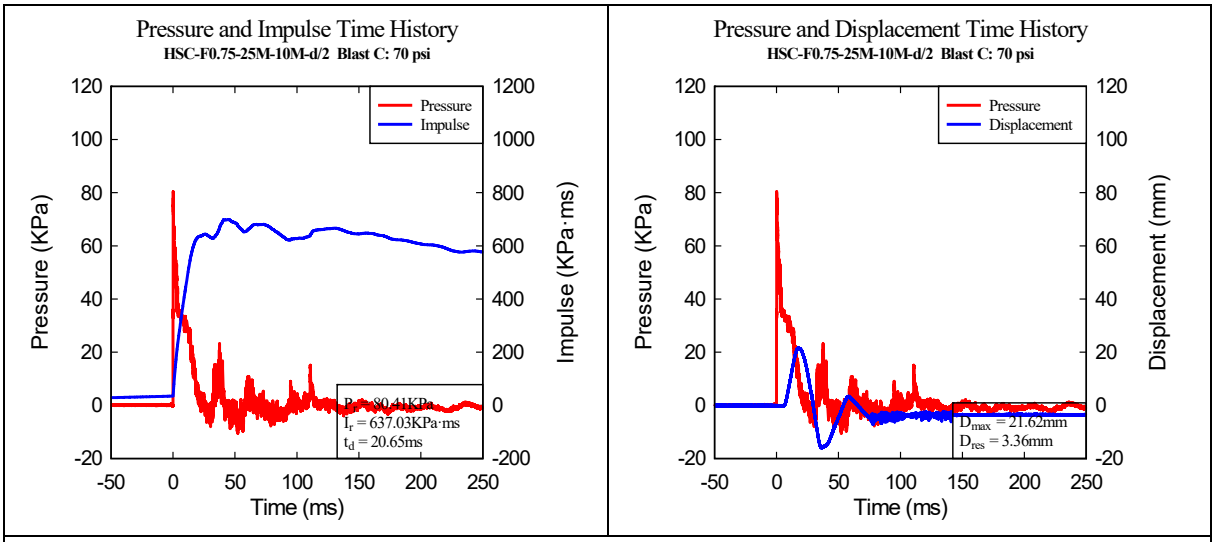

(a) Blast C: Reflected pressure, impulse, and displacement time histories

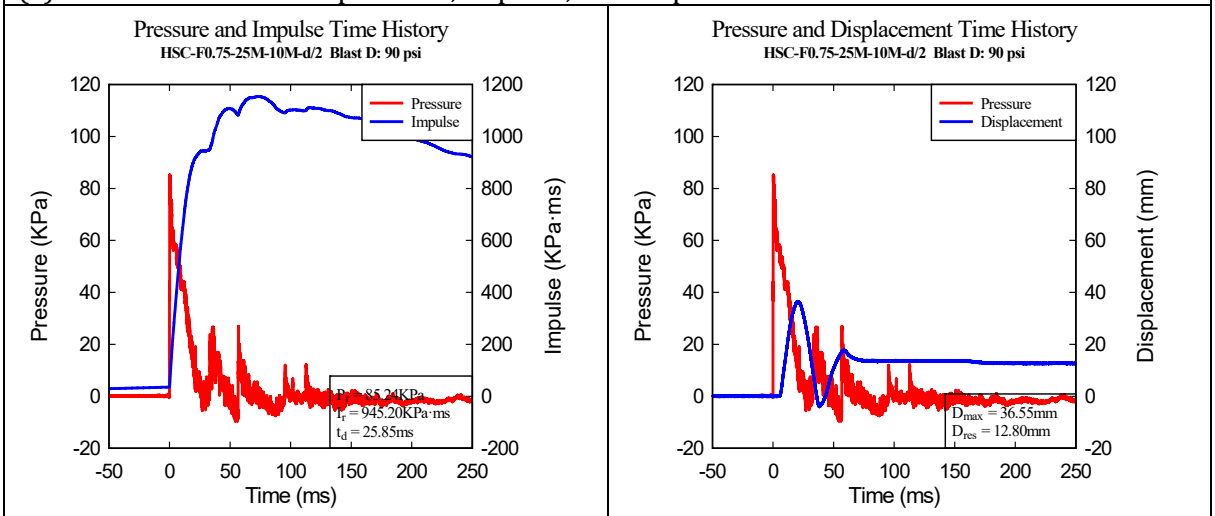

(b) Blast D: Reflected pressure, impulse, and displacement time histories

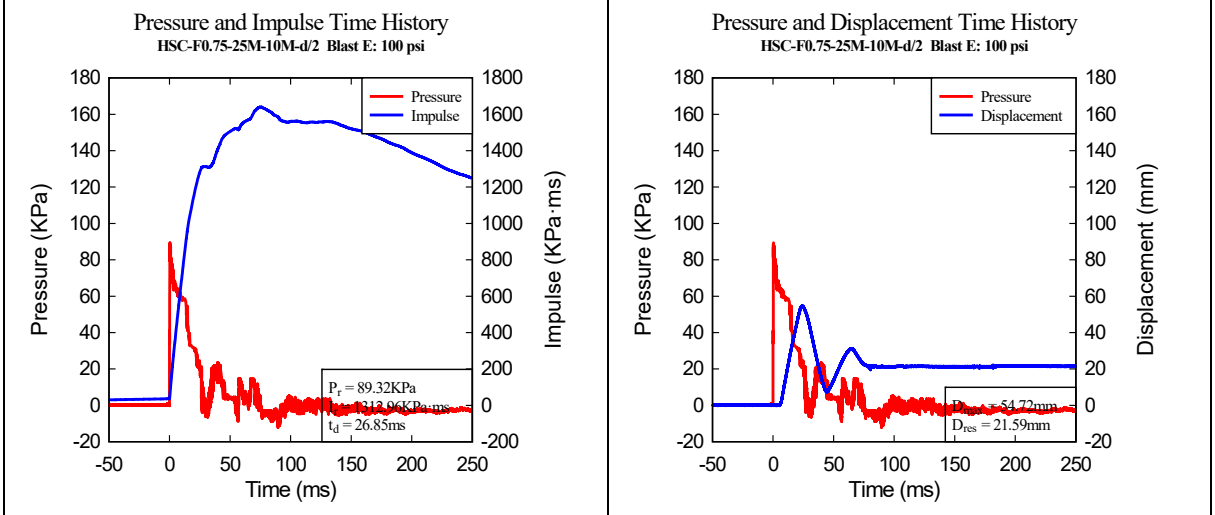

(c) Blast E: Reflected pressure, impulse, and displacement time histories

Figure 5-37 – HSC-F0.75-25M-10M-d/2 recorded reflected pressure, impulse and displacement for Blasts C to E

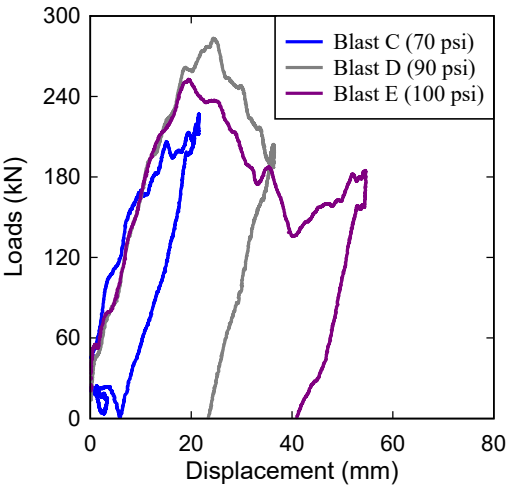

Dynamic resistance curves

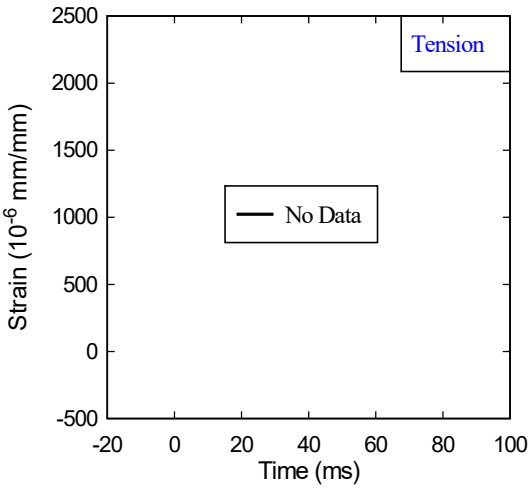

Strain data (tension bars)

Figure 5-38 Dynamic resistance curve and strain data (HSC-F0.75-25M-10M-d/2)

(a) Residual test load-deflection result

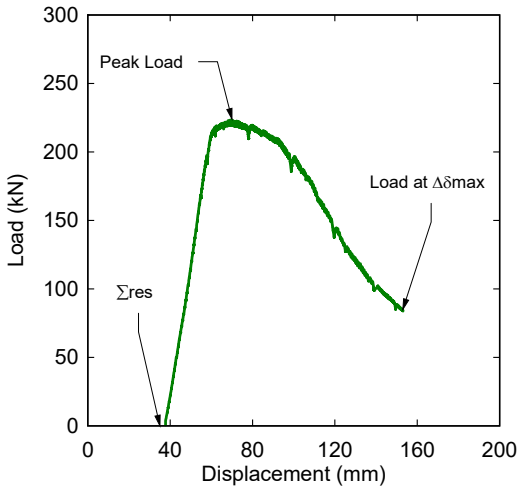

Data Summary	
∑res (mm)	37.7
P_{max}^{R} (kN)	223.4
$\Delta_{max}{}^{R}$ (mm)	153.1
P_{end}^{R} (kN)	83.7

(b) Condition of beam before residual test- after Blast E (100 psi)

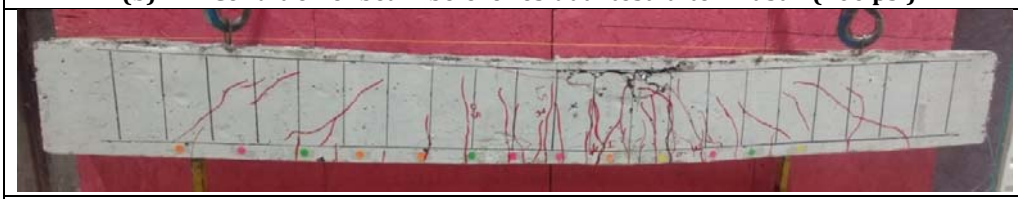

Comments

-Flexural cracks within the constant moment region of the beam.
-Some signs of crushing

(c) Condition of beam after Residual Test

Comments

-Pronounced Localized cracks and more severe concrete crushing in the midspan region
-Buckling of bars occurs between the ties

Figure 5-39 Residual test results for beam HSC-F0.75-25M-10M-d/2

CHAPTER 6: DISCUSSION OF EXPERIMENTAL RESULTS

6.1 CHAPTER OVERVIEW

This chapter presents a discussion examining the results of the HSC and HSFRC beams tested under quasi-static and simulated blast loads. The effects of blast detailing, fibers, longitudinal steel ratio, transverse reinforcement ratio, compression steel ratio, and repeated loading are investigated. In addition, the effects of test variables on the dynamic reaction curves, and the residual post-blast capacity of the beams are investigated.

6.2 SUMMARY OF RESULTS

This study included seventeen beams, including seven beams tested under static loads, and ten beams tested under dynamic loading. In order to investigate the effect of blast detailing, an additional two beams tested by Algassem (2016) are included in the discussions: HSC-F0-15M-0M* and HSC-F0-20M*. These beams were designed with plain HSC and nominal detailing, consisting of 2-15M or 2-20M bars, with open stirrups in the shear spans only.

The static load-deflection curves for all beam tested in this study are shown in **Figure 6-1**, while key parameters from these curves are summarized in **Table 4-1**including: maximum load (P_{max}), secant stiffness (K), yield displacement (Δ_y), displacement (Δ_{end}), ductility ($\Delta_{end}/\Delta_{yield}$) and toughness ($A_{end}$) at the end of testing, defined as the area under the curves up to Δ_{end}.

The results from the blast tests are summarized in **Table 5-2,** which reports the shockwave data (P_r , I_r and t_d = peak reflected pressure, impulse, and positive phase duration) as well as specimen response after each test (D_{max}, D_{res} and θ_{max} = maximum displacement, residual displacement, and support rotation). **Table 5-2** also compares the results with the response limits in the CSA S850 blast standard. **Figure 6-2-Figure 6-4** also provides an overview of the blast test results, in terms of displacements, failure blasts and photos illustrating failure mode.

The majority of beams in this study had significant post-blast resistance. The residual resistance of the beams was assessed by testing the blast-damaged beams under static four-point bending. **Figure 6-1-b** provides a summary of these tests.

The following sections review the effects of detailing, tension-steel ratio, fibers and compression/transverse steel ratio on the static, blast and post-blast responses of the beams

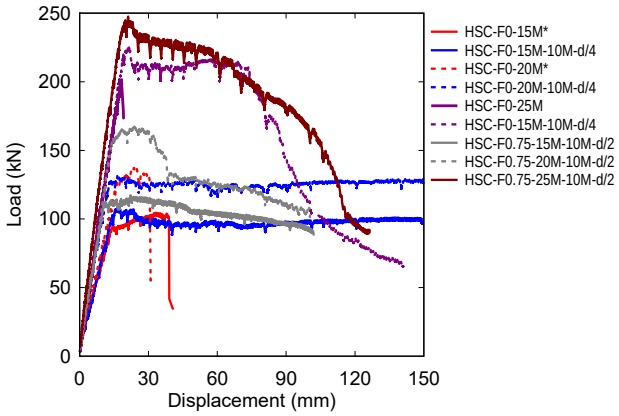

(a) Static test results

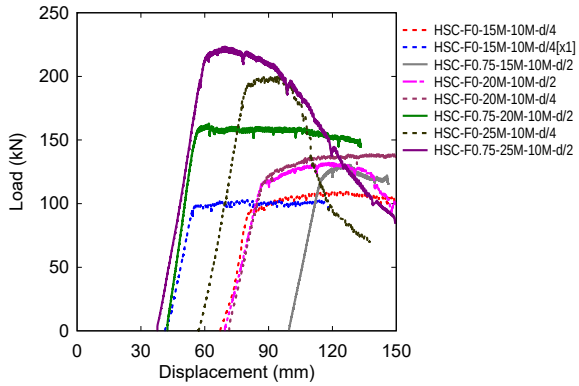

(b) Residual static test results

Figure 6-1 - Load displacement curves for all specimens

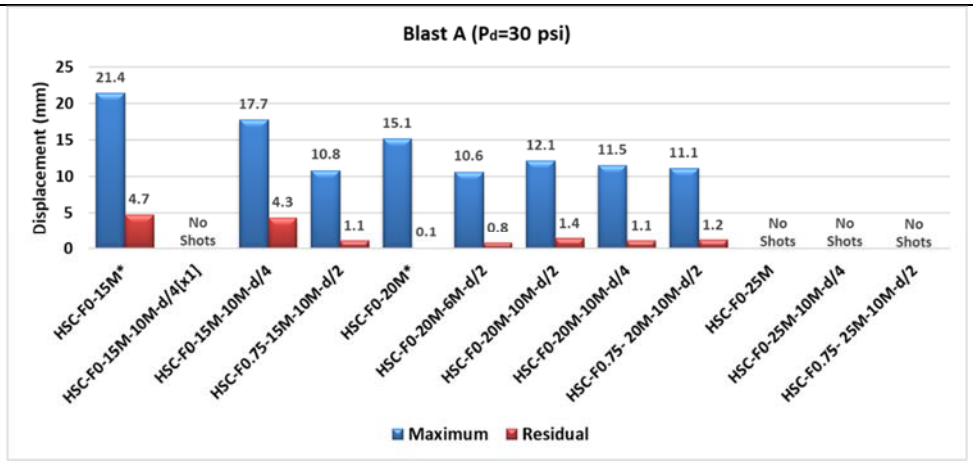

(a) Blast A (30 psi)

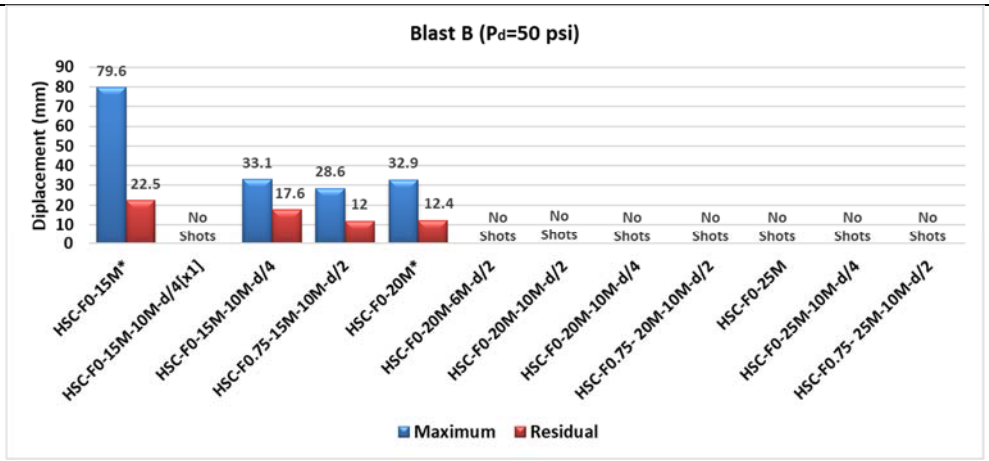

(a) Blast B (50 psi)

*: Tested by Algassem (2016).

[x1]: Sigle Shot

Figure 6-2 - Maximum and residual displacements for Blast A and B (30 and 50 psi)

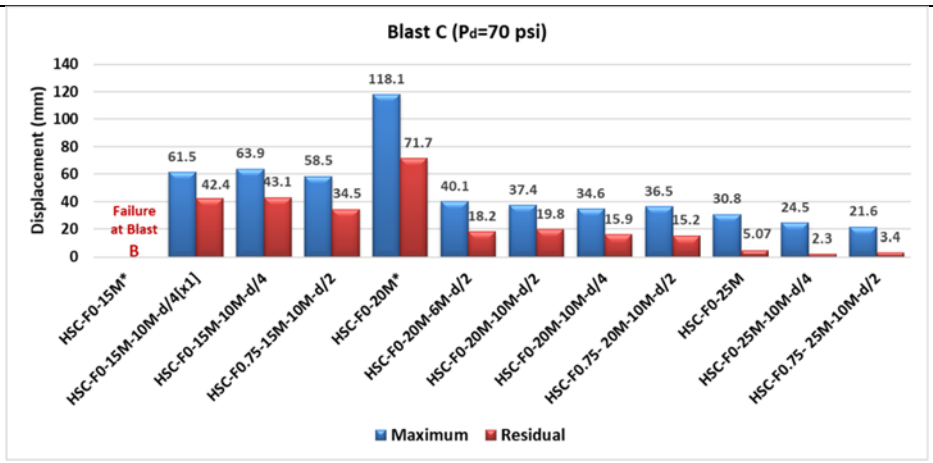

(a) Blast C (70 psi)

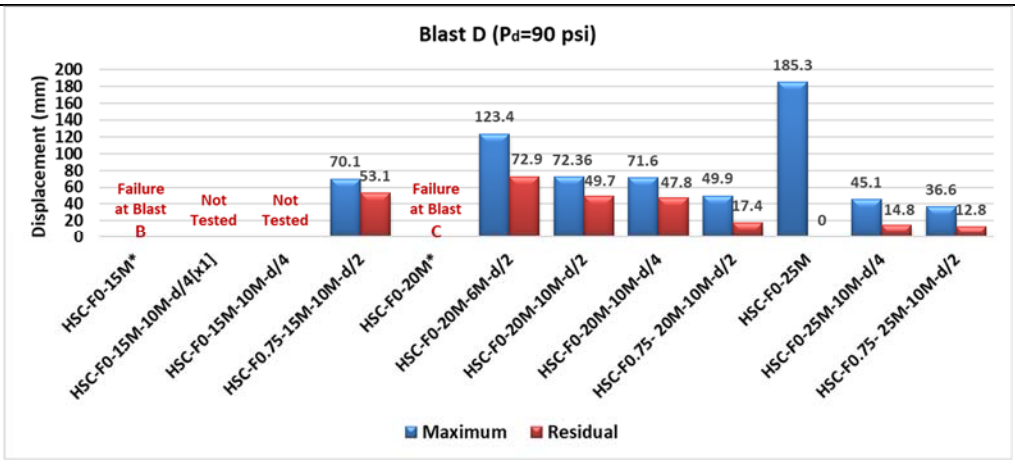

(b) Blast D (90 psi)

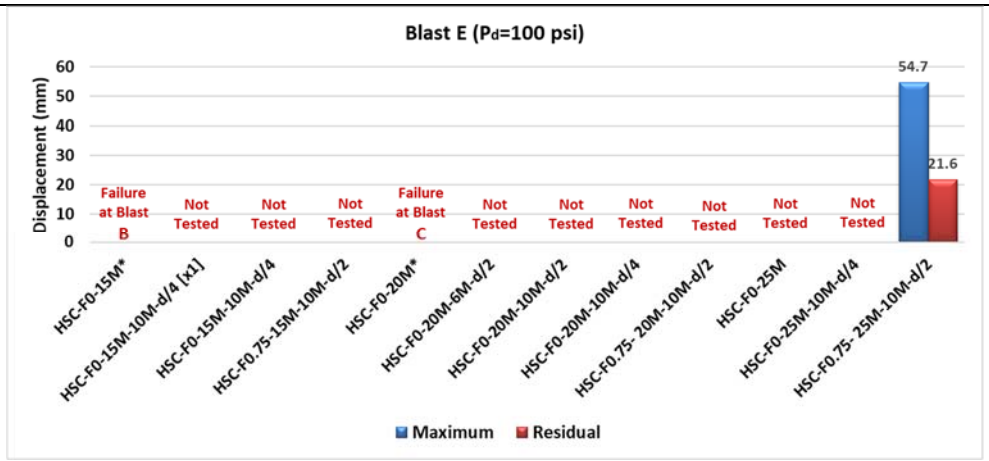

(c) Blast E (100 psi)

Figure 6-3 - Maximum and residual displacements for Blast C, D, and E (70, 90, and 100 psi)

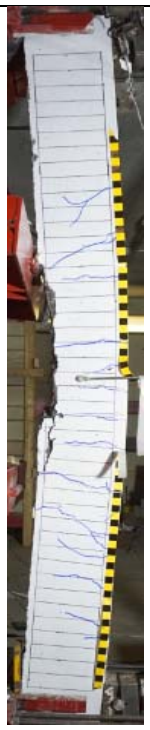 HSC-F0-15M-10M-d/4 Blast C (70 psi)	 HSC-F0-15M-10M-d/4[x1] Blast C (70 psi)	 HSC-F0.75-15M-10M-d/2 Blast D (90 psi)	 HSC-F0-20M-6M-d/2 Blast D (90psi)	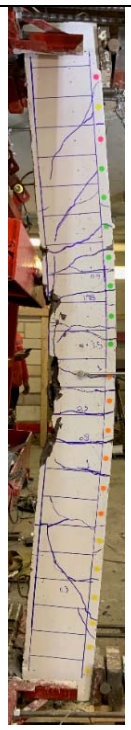 HSC-F0-20M-10M-d/2 Blast D (90psi)
 HSC-F0-20M-10M-d/4 Blast D (90psi)	 HSC-F0.75-20M-10M-d/2 Blast D (90psi)	 HSC-F0- 25M Blast D (90psi)	 HSC-F0-25M-10M-d/4 Blast D (90psi)	 HSC-F0.75-25M-10M-d/2 Blast D (100psi)

Figure 6-4 –Photos of all beams indicating Final Blasts

6.3 EFFECT OF BLAST DETAILING

The effect of blast detailing on the static and dynamic response of the HSC beams can be examined by comparing the responses of the blast-detailed HSC beams (HSC-F0-15M-10M-d/4, HSC-F0-20M-10M-d/4, and HSC-F0-25M-10M-d/4), with the companion nominally-detailed beams (HSC-F0-15M, HSC-F0-20M, and HSC-F0-25M). Detailing in the blast-detailed beams included top continuity (compression) bars and closed ties spaced at s = 50 mm (d/4) throughout the span, while the nominally-detailed beams were singly-reinforced with open-stirrups at s = 100 mm (d/2) in the shear spans only.

6.3.1 STATIC TEST RESULTS

Figure 6-5 and **Table 6.1** summarize the static results for the beams with blast and nominal detailing. It can be observed that the improved detailing enhanced all aspects of structural response and failure mode under static loading.

No clear trend emerges when examining the effect on peak strength and stiffness. In the 15M series, beam HSC-F0-15M-10M-d/4 shows an increase of 3% in strength (P_{max}) when compared to beam HSC-F0-15M*, with similar stiffness. A similar effect is observed in the 25M series, where beam HSC-F0-25M-10M-d/4 shows an 11% in peak strength (owing to the change in failure mode) with similar stiffness when compared to HSC-F0-25M. On the other hand, in the 20M series, beam HSC-F0-20M-10M-d/4 shows similar strength to HSC-F0-20M*, with a 24% increase in stiffness. It can be concluded that the reinforcement detailing did not significantly affect peak strength and stiffness in the HSC beams.

On the other hand, the enhancement in post-peak ductility is clear. In the 15M and 20M series, the nominally detailed HSC beams reached yielding but eventually failed in flexure due to crushing of HSC concrete in the midspan compression zone at maximum displacements of Δ_{max} = 41 mm [L/54] and 31 mm [L/72]. In comparison, provision of compression bars and transverse ties in the companion beams with blast detailing allowed the beams to carry sustained post-peak loads until very large deflections of $\sim \Delta_{max}$ = 150 mm [L/13]. As a result, beams HSC-F0-15M-10M-d/4 and HSC-F0-20M-10M-d/4 show impressive increases in ductility (Δ_{max}/Δ_y) [↑ 233% & 376%] and overall toughness (A_{max}) [↑ 328% & 531%] when compared to the companion beams with nominal detailing (see **Table 1**). The enhancement in behavior can be explained by the improvement in toughness and confinement in the midspan compression zone which controlled and delayed concrete crushing. Similarly, owing to the reduced tie spacing (from d/2 to d/4) changed the failure mode from shear to flexure in the beam with 25M bars. Moreover, the improved concrete response in the midspan zone allowed the beam to carry significant post-peak deformations despite the high-tension steel ratio, representing significant improvements when compared to the sudden shear failure in the companion with nominal stirrups.

A ductility index of 3 is generally considered as adequate in the study of reinforced concrete beams (Rashid and Mansur, 2005). This minimum is approximately met in the nominally-detailed beam with 15M bars (HSC-F0-15M: Δ_{max}/Δ_y= 2.74), but not satisfied in beam HSC-F0-20M which had 20M bars and a reinforcement ratio ρ = 2.4%, which was only slightly lower than the maximum permitted by the CSA S850 blast standard (ρ = 2.5%). Previous research shows that the ductility of conventionally reinforced HSC beams significantly reduces as the ratio ρ/ρ_b approaches 0.4-0.5 (Wu et al., 2005); the result for beam HSC-F0-20M which had a ratio ρ/ρb = 0.42 fits this trend. In comparison, the blast-detailed beams with 15M and 20M bars show ductility ratios of 9.3 and 11.5, with an ability to continue to carry the load until the end of testing (150 mm). Even beam HSC-F0-25M-10M-d/4 which had 25M bars, with ρ = 4.1% (well above the CSA S850 limit), shows important ductility of Δ_{max}/Δ_y= 4.2 (where Δ_{max} is taken at 85% drop in load). In summary, the results demonstrate the significant response characteristics that can be gained from the use of blast detailing in HSC beams, even under quasi-static loads.

6.3.2 BLAST TEST RESULTS

The previous sub-section demonstrated the benefits of improved steel detailing on the static response of the HSC beams. As demonstrated in this section, the use of blast detailing also improved all aspects of blast response in the HSC beams**. Figure 6-6, Figure 6-9** and **Figure 6-12** compare the responses of the blast-detailed and nominally-detailed HSC beams under dynamic loading. Photos of the beams at the end of blast testing are shown in **Figure 6-7**, **Figure 6-10** and **Figure 6-13**.

Beginning with the 15M series (**Figure 6-6**), it can be observed that beam HSC-F0-15M-10M-d/4 shows reductions of 21% and 9% in maximum displacements when compared to HSC-F0-15M at Blast A (30 psi). In addition, the use of compression bars results in significant reductions in the rebound displacement (reduction of 92%) at this blast. The next blast (Blast B – 50 psi; I_r = 516582 kPa·ms) resulted in a support rotation of θ_{max} = 6.41° ("Hazardous" damage) and severe concrete failure in the HSC beam with nominal detailing (see **Figure 6-7**). In comparison, beam HSC-F0-15M-10M-d/4 survived this shot, and further tested at Blast C (70psi), with support rotations of 1.58° and 3° ("moderate" damage). As shown in **Figure 6-7,** the beam showed high damage tolerance at Blast C (I_r = 701 kPa·ms), which was limited to the loss of the top concrete cover in the midspan region.

Figure 6-9 compares the responses of the beams in the 20M series. Like the previous series, the blast design significantly improved the dynamic response of the beams at every blast. For example, beam HSC-F0-20M-10M-d/4 had a 24% reduction in maximum displacement at Blast A (30 psi), with an important reduction in the rebound displacement. As shown in **Figure 6-10**, the absence of compression bars and confinement steel caused specimen HSC-F0-20M* to fail in flexure at Blast C (70 psi) (I_r = 703 kPa·ms) which resulted in a support rotation of θ_{max} = 6.06° ("hazardous" damage). The failure was associated with significant

concrete crushing in the midspan zone, with the generation of important secondary fragments at failure. On the other hand, damage remained well controlled in the beam with blast detailing at Blast C, with the beam also tested under Blast D (90 psi) (I_r = 837 kPa-ms), with support rotations of θ_{max} = 1.65° and 3.4° ("moderate" damage) at these two blasts. As shown in **Figure 6-10**, after Blast D, damage was limited to spalling of top concrete cover in the mid-span compression region, with the use of closely spaced ties ensuring the integrity of the core concrete region and preventing bar buckling.

The effect of blast detailing in the 25M series can be observed in **Figure 6-12**. To recall the beams in this series were heavily reinforced in tension with ρ = 4.1%. Under static loading, the use of closely spaced ties and blast-detailing prevented shear failure and allowed for high ductility. Under blast loading, both the beams with nominal and improved detailing failed in flexure, but with improved response for beam HSC-F0-25M-10M-d/4. Examining the results, the beam with 25M bars and blast detailing shows reductions of 21% and 55% in maximum and residual displacements when compared to beam HSC-F0-25M which only had stirrups in the shear spans. Failure of beam HSC-F0-25M occurs in a severe manner under Blast D (90 psi), with a very large maximum displacement, large support rotation of θ_{max} = 8.6° ("hazardous") owing to the nominal detailing and over-reinforced conditions. As shown in **Figure 6-13** the lack of compression bars and ties resulted in severe damage and complete loss of concrete in the midspan compression zone. In comparison, the beam with blast detailing survived Blast D, experiencing a support rotation of θ_{max} = 2.1o ("moderate"), with damage limited to spalling of the top cover concrete cover and visible protection of the midspan core region.

In summary, the results demonstrate the significant increases in blast resistance (ability to withstand higher blast loads before failure) and ductility (ability to withstand larger displacements/support rotations without damage) that can be gained from the use of improved detailing in high-strength concrete beams designed using the guidelines in the CSA S850 blast standard.

In addition to the enhancements in displacement control, blast capacity and damage tolerance, the use of blast detailing also allowed for significant post-blast residual capacity as will be discussed in the next sections.

Table 6.1 - Effect of blast detailing - 15M Series Static Test Results

ID	Load		Displacement			Stiffness	Ductility		Toughness (kN-mm)		Failure Mode
	P_y (kN)	P_{max} (kN)	Δ_{yield} (mm)	Δ_{max} (mm)	Δ_{end} (mm)	K (N/mm)	$\frac{\Delta_{max}}{\Delta_{yield}}$	$\frac{\Delta_{end}}{\Delta_{yield}}$	A_{max}	A_{end}	
HSC-F0-15M*	95	105	15	41	41	6518	2.7	2.7	3273	3273	Flexure
HSC-F0-15M-10M-d/4	105	108	16	149	149	6562	9.3	9.3	14018	14018	Flexure

(a) Load Displacement Curves for 15M series

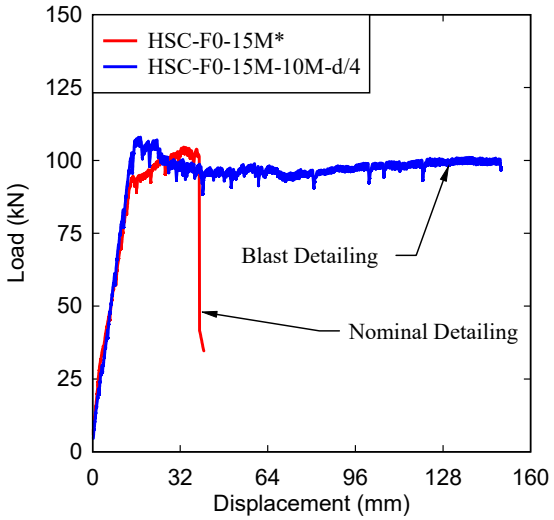

(b) Condition of beams at Failure		Δ_{max}	Failure
HSC-F0-15M*		41	Flexure
HSC-F0-15M-10M-d/4		149	Flexure

Figure 6-5 - Load Displacement Curves and photos of the beams under static loads - 15M series

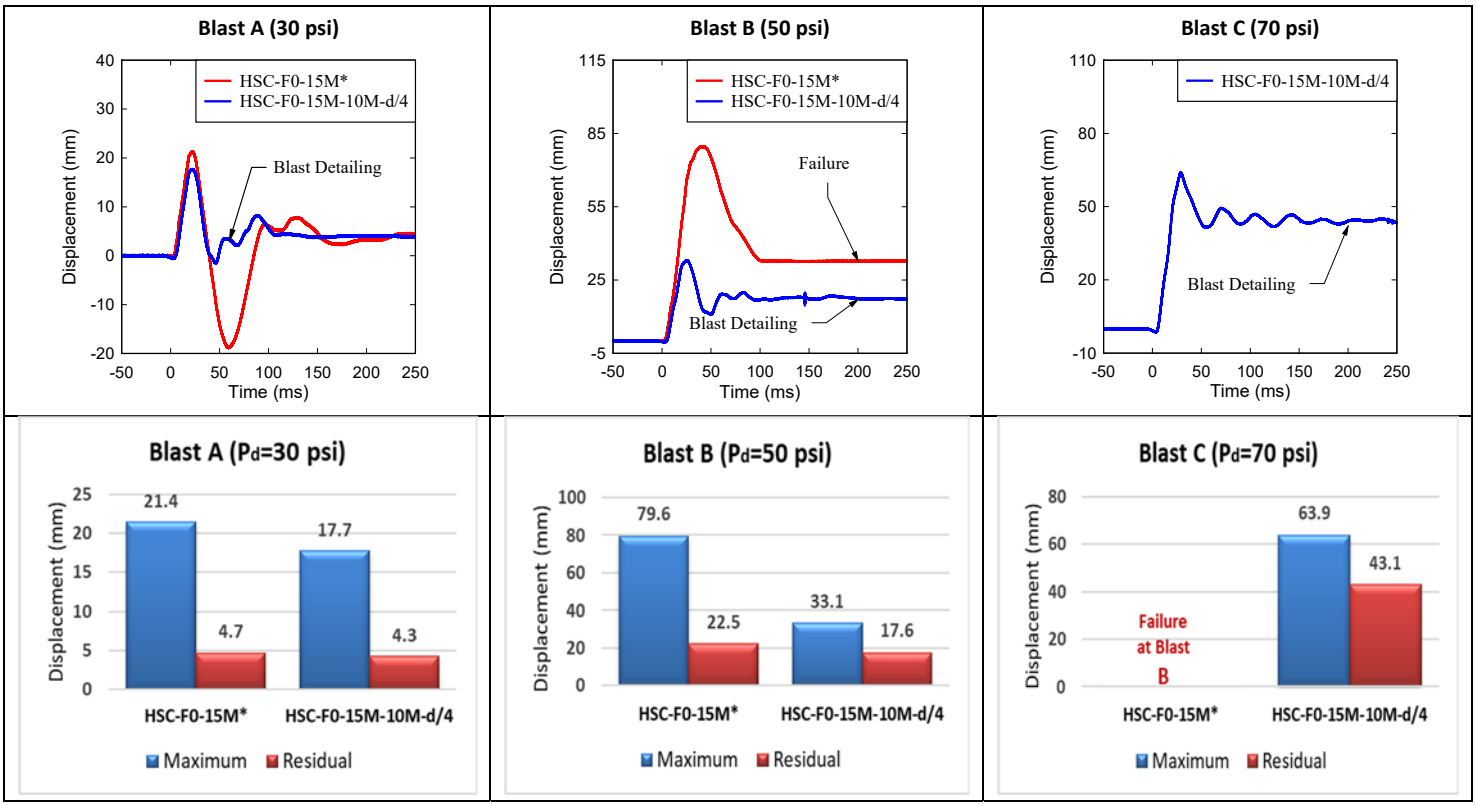

Figure 6-6 - Effect of blast detailing on displacements: Series 15M

HSC-F0-15M*		HSC-F0-15M-10M-d/4	
Blast B (50 psi) – Flexure Failure		Blast B (50 psi)	Blast C (70 psi) – Flexure Failure

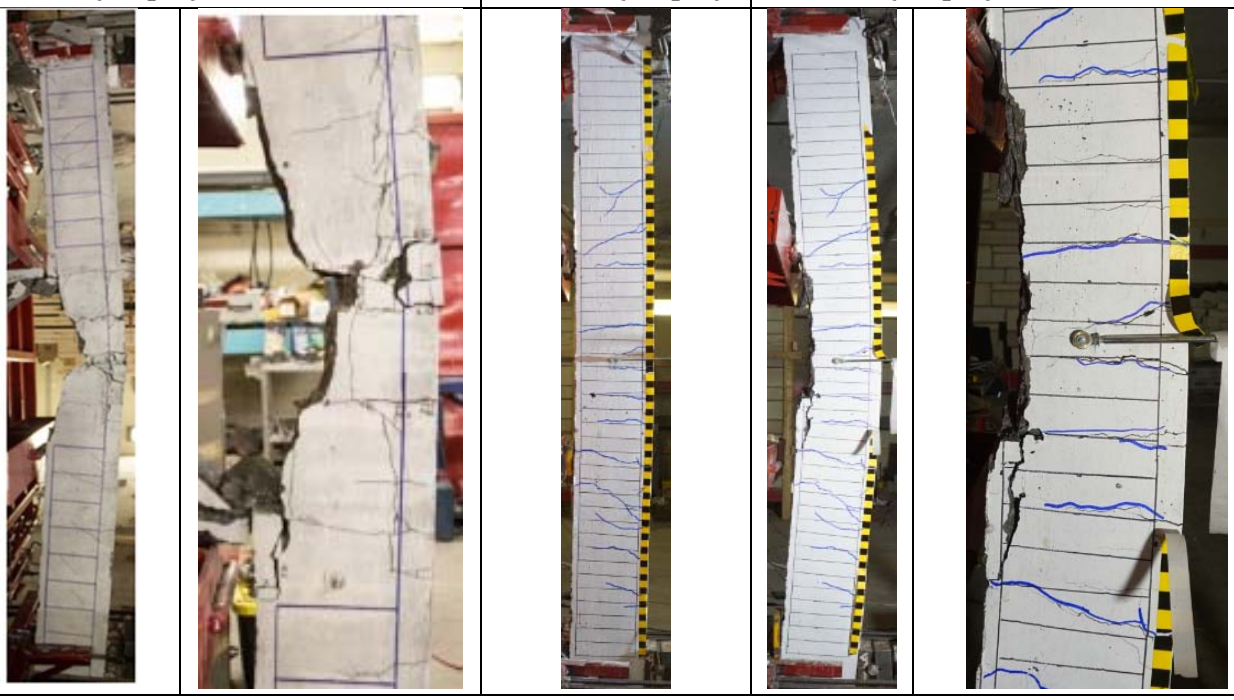

Figure 6-7 - Damage and Failure Modes of the 15M series beams with nominal detailing and blast detailing

Table 6.2 – Effect of blast detailing - 20M Series Static Test Results

ID	Load		Displacement			Stiffness	Ductility		Toughness (kN-mm)		Failure Mechanism
	P_y (kN)	P_{max} (kN)	Δ_{yield} (mm)	Δ_{max} (mm)	Δ_{end} (mm)	K (N/mm)	$\frac{\Delta_{max}}{\Delta_{yield}}$	$\frac{\Delta_{end}}{\Delta_{yield}}$	A_{max}	A_{end}	
HSC-F0-20M*	126	137	16	31	31	7615	2.1	2.1	2994	2994	Flexure
HSC-F0-20M-10M-d/4	127	131	13	150	150	9411	11.5	11.5	18889	18889	Flexure

(a) Load Displacement Curves for 20M series

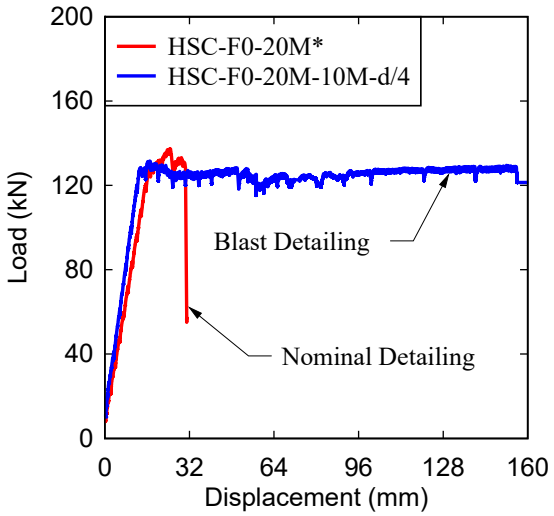

(b) Condition of beams at Failure		Δ_{max}	Failure
HSC-F0-20M*	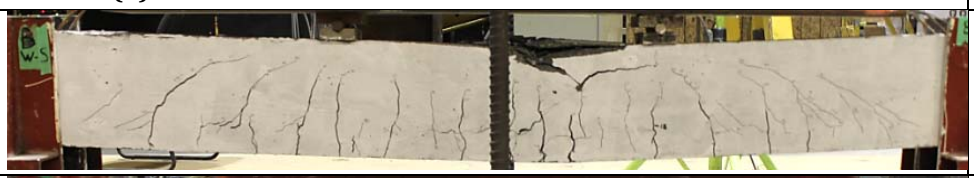	31	Flexure
HSC-F0-20M-10M-d/4		150	Flexure

Figure 6-8 - Load Displacement Curves for 20M series tested under static load

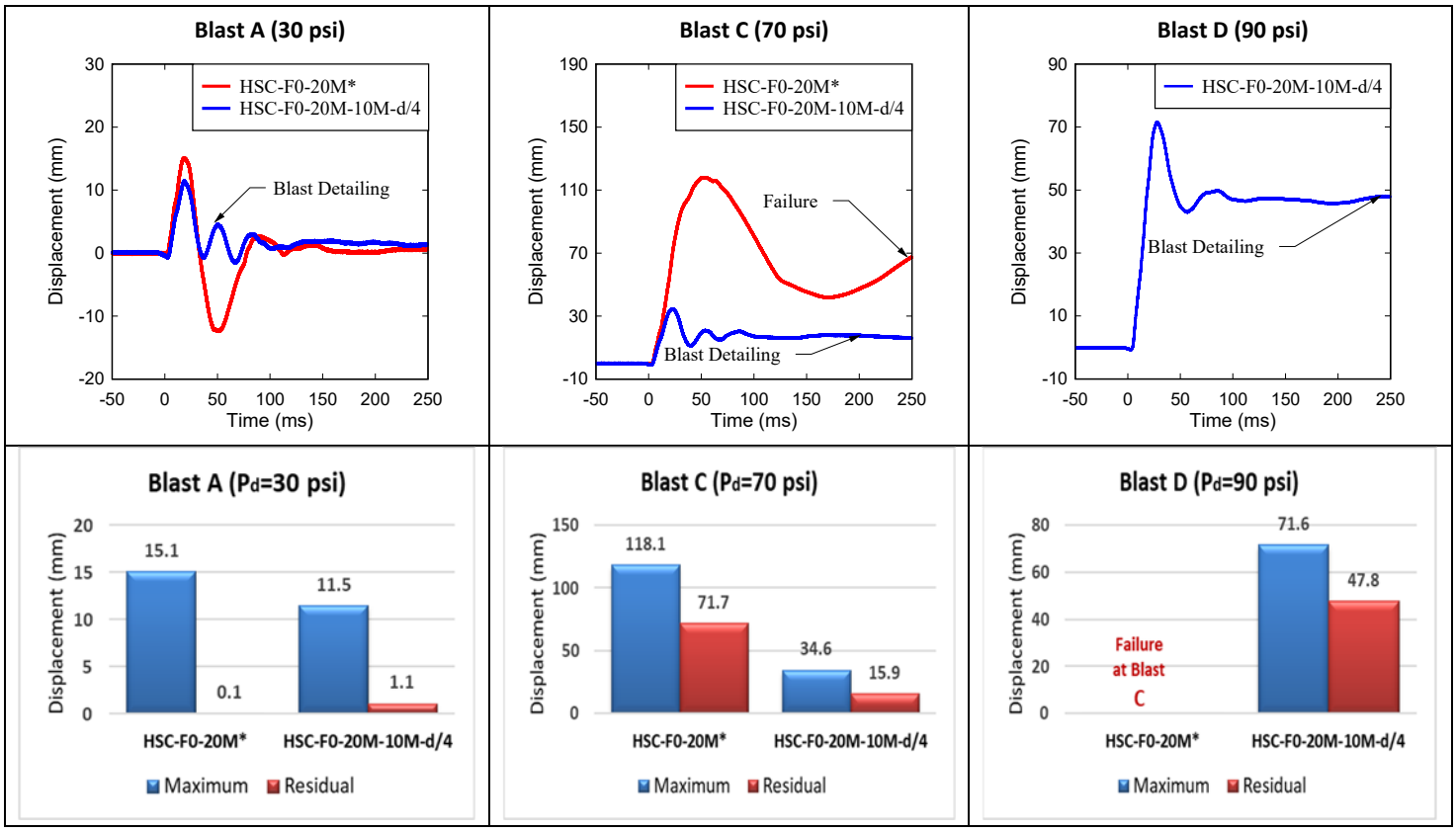

Figure 6-9 - Displacement time histories; Effect of blast detailing on HSC specimens: Series 20M

HSC-F0- 20M*		HSC- F0-20M-10M-d/4	
Blast B (70 psi) – Flexure Failure		Blast B (70 psi)	Blast C (90 psi) – Flexure Failure
			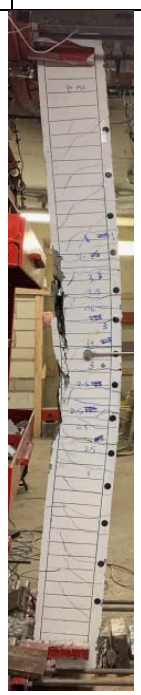 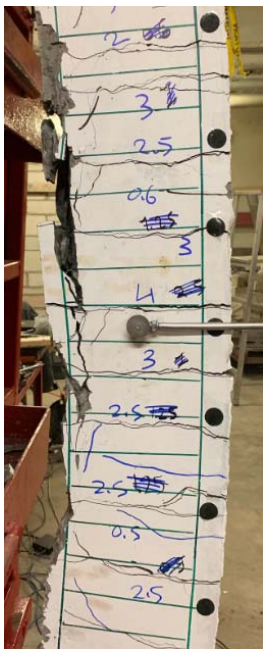

Figure 6-10 - Damage and Failure Modes of the 20M series with nominal detailing and blast detailing

Table 6.3 – Effect of blast detailing - 25M Series Static Test Results

ID	Load		Displacement			Stiffness	Ductility		Toughness (kN-mm)		Failure Mechanism
	P_y (kN)	P_{max} (kN)	Δ_{yield} (mm)	Δ_{max} (mm)	Δ_{end} (mm)	K (N/mm)	$\frac{\Delta_{max}}{\Delta_{yield}}$	$\frac{\Delta_{end}}{\Delta_{yield}}$	A_{max}	A_{end}	
HSC-F0- 25M	-	202	-	-	18	11098	-	-	-	1920	Shear
HSC-F0-25M-10M-d/4	220	225	19.2	80	120	11458	4.17	6.25	14734	19734	Flexure

(a) Load Displacement Curves for 25M series

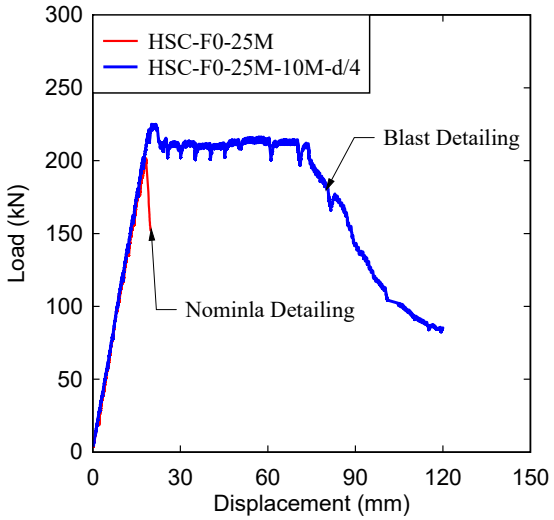

(b) Condition of beams at Failure		Δ_{max}	Failure
HSC-F0- 25M		18	Shear
HSC-F0-25M-10M-d/4		120	Flexure

Figure 6-11 - Load Displacement Curves for 25M series tested under static load

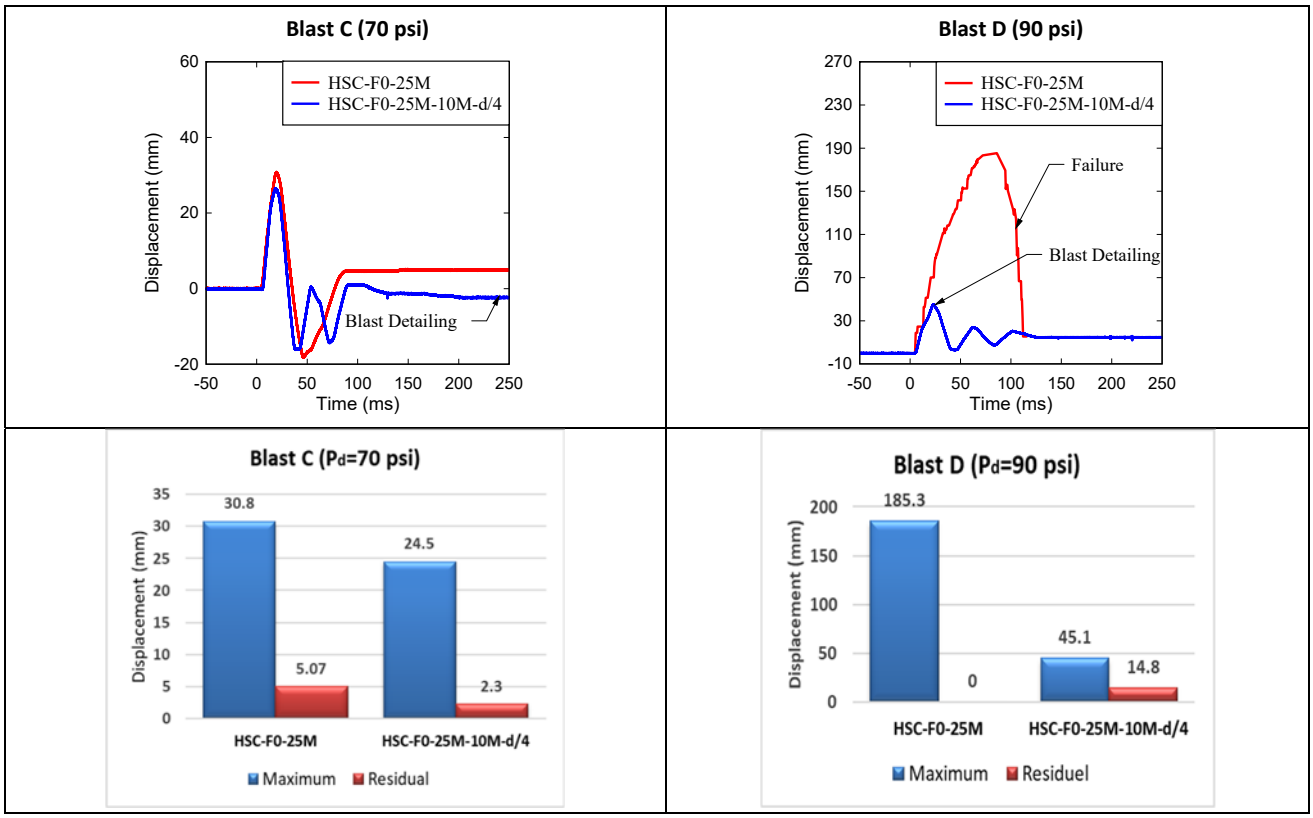

Figure 6-12 - Displacement time histories; Effect of blast detailing on HSC specimens Series 25M

HSC-F0- 25M		HSC- F0-25M-10M-d/4	
Blast D (90 psi) – Severe Crushing Failure		Blast C (90 psi) – Flexure Failure	
			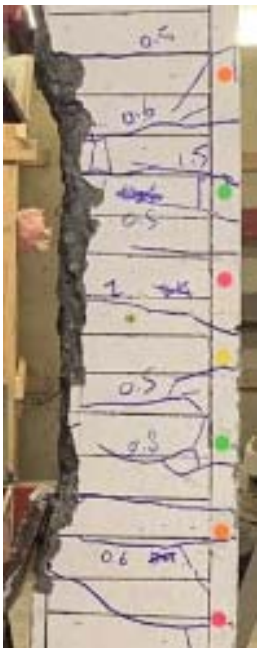

Figure 6-13 - Damage and Failure Modes of the 25M series with nominal detailing and blast detailing

6.4 EFFECT OF FIBERS

The effect of Fibers is examined by comparing the static and dynamic responses of the following three sets of specimens: (1) HSC-F0-15M-10M-d/4 and HSC-F0.75-15M-10M-d/2; (2) HSC-F0-20M-10M-d/4 and HSC-F0.75-20M-10M-d/2 and (3) HSC-F0-25M-10M-d/4 and HSC-F0.75-25M-10M-d/2, which were built with plain HSC and HSFRC containing 0.75% of hybrid fibers, respectively. Traverse reinforcement in the plain HSC specimens consisted of close hoops spaced at 50 mm (s=d/4), while a larger "intermediate" tie spacing of 100 mm (s=d/2) was used in the beams with fibers.

6.4.1 STATIC TEST RESULTS

Table 6.4 to **Table 6.6** present the static results, while **Figure 6-14**, **Figure 6-17**, and **Figure 6-20** show the load-defection curves and the damage profile of the beams with steel fibers. The experimental results show that a moderate amount of steel fibers can be used to enhance the overall performance of the beams and relax detailing while also improving the control of cracking and damage. First, it can be observed that the beams with fibers show increased peak strength and stiffness when compared to their plain HSC companions. Examining the results, beams HSC-F0.75-15M-10M-d/2, HSC-F0.75-20M-10M-d/2, and HSC-F0.75-25M-10M-d/2 in the 15M, 20M and 25M series, show improvements of 8%, 13% and 10% in peak load (P_{max}) with enhancements of 55%, 28%, and 9% in initial stiffness (K), when compared to beams HSC-F0-15M-10M-d/4, HSC-F0-20M-10M-d/4, and HSC-F0-25M-10M-d/4. The ability of steel fibers to bridge cracks was also evident at the early stage of testing, delaying the formation of the first hairline cracks and reducing crack widths prior to yielding.

In general, the use of fibers delayed concrete crushing in the midspan region, and the excellent toughness of the HSFRC concrete in compression allowed for minimum damage in the midspan compression zone throughout testing. The ability of fibers to delay crushing is most clear in the beams with 25M bars, where beam HSC-F0.75-25M-10M-d/2 shows improvements of 4% and 16% in ductility and overall toughness when compared to HSC-F0-25M-10M-d/4. In general, it can be seen that the fibers allowed for high ductility and toughness in all three series. On the other hand, the use of fibers resulted in crack localization, where the crack widths extended rapidly at one or two cracks, resulting in high strains in the tension steel bars at these locations. This translated into early bar rupture in the HSFRC beam with 15M bars (ρ=1.5%), resulting in a relative loss of ductility and a more brittle failure mode when compared to its HSC companion. Increasing the tension bar area prevented such failure in the HSFRC beam with 25M bars (ρ=4.1%), whereas crack localization is also apparent in the HSFRC beam with 20M bars (ρ=2.5%). It is also noted that while the increased tie spacing (d/2) did not affect damage in the midspan concrete zone, it led to compression bar buckling in the HSFRC beams with 15M and 25M bars.

6.4.2 BLAST TEST RESULTS

The previous sub-section demonstrated the benefits of steel fibers on the static response of the HSC beams in terms of strength and stiffness. The fiber-reinforced concrete beams also showed post-peak behavior which at least matched that of the more-heavily detailed HSC beams, except that earlier bar rupture was observed when using low steel ratio.

This section compares the dynamic responses of the companion HSC beams and HSFRC beams to examine if fibers can relax blast detailing (i.e. increase tie spacing) and further improve blast response. **Figure 6-15, Figure 6-18** and **Figure 6-21** present the dynamic responses of beams HSC-F0.75-15M-10M-d/2, HSC-F0.75-20M-10M-d/2, and HSC-F0.75-25M-10M-d/2 (which were built with HSFRC and d/2 ties) and beams HSC-F0-15M-10M-d/4, HSC-F0-20M-10M-d/4, and HSC-F0-25M-10M-d/4 (which were built with plain HSC and d/4 ties). The damage and failure photos of the beams are shown in **Figure 6-16, Figure 6-19** and **Figure 6-22.**

Examining the results, HSFRC beams were effective in controlling the displacements, cracks and secondary fragmentation at each blast (Blast A, B, C, D, and E). Blast A (30 psi) was intended to test beams within the elastic range and resulted in similar responses for the companion HSFRC and HSC beams. The contribution of fibers becomes more pronounced at higher blast intensities. In the 15M series, the use of fibers resulted in reductions of 14% and 8% in maximum displacements, and reductions of 33% and 24 in residual displacements at Blasts B (50 psi) and C (70 psi). Likewise, the beams in the 20M series show similar responses at Blast A, but the fibers reduce maximum and residual displacements by 30% and 43% at Blast D (90 psi). In the same way, the use of fibers, in the 25M series reduced maximum and residual deformations by 19% and 14% at this same blast.

The use of fibers also improved the damage tolerance in the beams. As noted in the previous sections the use of blast detailing allowed for high damage control in the HSC beams with compression bars and d/4 ties, however, these beams suffered spalling/crushing of the top cover region. This spalling is clear in the final test photos of the HSC beams in the 15M, 20M, and 25M sets. In comparison, this cover damage remained well controlled in the companion HSFRC beams which were subsequently tested at larger blast intensity without failure. This is also clear when examining the high-speed videos of the companion beams (see **Figure 6-39** to **Figure 6-41**). All HSFRC beams did not fail under intense blast testing, showing significant post-blast residual capacity as will be discussed in the following sections.

In summary, the use of fibers in HSC was effective in controlling blast-induced displacements and damage with responses that matched or outperformed the responses of the companion beams with blast detailing. Keeping in mind the potential of bar rupture, the results show that the use of a moderate amount of fibers (0.75% volume content in this study) can be used to relax transverse reinforcement detailing while enhancing the blast performance.

Table 6.4 - Effect of Fibers - 15M Series Static Test Results

ID	Load		Displacement			Stiffness	Ductility		Toughness (kN-mm)		Failure Mechanism
	P_y (kN)	P_{max} (kN)	Δ_{yield} (mm)	Δ_{max} (mm)	Δ_{end} (mm)	K (N/mm)	$\frac{\Delta_{max}}{\Delta_{yield}}$	$\frac{\Delta_{end}}{\Delta_{yield}}$	A_{max}	A_{end}	
HSC-F0-15M-10M-d/4	105	108	16	149	149	6562	9.3	9.3	14018	14018	Flexure
HSC-F0.75-15M-10M-d/2	112	117	11	98.8	102	10181	8.9	9.3	9997	10234	Flexure Bar Rupture

(a) Load Displacement Curves for 15M series

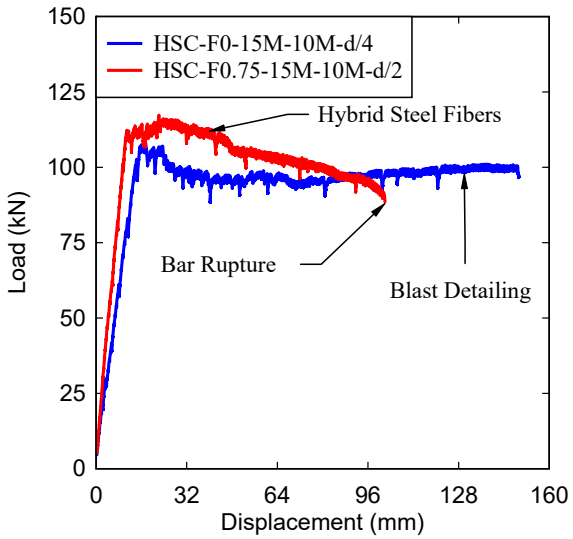

(b) Condition of beams at Failure		Δ_{max}	Failure
HSC-F0-15M-10M-d/4		149	Flexure
HSC-F0.75-15M-10M-d/2		102	Flexure Bar Rupture

Figure 6-14 - Load Displacement Curves for 15M series tested under static load

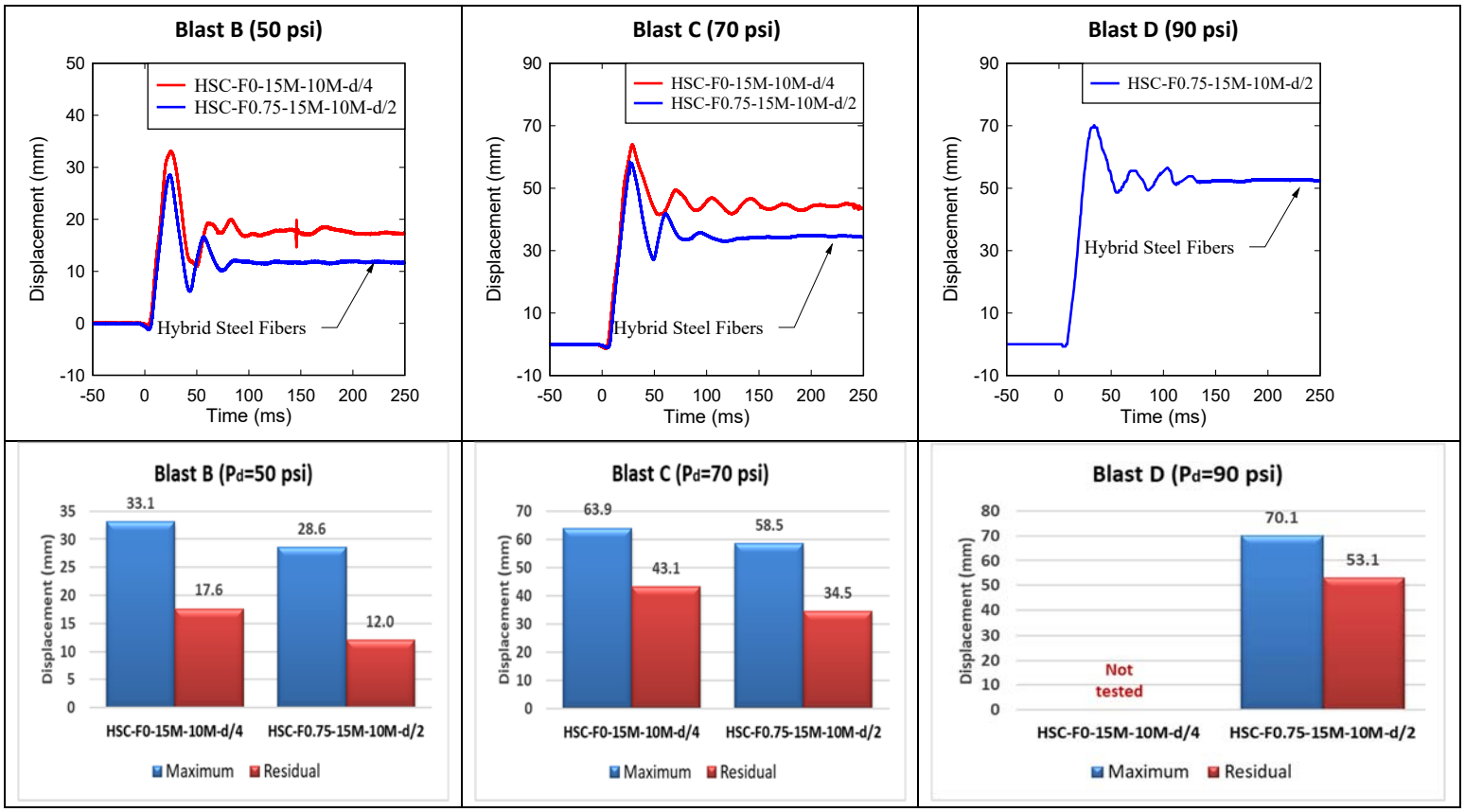

Figure 6-15 - Displacement time histories: Effect of fibers in 15M series

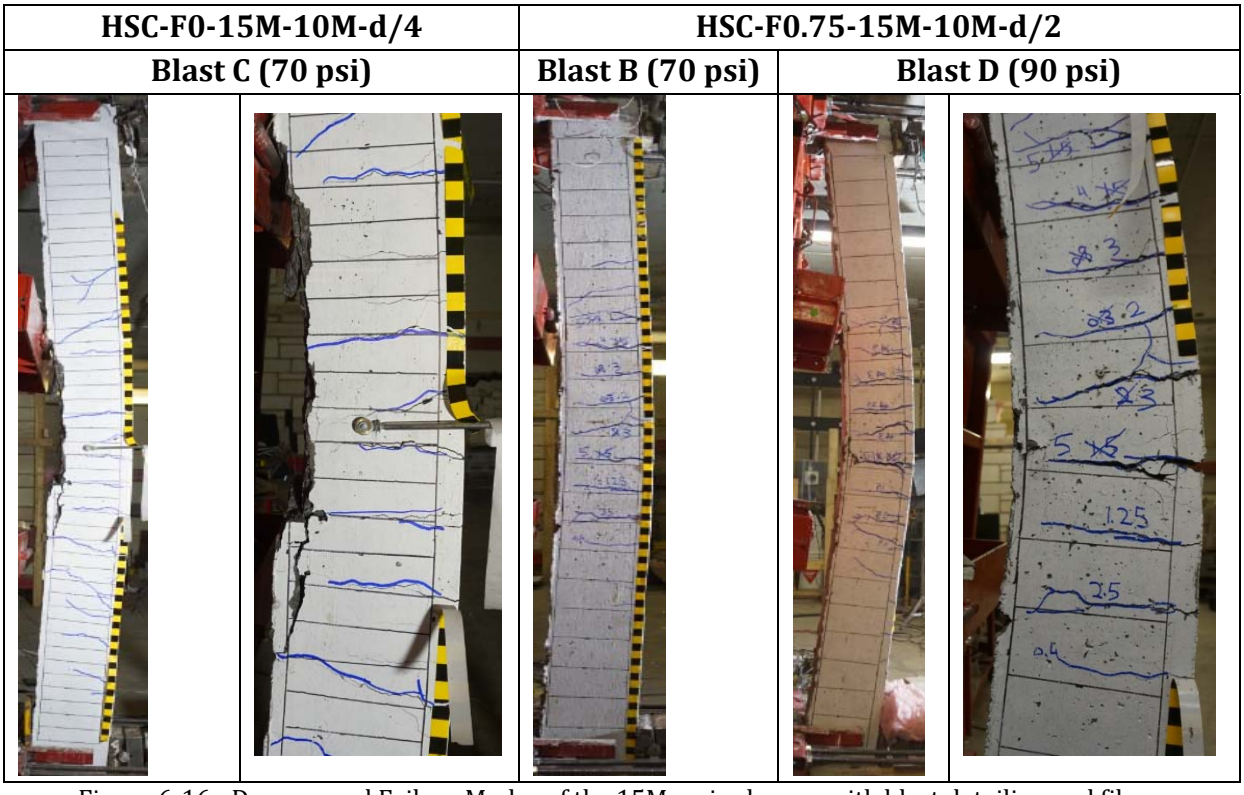

Figure 6-16 - Damage and Failure Modes of the 15M series beams with blast detailing and fibers

Table 6.5 - Effect of Fibers - 20M Series Static Test Results

ID	Load		Displacement			Stiffness	Ductility		Toughness (kN-mm)		Failure Mechanism
	P_y (kN)	P_{max} (kN)	Δ_{yield} (mm)	Δ_{max} (mm)	Δ_{end} (mm)	K (N/mm)	$\frac{\Delta_{max}}{\Delta_{yield}}$	$\frac{\Delta_{end}}{\Delta_{yield}}$	A_{max}	A_{end}	
HSC-F0-20M-10M-d/4	127	131	13	150	150	9411	11.5	11.5	18889	18889	Flexure
HSC-F0.75-20M-10M-d/2	160	168	15	37	100	10667	2.5	6.8	4781	12494	Flexure

(a) Load Displacement Curves for 15M series

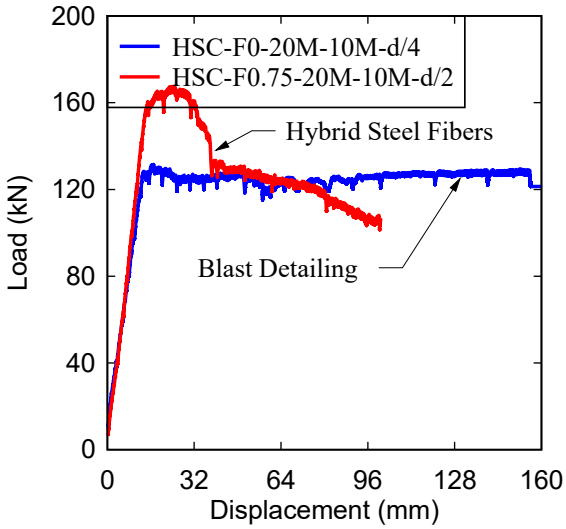

(b) Condition of beams at Failure		Δ_{max}	Failure
HSC-F0-20M-10M-d/4		150	Flexure
HSC-F0.75-20M-10M-d/2		100	Flexure

Figure 6-17 - Load Displacement Curves for 20M series tested under static load

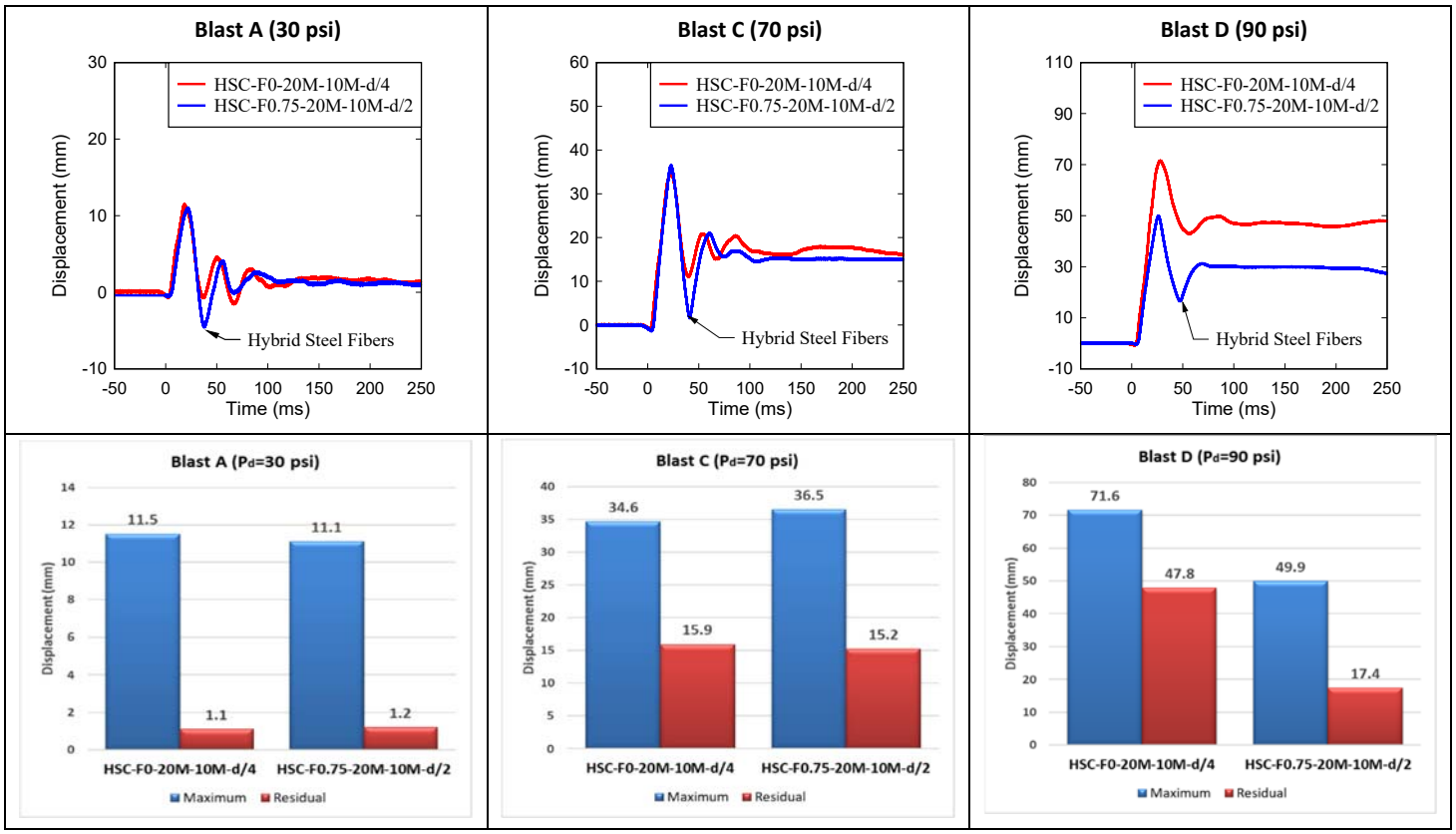

Figure 6-18 - Displacement time histories; Effect of fibers in 20M series

HSC-F0-20M-10M-d/4		HSC-F0.75-20M-10M-d/2	
Blast D (90 psi)		Blast D (90 psi)	
	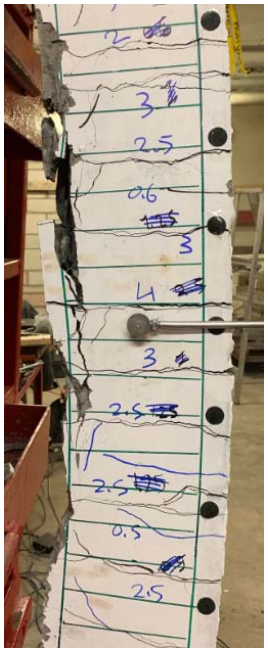		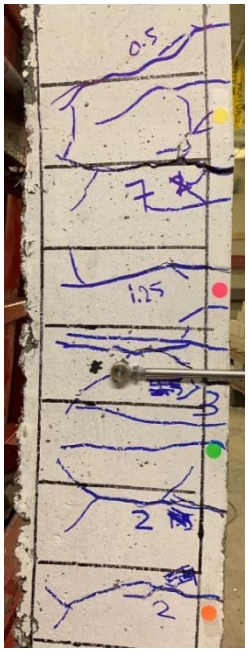

Figure 6-19 - Damage and Failure Modes of the 20M series with blast detailing and fibers

Table 6.6 – Effect of Fibers - 25M Series Static Test Results

ID	Load		Displacement			Stiffness	Ductility		Toughness (kN-mm)		Failure Mechanism
	P_y (kN)	P_{max} (kN)	Δ_{yield} (mm)	Δ_{max} (mm)	Δ_{end} (mm)	K (N/mm)	$\frac{\Delta_{max}}{\Delta_{yield}}$	$\frac{\Delta_{end}}{\Delta_{yield}}$	A_{max}	A_{end}	
HSC-F0-25M-10M-d/4	220	225	19.2	80	120	11458	4.17	6.25	14734	19734	Flexure
HSC-F0.75-25M-10M-d/2	240	248	19.3	70	125	12435	3.5	6.47	13931	22811	Flexure

(a) Load Displacement Curves for 25M series

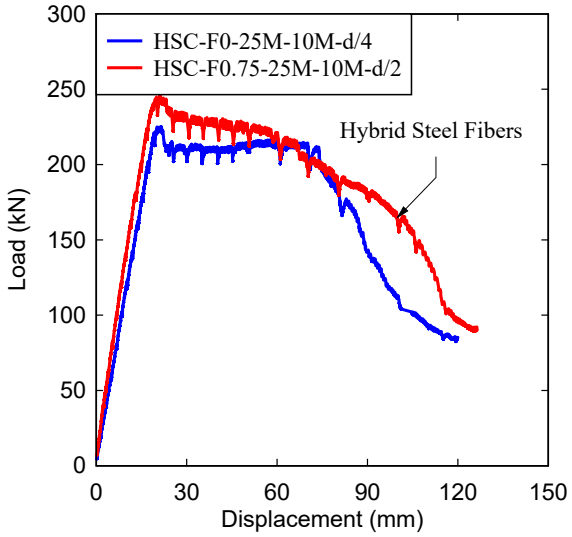

(b) Condition of beams at Failure		Δ_{max}	Failure
HSC-F0-25M-10M-d/4		120	Flexure
HSC-F0.75-25M-10M-d/2		125	Flexure

Figure 6-20 - Load Displacement Curves for 25M series tested under static load

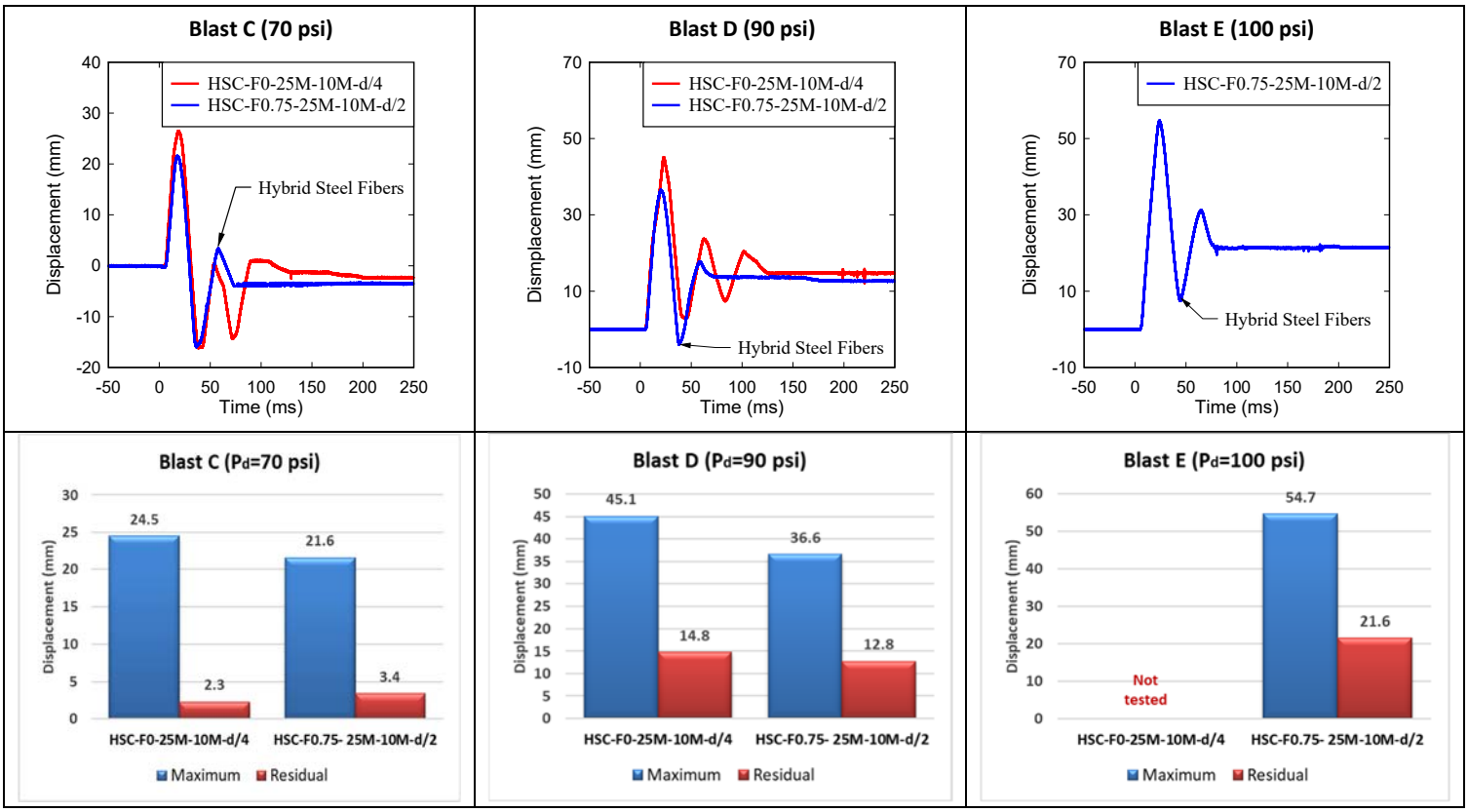

Figure 6-21 - Displacement time histories; Effect of fibers: Series 25M

HSC-F0-25M-10M-d/4	HSC-F0.75-25M-10M-d/2
Blast D (90 psi)	Blast E (100 psi)

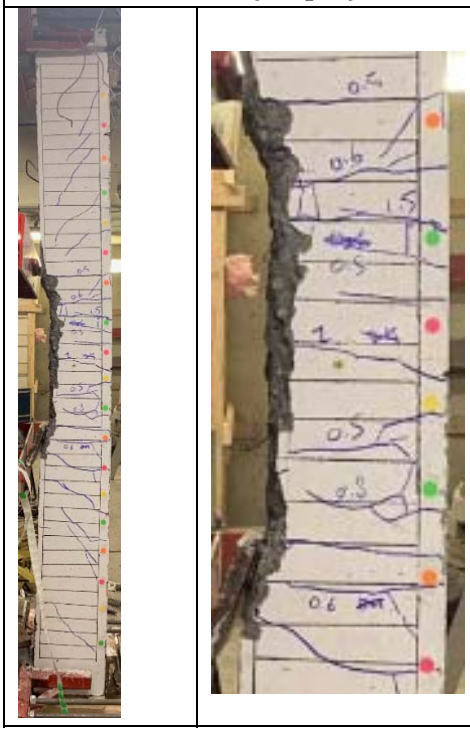

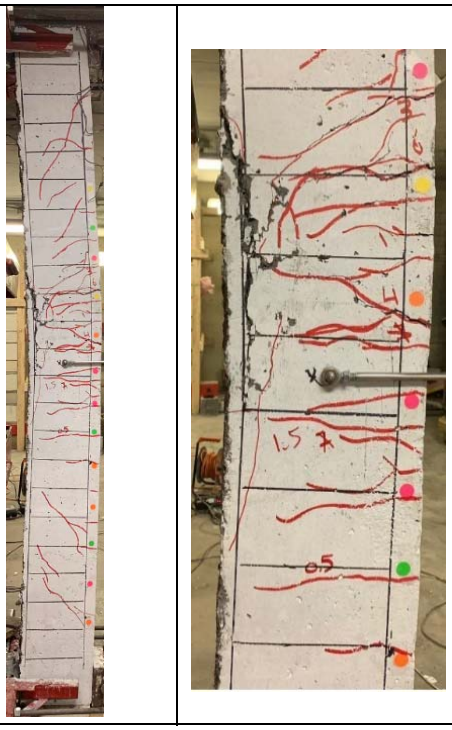

Figure 6-22 - Damage and Failure Modes of the 25M series with blast detailing and fibers

6.5 SINGLE VS REPEATED BLAST: SERIES 15M

The majority of the beams in this research were tested under repeated blasts which can result in accumulated damage. The effect of repeated loading is examined by comparing the results for beams HSC-F0-15M-10M-d/4[x1] and HSC- F0-15M-10M-d/4 which were tested under single and repeated blasts, respectively. Both beams had identical properties and were built with plain HSC and blast detailing, with 2-15M bars in tension, 2-10M bars in compression, and ties spaced at 50 mm (s = d/4) throughout the beam span.

The results of the beams are shown in **Figure 6-23** and **Figure 6-24**. Beam HSC- F0-15M-10M-d/4, was subjected to two blast loads, Blasts A-B (30-50 psi), prior to the application of Blast C (70 psi), while specimen HSC-F0-15M-10M-d/4[x1] was tested under a single shot corresponding to Blast C.

Comparing the results at Blast C, it can be observed that both beams show similar maximum and residual displacements, with D_{max} = 61.5 mm and D_{res} = 45.2 mm for HSC-F0-15M-10M-d/4[x1], corresponding to minor reductions of 3% and 6% when compared to the beam tested under repeated shots (D_{max} = 63.9 mm and D_{res} = 43.1 mm). Thus, it can be concluded that the repeated blast testing did not significantly affect the displacement responses of the blast-detailed HSC beams.

Figure 6-24 compares the photos of the specimens after Blast C. It can be observed that the beam tested under repeated tests shows loss of top cover concrete, whereas the midspan cover damage is reduced in the companion tested under the single blast. The increased damage can be explained by the "rebound" displacements experienced by beam HSC-F0-15M-10M-d/4 during blasts A/B, which weakened the unreinforced cover region prior to application of Blast C.

Figure 6-25 compares the post-blast residual static results for the companion beams tested under single and repeated blasts. It can be observed that despite the relatively greater damage in beam HSC-F0-15M-10M-d/4 before the residual static testing, both beams show similar residual post-blast resistance and ductility (in fact the beam tested under repeated blasts shows a slightly higher residual capacity). Indeed, both beams continued to carry significant loads until the end of residual static testing, demonstrating the high resilience of both blast-detailed beams.

In summary, the dynamic response of the beams didn't show large differences under single and repeated loading, with the exception of greater damage in the unreinforced cover region in the beam tested under repeated blasts.

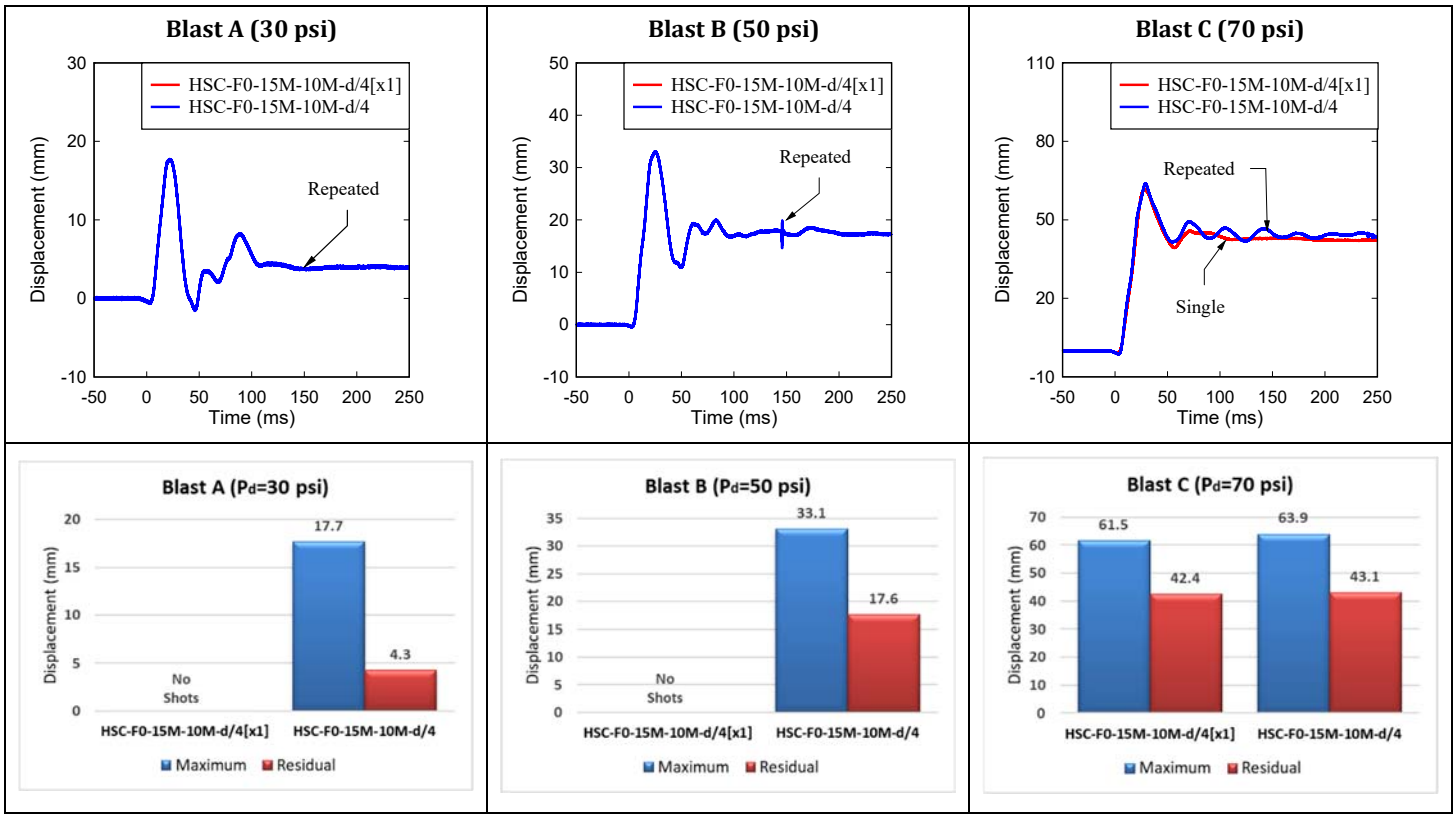

Figure 6-23 - Displacement time histories; Single vs Repeated Blast: Series 15M

HSC-F0-15M-10M-d/4[x1]	HSC- F0-15M-10M-d/4
Blast C (70 psi)	Blast C (70 psi)

Figure 6-24 - Damage and Failure Modes of the beams tested under single and repeated blasts

Comparison of residual load-deflecting curves

Shifting based on residual blast displacement	Without shifting
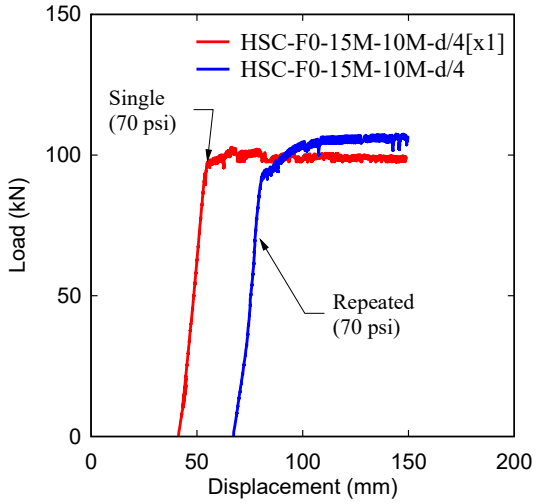	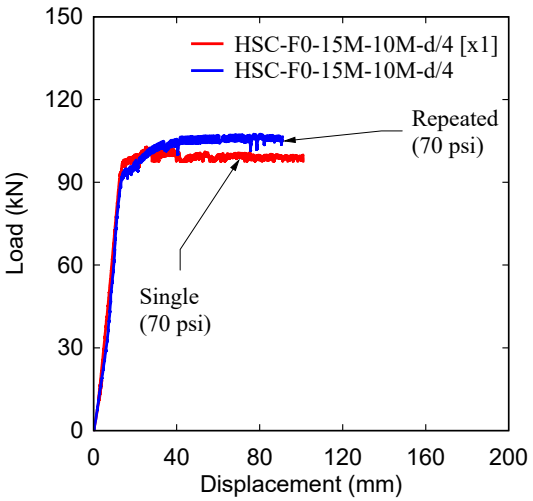

Beams after residual static testing

HSC-F0-15M-10M-d/4[x1]

($\Delta_{max}{}^{R}$ = 147.4 mm)

HSC- F0-15M-10M-d/4

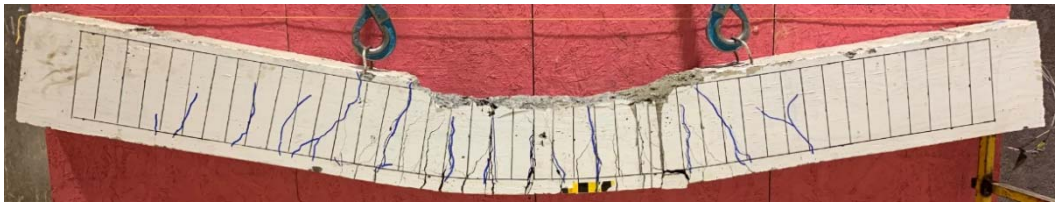

($\Delta_{max}{}^{R}$ = 151 mm)

Figure 6-25 – Residual test results for beams tested under single and repeated blasts

6.6 EFFECT OF TIE SPACING

The effect of tie spacing in the constant moment region can be examined by comparing the responses of beams HSC-F0-20M-10M-d/4 and HSC-F0-20M -10M-d/2 under blast and post-blast loading. Both beams were built with plain HSC and were double-reinforced with 20M and 10M bars in tension and compression but were detailed with closed hoops spaced at s = 50 mm (d/4; $\rho_t = 1\%$) and s = 100 mm (d/2, $\rho_t = 0.5\%$), representing blast and intermediate detailing, respectively.

Figure 6-26 compares the displacement results for the beams which were tested under Blasts A, C, and D (30, 70 and 90 psi). It can be observed that the tie spacing had limited effects on the blast deformations. Blast A tested the beams within the elastic range, with both beams showing similar responses. Examination of the results shows slight reductions of 5% in D_{max} and 21% in D_{res}, with a lower first-rebound displacement for the beam with blast detailing. Blast C pushed the tension steel into the inelastic range, with good control of damage in both specimens. Nonetheless, the beam with d/4 ties shows reductions of 7% and 20% in maximum and residual displacements when compared to HSC-F0-20M-10M-d/2. The first rebound is the same however, the rebound displacements in the second and third cycles are larger in the beam with d/2 ties. Blast D was the final shot applied on the specimens and resulted in similar responses in both beams, though the beam with d/2 ties shows slightly higher residual and 2nd rebound displacements (differences of less than 5%).

Figure 6-27 compares the damage in the beams at the end of blast testing. Both beams show similar cracking patterns and spalling of top concrete cover in compression, though the extent of the cover damage zone is greater in the beam with d/2 ties.

Figure 6-28 compares the post-blast residual static results of the companion beams with d/4 and d/2 ties. It can be observed that the beam with intermediate ties shows similar peak resistance but a more rapid strength decay, with an eventual loss of load-carrying capacity due to buckling of the 10M compression bars. In comparison, the post-blast capacity remains stable, with bar buckling prevented, in the beam with d/4 ties.

In conclusion, the results show the significant blast performance that can be gained from the use of improved detailing in HSC beams (i.e. provision of top continuity (compression) bars and transverse reinforcement throughout the beam span), even when using intermediate ties. However, the post-blast tests demonstrate that the use of d/4 ties is more effective in preventing bar buckling and confining the core concrete in the beam midspan region. Indeed, the use of such detailing ensures high post-blast residual capacity, even after intense blast testing and the applications of significant residual static loads.

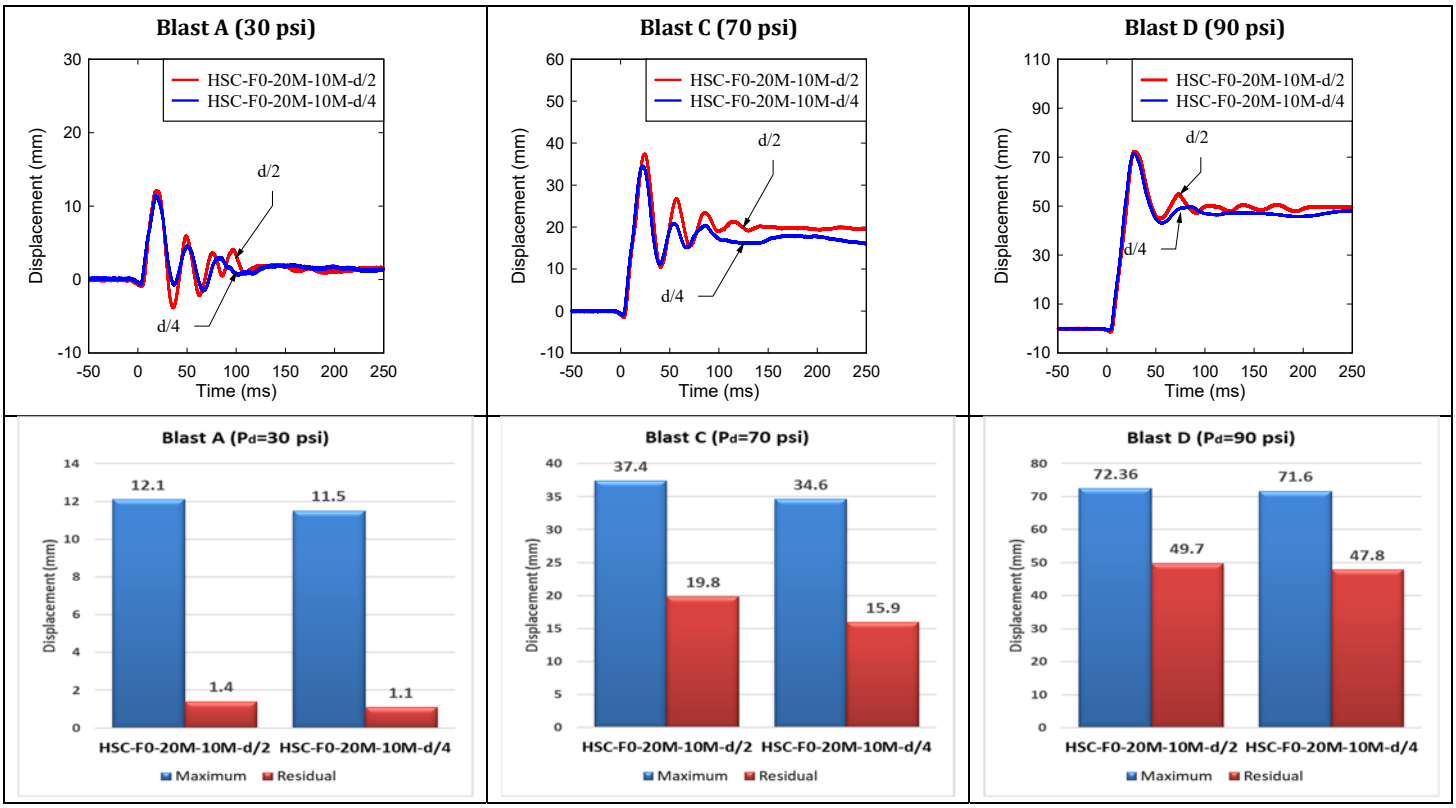

Figure 6-26 - Displacement time histories: Effect of tie spacing (d/2 vs d/4)

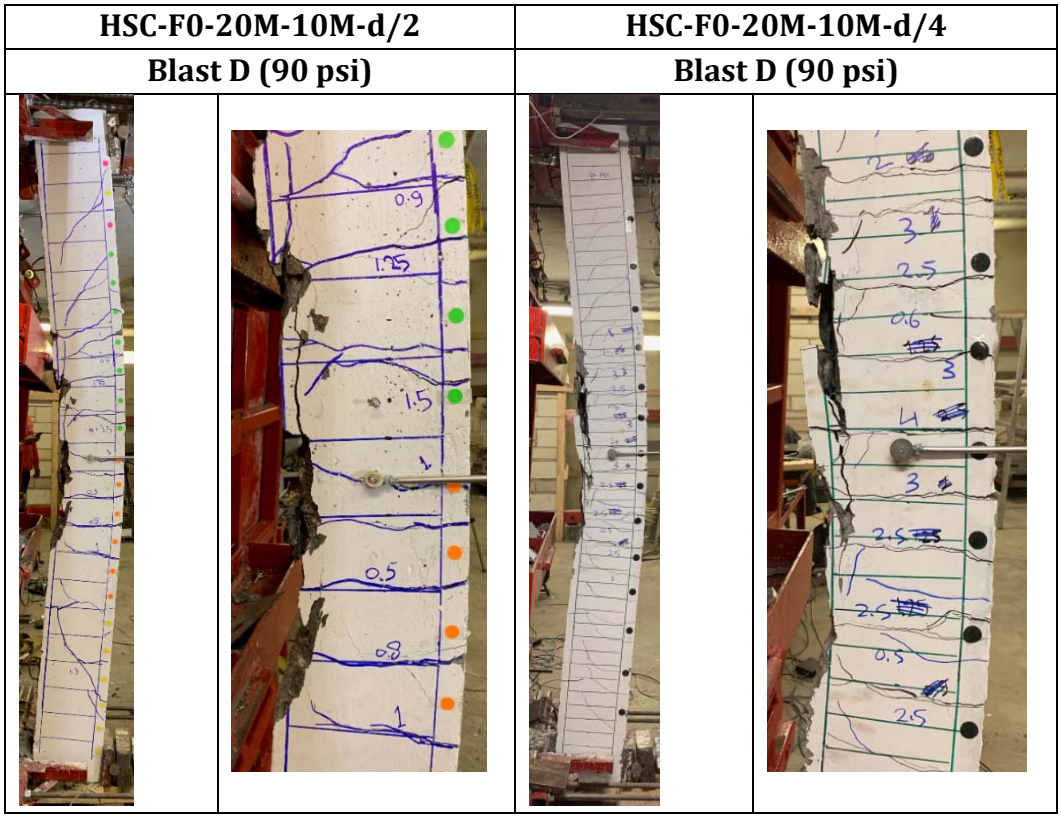

Figure 6-27 - Damage and Failure Modes of the HSC beams with d/2 and d/4 ties

Comparison of residual load-deflecting curves

Shifting based on residual blast displacement	Without shifting
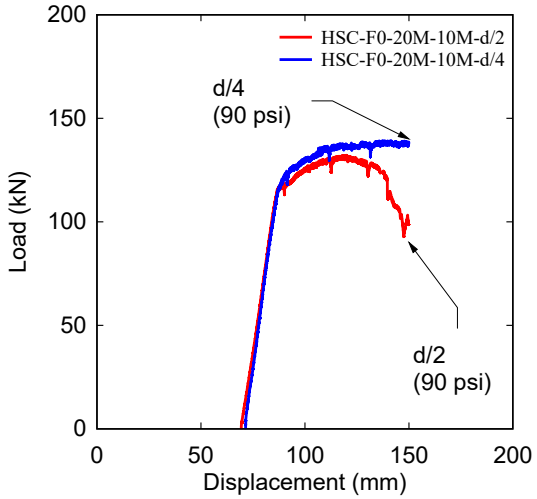	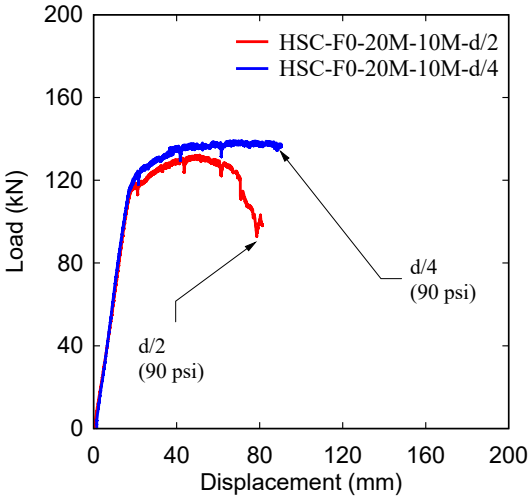

Beams after residual static testing

HSC-F0-20M-10M-d/2

($\Delta_{max}{}^{R}$ = 151.8 mm)

HSC-F0-20M-10M-d/4

($\Delta_{max}{}^{R}$ = 150.4 mm)

Figure 6-28 – Residual test results for beams with intermediate (d/2) and blast (d/4) detailing

6.7 EFFECT OF COMPRESSION STEEL RATIO

The results of specimens HSC-F0-20M-6M-d/2 and HSC-F0-20M-10M-d/2 can be compared to study the effect of the compression reinforcement ratio. Both beams were built with plain HSC and intermediate ties spaced at s = 100 mm throughout their span, however compression steel consisted of 6 mm wire ($\rho' = 0.25\%$, $A_s' = 63$ mm^2) and 10M deformed bars ($\rho' = 0.8\%$, $A_s' = 200$ mm^2) in the two beams.

Figure 6-29 compares the displacement responses of the beams at Blasts A, C, and D (30, 70, 90 psi), and **Figure 6-30** shows the damage in the beams after the final shot. Examining the dynamic test results, it can be observed that the compression steel ratio had limited effects at Blasts A and C. Indeed, the maximum displacements are similar (and in some cases slightly higher for the beam with increased amount of compression bars). However, the negative effect of the insufficient compression bar area is clear at Blast D. Beam HSC-F0-20M-6M-d/2 shows significantly larger maximum and residual deformations (increases of 42% and 32%) when compared to beam with 10M compression bars. Moreover, the beam with 6 mm wire experiences severe failure which was associated with bar buckling, significant crushing of concrete and cover spalling. In comparison, the damage is limited to the top cover region, without bar buckling, in the beam with 10M bars. As noted in the previous section, this beam was able to carry significant residual static loads after blast testing, whereas all capacity was lost in the beam with insufficient compression steel.

The CSA S850 standard requires that the area of the top and bottom reinforcement in beams at any section not be less than $1.4 b_w \frac{d}{f_y}$, where b_w, d, f_y = beam width, beam depth and specified yield strength (Cl. 9.2.4.3) = 85 mm^2, with $\rho \leq 2.5\%$. In addition, Cl. 9.2.4.4 requires that the positive and negative moment not differ significantly (this clause is intended for continuous beam members; however, it ensures a minimum level of positive and negative moment resistance throughout the beam span).

It can be observed that the requirements of Cl. 9.2.4.3 (and Cl. 9.2.4.4) are not met in beam HSC-F0-20M-6M-d/2. The results clearly demonstrate the importance of carefully detailing the compression reinforcement in HSC beams designed for blast effects.

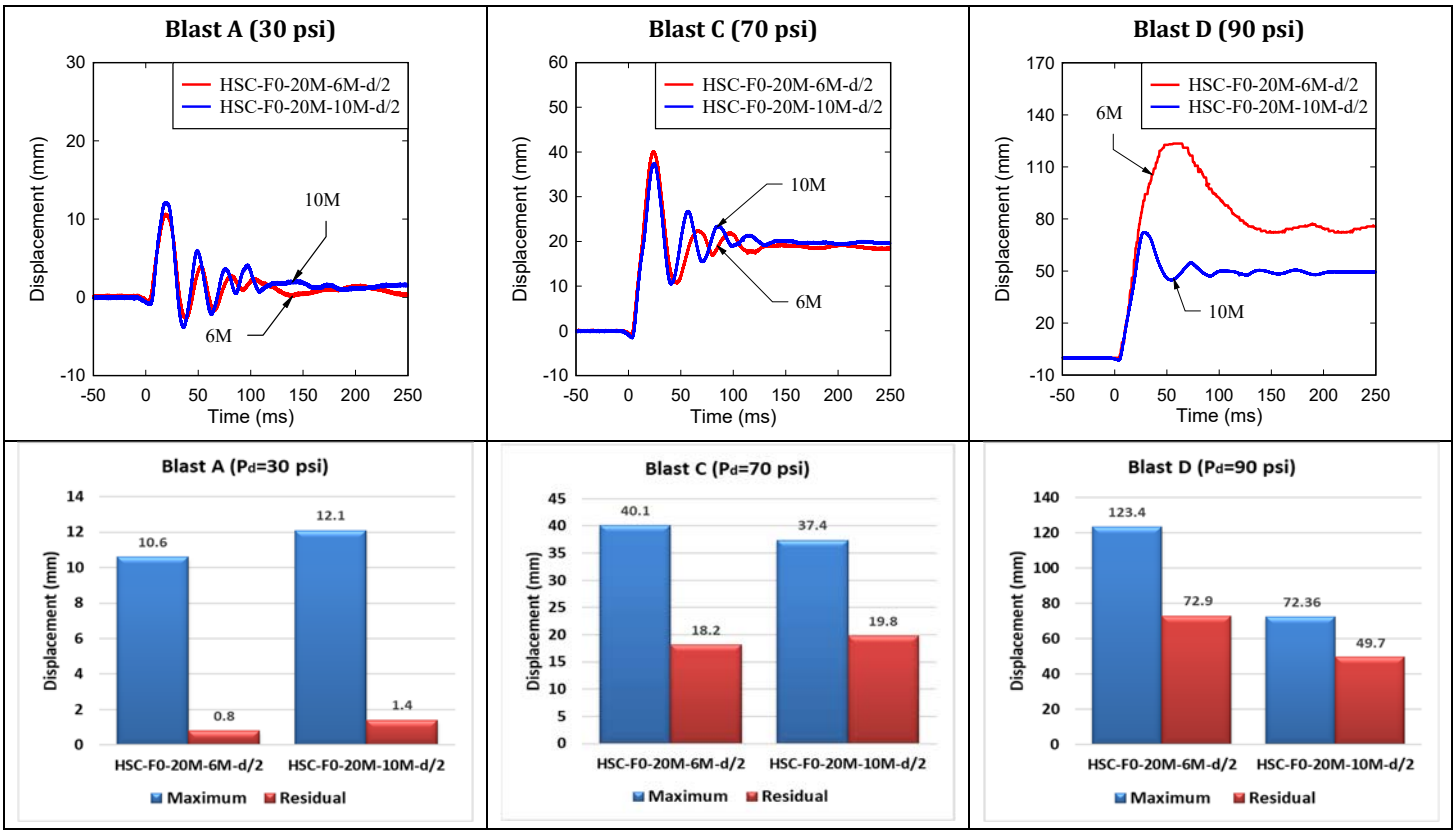

Figure 6-29 - Displacement time histories; Effect of compression reinforcement (6M vs 10M)

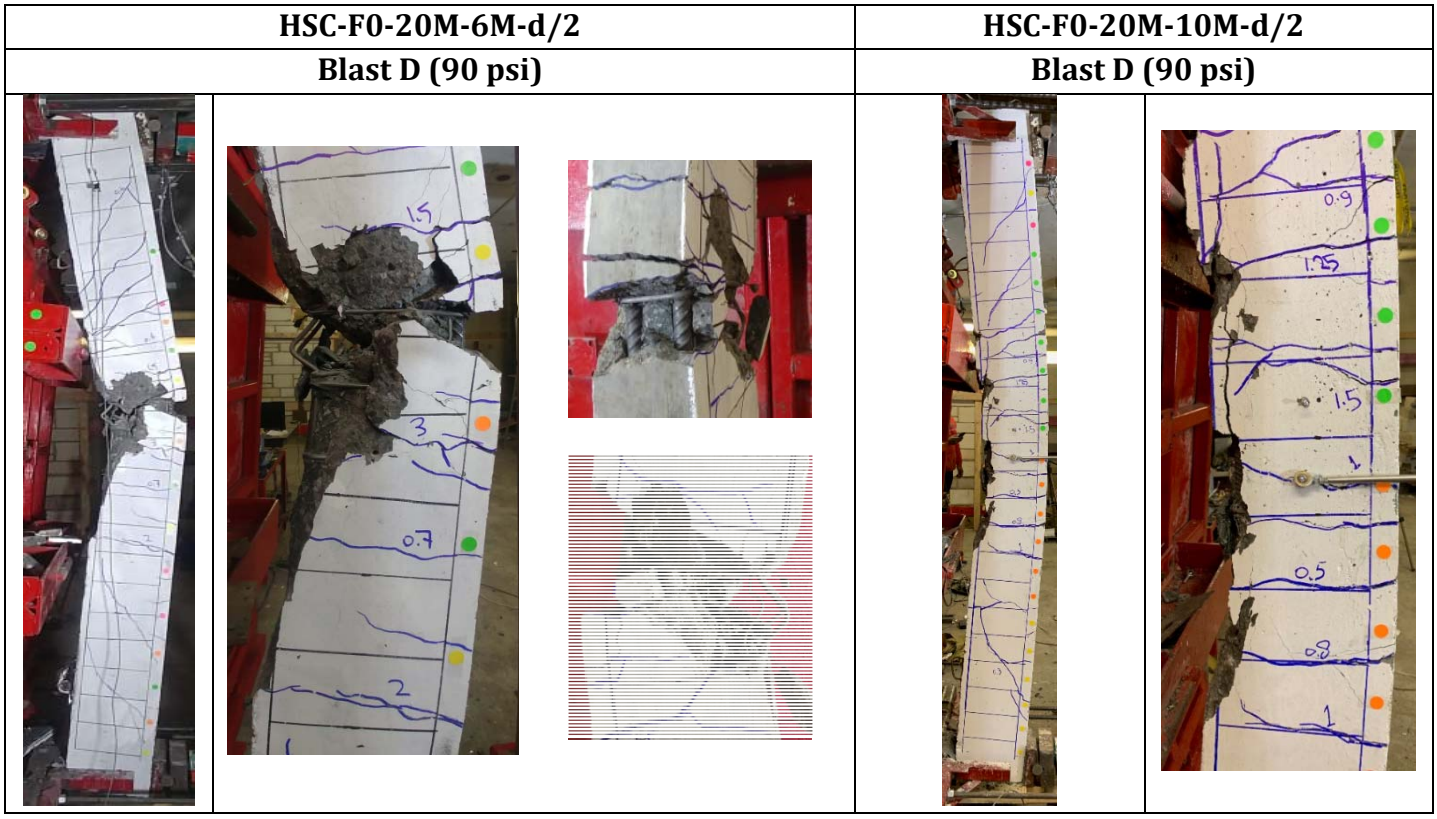

Figure 6-30 - Damage and Failure Modes: Effect of compression reinforcement (6M vs 10M)

6.8 EFFECT OF TENSION STEEL RATIO (HSC SERIES)

The effect of tension reinforcement ratio can be examined by comparing the responses of beams HSC-F0-15M-10M-d/4, HSC-F0-20M-10M-d/4 and HSC-F0-25M-10M-d/4. All three specimens were built with plain HSC and were designed in accordance with the CSA-S850 blast detailing requirements, with 2-10M bars in compression and closed ties spaced at 50 mm (s=d/4) throughout the beam span. However, the tension steel ratio varied with longitudinal reinforcement ratio (ρ) of 1.6% (2-15M), 2.4% (2-20M), and 4.1% (2-25M), respectively.

6.8.1 STATIC TEST RESULTS

Static results are summarized in **Table 6.7** and **Figure 6-31.** For comparison, the responses of the companion nominally detailed HSC beams are also included in **Figure 6-31.** It can be observed that increasing the tension steel ratio led to increases in strength and stiffness in the blast-detailed HSC beams. For example, the beam with 25M bars shows increases of 22% and 73% in strength (P_{max}), and 75% and 109% in stiffness (K) when compared to the companions with 20M and 15M bars. Importantly, all three blast-detailed beams fail in flexure with high ductility, whereas increasing the steel ratio in the nominally-detailed specimens reduces ductility ($\Delta_{max}/\Delta_{yield}$ = 2.74 and 2.05 in the singly-reinforced HSC beams with 15M and 20M bars), with shear failure (and no ductility) in the case of the nominally-detailed HSC beam with 25M bars.

The blast-detailed beams with 15M and 20M bars (ρ = 1.5% and 2.4%) show similar ductility of $\Delta_{max}/\Delta_{yield}$ = 9.3 & 11, with testing, stopped at 150 mm due to excessive deformations. In addition, damage in both beams was limited to spalling of top cover concrete and flexural/shear cracking, with no damage to the core region in the midspan zone. On the other hand, increasing the tension steel ratio to ρ = 4.1% in the beam with 25M bars led to buckling of the 10M compression bars, and more intense crushing in the midspan beam zone, which resulted in a relative loss in ductility to $\Delta_{max}/\Delta_{yield}$. The results show that HSC beams designed with tension-steel ratios beyond ρ = 2.5% (CSA S850 limit) show reduced ductility. Moreover, the results point to the importance of properly detailing the compression steel in doubly reinforced HSC beams, especially as the tension steel is increased.

6.8.2 BLAST TEST RESULTS

Figure 6-32 compares the dynamic responses and displacements of the HSC beams with varying steel ratios, while **Figure 6-33** shows photographs of the beams at the end of testing. It can be observed that increasing the tension steel ratio led to better control of displacements at equivalent blasts. The beams with 15M and 20M bars were tested under Blast A (30 psi), where it can be that the beam with increased tension steel area showed reductions of 35% and 77 in maximum and residual displacements. The same trend continues at the subsequent blasts. At Blast C (70 psi) a gradual decrease in maximum and residual deformations is observed as the steel ratio is increased. The beam with 25M bars (ρ = 4.1%) shows reductions of 62% and 95% in D_{max} and D_{res} displacements when compared

to the beam with 20M bars (ρ = 2.4%), which in turn shows reductions of 37% and 56% for the beam with 15M bars (ρ = 1.5%). Crushing of cover concrete occurs in the beam with 15M bars at Blast C, while damage remained well controlled in the 20M and 25M companions which were tested under a further blast. At Blast D (90 psi), the use of increased steel ratio in the 25M specimen once again led to improved control of maximum and residual displacements (reductions of 38% and 70% when compared to the 20M beam). Both beams experienced damage in the top cover concrete region at this blast.

Figure 6-34 compares the post-blast residual static results for the three beams. All three beams show significant residual strength, with larger residual capacity but lower ductility in the beam with 25M bars. Similar to the static results, the beam with 25M bars experiences buckling of the 10M compression bars, whereas the extent of buckling is limited in the beams with 15M and 20M bars.

In summary, increasing the tensile reinforcement ratio increased the overall capacity of the beams under static loading, with improved control of displacements under blast loads. On the other hand, increasing the steel ratio beyond the CSA S850 limits led to a more rapid loss in static and post-blast residual strength, with a greater susceptibility to bar buckling and concrete damage at failure.

Table 6.7 - Effect of Tension Reinforcement – Plain HSC Static Test Results

ID	Load		Displacement			Stiffness	Ductility		Toughness (kN-mm)		Failure Mechanism
	P_y (kN)	P_{max} (kN)	Δ_{yield} (mm)	Δ_{max} (mm)	Δ_{end} (mm)	K (N/mm)	$\frac{\Delta_{max}}{\Delta_{yield}}$	$\frac{\Delta_{end}}{\Delta_{yield}}$	A_{max}	A_{end}	
HSC-F0-15M-10M-d/4	105	108	16	149	149	6562	9.3	9.3	14018	14018	Flexure
HSC-F0-20M-10M-d/4	127	131	13	150	150	9411	11.5	11.5	18889	18889	Flexure
HSC-F0-25M-10M-d/4	220	225	19.2	80	120	11458	4.17	6.25	14734	19734	Flexure

(a) Load Displacement Curves for plain HSC series

Nominal Detailing

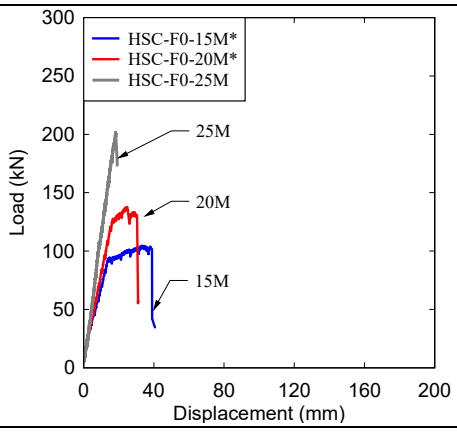

Blast Detailing

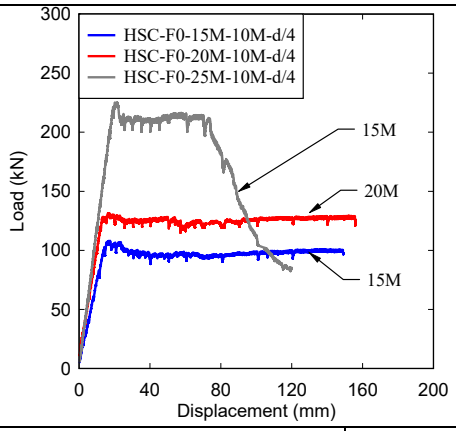

(b) Condition of beams at Failure		Δ_{max}	Failure
HSC-F0-15M-10M-d/4	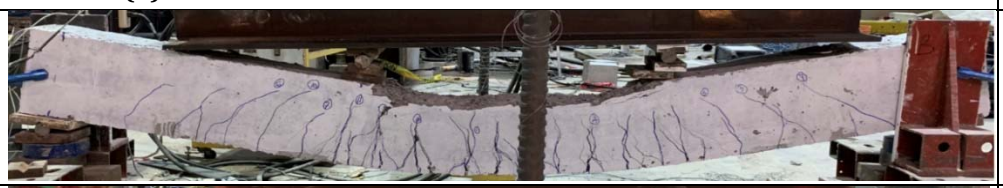	149	Flexure
HSC-F0-20M-10M-d/4		150	Flexure
HSC-F0-25M-10M-d/4		120	Flexure

Figure 6-31 – Results and photos at end of static testing: Effect of steel ratio in HSC beams

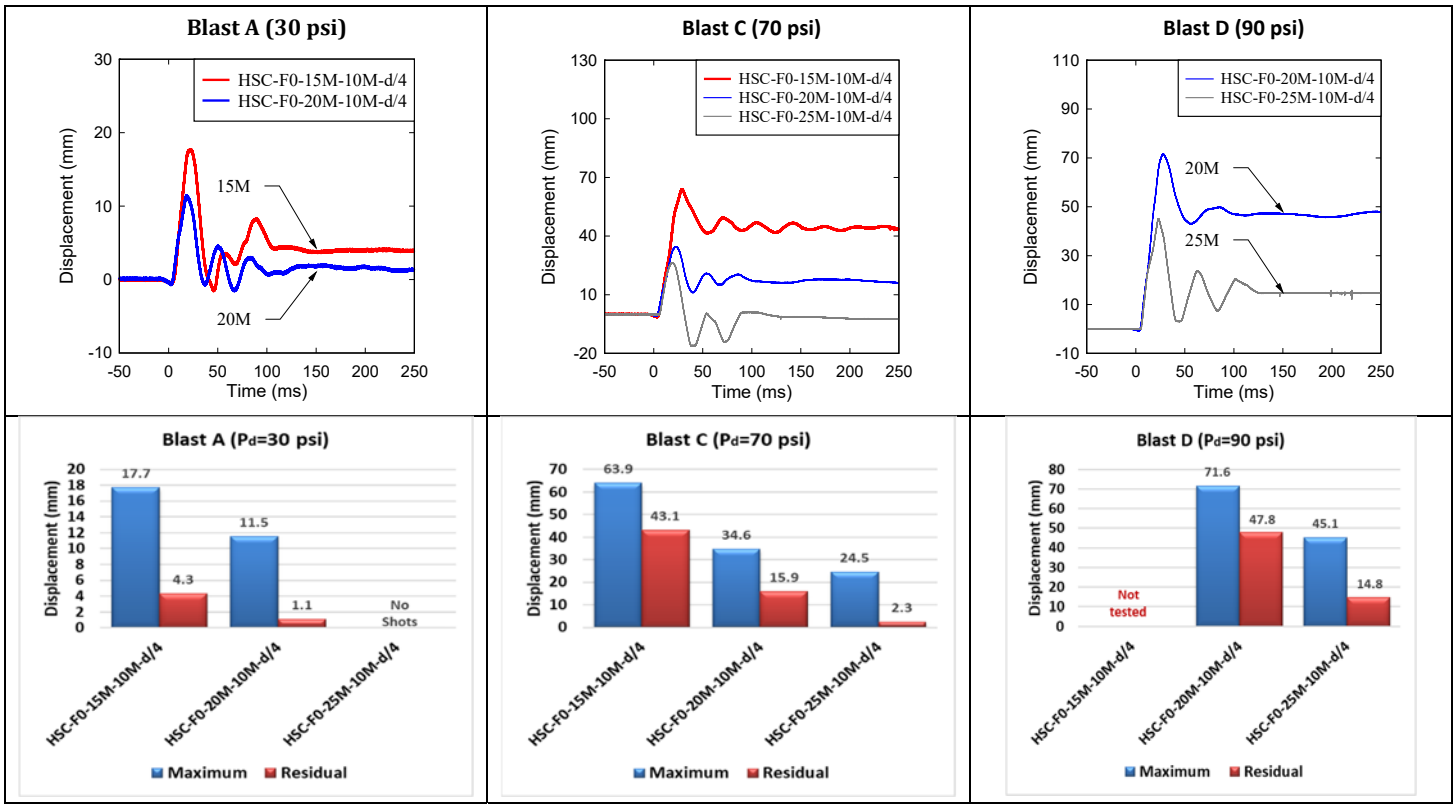

Figure 6-32 –Displacement time histories: Effect of steel ratio in HSC beams

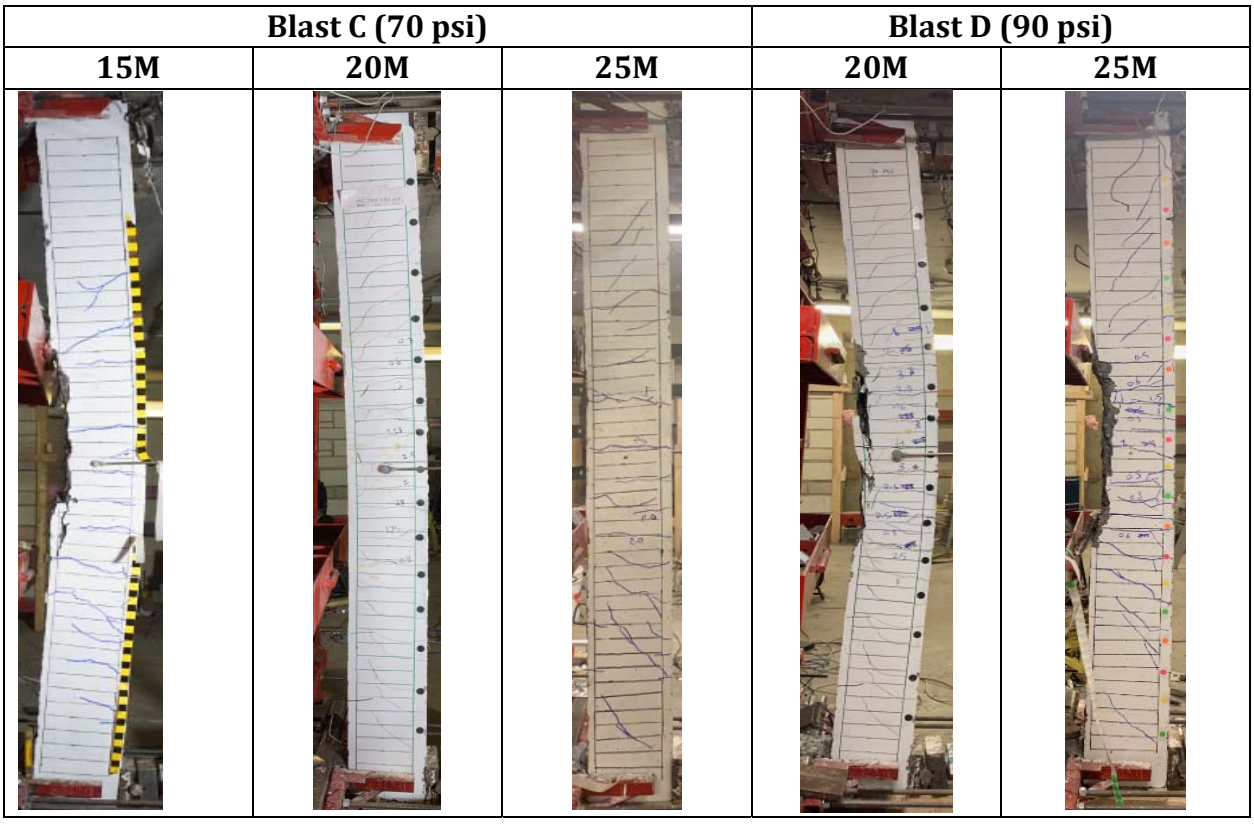

Figure 6-33 - Damage and Failure Modes: Effect of steel ratio in HSC beams

Comparison of residual load-deflecting curves

Shifting based on residual blast displacement	Without shifting
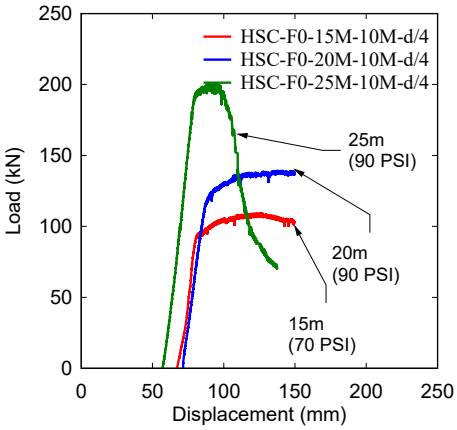	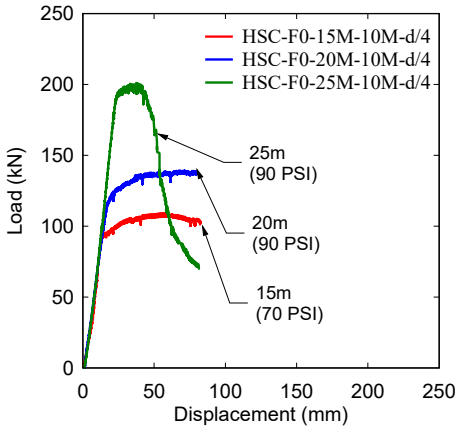

Beams after residual static testing

HSC-F0-15M-10M-d/4

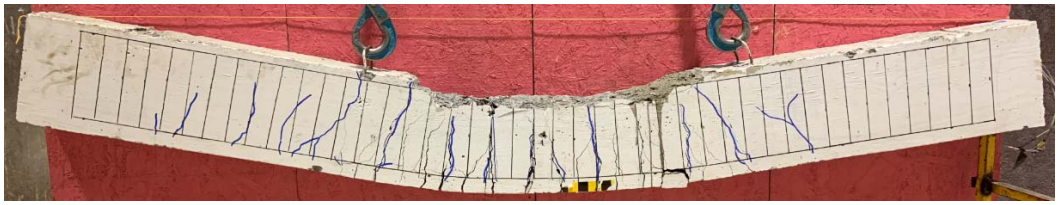

($\Delta_{max}{}^{R}$ = 151 mm)

HSC- F0-20M-10M-d/4

($\Delta_{max}{}^{R}$ = 150.4 mm)

HSC-F0-25M-10M-d/4

($\Delta_{max}{}^{R}$ = 137.40 mm)

Figure 6-34 – Residual test results for beams tested Effect of reinforcement ratio (HSC beams)

6.9 EFFECT OF REINFORCEMENT RATIO (HSFRC BEAMS)

The effect of tension steel ratio for the specimens with hybrid fibers is examined by comparing the responses of beams HSC-F0.75-15M-10M-d/2, HSC-F0.75-20M-10M-d/2 vs HSC-F0.75-25M-10M-d/2. All specimens were built with HSFRC, 2-10M bars in compression and intermediate ties spaced at 100 mm (s= d/2) but had varying steel ratios of (ρ): 1.6% (2-15M), 2.4% (2-20M), and 4.1% (2-25M).

6.9.1 STATIC TEST RESULTS

Figure 6-35 compares the responses of the specimens under static loading. As in the previous series increasing the tension steel ratio increased the maximum capacity (Pmax) and stiffness (K) of the beams. In addition, the use of increased steel ratio increased overall toughness (Amax). Beam HSC-F0.75-25M-10M-d/2 with 25M bars (ρ=4.1%) recorded values of Pmax= 248 kN , K= 12435 N/mm, and Amax,=22811 kN-mm, representing increases of 112%, 23% and 123% compared to HSC-F0.75-20M-10M-d/2, and 50%, 25% and 83% when compared to beam HSC-F0.75-25M-10M-d/2. All beams show significant post-blast deformations, however the strength decay after peak was more rapid with the increase in steel ratio. On the other hand, the beam with 10M bars (ρ =1.5%) experiences earlier failure due to tension bar rupture, whereas this failure mode is prevented in the beams with 20M (ρ =2.5%) and 25M bars (ρ =4.1%). The results point to the importance of carefully considering the tension steel ratio in HSFRC beams. This is especially important since the 15M beam had a relatively moderate amount of steel. Previous research shows that the use of fibers can result in crack localization and bar rupture in HSC beams, especially as the tension steel ratio reduces below ρ = 0.5-1% ((Dancygier and Karinski 2019).

6.9.2 BLAST TEST RESULTS

Figure 6-36 and **Figure 6-37** shows the blast results of the specimens with fibers. Similar to the previous test series, increasing the tensile reinforcement ratio led to enhanced control of displacements at equivalent blasts. For example, at Blast C (70 psi), the beam with 25M bars (ρ= 4.1%) shows reductions of 41% and 78% in maximum and residual displacements when compared to the beam with 20M bars, which in turns shows reduction of 37% and 56% when compared to the specimen with 15M bars. All specimens showed good control of cracking and cover damage, even as the steel ratio was increased. As a result, all beams were tested under Blast D (90 psi) loading. Once again increasing the steel ratio in the beam with 25M bars led reductions of 27 % and 53% in maximum and residual deformations compared to the 20M specimen, which in turn showed reductions of 29% and 49% compared to the 15M beam.

Figure 6-38 compares the post-blast residual static results of the HSFRC beams. The specimens with fibers show significant residual capacity, where the beam with the largest tension bars (2-25M) showed greater residual capacity but lower ductility. Similar to the static results, the beam with 25M bars experience buckling of the 10M compression bars.

Moreover, similar to the static results, the beam with 15M bars suffered bar rupture failure during the residual tests, while this failure is prevented in the beam with 20M bars which eventually failed due to buckling of the 10M bars in compression bars.

In summary, increasing the tensile reinforcement ratio increased the static resistance of the beams and led to better control of displacements under blast loading. Results also indicate that HSFRC with low to moderate steel ratios may be susceptible to tension steel bar rupture due to crack localization, and this point should be considered when designing such beams.

Table 6.8 - Effect of Tension Reinforcement – Plain HSC Static Test Results

ID	Load		Displacement			Stiffness	Ductility		Toughness (kN-mm)		Failure Mechanism
	P_y (kN)	P_{max} (kN)	Δ_{yield} (mm)	Δ_{max} (mm)	Δ_{end} (mm)	K (N/mm)	$\frac{\Delta_{max}}{\Delta_{yield}}$	$\frac{\Delta_{end}}{\Delta_{yield}}$	A_{max}	A_{end}	
HSC-F0.75-15M-10M-d/2	112	117	11	98.8	102	10181	8.9	9.3	9997	10234	Flexure
HSC-F0.75-20M-10M-d/2	160	168	15	37	100	10667	2.5	6.8	4781	12494	Flexure
HSC-F0.75-25M-10M-d/2	240	248	19.3	70	125	12435	3.5	6.47	13931	22811	Flexure

(a) Load Displacement Curves for plain HSFRC series

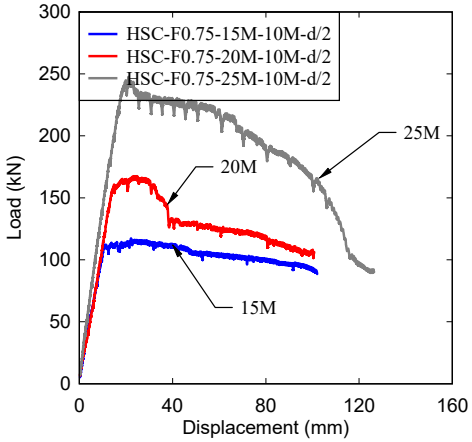

(b) Condition of beams at Failure		Δ_{max}	Failure
HSC-F0.75-15M-10M-d/2		102	Flexure Bars Rupture
HSC-F0.75-20M-10M-d/2		100	Flexure
HSC-F0.75-25M-10M-d/2	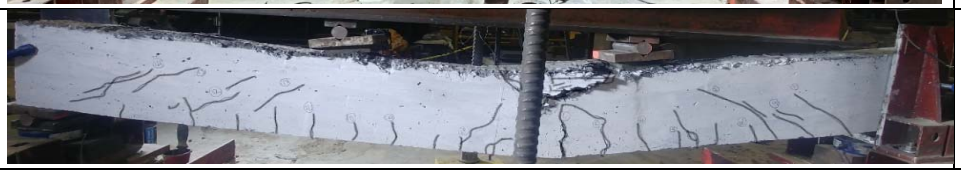	125	Flexure

Figure 6-35 - Load Displacement Curves and Failure Profile of the HSFRC beams tested under static load

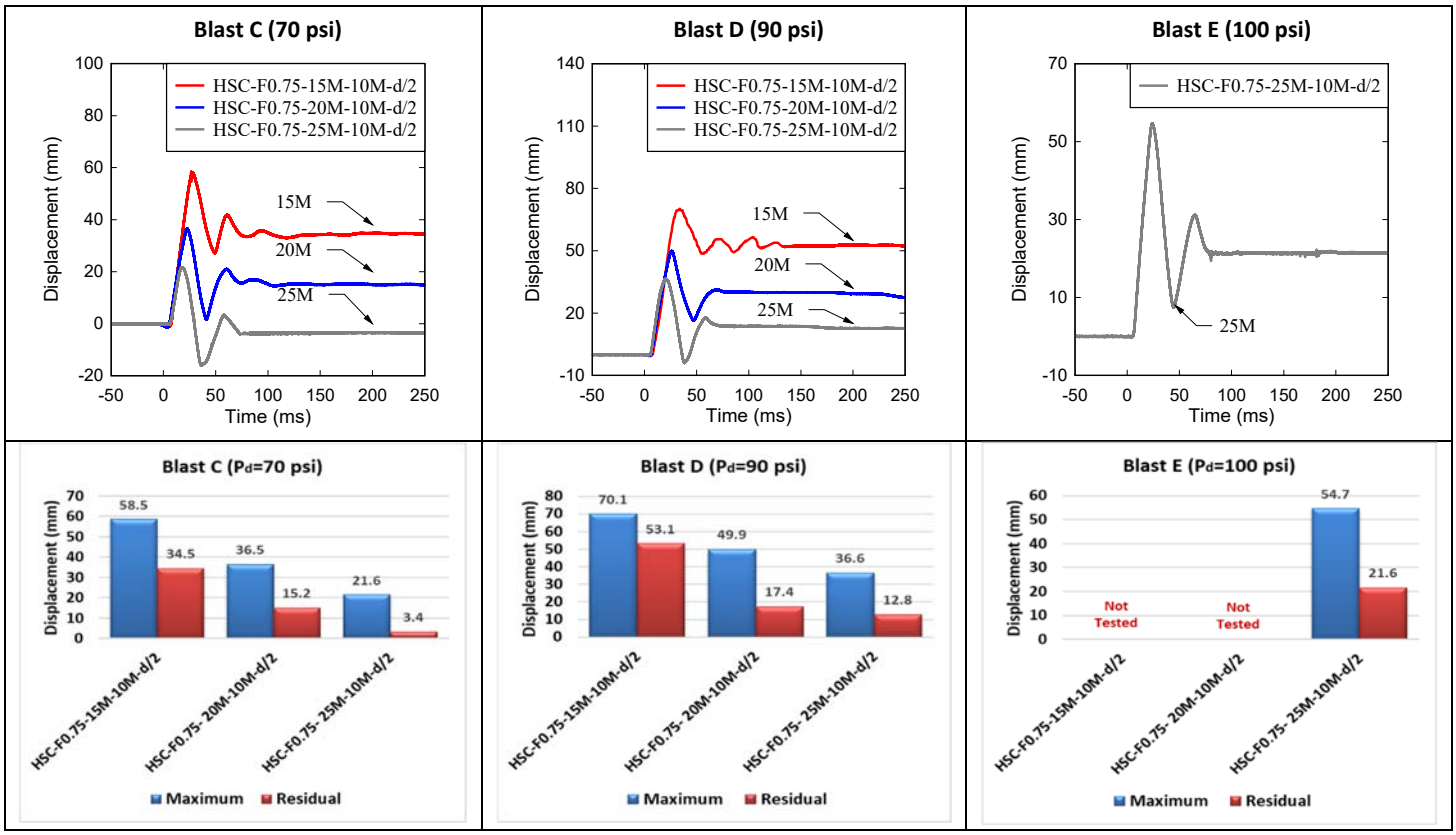

Figure 6-36 - Displacement time histories: Effect of reinforcement ratio in HSFRC beams

Blast C (90 psi)			Blast D (100 psi)
15M	20M	25M	25M

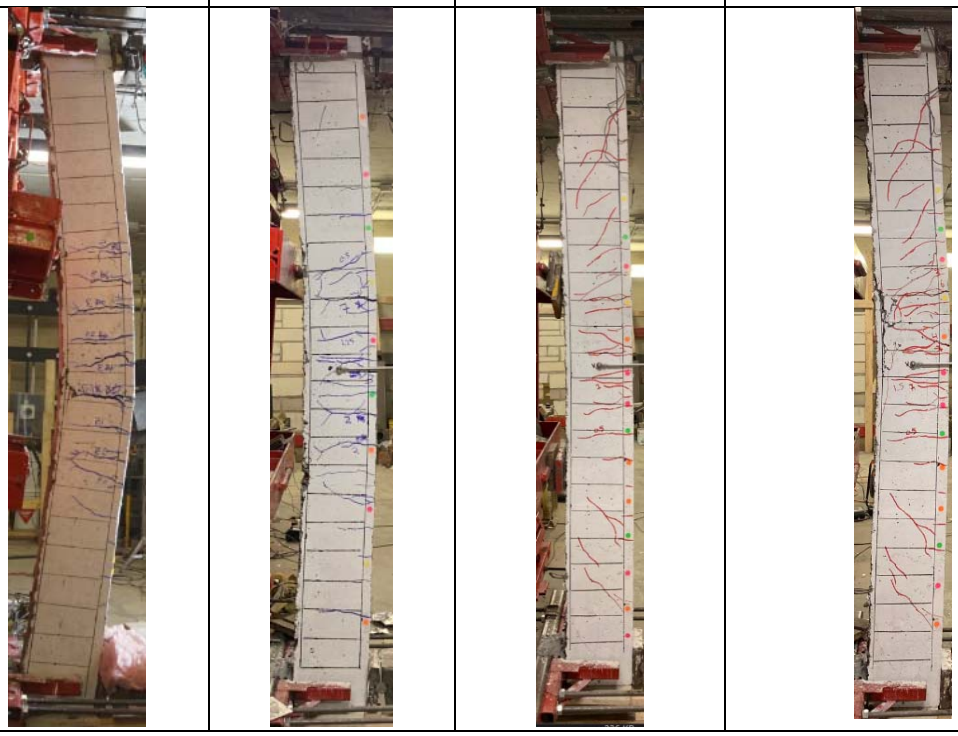

Figure 6-37 - Damage and Failure Modes of the 15M, 20M, and 25M HSFRC beams

Comparison of residual load-deflecting curves

Shifting based on residual blast displacement	Without shifting
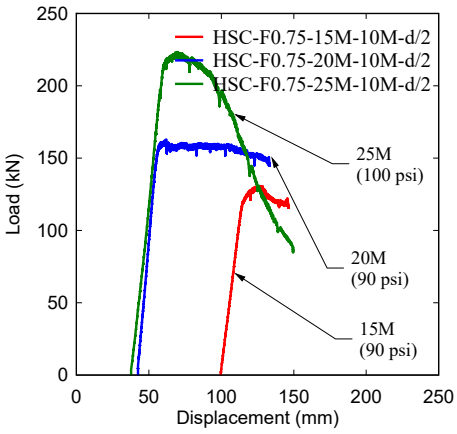	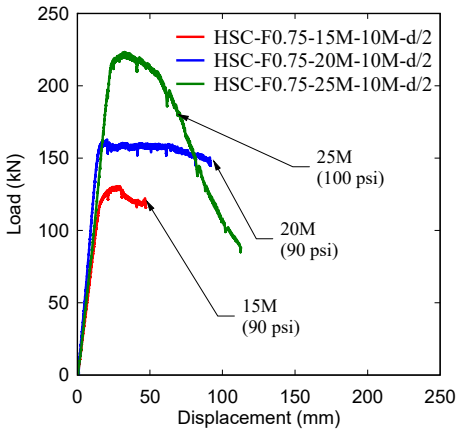

Beams after residual static testing

HSC-F0-15M-10M-d/2

($\Delta_{max\ R}$ = 151.02 mm)

HSC- F0-20M-10M-d/2

($\Delta_{max\ R}$ = 133.99 mm)

HSC-F0-25M-10M-d/2

($\Delta_{max\ R}$ = 153.06 mm)

Figure 6-38 – Residual test results for beams tested under the Effect of reinforcement ratio (HSFRC beams)

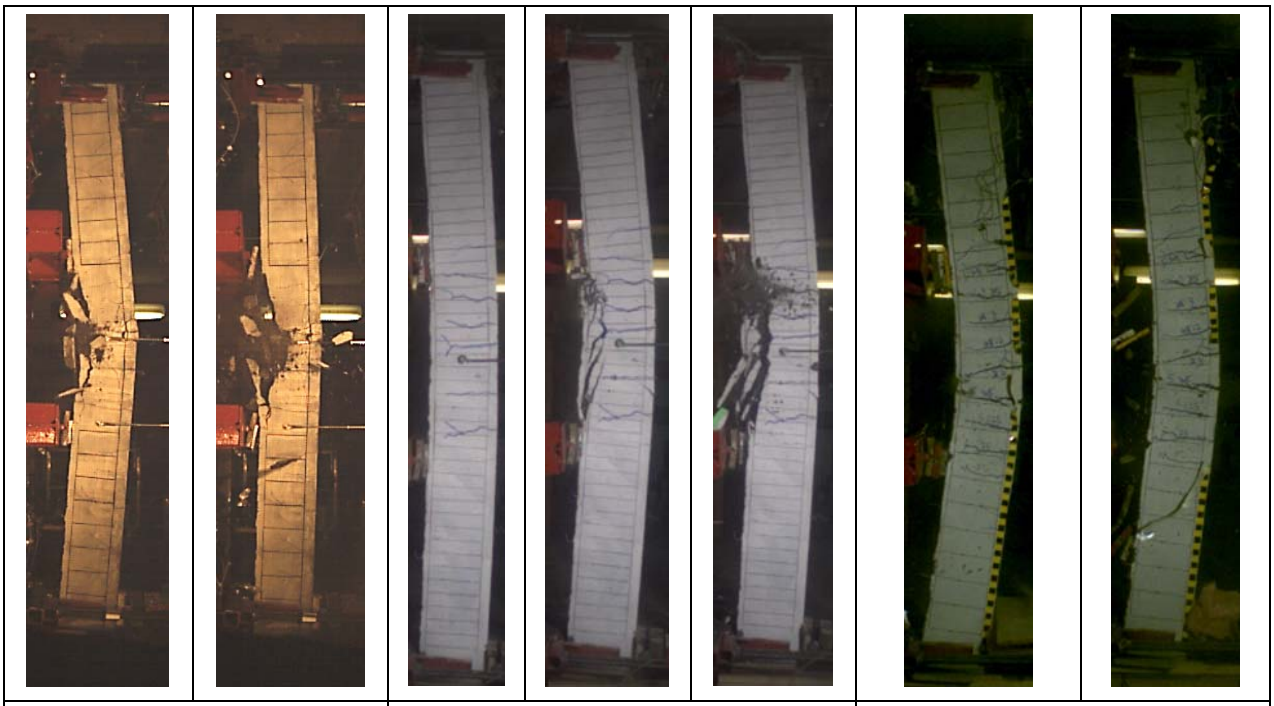

a) HSC-F0-15M-0M-d/2* Blast B (50 psi)	b) HSC-F0-15M-10M-d/4 Blast C (70 psi)	c) HSC-F0.75-15M-10M-d/2 Blast D (90 psi)

Figure 6-39 - Speed videos showing secondary blast fragments (15M Series)

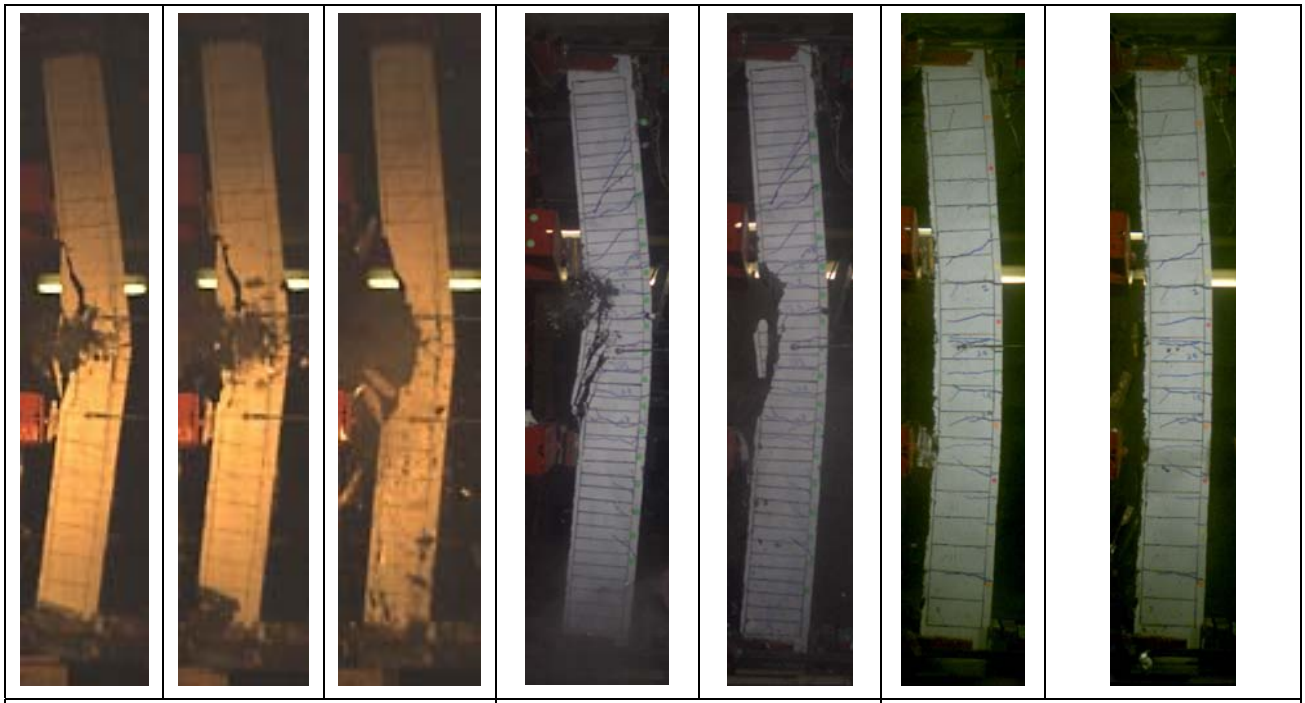

a) HSC-F0-20M-0M-d/2* Blast C (70 psi)	b) HSC-F0-20M-10M-d/4 Blast D (90 psi)	c) HSC-F0.75-20M-10M-d/2 Blast D (90 psi)

Figure 6-40 - Speed videos showing secondary blast fragments (20M Series)

a) HSC-F0-25M-0M-d/2* Blast D (90 psi)	b) HSC-F0-25M-10M-d/4 Blast D (90 psi)	c) HSC-F0.25M-15M-10M-d/2 Blast E (100 psi)

Figure 6-41 - Speed videos showing secondary blast fragments (25M Series)

6.10 DYNAMIC REACTION – LOAD-DISPLACEMENT CURVES

This research program included companion beams with identical properties that were tested under static and dynamic conditions using the same loading pattern. The dynamic results were obtained by summing the support reactions recorded by the load-cells during testing. This section presents a comparison of the dynamic reactions (dynamic resistance curves) at different blast intensities and compares the load-deformation responses and peak loads under static (P^{S}_{max}) and dynamic (P^{D}_{max}) conditions.

Dynamic resistance curves:

Figure 6-42 shows the dynamic resistance curves for all beams at all blasts. In most cases, the maximum dynamic load (P^{D}_{max}) increased with increasing blast intensity. For example, at Blast C (70 psi), beam HSC-F0-15M-10M-d/4 showed a 30% increase in P^{D}_{max} when compared to Blast A (30 psi) which tested the beam in the elastic range. Blast B (50 psi) brought the beam to yield levels and therefore the capacities are quite similar at Blasts B and C. Lower peak dynamic loads are observed at later blasts (e.g. Blast D – 90 psi) for some beams since these shots tested the specimens well into the inelastic range, resulting in reduced dynamic capacities. The envelope resistance curves (obtained by overlapping the individual blast responses) are therefore used when comparing the results in the next section, where P^{D-E}_{max} and A^{D-E}_{u} represent the maximum capacity and toughness (total area) in the envelope resistance curves.

Dynamic vs Static resistance:

Figure 6-43 compares the resistance curves of the HSC and HSFRC beams under static and dynamic loading. The maximum loads under dynamic and static loading, and their ratio ($P^{D-E}_{max}/P^{s}_{max}$) are also reported in the plots and in **Table 6.9**. The results show that the beams experience an increase in maximum capacity under dynamic loading. For example, beams HSC-F0-15M-10M-d/4, HSC-F0-20M-10M-d/4, and HSC-F0-25M-10M-d/4 (plain HSC and blast detailing) show dynamic and static loads of: P^{D-E}_{max}= 136 kN vs. P^{S}_{max} = 108 kN; P^{D-E}_{max} = 207 kN vs. P^{S}_{max} = 131 kN ; and P^{D-E}_{max}= 299 kN vs. P^{S}_{max} =225 kN, with dynamic-to-static load ratios of 1.2, 1.6 and 1 .3. The increase in capacity can be explained by the increase in concrete and reinforcement strengths under high strain-rate loading.

The same trend is observed for the beams with fibers, with higher peak loads under dynamic vs. static conditions. The HSFRC specimens with 15M, 20M and 25M bars show $P^{D-E}_{max}/P^{s}_{max}$ ratios of 1.5, 1.3 and 1.1. It is interesting to note that the HSFRC beams show larger dynamic loads when compared to their plain HSC counter-parts, however, the $P^{D-E}_{max}/P^{s}_{max}$ ratios are generally lower for the beams with fibers (see **Figure 6-43**).

Effect of parameters on dynamic resistance curves

The dynamic resistance functions of beams with different designs are compared in **Figure 6-44.** The effect of steel detailing can be observed in **Figure 6-44a-c** which compares the dynamic load-deflection curves of the beams with blast and nominal detailing. It can be observed that the improved detailing (use of compression bars and ties throughout the span) results in similar dynamic resistance (P_{max}^{D-E}) but increased dynamic toughness (A_u^{D-E}). The results show that the A_u^{D-E} toughness is 52%, 50% and 44% larger for the blast-detailed HSC beams with 15M, 20M, and 25M bars when compared to the companions with nominal details.

Figure 6-44 d-e-f compares the resistance curves of the HSFRC beams with intermediate ties (d/2) with the companion blast-detailed HSC beams (d/4). It can be observed that the beams with fibers show similar dynamic loads (P_{max}^{D-E}) but increases by 40%, 25%, and 22% in overall A_u^{D-E} toughness when compared to the companion HSC beams with 15M, 20M, and 25M bars.

Figure 6-44g compares the dynamic resistance curves of the beams tested under single and repeated blasts. It can be observed that both beams show similar resistance functions. In fact, the beam tested under repeated blasts shows increases of 9% and 32% in peak resistance (P_{max}^{D-E}) and overall toughness (A_u^{D-E}). The results confirm that repeated tests had minimal effects on the dynamic responses of the beams in this series. The increased strength can possibly be explained by the built-up residual deformations which may have pushed the tension steel into strain-hardening.

Figure 6-44h compares the HSC beams in the 20M series which had d/2 (s=100 mm) and d/4 (s=50mm) ties. It can be observed beam HSC-F0-20M-10M-d/4 shows only slight increases of 7% and 3% in load (P_{max}^{D-E}) and toughness (A_u^{D-E}) when compared to beam HSC-F0-20M-10M-d/2.

Finally, **Figure 6-44i-j** compares the resistance functions of the HSC and HSFRC beams with varying steel ratios. As expected, larger dynamic resistance is observed as the steel ratio is increased in both series. In the HSC series, beam HSC-F0-25M-10M-d/4 (ρ_t = 4.1%) shows increases of 120% and 44% in P_{max}^{D-E} when compared to beams HSC-F0-15M-10M-d/4 (ρ_s = 1.6%) and HSC-F0-20M-10M-d/4 (ρ_s = 2.4%). On the other hand, the HSC beam with 25M bars shows a reduction of 16% in A_u^{D-E} toughness when compared with the companion with 20M bars. In the HSFRC series, beam HSC-F0.75-25M-10M-d/2 (ρ_t = 4.1%) shows increases of 60% and 13% in $\mathbf{P_{max}^{D-E}}$, and improvements of 25% and 18% in $\mathbf{A_u^{D-E}}$ toughness when compared to the companions with 15M (ρ_t =1.6%) and 20M (ρ_t = 2.4%) bars.

Table 6.9 - Summary of Static and Dynamic resistance curve results

Series		P_{max}^{S}	P_{max}^{D}					P_{max}^{D-E}	P_{max}^{D-E} / P_{max}^{S}	A_u^{D-E}
		kN	kN					kN	ratio	kN-mm
			30 psi	50 psi	70 psi	90 psi	100 psi			
15M	**HSC-F0-15M-10M-d/4[x1]**	108.03	‡	‡	125.39	‡	‡	125.39	1.16	5171
	HSC- F0-15M-10M-d/4	108.03	103.66	135.77	134.68	‡	‡	135.77	1.26	6805
	HSC- F0.75-15M-10M-d/2	117.28	93.67	151.61	177.22	140.70	‡	177.22	1.52	9435
20M	**HSC-F0-20M-6M-d/2**	‡	102.03	‡	182.85	156.03	‡	182.85	‡	10801
	HSC-F0-20M-10M-d/2	‡	103.88	‡	186.69	193.57	‡	193.57	‡	9881
	HSC- F0-20M-10M-d/4	131.51	107.11	‡	206.90	196.45	‡	206.90	1.57	10425
	HSC- F0.75-20M-10M-d/2	167.57	81.50	‡	226.90	222.12	‡	226.90	1.35	9058
25M	**HSC- F0-25M-0M-d/2**	201.67	‡	‡	240.45	289.46	‡	289.46	1.44	6051
	HSC- F0-25M-10M-d/4	225.02	‡	‡	250.98	298.87	‡	298.87	1.33	8719
	HSC- F0.75-25M-10M-d/2	247.61	‡	‡	226.89	283.41	252.84	283.41	1.14	10654

P_{max}^{S}: Static resistance; P_{max}^{D}: Dynamic resistance; P_{max}^{D-E}: Envelope dynamic resistance $\mathbf{A_u^{D-E}}$**:** Envelope dynamic toughness; $\frac{P_{max}^{D-E}}{P_{max}^{S}}$: Dynamic-to-static resistance ratio

‡: No Data

15M Series

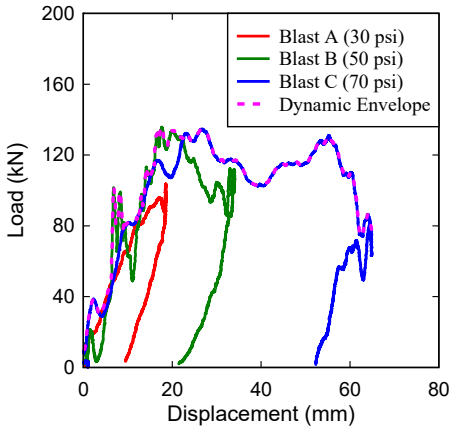

(a) HSC- F0-15M-10M-d/4

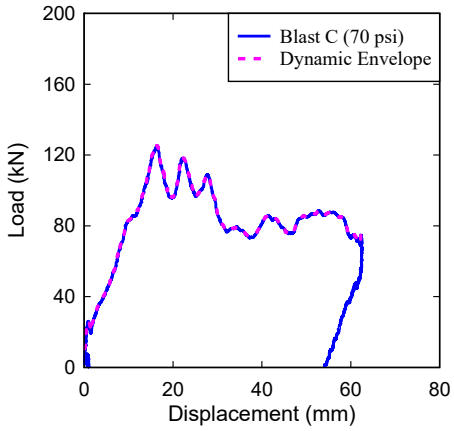

(b) HSC- F0-15M-10M-d/4[x1]

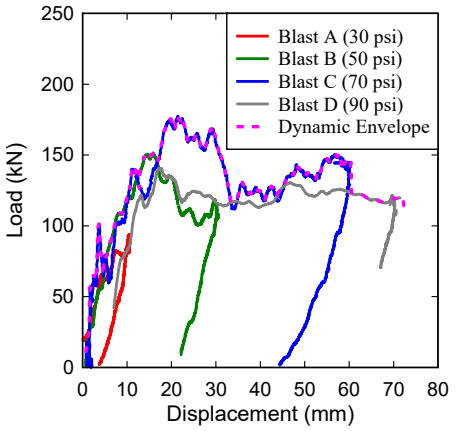

(c) HSC- F0.75-15M-10M-d/2

20M Series

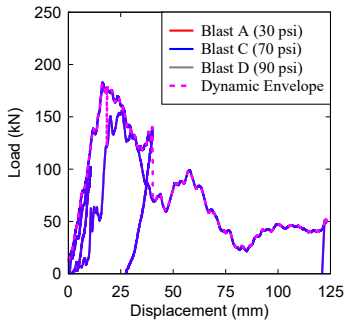

(d) HSC-F0-20M-6M-d/2

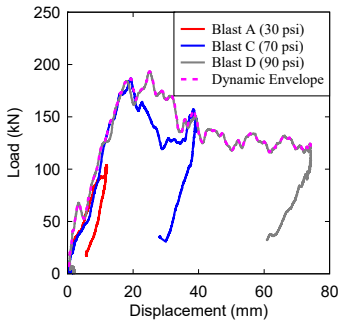

(e) HSC-F0-20M-10M-d/2

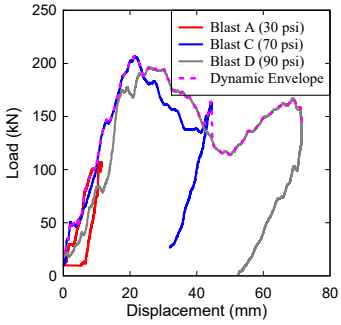

(f) HSC-F0-20M-10M-d/4

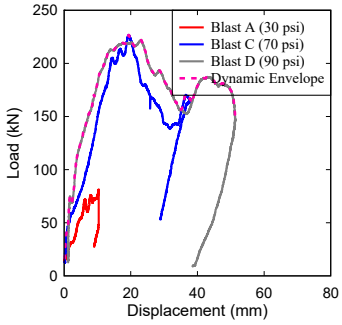

(g) HSC- F0.75-20M-10M-d/2

25M Series

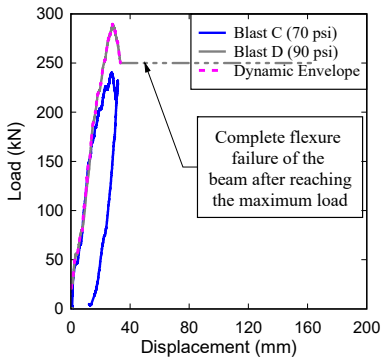

(h) HSC- F0-25M-0M-d/2

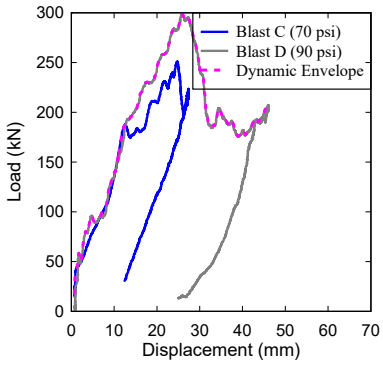

(i) HSC- F0-25M-10M-d/4

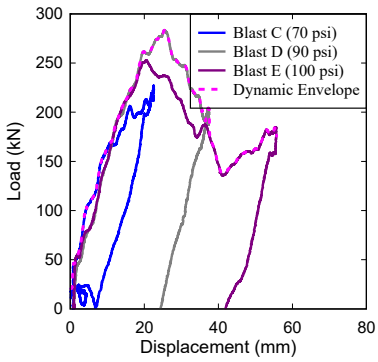

(j) HSC-F0.75-25M-10M-d/2

Figure 6-42 - Dynamic resistance curves at varying blast intensities

15M Series: Static vs. Dynamic

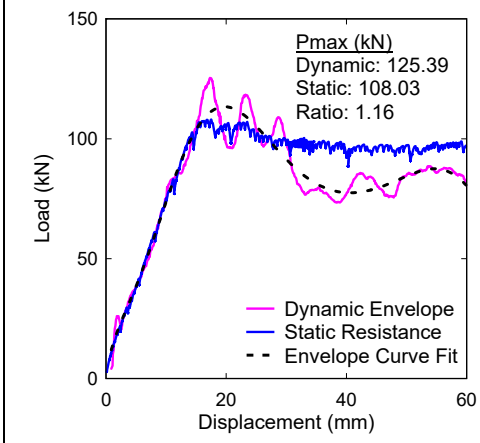

(a) HSC- F0-15M-10M-d/4[x1]

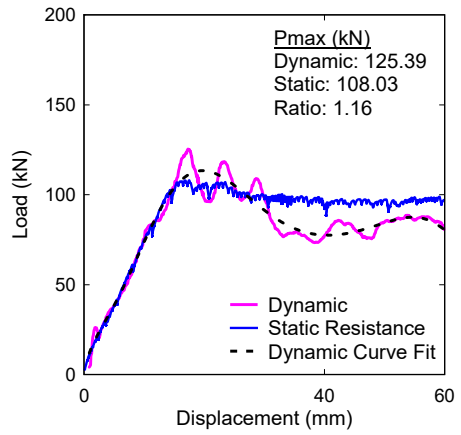

(b) HSC- F0-15M-10M-d/4

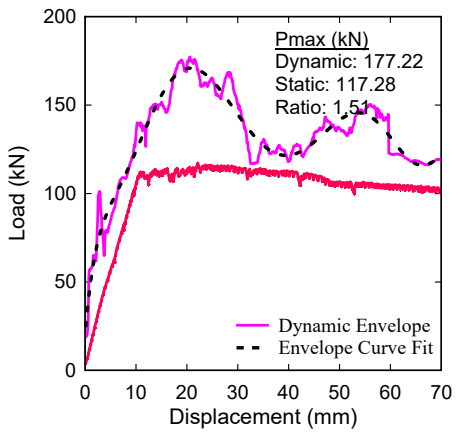

(c) HSC- F0.75-15M-10M-d/2

20M Series: Static vs. Dynamic

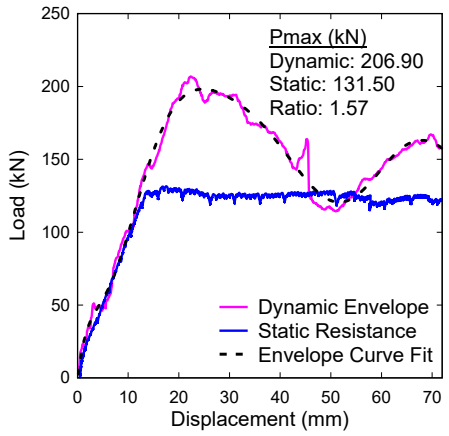

(d) HSC-F0-20M-10M-d/4

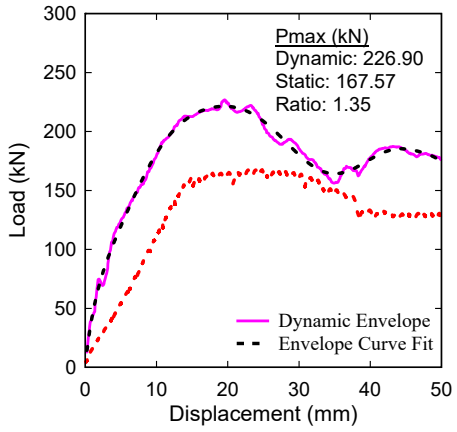

(e) HSC- F0.75-15M-10M-d/2

25M Series: Static vs. Dynamic

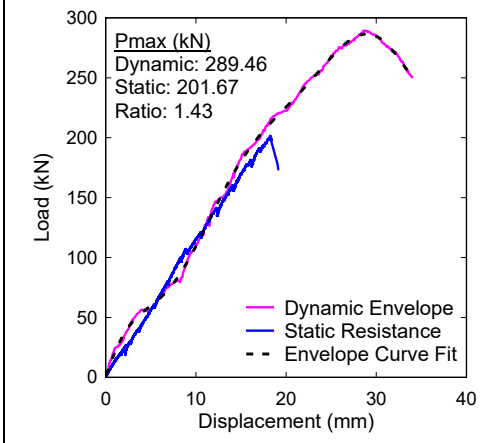

(k) HSC- F0-25M-0M-d/2

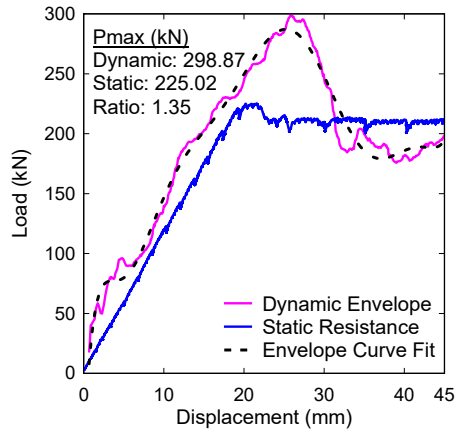

(l) HSC- F0-25M-10M-d/4

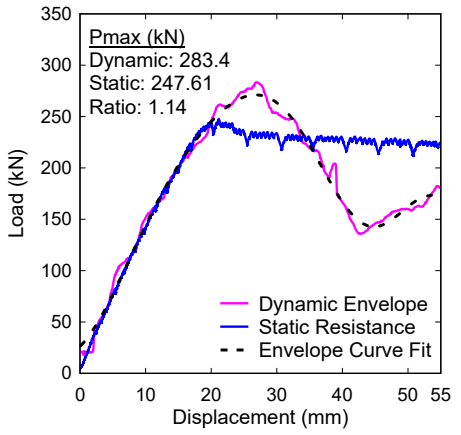

(m) HSC-F0.75-25M-10M-d/2

Figure 6-43 - Dynamic vs. static resistance curves

Effect of Blast Detailing

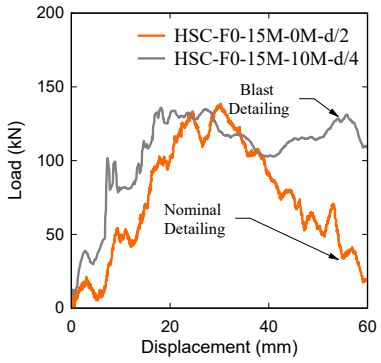

(a) 15M Series

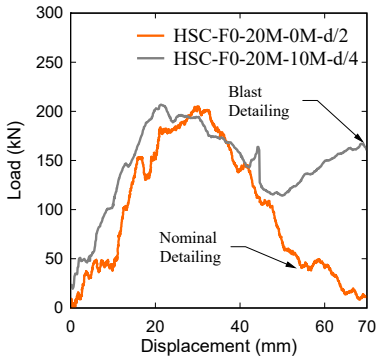

(b) 20M Series

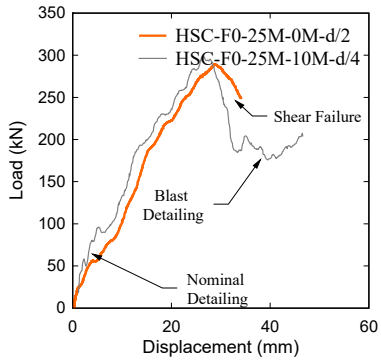

(c) 25M Series

Effect of Fibers

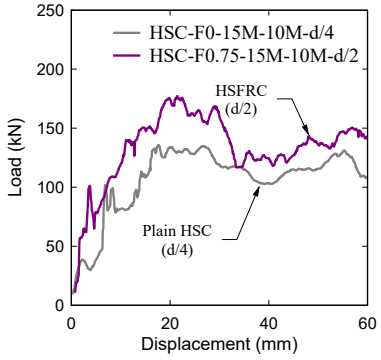

(d) 15M Series

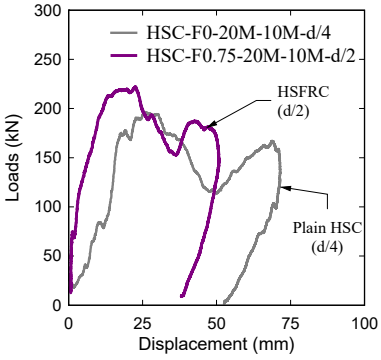

(e) 20M Series

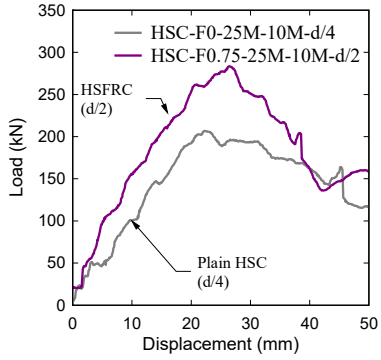

(f) 25M Series

Single vs Repeated loads

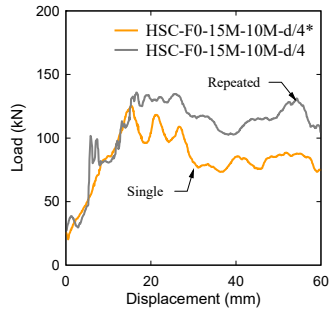

(g)

Tie spacing (d/2 vs d/4)

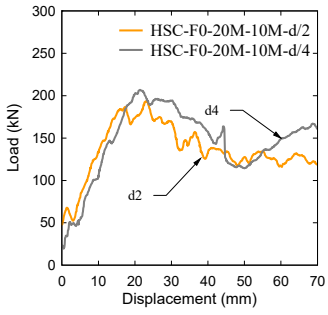

(h)

Tension steel ratio

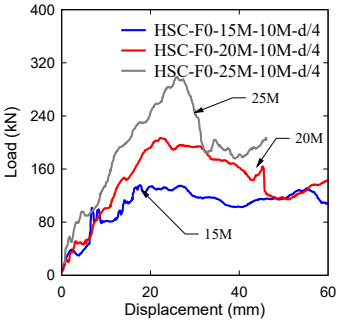

(i) HSC beams

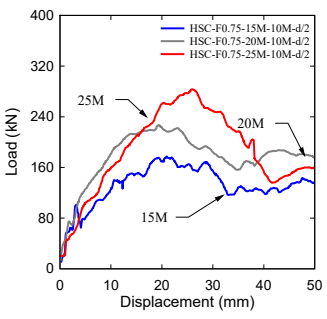

(j) HSFRC beams

Figure 6-44 - Effects of different parameters on the dynamic curves

6.11 RESIDUAL CAPACITY AND ENERGY DISSIPATION

This test program included companion beams with identical properties tested under static and dynamic conditions. The dynamically tested beams were subsequently tested under static four-point bending to assess their post-blast residual capacity. The results of these tests, along with the results from the original undamaged beams are shown in **Figure 6-46** while **Figure 6-47** shows photos of the beams after residual testing. The maximum residual capacity (P_{max}^{R}), residual secant stiffness (k^{R}) and maximum post-blast residual displacement Δ_{max}^{R} are reported in **Table 6.10**.

Adhikary et al. (2015) proposed a residual resistance index defined as $RRI = P_{max}^{R}/P_{max}^{S}$ and damage index, $D = 1 - RRI$, to assess the post-blast resistance of impact-damaged beams. According to this study, the degree of damage caused by dynamic loading can be classified as "low", "medium", "high" and "severe" if the damage index is: D <0.2, D=0.2-0.5, D=0.5-0.8 and D=0.8-1.0, respectively. As shown in **Figure 6-46a-h**, all blast-detailed HSC beams showed significant residual capacities, with an ability to sustain significant load even after intense blast testing. Examining **Table 6.10,** all HSC beams with blast detailing show RRI above 0.89, with damage indices < 0.2, which confirms the low damage in the beams tested under blast loads. The same trend is observed in the beams with fibers intermediate detailing which shows RRI ≥ 0.90. It is interesting to note that near-perfect results are obtained for the beams with 15M and 20M bars, whereas the lowest RRI are observed for the specimens with 25M bars (RRI ≈ 0.9, with damage indices ≈ 0.1). As noted before these beams showed relatively higher compression concrete damage owing to the high strain demands imposed by the increased tension-steel ratio. Indeed, both the undamaged and blast-damaged beams showed buckling of the 10M longitudinal compression bars after static testing, however, this effect is more evident in the blast-damaged specimens.

No "undamaged" static test was conducted on beam HSC-F0-20M-10M-d/2 (ties at s = 100 mm, d/2), however, it can be observed that this beam has a lower peak residual strength (P_{max}^{R} = 132 kN) when compared to beam HSC-F0-20M-10M-d/4 (ties at s = 50 mm, d/2; P_{max}^{R} = 139 kN), though both beams show significant post-blast resistance. In general, the results demonstrate the high residual capacity of HSC and fiber-reinforced concrete beams with improved detailing.

Adhikary et al. (2015) also proposed a "Residual stiffness index" (RSI) defined as the ratio of secant stiffness of impact-damaged to undamaged specimens ($RSI = k^{R}/k^{S}$) and noted higher RSI indices (lower stiffness degradation) in doubly-reinforced beams compared to singly-reinforced specimens. The results from the current tests show that the RSI varied between 0.73 to 0.82 and 0.74 to 0.95 for the HSC and HSFRC beams with improved detailing, which indicates that all beams showed high residual stiffness even after intense blast testing.

Zanuy and Ulzurrun (2018) proposed the "Total Energy Index" (TEI) to better assess the energy absorbed after dynamic loading. **Figure 6-45a-c** shows the procedure to calculate

the “Impact Energy Index” (IEI), “Residual Energy Index” (REI) and “Total Energy Index” (TEI), and the results of this analysis are presented in **Table 6.10**. The IEI index is calculated using only the undamaged quasi-static response, with IEI $= \mathrm{A}/A + B$, and where A is the energy calculated up to the residual deflection, and A+B equals the total energy-absorption capacity of the undamaged beam. After dynamic testing, the energy absorbed in the residual test, denoted as C in **Figure 6-45a** can be calculated, with REI $= \mathrm{C}/A + B$. In the last step the total energy index can be calculated as TEI $=$ IEI $+$ REI.

It is interesting to note that the REI values show a reducing trend (0.69 > 0.53 > 0.36) as the tension steel ratio is increased (ρ = 1.5% [15M] > 2.5% [20M] > 4.1% [25M]) in the blast-detailed plain HSC beams, whereas the REI values remain somewhat constant (and in fact show an increasing trend) for the companion HSFRC beams (REI = 0.53, 0.58 and 0.67 for the beams with 15M, 20M and 25M bars).

According to Zanuy and Ulzurrun (2018) the IEI and REI “do not provide in itself an easy identification of residual failure mode or ductility”. On the other hand, the TEI can provide a better indication of ductility and failure mode, with a TEI of ≈ 1.0 indicating similar failure mode/ductility for undamaged and damaged beams, and TEI ≤ 0.85 indicating a change of behavior from “ductile” to “brittle” in undamaged versus damaged specimens. Examining the results in **Table 6.10**, most beams show TEI indices ≥ 1.0 (average of 1.11), which indicates the high post-blast resilience and energy-absorption capacity of the HSC and HSFRC beams with blast/intermediate detailing. While damage was sometimes more severe in the blast-damaged beams after residual static loading, all beams carried significant residual deflections with similar, but sometimes more intense failure modes (e.g. more severe buckling of compression steel, which can be linked to the damage of the concrete cover region, and built-up residual strains in the compression bars, prior to residual static testing – see **Figure 6-47**).

Table 6.10 - Summary of the results of Static and Residual Test

Series		Last Blast	Load			Stiffness			Displacement				
			P^{S}_{max}	P^{R}_{max}	*RRI*	K^{S}	K^{R}	RSI	Δ^{R}_{max} (mm)	Δ^{Total}_{max} (mm)	IEI	REI	TEI
		psi	kN	kN		(N/mm)	(N/mm)						
15M	HSC-F0-15M-10M-d/4 [x1]	70	108.03	102.94	0.95	‡	‡	‡	106.01	148.38	0.36	0.69	1.06
	HSC- F0-15M-10M-d/4	70	108.03	107.49	1.00	6562	5392	0.82	87.74	150.91	0.54	0.53	1.06
	HSC- F0.75-15M-10M-d/2	90	117.28	130.56	1.11	10181	7583	0.74	51.29	151	‡	‡	‡
20M	HSC-F0-20M-10M-d/2	90	‡	132.15	‡	‡	‡	‡	76.76	147.61	‡	‡	‡
	HSC- F0-20M-10M-d/4	90	131.51	139.26	1.06	9411	7250	0.77	83.16	150.35	0.59	0.53	1.12
	HSC- F0.75-20M-10M-d/2	90	167.57	162.96	0.98	10667	10085	0.95	90.33	133.99	0.55	0.58	1.14
25M	HSC- F0-25M-10M-d/4	90	225.02	200.98	0.89	11458	8319	0.73	79.7	136.86	0.79	0.36	1.14
	HSC- F0.75-25M-10M-d/2	100	247.61	223.44	0.90	12435	9818	0.79	111.36	149.10	0.48	0.67	1.15

Note: P^{S}_{max} : Maximum Static Resistance Load; P^{R}_{max}: Maximum Dynamic Resistance Load; *RRI*: Ratio of the Maximum Residual and Static Resistance Loads
K^{S}: Static stiffness; K^{R}: Residual stiffness; RSI: Ratio of the residual and static secant stiffness; Δ^{R}_{max} : Maximum post-blast residual displacement, Δ^{total}_{max}: Total displacement (Blast residual displacement + Maximum post-blast residual displacement)
IEI: Impact Energy Index; REI: Residual Energy Index; TEI: Total Energy Index; ‡: No Data

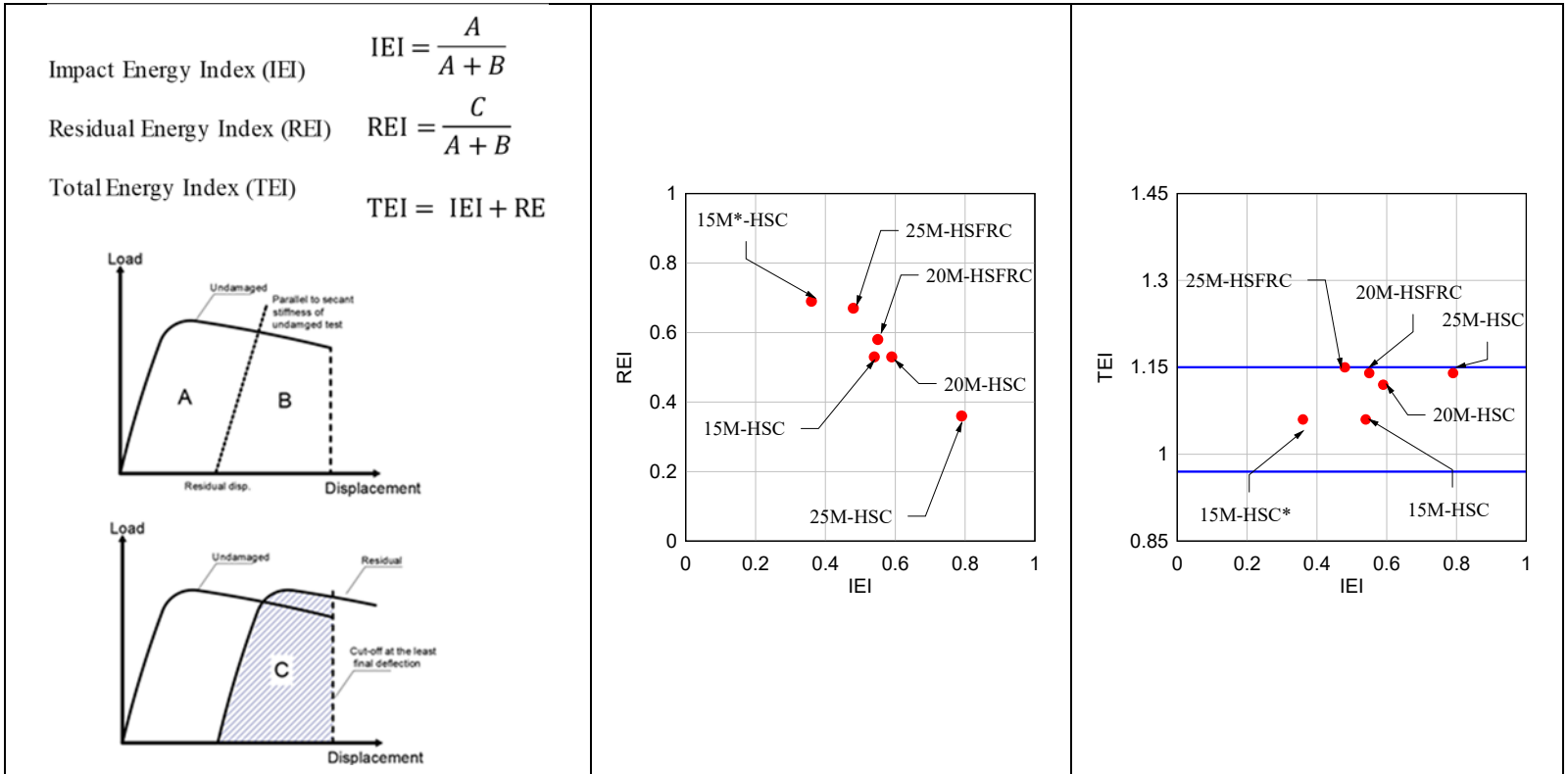

(a) Areas used for the damage indices (b) REI - IEI (c) TEI - IEI

Figure 6-45 – (a) Areas used for calculating the residual damage indices (b REI as a function of IEI (c) TEI as a function of IEI

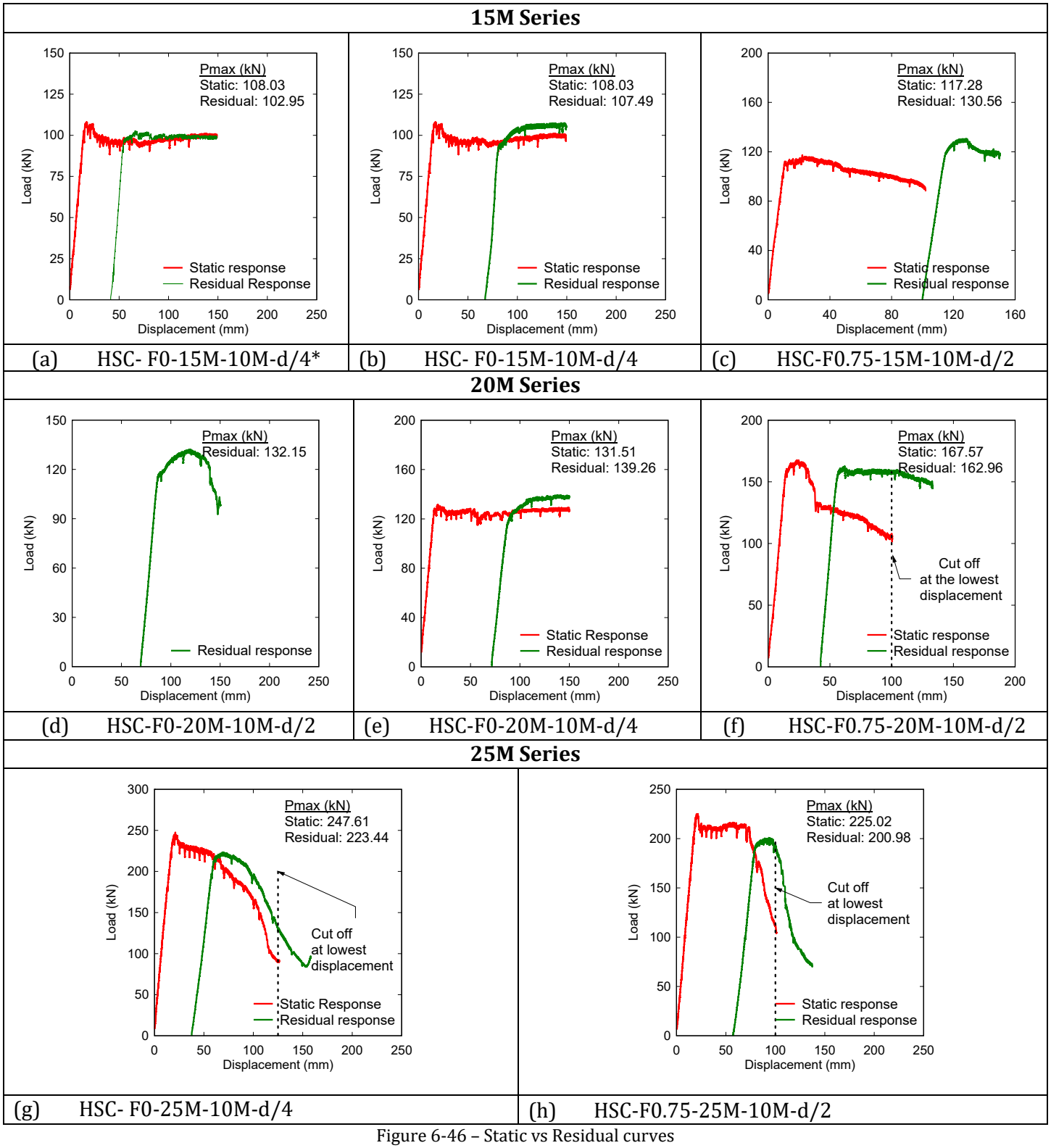

Figure 6-46 – Static vs Residual curves

<table>
<tr><td>(a) HSC-F0-15M-10M-d/4</td><td>(b) HSC-F0-15M-10M-d/4 [x1] (single blast)</td></tr>
<tr><td> 
Δ^R_{max}= 150.91 mm</td><td> 
Δ^R_{max}= 147.38 mm</td></tr>
<tr><td>(c) HSC-F0.75-15M-10M-d/2</td><td>(d) HSC-F0-20M-10M-d/2</td></tr>
<tr><td> 
Δ^R_{max}= 147.27 mm</td><td> 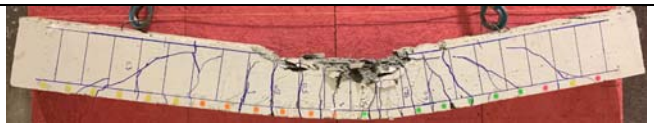
Δ^R_{max}= 151.72 mm</td></tr>
<tr><td>(e) HSC-F0-20M-10M-d/4</td><td>(f) HSC-F0.75-20M-10M-d/2</td></tr>
<tr><td> 
Δ^R_{max}= 150.35 mm</td><td> 
Δ^R_{max}= 147.38 mm</td></tr>
<tr><td>(g) HSC-F0-25M-10M-d/4</td><td>(h) HSC-F0.75-25M-10M-d/2</td></tr>
<tr><td> 
Δ^R_{max}= 137.40 mm
 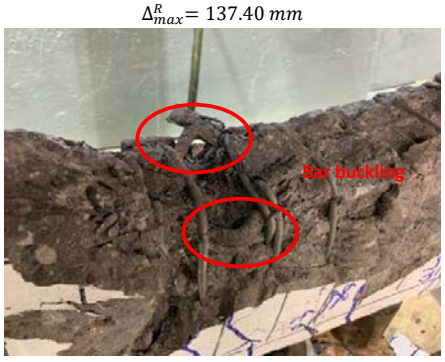 </td><td> 
Δ^R_{max}= 153.06 mm
  </td></tr>
</table>

Figure 6-47 – Failure modes of beams after the post-blast residual static tests

CHAPTER 7: ANALYSIS

7.1 PREDICTION OF BLAST RESPONSE OF HSC AND HSFRC BEAMS

Non-linear single degree of freedom (SDOF) analysis was used to predict the dynamic response of the HSC and HSFRC beams tested in this research study. This was accomplished by: 1) defining stress-strain relationships for concrete, HSFRC and steel reinforcement at high-strain rates, 2) predicting moment-curvature relationships for the beam sections using sectional analysis; 3) developing resistance functions using member analysis and 4) transforming each beam into an equivalent SDOF system and solving the equation of motion for maximum displacement response.

7.2 MATERIALS

The following sections provide an overview of the material's constitutive models as well as the dynamic increase factors used in the sectional analysis. A summary of the material models and DIF equations are provided in **Figure 7.1**, **Figure 7.3**, and **Figure 7.4**.

7.2.1 HSC CONCRETE MODELS

The blast-detailed beams were built with high-strength concrete and provided with closely spaced ties which provided confinement. To account for these effects, the models proposed by Popovics (1973) and Mander et al. (1988) were used to define the static stress-strain behavior of unconfined and confined high-strength concrete in compression. The equations to develop the stress-strain-relationships, as well as the equations for peak confined stress and strain are presented in **Figure 7.1**. In the equations: f_c = unconfined stress at strain ε_c; f'_c and ε_{co} = peak unconfined stress and strain; f_{cc} = confined stress at strain ε_{cc}; f'_{cc} and ε'_{cc} = peak unconfined stress and strain. The Mander model accounts for the arrangement and distribution of transverse reinforcement on confinement using the confinement effectiveness parameter, K_e, with f'_l defined as the effective confinement pressure. A linear relationship with maximum tensile stress equal to $f'_t = 0.33\sqrt{f'_c}$ and slope equal to E_c (modulus of elasticity of concrete) was used for HSC in tension.

Concrete exhibits an increase in strength under dynamic loading (Bishop and Perry Bischoff and Perry (1991), To consider the effect of high strain rates, the dynamic increase factor (DIF) models shown in **Figure 7.4** were used to determine the dynamic properties of the HSC concrete. The CEB model CEB (1991) code (1990) expressions were used to determine the DIF for plain HSC in compression (DIF_c), while the model proposed by Malvar (1998)& Ross (1998) was used for concrete in tension (DIF_t). Assuming a constant strain rate ($\dot{\varepsilon}$) of 1 s-1 for the shock-tube experiments, the models predict the: DIF_c= 1.14 and DIF_t= 1.22.

7.2.2 FIBER-REINFORCED CONCRETE MODELS

The addition of fibers enhances the performance of concrete in compression and improves its tensile post-cracking response. The Mansur et al model. (1999) was used to predict the response of high-strength fiber-reinforced concrete in compression. This model adopts an earlier model proposed by Carreira and Chu (1985) and was developed specifically for steel fiber-reinforced HSC. The equations used to define the stress-strain relationship are shown in **Figure 7.2**. In the equations: f_{cf} = stress in HSFRC at strain ε_{cf}; f'_{cf} and ε'_{cf} = peak HSFRC stress, with fiber parameters (fiber content, length and diameter) are defined using v_f, l_f and d_f, with $(\frac{v_f l_f}{d_f})$ defined as the fiber-factor. In the model, the factors k_1 and k_2 are used to account for the influence of steel fibers on post-peak response and are taken as 1.0 until the stress-strain curve reaches the peak stress.

The tension response of HSFRC was modeled using a simplified tri-linear model originally developed by Lok and Pei (1998) and modified by Burrell et al. (2014) The model is composed of three segments. The response before cracking is linear up to stress $f_{ct} = 0.33 \times {f'_{cf}}^{1/2}$, with slope taken as E_{cf}, with the second branch defined using stress f_2^* and strain ε_2^* (linear descending for the fiber content and type used in this study). The final branch represents the pullout stage and is linear descending from strain ε_2^* to a strain of 0.02 mm/mm at zero stress. In the current study the matrix bond strength (τ_{bond}) was taken as $\tau_{bond} = 0.66 \times {f'_{cf}}^{1/2}$ (two times the cracking stress). The fiber parameters v_f, L_f and d_f are as defined before, with the modulus of elasticity for the steel fibers taken as 200 GPa.

Previous research indicates that the material response of fiber reinforced concrete is strain rate dependent under dynamic compression and tension. In this research, the model proposed by Wang et al. (2011) was used to account for rates effects in HSFRC in compression (${DIF_c}^F$). This model modifies the CEB formulation for the influence of fibers in HSC. Due to the lack of an available model, the DIF equation proposed by Malvar and Ross (1998) was used to determine the dynamic increase factor of HSFRC in tension (DIF_t). These models are defined in **Figure 7.4** and predict ${DIF_c}^F$=1.14, DIF_t= 1.22 at $\dot{\varepsilon}$ = 1 s^{-1}.

7.2.3 TENSION STEEL MODEL

The Jacques et al. (2012) model was used to predict the static tensile stress-strain response of the longitudinal steel reinforcement in tension. As shown in **Figure 7.2**, the model consisted of two linear segments and a parabolic function to account for elastic, post-yield, and strain-hardening response. In the equations, f_s = steel stress at strain ε_s; f_y = steel yield stress at strain ε_y; f_{sh} = steel hardening stress at strain ε_{sh}; f_u = steel ultimate stress at strain ε_u. Research shows that the properties of steel are affected by high strain-rates, with the effect on yield stress being greater than at ultimate. In this study, the expressions proposed by Saatcioglu et al. (2011) were used for DIF_y (dynamic factor at yield stress) and DIF_u

(dynamic factor at ultimate stress). Using the assumed strain rate of $\dot{\varepsilon}$ = of 1 s^{-1} the model predicts DIF_y= 1.30 and DIF_u= 1.10.

7.2.4 ADDITIONAL DIF CASES

To examine the effect of the dynamic increase factors, additional analyses were run using design DIFs (Case 2) and ignoring dynamic increase factors (DIF = 0, Case 3). Case 2 factors were applied using the recommendations in the CSA S850 Blast Standard for reinforced concrete beams in the far range: DIF_c & $DIF_c{}^F$= 1.19, DIF_t= 1.0, DIF_y= 1.17 and DIF_u= 1.05. It is noted that these factors are not dependant on strain-rate. The default analysis (Case 1) was run using the strain-rate dependent DIF factors defined in the previous sections.

<table>
<tr><th colspan="3">HSC Materials Models</th></tr>
<tr><td rowspan="2">Concrete in compression</td><td> 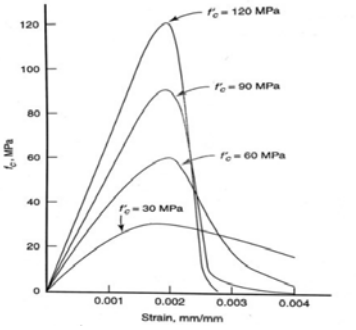
</td><td><u>Stress-strain relationship:</u>
$$f_c = \frac{f'_c\,\beta_c\left(\frac{\varepsilon_c}{\varepsilon_{c0}}\right)}{\beta_c - 1 + \left(\frac{\varepsilon_c}{\varepsilon_{c0}}\right)^{\beta_c k}}$$
$\beta_c = 0.8 + \frac{f'_c}{17}$; $E_c = 3320\sqrt{f'_c} + 6900$;
$\varepsilon_{c0} = \frac{f'_c}{E_c} * \frac{\beta_c}{\beta_c - 1}$; $k = \begin{cases} 1.0 & \text{Ascending} \\ 0.67 + \frac{f'_c}{62} & \text{Descending} \end{cases}$</td></tr>
<tr><td> 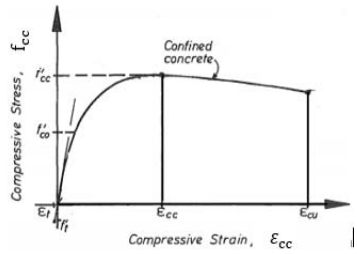
</td><td><u>Stress-strain relationship</u>:
$f_{cc} = \frac{f'_{cc}xr}{r-1-x^r}$; $x = \frac{\varepsilon_{cc}}{\varepsilon'_{cc}}$; $r = \frac{E_c}{E_c - E_{sec}}$;
$E_c = 3320\sqrt{f'_c} + 6900$; $E_{sec} = \frac{f'_{cc}}{\varepsilon_{cc}}$
$\varepsilon'_{cc} = \varepsilon_{c0}\left[1 + 5\left(\frac{f'_{cc}}{\varepsilon_{cc}} - 1\right)\right]$;
$f'_{cc} = f'_c(1.254 + 2.254\sqrt{1 + 7.94\frac{f'_l}{f'_c}} - 2\frac{f'_l}{f'_c})$; $f'_l = k_e\rho f_{yh}$; $k_e = \frac{\left(1-\frac{s'}{2d_s}\right)^2}{1-\rho}$</td></tr>
<tr><td>Concrete in tension</td><td> 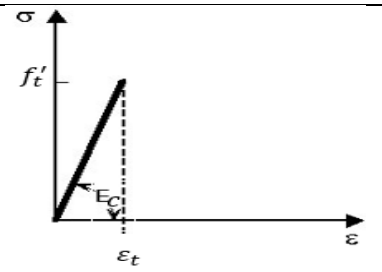
</td><td><u>Linear stress-strain relationship</u>:
Linear – elastic model with:
Peak stress: $f'_t = 0.33\sqrt{f'_c}$
Peak strain: $\varepsilon_t = \frac{f'_t}{E_c}$</td></tr>
</table>

Note: f'_t – peak concrete tensile stress at strain ε_t; f_c – unconfined concrete stress at strain ε_c ; f'_c – peak unconfined concrete stress; ε_{co} – peak unconfined concrete strain; E_c – concrete elastic modulus; k – slope control parameter; f_{cc} – confined concrete stress at strain ε_{cc} ; f'_{cc}– peak confined stress; ε'_{cc}– peak confined strain; ρ = ratio of the volume of transverse confining steel to the volume of the confined concrete in the core; k_e= confinement effectiveness coefficient; f'_l = lateral confining pressure on concrete; s = center to center spacing of the transverse reinforcement; f_{yh}: yield strength of the transverse reinforcement.

Figure 7.1 Constitutive material models for HSC

	HSFRC Materials Models	
FRC in compression	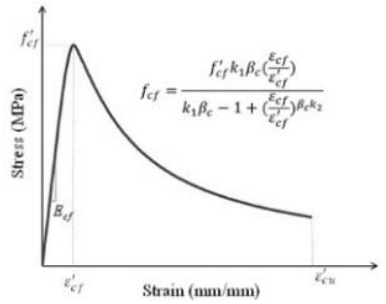	Stress-strain relationship: $f_{cf} = \frac{f'_{cf}\, k_1 \beta_c \left(\frac{\varepsilon_{cf}}{\varepsilon'_{cf}}\right)}{k_1 \beta_c - 1 + \left(\frac{\varepsilon_{cf}}{\varepsilon'_{cf}}\right)^{\beta_c k_2}}; \rightarrow \begin{cases} k_1 = k_2 = 1.0 & \text{if } \varepsilon_{cf}/\varepsilon'_{cf} \le 1.0 \\ k_1 = \left(\frac{50}{f'_{cf}}\right)^{3.0}\left[1 + 2.5\left(\frac{v_f l_f}{d_f}\right)^{2.5}\right] \\ k_2 = \left(\frac{50}{f'_{cf}}\right)^{1.3}\left[1 - 0.11\left(\frac{v_f l_f}{d_f}\right)^{-1.1}\right] & \text{if } \varepsilon_{cf}/\varepsilon'_{cf} \ge 1.0 \end{cases}$ $\beta_c = \frac{1}{1 - \frac{f'_{cf}}{\varepsilon'_{cf} E_{cf}}}$; $E_{cf} = (10{,}300 - 400 v_f) f'^{1/3}_{cf}$; $\varepsilon'_{cf} = \left[5 \times 10^{-4} + 7.2 \times 10^{-7}\left(\frac{v_f l_f}{d_f}\right)\right]$
FRC in tension	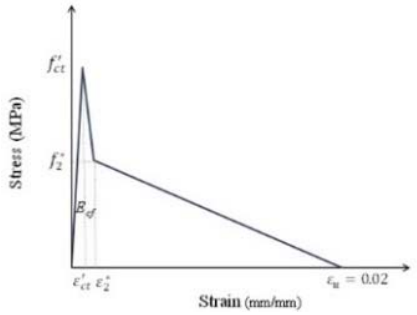	Tri-linear stress-strain relationship: Branch 1: 0 to stress $f'_{ct} = 0.33 f'^{1/2}_{cf}$; slope = E_{cf} Branch 2: linear descending to stress f^*_2 and strain ε^*_2 Branch 3: linear to failure stress (f_{ct} = 0 MPa) at strain =0.02 $f^*_2 = \frac{1}{2} v_f \tau_{bond} \frac{l_f}{d_f}$, $\varepsilon^*_2 = \tau_{bond} \frac{l_f}{d_f} \frac{1}{E_{fp}}$ and $\tau_{bond} = 0.66 \times f'^{1/2}_{cf}$

Note: f_{cf} – FRC stress at strain ε_{cf} ; f'_{cf} – peak FRC stress at strain ε'_{cf}; E_{cf} – FRC elastic modulus; k1, k2 , β_c – various curve fitting parameters; f'_{ct} – peak FRC tensile stress at strain ε'_{ct}; f^*_2– FRC post-cracking stress at strain ε^*_2; τ_{bond} – matrix bond stress; v_f, L_f, d_f and E_{fp}– fiber content, length, diameter, and modulus;

Figure 7.2 Constitutive material models for HSFRC

Steel Model	
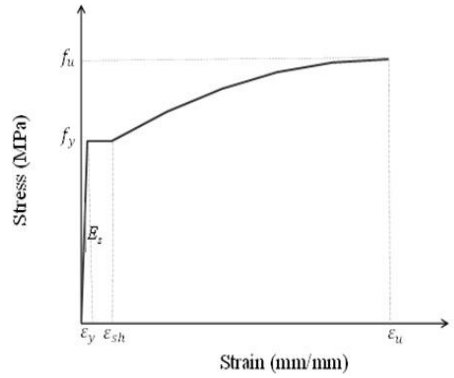	Stress-strain relationship: $f_s = \begin{cases} E_s \varepsilon_s & \text{for } \varepsilon_s \le \varepsilon_y \\ f_y + (\varepsilon_s - \varepsilon_y)\left(\frac{f_{sh} - f_y}{\varepsilon_{sh} - \varepsilon_y}\right) & \text{for } \varepsilon_y < \varepsilon_s \le \varepsilon_{sh} \\ f_y + (f_u - f_y)\left[2\left(\frac{\varepsilon_s - \varepsilon_{sh}}{\varepsilon_u - \varepsilon_{sh}}\right) - \left(\frac{\varepsilon_s - \varepsilon_{sh}}{\varepsilon_u - \varepsilon_{sh}}\right)^2\right] & \text{for } \varepsilon_{sh} < \varepsilon_s \le \varepsilon_u \end{cases}$

Note: f_s – steel stress at strain $\mathcal{E}_s$; f_y – steel yield stress; $\mathcal{E}_y$ – steel yield strain; f_{sh} – steel hardening stress; $\mathcal{E}_{sh}$ – steel hardening strain; f_u – steel ultimate stress; $\mathcal{E}_u$ – steel ultimate strain;

Figure 7.3 Constitutive material model for Steel

<table>
<tr><th></th><th colspan="2">Dynamic Increase factor (DIF) models</th></tr>
<tr><th></th><th>Concrete in compression</th><th>Concrete in tension</th></tr>
<tr><td>HSC</td><td>CEB model:
$\mathrm{DIF_c} = \begin{cases} \left(\frac{\dot{\varepsilon}}{\dot{\varepsilon}_s}\right)^{1.026\alpha} & \text{for } \dot{\varepsilon} \le 30\mathrm{s}^{-1} \\ \gamma\left(\frac{\dot{\varepsilon}}{\dot{\varepsilon}_s}\right)^{1/3} & \text{for } \dot{\varepsilon} > 30\mathrm{s}^{-1} \end{cases}$
Where: $\log\gamma = 6.156\alpha - 2;\ \alpha = \frac{1}{(5+9f'_c/10)};\ \dot{\varepsilon}_s = 30\cdot 10^{-6}\mathrm{s}^{-1}$
Case 2: $\mathrm{DIF_c}$ = 1.19 (Design DIF), Case 3: $\mathrm{DIF_c}$ = 1.0 (no dynamic factor)</td><td rowspan="2">Malvar and Ross:
$\mathrm{DIF_t} = \begin{cases} \left(\frac{\dot{\varepsilon}}{\dot{\varepsilon}_s}\right)^{\delta}, & \dot{\varepsilon} \le 1\mathrm{s}^{-1} \\ \beta^*\left(\frac{\dot{\varepsilon}}{\dot{\varepsilon}_s}\right)^{1/3}, & \dot{\varepsilon} > 1\mathrm{s}^{-1} \end{cases}$
$\mathrm{Log}\,\beta^* = 6\delta - 2;\ \delta = \frac{1}{(1+8f'_{cf}/10)};\ \dot{\varepsilon}_s = 10^{-6}\mathrm{s}^{-1}$
Case 2: $\mathrm{DIF_t}$ = 1.0 (no dynamic factor)
Case 3: $\mathrm{DIF_t}$ = 1.0 (no dynamic factor)</td></tr>
<tr><td>HSFRC</td><td>Wang et al.:
$\mathrm{DIF_c^F} = \begin{cases} \left(\frac{\dot{\varepsilon}}{\dot{\varepsilon}_s}\right)^{1.026\alpha} & \text{for } \dot{\varepsilon} \le (30+23i)\mathrm{s}^{-1} \\ \eta\left(\frac{\dot{\varepsilon}}{\dot{\varepsilon}_s}\right)^{\kappa} & \text{for } \dot{\varepsilon} > (30+23i)\mathrm{s}^{-1} \end{cases}$
Where: i =1 and 0 for FRC and plain concrete, respectively;
$\eta = \gamma(1-0.3392i);\ \kappa = (1+0.05i)/3;$
$\log\gamma = 6.156\alpha - 2;\ \alpha = \frac{1}{(5+9f'_{cf}/10)}$; and
Case 2: $\mathrm{DIF_c^F}$ = 1.19 (Design DIF), Case 3: $\mathrm{DIF_c^F}$ = 1.0 (no dynamic factor)</td></tr>
<tr><td>Steel</td><td colspan="2">Saatcioglu et al:
At yield → $\mathrm{DIF_y} = 0.034\ln(\dot{\varepsilon}) + 1.30 \ge 1.0$ - At ultimate → $\mathrm{DIF_u} = 0.0101\ln(\dot{\varepsilon}) + 1.10 \ge 1.0$
Case 2: $\mathrm{DIF_y}$ = 1.17 and $\mathrm{DIF_u}$ = 1.05 (Design DIF) - Case 3: $\mathrm{DIF_y} = \mathrm{DIF_u}$ = 1.0 (no dynamic factor)</td></tr>
</table>

Note: $\dot{\varepsilon}_s$ – static strain rate; $\dot{\varepsilon}$ – dynamic strain rate; $\mathrm{DIF_c}$, $\mathrm{DIF_t}$, $\mathrm{DIF_y}$ & $\mathrm{DIF_u}$: Dynamic increase factors for concrete in compression & tension and steel at yield & ultimate; α, η, γ, κ, β*and δ – various curve fitting parameters; i – fiber parameter taken as = 1 for FRC and 0 for plain concrete.

Figure 7.4 Dynamic increase factor (DIF) models for HSC, HSFRC, and Steel

7.3 SECTIONAL AND MEMBER ANALYSIS PROCEDURES

Sectional analysis was used to generate the M-ϕ (moment-curvature) relationships for each beam section. The analysis began by defining the constitutive material models for concrete and steel at high-strain rates using the models defined in the previous section. **Figure 7.5** shows sample stress-strain curves for HSC, HSFRC, and steel, with and without DIF factors applied. With the dynamic properties defined, the procedure is shown in **Figure 7.6 (a)** was used to determine the moment-curvature relationship.

The analysis involved discretizing the beam section into n = 50 equal segments, setting a strain in the top compression fiber, assuming a neutral axis depth, and then using force equilibrium and summation of moments to determine the curvature and moment. This iterative procedure was repeated to find the complete $(\mathrm{M}-\phi)$ relationship for each beam.

Next, the load-deflection relationships were determined by plotting the curvature along the beam length ad using the moment area method ($\delta = \int_0^{\mathrm{L}/2} \phi(\mathrm{x})\cdot \mathrm{x}\cdot \mathrm{dx}$) as outlined in **Figure 7.6 (b)** to determine the deflections. Before yielding ($\delta \le \delta_y$), the deflection was obtained using the following relationship based on the integration of the curvature:

$$\delta_y = \int_0^{L/2} \phi(x) \cdot x \cdot dx = \phi_y \cdot \left(\frac{a^2}{3}\right) + \phi_y \cdot \left(\frac{L_{cm}}{2}\right)\left(\frac{L}{2} - \frac{L_{cm}}{4}\right) \quad (5)$$

After yielding, non-linear behavior (cracking and concrete damage) was assumed to be concentrated in the beam plastic hinge length (l_p), with the plastic deflection determined using the following equation:

$$\delta_p = \int_0^{L/2} \phi(x) \cdot x \cdot dx = \delta_y + (\phi_u - \phi_y) \cdot (l'_p) \cdot \left(\frac{L}{2} - \frac{l'_p}{2}\right) \quad (6)$$

Ashour and Wafa (1993) have observed that the actual hinge length in reinforced concrete beams tested under four-point bending varies and can be shorter or longer than the constant moment region length. In addition, fibers affect cracking behavior in reinforced concrete beams and can either extend the hinge length if they cause more diffused cracking or shorten the hinge length if they cause crack localization. To examine these effects various hinge length cases were considered in the analysis including : $l_p = l_{cm}$ (Case 1), where l_{cm} is the length of the constant moment region, and $l_p = 2d$ or $l_p = d$ (Cases 1b, 1c) where d = the beam section depth.

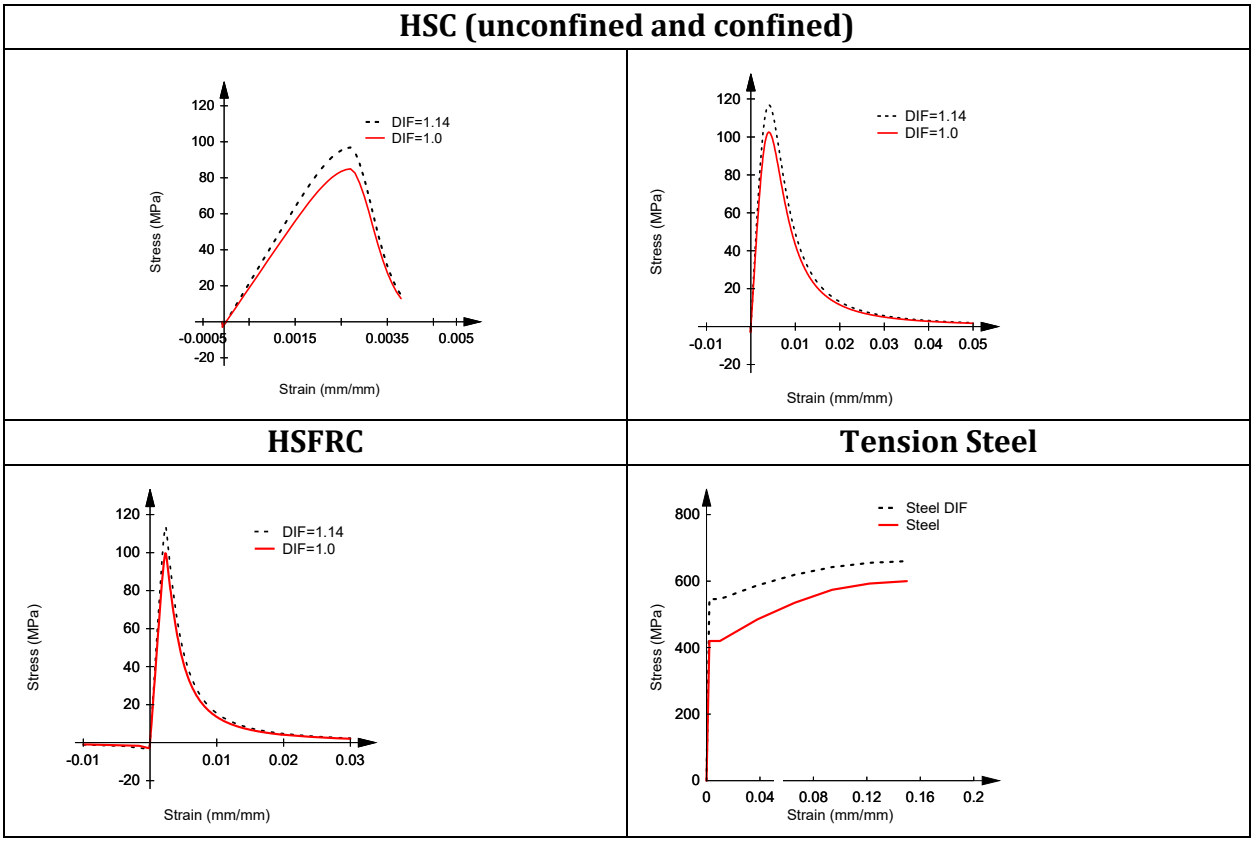

Figure 7.5 Sample stress-strain relationships (with and without DIF)

Multi-layer sectional analysis procedure used to determine M-Φ relationship	Procedure for determining load-displacement resistance relationship
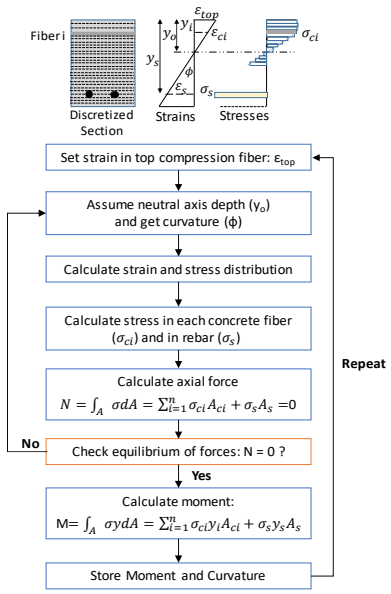	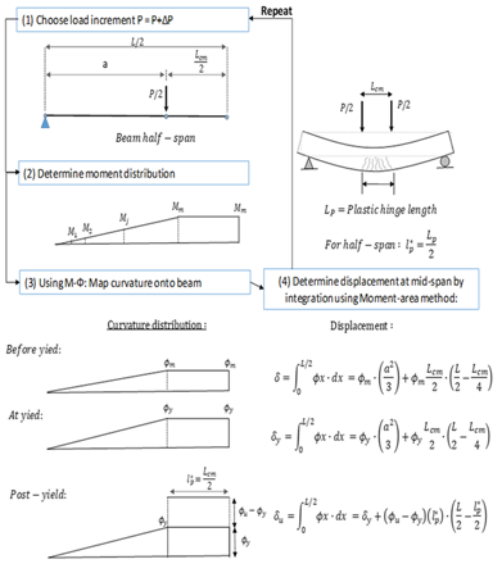

Figure 7.6 Procedures used to develop the analytical resistance curves (Algassem et al., 2016)

7.4 DYNAMIC ANALYSIS (SDOF PROCEDURE)

Single degree of freedom (SDOF) analysis was used to predict the dynamic displacement response of each specimen by solving the equation of motion shown in (3):

$$\boldsymbol{K_{LM} m \ddot{u}(t) + R(u(t)) = AP_r(t)} \quad (7)$$

The analysis involved transforming the actual structure (beam) into an equivalent SDOF system were mass and stiffness are lumped. This is accomplished using the factor K_{LM}, which is a load-mass transformation factor that takes into account the loading, deformed shape and boundary conditions in the actual structure. In this study, factors of 0.6 and 0.56 were used before and after yield based on the recommendations in Biggs (1964).

The mass (m) of the system was taken as 450 kg, equivalent to the mass of the beam and load-transfer device (LTD). The remaining parameters include: u(t) = beam mid-span displacement, ü(t) = beam mid-span acceleration and R(u(t)) = beam resistance as a function of displacement.

Finally, $AP_r(t)$ represents the loading function, where A is the loaded area of the load-transfer device (taken as 3.4 m2 for the setup used in this research) and $P_r(t)$ is the blast pressure as a function of time, which was idealized using a triangular function having the same peak reflected pressure and impulse observed in the experiments.

With the resistance functions, load-mass factors, and forcing function defined, software RCBlast was used o solve the equation of motion using the average acceleration method. Some of the steps used in the analysis procedure are shown in Figure 7.7.

a) Define General Member Properties

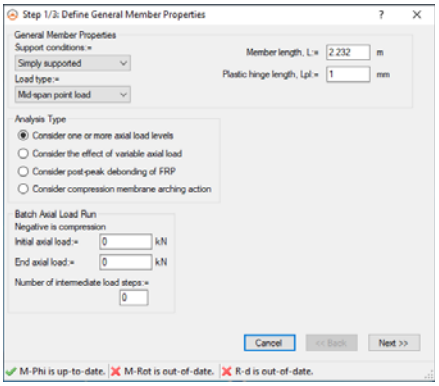

b) Input material properties (models are developed in separate excel spreadsheet and then input in RCBlast)

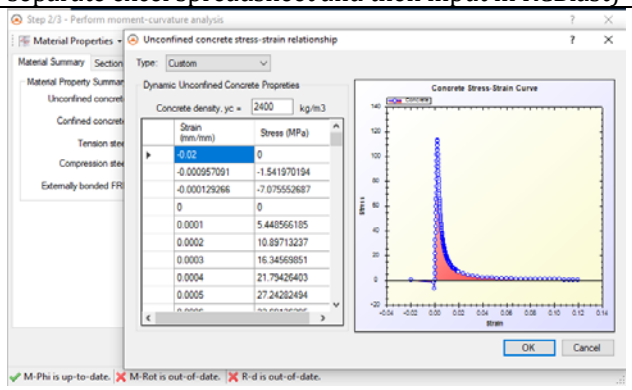

c) Generate moment-curvature using RCBlast software

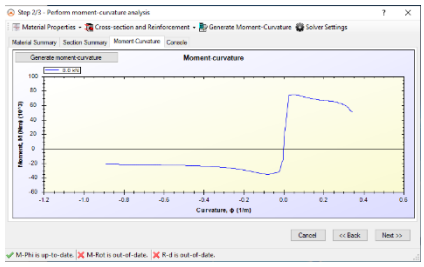

d) Generate load-displacement curve in excel spread-sheet, then plug back into RCBlast software

φ (1/m)	M (Nm)	εtop	εbtm	Delta	Load	Klm
-0.888629716	-21490.43	-0.04554	0.176617	-129.0853	-57.84773	0.56
-0.884423491	-21499.68	-0.04532	0.175786	-128.6369	-57.87263	0.56
-0.880217986	-21509.46	-0.04510	0.174954	-128.1886	-57.89895	0.56
-0.87601624	-21518.85	-0.04488	0.174124	-127.7407	-57.92423	0.56
-0.871814714	-21528.28	-0.04466	0.173294	-127.2928	-57.9496	0.56
-0.867613966	-21537.79	-0.04444	0.172463	-126.845	-57.97522	0.56
-0.863413833	-21547.31	-0.04422	0.171633	-126.3973	-58.00083	0.56
-0.859215004	-21557.38	-0.04400	0.170804	-125.9497	-58.02794	0.56
-0.85501958	-21567.05	-0.04378	0.169975	-125.5024	-58.05396	0.56
-0.850824476	-21576.75	-0.04356	0.169146	-125.0552	-58.08007	0.56
-0.846630363	-21586.57	-0.04334	0.168318	-124.6081	-58.10651	0.56
-0.842437351	-21596.45	-0.04312	0.167489	-124.1612	-58.13311	0.56
-0.838247871	-21606.86	-0.04290	0.166662	-123.7146	-58.16114	0.56
-0.834062747	-21617.04	-0.04268	0.165836	-123.2684	-58.18854	0.56
-0.829879547	-21627.54	-0.04246	0.16501	-122.8225	-58.21679	0.56
-0.825699009	-21638.29	-0.04224	0.164185	-122.3769	-58.24573	0.56
-0.82152019	-21649.47	-0.04202	0.16336	-121.9314	-58.27583	0.56
-0.81734613	-21661.22	-0.04180	0.162537	-121.4864	-58.30746	0.56
-0.81317359	-21672.66	-0.04158	0.161713	-121.0416	-58.33826	0.56
-0.80900203	-21684.22	-0.04136	0.160891	-120.597	-58.36937	0.56
-0.804773695	-21716.37	-0.04114	0.160053	-120.1462	-58.4559	0.56
-0.800603749	-21728.58	-0.04092	0.159231	-119.7017	-58.48877	0.56
-0.796439069	-21740.48	-0.04070	0.15841	-119.2577	-58.5208	0.56
-0.792274901	-21752.41	-0.04048	0.157589	-118.8138	-58.55291	0.56
-0.788112086	-21764.47	-0.04026	0.156768	-118.3701	-58.58538	0.56

e) Define the mass of the system and the pressure-time history, then run the SDOF analysis to obtain the maximum displacement using RCBlast software

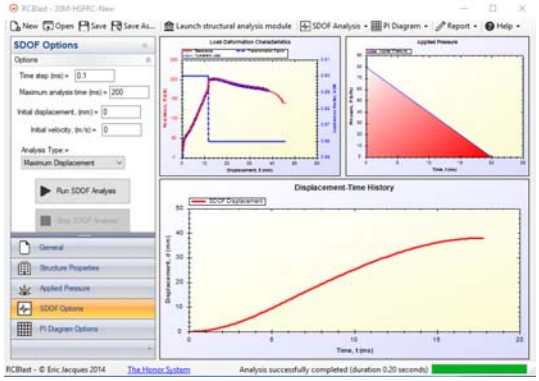

Figure 7.7 SDOF analysis procedure: steps used to predict maximum displacement.

7.5 STATIC ANALYSIS RESULTS

Before presenting the results of the dynamic analysis, it is useful to examine the predictions of the beams under static loads. The analytical static load-deflection responses of the test beams were determined using the procedure defined in **Section 7.3** but ignoring strain-rate effects. The results of the analysis are summarized in **Table 7-1**and **Figure 7.8**, while the comparison of the experimental and analytical load-deflection curves for the HSC and HSFRC beams are shown in **Figure 7.9** and **Figure 7.11**.

As seen in **Figure 7.9** and **Figure 7.11**, the analytical load-deflection curves correlate well with the experimental load-deflection curves, with a good prediction of peak load (P_{anls}) when compared to the experiments (P_{max}), with an average P_{anls}/P_{max} ratio of 0.98 when considering the results for all beams (standard deviation [SD] of 0.04 and the coefficient of variation [cov] of 4.1%). While the post-peak responses closely match the experimental curves, it can be seen that analytical curves over-predict the initial stiffness. Considering all beams, the mean analytical to experimental stiffness ratio (K_{anls}/K_{max}) is found to be 1.44, with SD = 0.17 and cov =12%.

Table 7-1 -Comparison of experimental vs. analytical peak loads and stiffness (static tests)

Series	ID	Load			Stiffness		
		P_{exp} (kN)	P_{anls} (kN)	P_{anls}/P_{exp}	K_{exp} (N/mm)	K_{anls} (N/mm)	K_{anls}/K_{exp}
15M	HSC-F0-15M-10M-d/4	108	106	0.98	6562	10771	1.64
	HSC-F0.75-15M-10M-d/2	117	110	0.94	10181	11778	1.16
20M	HSC-F0-20M-10M-d/4	131	135	1.03	9411	13804	1.47
	HSC-F0.75-20M-10M-d/2	168	156	0.93	10667	14380	1.35
25M	HSC-F0-25M-10M-d/4	225	227	1.01	11458	17460	1.52
	HSC-F0.75-25M-10M-d/2	248	247	1.00	12435	18712	1.50
Mean		0.98	Mean		1.44		
Std. Dev.		0.04	Std. Dev.		0.17		
COV		4.1%	COV		12%		

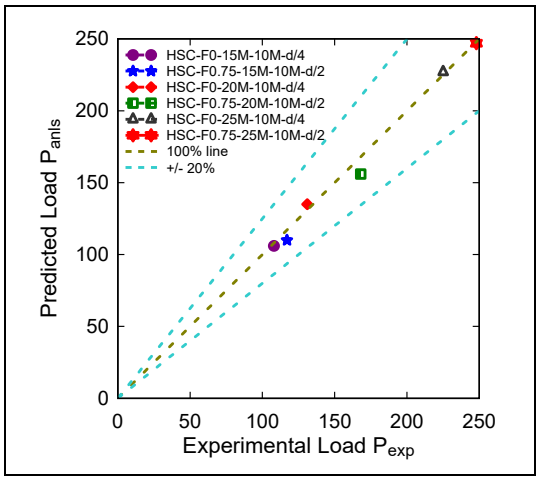

Figure 7.8 -Predicted vs. experimental loads peak loads

7.6 DYNAMIC ANALYSIS RESULTS

Figure 7.9 and **Figure 7.10** present the results of the dynamic analysis in terms of maximum displacement and response time histories for plain HSC beams (HSC-F0-15M-10M-d/4, HSC-F0-20M-10M-d/4, and HSC-F0-25M-10M-d/4) at Blast A-D, while **Figure 7.11** and **Figure 7.12** show the results for the HSFRC beams (HSC-F0.75-15M-10M-d/4, HSC-F0.75-20M-10M-d/4, and HSC-F0.75-25M-10M-d/4) at Blast A-E. The dynamic resistance functions for the beams considering the three cases of DIF and the different plastic hinge length cases are also shown in the figures. **Table 7-2** and

Table 7-3 summarizes the analysis results in terms of predicted displacements for the HSC and HSFRC beams, respectively.

Considering the plain HSC specimens and all blasts, the mean maximum displacement ratio (D_{anls}/D_{max}) for Case 1 (default DIF and plastic hinge length = lcm) is found to be 0.98 (with SD=0.14 and cov = 14%) which demonstrates that the analytical procedure was able to predict the maximum displacement responses of the beams with good accuracy. The analytical displacements for the specimens with fibers (HSFRC) showed similar accuracy for Case 1 with mean D_{anls}/D_{max} ratio = 0.97, SD =0.11, and cov =12%.

Examining the individual results for the HSC beams, it can be seen that the displacement ratios show a decreasing trend (underprediction of response) as the blast intensity increases, with mean ratios of 1.2, 0.92, and 0.79 at Blast A. C, and D. This result can be attributed to the effects of repeated loading and accumulated damaged which were not considered in the analysis. The same trend is observed for the specimens with fibers, where the displacement ratios reduce at higher blasts (mean ratios at Blast A: 1.05; Blast C: 0.94; and Blast C: 0.89).

Examining the specimens tested under single and repeated blasts, it can be seen that beam HSC-F0-15M-10M-d/4, which was subjected to three Blast loads (Blast A, B, and C), shows a D_{anls}/D_{exp} = 0.87 at Blast C which is lower when compared to the companion beam tested under a single shot (Blast C): D_{anls}/D_{exp} = 0.90 which further confirms the above conclusions.

The effect of DIF model in the HSC and HSFRC series predictions is presented in **Figure 7.9-f** and **Figure 7.11-f.** Considering all blasts the D_{anls}/D_{exp} ratios for Cases 1, 2 and 3 are found to be 0.98, 1.05 and 1.18 for the HSC beams, and 0.97, 1.02, and 1.10 for the HSFRC specimens. The results follow the expected trend; that is, lower displacement ratios for the analyses that incorporated the strain rate dependent DIFs (Case 1) when compared to Case 2 (design DIF) and Case 3 (DIF=0). Case 1 was found to result in the most accurate results, while more conservative predictions were obtained when ignoring the DIF factors. On the other hand, the results for Case 2 (design DIF) are reasonably accurate.

Figure 7.9-d and **Figure 7.11-d** show the effects of hinge length assumption ($l_p = l_{cm}$, $l_p = 2d$, $l_p = d$; Cases 1, 1b and 1c) on the predicted dynamic load-deflection responses. It can be

seen that this parameter does not influence the strength nor the stiffness properties of the resistance functions but affects the ultimate displacements. The effect of this parameter on the dynamic analysis results at Blast C and D can be seen in **Figure 7.9-g** and **Figure 7.11-g**. The results show that decreasing the hinge length from the default value ($l_p = l_{cm}$) to 2d or d increased the analytical displacements at these blasts. The same trend was observed for the beams with fibers, indicating that the lower plastic hinge resulted in higher analytical displacements. It can, however, be concluded that increasing the plastic hinge length did not considerably affect the analytical displacements, with reasonable predictions when using Case 1 (Default value, $l_p = lcm$).

Table 7-2-Idealized blast properties and results of SDOF analysis for HSC beams

Beam ID	Shot #	Blast ID	Idealized Shockwave properties[1]			Maximum Mid-Span Displacement[2]			
			P_r (kPa)	I_r (kPa·msec)	t_{di} (msec)	D_{exp} (mm)	D_{anls} (mm)	Results	
								D_{anls}/D_{exp}	% Error
HSC-F0-15M-10M-d/4	1	A	46.3	373	16.1	17.7	19.8	1.11	11%
	2	B	57.8	582	20.2	33.1	36.4	1.10	10%
	3	C	70.8	701	19.8	63.4	55.0	0.87	13%
HSC-F0-15M-10M-d/4 [x1]	1	C	69.8	712	20.4	61.6	55.7	0.90	10%
HSC-F0-20M-10M-d/4	1	A	45.1	370	16.4	11.5	14.7	1.28	28%
	2	C	74.9	704	18.8	34.6	38.8	1.12	12%
	3	D	88.7	837	18.9	71.6	58.6	0.82	18%
HSC-F0-25M-10M-d/4	1	C	72.1	819	22.7	26.5	20.3	0.77	23%
	2	D	97.7	1001	20.5	45.1	34.6	0.77	23%
								D_{anls}/D_{exp}	
								Mean	0.97
								Std. Dev.	0.19
								COV	19%

Table 7-3-Idealized blast properties and results of SDOF analysis for HSFRC beams

Beam ID	Shot #	Blast ID	Idealized Shockwave properties[1]			Maximum Mid-Span Displacement[2]			
			P_r (kPa)	I_r (kPa·msec)	t_{di} (msec)	D_{exp} (mm)	D_{anls} (mm)	Results	
								D_{anls}/D_{exp}	% Error
HSC-F0.75-15M-10M-d/2	1	A	33.4	335	20.1	10.8	12.1	1.11	11%
	2	B	55.9	565	20.2	28.6	30.3	1.06	6%
	3	C	70.1	731	20.8	58.5	57.1	0.98	2%
	4	D	86.3	921	21.3	70.1	66.6	0.95	5%
HSC-F0.75-20M-10M-d/2	1	A	43.1	315	14.6	11.1	10.9	0.99	1%
	2	C	68.7	706	20.6	36.5	32.9	0.91	9%
	3	D	89.9	897	19.9	49.9	44.3	0.89	11%
HSC-F0.75-25M-10M-d/2	1	C	80.4	637	15.8	21.6	20.3	0.94	6%
	2	D	85.2	945	22.2	36.6	29.8	0.82	18%
	3	E	89.3	1313	29.4	54.7	44.0	0.80	20%
								D_{anls}/D_{exp}	
								Mean	0.97
								Std. Dev.	0.11
								COV	12%

[1]: P_r = Reflected pressure; I_r = Reflected impulse; t_{di} = idealized positive phase duration in triangular blast = I_r *2/ P_r;
[2]: D_{max} = experimental mid-span displacement; D_{anls} = analytical mid-span displacement; AD = accumulated damage

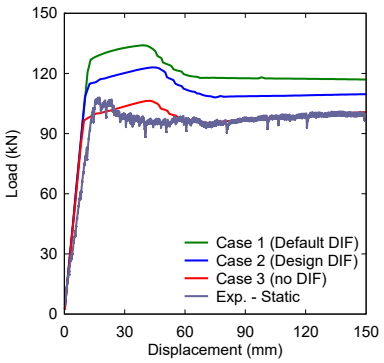

(a) HSC-F0-15M-10M-d/4

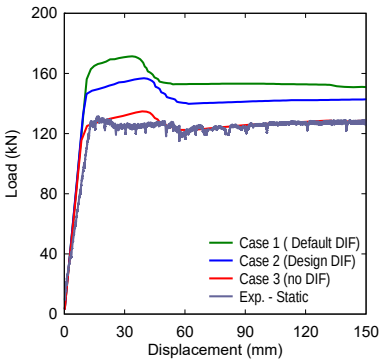

(b) HSC-F0-20M-10M-d/4

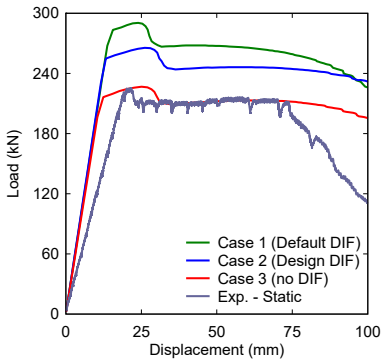

(c) HSC-F0-25M-10M-d/4

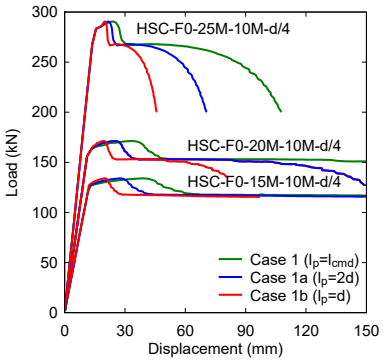

(d) Effect of plastic hinge length on dynamic resistance curves

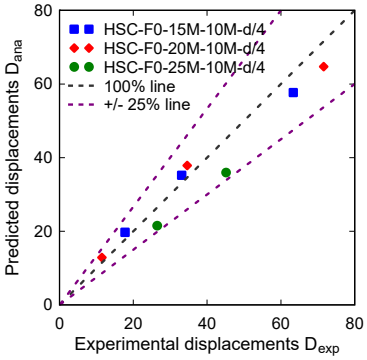

(e) Predicted versus Experimental midspan displacements (Case 1 assumptions)

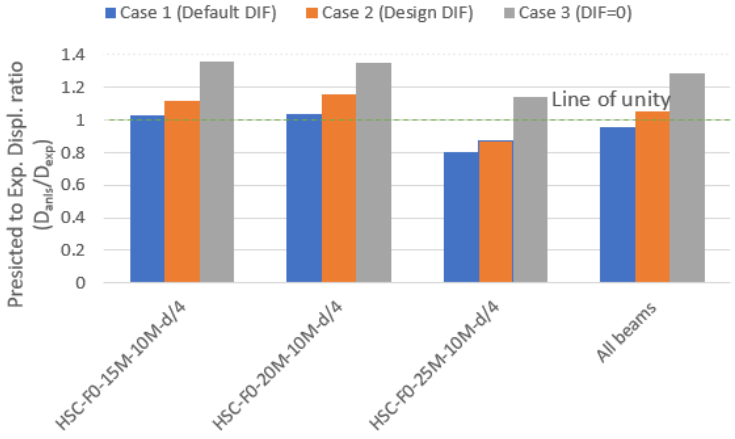

(f) Effect of DIF model on dynamic displacements (average results - all blasts)

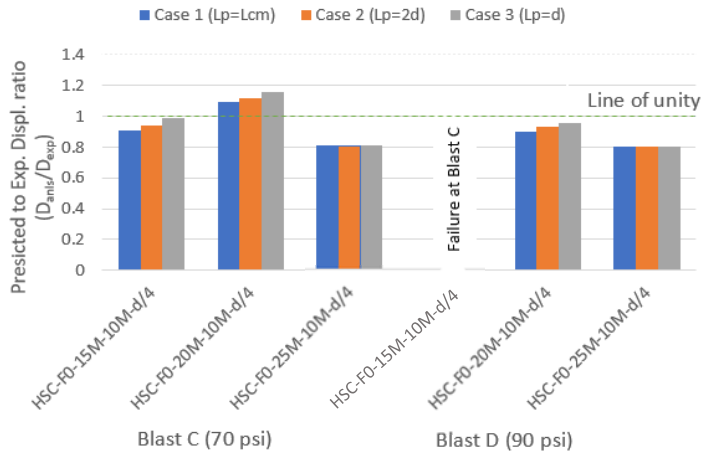

(g) Effect of hinge length assumption on dynamic displacements (Results at Blast C and Blast D)

Figure 7.9 - Analytical static and dynamic resistance curves and sensitivity analysis for HSC beams

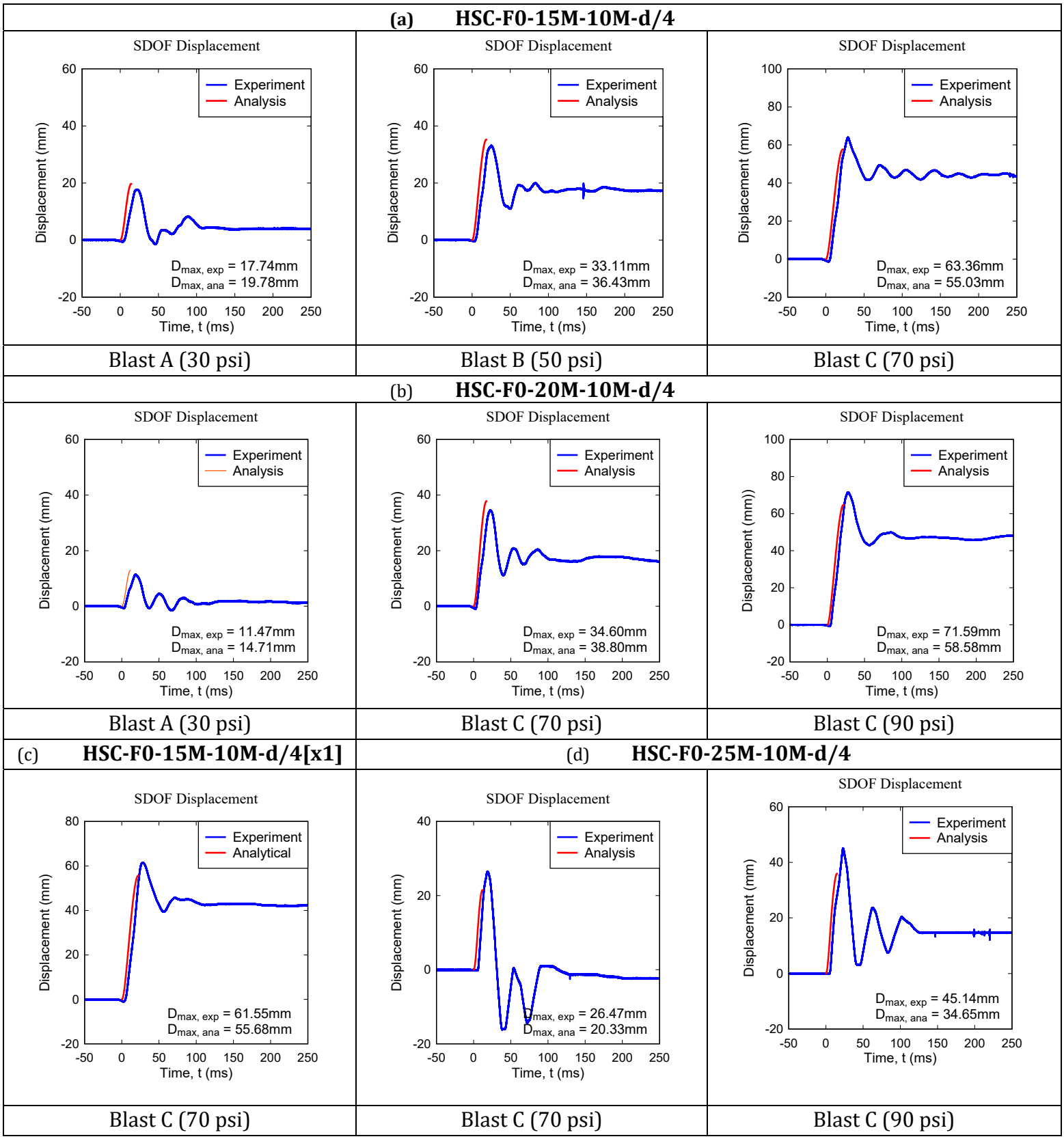

Figure 7.10 Displacement time-history predictions for HSC beams

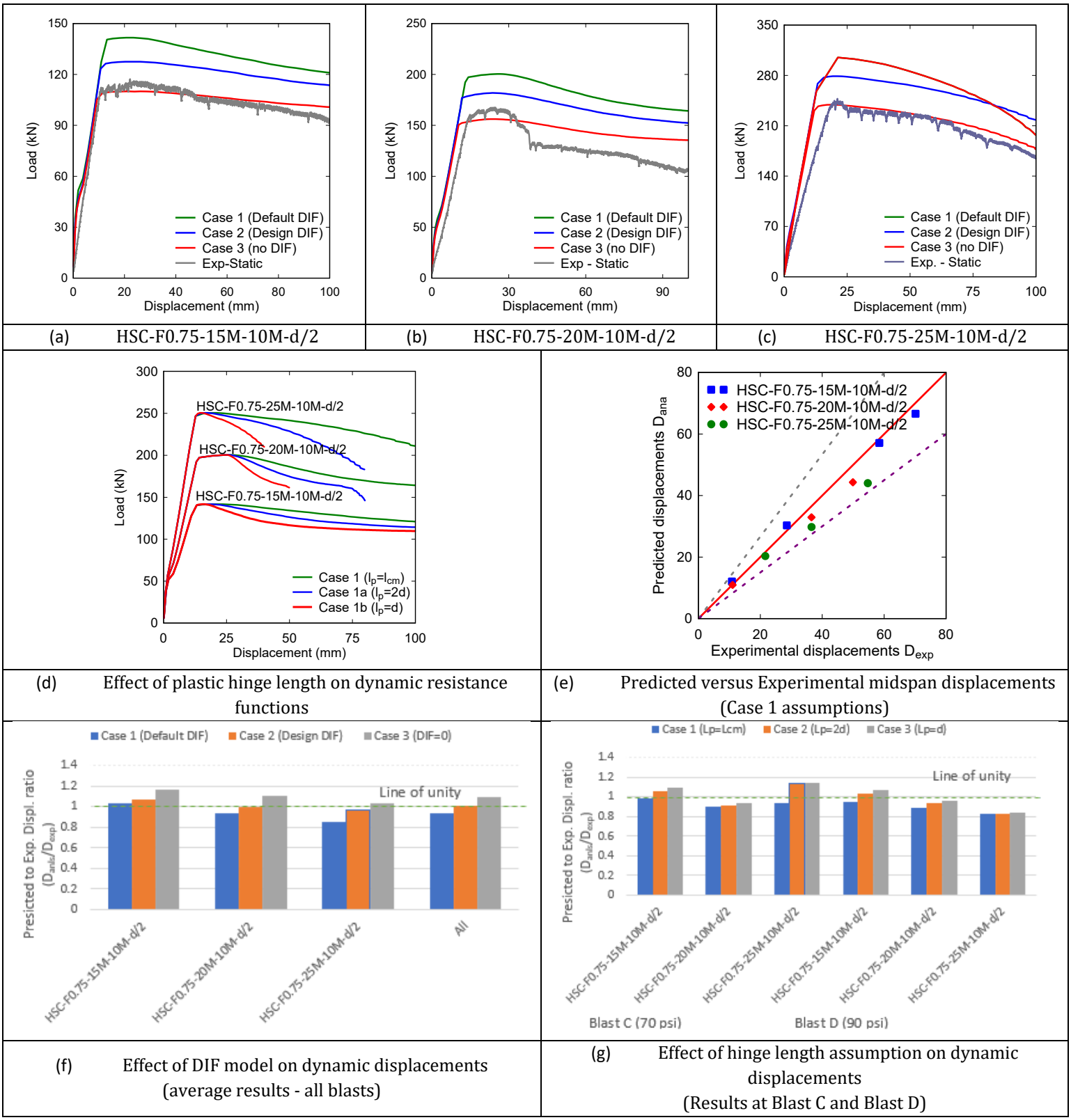

(a) HSC-F0.75-15M-10M-d/2

(b) HSC-F0.75-20M-10M-d/2

(c) HSC-F0.75-25M-10M-d/2

(d) Effect of plastic hinge length on dynamic resistance functions

(e) Predicted versus Experimental midspan displacements (Case 1 assumptions)

(f) Effect of DIF model on dynamic displacements (average results - all blasts)

(g) Effect of hinge length assumption on dynamic displacements (Results at Blast C and Blast D)

Figure 7.11 - Analytical static and dynamic resistance curves and sensitivity analysis for HSFRC beams

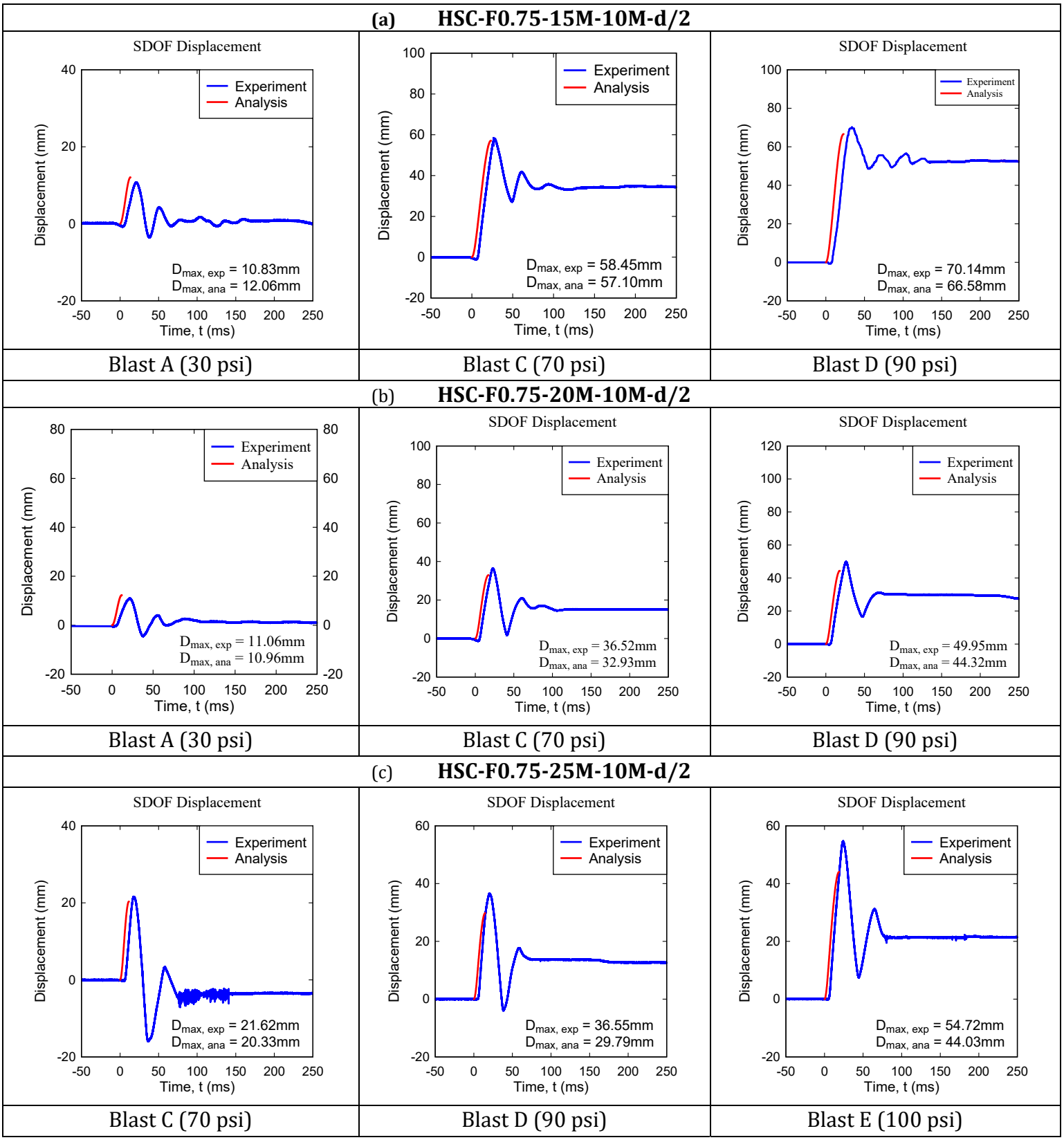

Figure 7.12 Displacement time-history predictions for HSFRC beams

CHAPTER 8: CONCLUSION & RECOMMENDATIONS

8.1 CONCLUSION

This research presented an experimental and analytical study that investigated the performance of high strength concrete (HSC) beams designed in accordance with the CSA-S850 blast detailing requirements. In addition, the study examined the potential of using steel fibers to relax such detailing. The main parameters investigated in this research included the effects of blast detailing, fibers, single vs repeated blasts, tension reinforcement ratio, compression reinforcement ratio, and transversal detailing.

A total of seventeen beams were included in this research, seven of which were tested under quasi-static four-point bending, with the remaining ten beams tested under simulated blast loads using the University of Ottawa shock tube. In total, eight beams with significant post-blast capacity were tested under quasi-static four-point bending to investigate their residual post-blast capacity. Conclusions of the experimental research are summarized below:

- The use of blast detailing was found to improve the overall response of plain HSC beams under static loads, significantly increasing the ductility and toughness. The blast detailing was also effective in enhancing the blast response of the specimens by reducing maximum and residual displacements and increasing blast resistance. Failure mode was also significantly improved, with limited damages and concrete crushing in the midspan region.
- All blast detailed HSC beams had significant post-blast capacity (RRI =0.9-1), with large energy dissipation (TEI > 1) and an ability to sustain large post-blast displacements. The blast damaged beams showed similar failure mode when compared to the undamaged specimens tested under static loads.
- The use of fibers increased the strength and stiffness of the beams under static loads, with important ductility. However, the use of low steel ratio (in the 15M specimens) led to earlier bar rupture and failure. Under blast loads, the use of fibers and intermediate tie spacing (d/2) not only matched but out-performed the blast performance of the blast-detailed HSC specimens with d/4 tie spacing, with improved damage tolerance. All HSFRC beams also showed significant post-blast resistance and energy-dissipation capacity even after intense blast testing. Keeping in mind the potential for bar rupture, the results show that moderate amount of fibers can be used to relax detailing requirements in modern blast codes.
- The effect of repeated blasts was examined by comparing responses of companion HSC beams with 15M bars and blast detailing tested under multiple and single blasts. In general, both beams showed similar displacement responses under blast loading. However, the damages in the unreinforced top cover region were more severe under repeated loads. Furthermore, both specimens showed similar post-blast behavior in terms of residual strength, ductility, and failure mode.

- Comparison between doubly reinforced beams with blast detailing (d/4, s= 50mm) and intermediate detailing (d/2, s= 100mm) in the 20M Series resulted in similar blast response and failure mode. However, during the residual satanic tests, the specimen with blast detailing prevented buckling of the compression bars which resulted in an increase of the overall residual capacity.
- The effect of tension steel ratio was examined in both the HSC and HSFRC series. In both cases, increasing eth steel ratio increased strength and stiffness under static loads, with improved displacement control under blast loading. However, increasing the steel ratio beyond the CSA S850 limits resulted in less ductile failures, with more rapid strength decay, increased concrete damage and bar buckling. On the other hand, the use of low steel ratio in the HSFRC series led to earlier bar rupture due to crack localization.

Dynamic inelastic analysis was conducted to predict the blast displacement response of the HSC and HSFRC beams. Materials and DIF models were used to develop the resistance curves and dynamic analysis using a SDOF approach was conducted to predict the analytical displacements of all specimens tested in the shock-tube. The conclusions from the analytical study are summarized below:

The SDOF method, with the development of dynamic resistance functions, predicted the dynamic responses of the HSC and HSFRC beams with reasonable accuracy. The accuracy of the analytical displacement was reduced at subsequent blasts due to the effects of accumulated damage.

- The strain-rate dependent DIF models proposed by and Wang et al. (2011); Malvar & Ross (1998); and Saatcioglu et al. (2011) led to accurate analytical predictions. Using, design DIF (CSA S850, 2012) also provided reasonably accurate predictions, while the use of DIF=0 resulted in more conservative predictions ($D_{anls}/D_{res} > 1$).

8.2 RECOMMENDATIONS FOR FUTURE RESEARCH

The following recommendations for future research are suggested:

- Further experimental and analytical research to examine the effects of single vs repeated blasts on the dynamic and residual post-blast behavior of HSC and HSFRC;
- Research on the development of reliable stress-strain models and dynamic increase factors (DIF) for fiber-reinforced concrete incorporating hybrid fibers;
- Further research the optimal fiber content that can be used to relax tie spacing without compromising on dynamic performance in HSC beams and columns.
- Performing further experimental research on different parameters (UHPC, High Strength steel, synthetic fiber) for reinforced concrete beams designed with blast detailing;
- Finite element modeling to better predicts the static and blast response of reinforced concrete beams built with HSC and HSFRC.

CHAPTER 9: REFERENCE

Adhikary, S.D., Li, B., and Fujikake, K. 2015. State-of-the-art review on low-velocity impact response of reinforced concrete beams. Magazine of Concrete Research, **68**(14): 701-723.

Algassem, O. 2016. PARAMETERS AFFECTING THE BLAST PERFORMANCE OF HIGH STRENGTH FIBRE REINFORCED CONCRETE BEAMS. Department of Civil Engineering, University of Ottawa.

Ashour, S.A. 2000. Effect of compressive strength and tensile reinforcement ratio on flexural behavior of high-strength concrete beams. Engineering Structures, **22**(5): 413-423.

Ashour, S.A., and Wafa, F.F. 1993. Flexural behavior of high-strength fiber reinforced concrete beams. ACI Structural Journal, **90**(3): 279-287.

Banthia, N.P. 1987. Impact resistance of concrete. University of British Columbia.

Biggs, J.M. 1964. Introduction to structural dynamics. McGraw-Hill New York.

Biolzi, L., and Cattaneo, S. 2017. Response of steel fiber reinforced high strength concrete beams: Experiments and code predictions. Cement and Concrete Composites, **77**: 1-13.

Bischoff, P., and Perry, S. 1991. Compressive behaviour of concrete at high strain rates. Materials and structures, **24**(6): 425-450.

Burrell, R.P., Aoude, H., and Saatcioglu, M. 2014. Response of SFRC columns under blast loads. Journal of structural engineering, **141**(9): 04014209.

CEB-FIP. Model Code 1990. Comite Euro-International Du Beton, Paris, 1991, p. 87-109.

Canadian Standards Association (CSA). Design and assessment of buildings subjected to blast loads. CSA S850-12, Mississauga, ON, Canada, 2012, p. 126.

Canadian Standards Association (CSA). Design of concrete structures. CAN/CSA A23.3-14, Mississauga, ON, 2014, p.

Dancygier, A.N., and Karinski, Y.S. 2019. Effect of cracking localization on the structural ductility of normal strength and high strength reinforced concrete beams with steel fibers. International Journal of Protective Structures, **10**(4): 457–469.

Feldman, A., Keenan, W., and Siess, C.P. 1962. Investigation of resistance and behavior of reinforced concrete members subjected to dynamic loading, part III. *In* SRS Report No. 165. Department of Civil Engineering, University of Illinois at Urbana Champaign, Urbana, IL. p. 354.

Fujikake, K., Li, B., and Soeun, S. 2009. Impact response of reinforced concrete beam and its analytical evaluation. Journal of structural engineering, **135**(8): 938-950.

Huynh, L., Foster, S., Valipour, H., and Randall, R. 2015. High strength and reactive powder concrete columns subjected to impact: experimental investigation. Construction and Building Materials, **78**: 153-171.

Jacques, E., Lloyd, A., & Saatcioglu, M. (2012). Predicting reinforced concrete response to blast loads. *Canadian Journal of Civil Engineering*, *40*(5), 427-444.

Jin, L., Zhang, R., Dou, G., Xu, J., and Du, X. 2017. Experimental and numerical study of reinforced concrete beams with steel fibers subjected to impact loading. International Journal of Damage Mechanics, **27**(7): 1058-1083.

Kwan, A., Chau, S., and Au, F. 2006. Improving flexural ductility of high-strength concrete beams. Proceedings of the Institution of Civil Engineers: Structures and Buildings.

Lee, J.-Y., Shin, H.-O., Yoo, D.-Y., and Yoon, Y.-S. 2018. Structural response of steel-fiber-reinforced concrete beams under various loading rates. Engineering Structures, **156**: 271-283.

Lloyd, A., Jacques, E., Saatcioglu, M., Palermo, D., Nistor, I., and Tikka, T. 2011. Capabilities and effectiveness of using a shock tube to simulate blast loading on structures and structural components. ACI SP-281: Behaviour of Concrete Structures Subjected to Blast and Impact Loadings: 1-20.

Lok, T.-S., and Pei, J.-S. 1998. Flexural behavior of steel fiber reinforced concrete. Journal of materials in civil engineering, **10**(2): 86-97.

Louw, M. 1992. The behaviour of RC columns under impact loading. The Civil Engineer in South Africa, **34**(11): 371-378.

Magnusson, J., Hallgren, M., and Ansell, A. 2010. Air-blast-loaded, high-strength concrete beams. Part I: Experimental investigation. Magazine of Concrete Research, **62**(2): 127-136.

Malvar, L.J. 1998. Review of static and dynamic properties of steel reinforcing bars. ACI Materials Journal, **95**(5): 609-616.

Malvar, L.J., and Ross, C.A. 1998. Review of strain rate effects for concrete in tension. ACI Materials Journal, **95**(6): 735-739.

Mander, J.B., Priestley, M.J., and Park, R. 1988. Theoretical stress-strain model for confined concrete. Journal of structural engineering, **114**(8): 1804-1826.

Mansur, M., Chin, M., and Wee, T. 1999. Stress-strain relationship of high-strength fiber concrete in compression. Journal of materials in civil engineering, **11**(1): 21-29.

Min, K.-H., Kwon, K.Y., Lee, J.-Y., and Yoon, Y.-S. 2014. Effects of steel fibre and shear reinforcement on static and impact load resistances of concrete beams. Magazine of Concrete Research, **66**(19): 998-1006.

Noghabai, K. 2000. Beams of fibrous concrete in shear and bending: experiment and model. Journal of structural engineering, **126**(2): 243-251.

Othman, H., and Marzouk, H. 2016. An experimental investigation on the effect of steel reinforcement on impact response of reinforced concrete plates. International Journal of Impact Engineering, **88**: 12-21.

Popovics, S. 1973. A numerical approach to the complete stress-strain curve of concrete. Cement and Concrete Research, **3**(5): 583-599.

Rashid, M., and Mansur, M. 2005. Reinforced high-strength concrete beams in flexure. ACI Structural Journal, **102**(3): 462-471.

Saatci, S., and Vecchio, F.J. 2009. Effects of shear mechanisms on impact behavior of reinforced concrete beams. ACI Structural Journal, **106**(1): 78-86.

Saatcioglu, M., Lloyd, A., Jacques, E., Braimah, A., and Doudak, G. 2011. Focused research for development of a CSA standard on design and assessment of buildings subjected to blast loads. University of Ottawa, Ottawa, Canada.

Sarkar, S., Adwan, O., and Munday, J. 1997. High strength concrete: an investigation of the flexural behaviour of high strength RC beams. Structural Engineer, **75**(7): 115-121.

Sharifi, Y., and Maghsoudi, A.A. 2014. An experimental study on the flexural behavior of heavily steel reinforced beams with high-strength concrete. Frontiers of Structural and Civil Engineering, **8**(1): 46-56.

Shin, S.-W., Yoo, S.-H., Ahn, J.-M., and Lee, K.-S. 1999. The ductile behaviour including flexural strength of high-strength concrete members subjected to flexure. ACI Special Publication, **172**: 247-280.

Song, P., and Hwang, S. 2004. Mechanical properties of high-strength steel fiber-reinforced concrete. Construction and Building Materials, **18**(9): 669-673.

Tachibana, S., Masuya, H., and Nakamura, S. 2010. Performance based design of reinforced concrete beams under impact. Natural Hazards and Earth System Sciences, **10**(6): 1069-1078.

Tahenni, T., Chemrouk, M., and Lecompte, T. 2016. Effect of steel fibers on the shear behavior of high strength concrete beams. Construction and Building Materials, **105**: 14-28.

Thiagarajan, G., Kadambi, A.V., Robert, S., and Johnson, C.F. 2015. Experimental and finite element analysis of doubly reinforced concrete slabs subjected to blast loads. International Journal of Impact Engineering, **75**: 162-173.

Ulzurrun, G.S.D., and Zanuy, C. 2017. Enhancement of impact performance of reinforced concrete beams without stirrups by adding steel fibers. Construction and Building Materials, **145**: 166-182.

Wang, S., Zhang, M.-H., and Quek, S.T. 2011. Effect of high strain rate loading on compressive behaviour of fibre-reinforced high-strength concrete. Magazine of Concrete Research, **63**(11): 813-827.

Yoo, D.-Y., Banthia, N., and Yoon, Y.-S. 2017. Impact Resistance of Reinforced Ultra-High-Performance Concrete Beams with Different Steel Fibers. ACI Structural Journal, **114**(1).